Phenotypic and genetic analysis of the hindshaker mutation

A thesis presented to the Faculty of Veterinary Medicine, University of Glasgow

for the degree of
Doctor of Philosophy

December 1997

Helen Anne King

ABSTRACT

Hindshaker (*hsh*) is a novel spontaneous murine mutation with autosomal recessive inheritance. Homozygous animals of both sexes exhibited a tremor of the hind end which commenced at about 2 weeks of age and largely disappeared in animals older than 6 weeks. The severity of tremor varied between mice of the same age and a small proportion did not develop a phenotype at all. Seizures, infertility and premature death were not features of the mutation. There was hypomyelination affecting predominantly the spinal cord, although optic nerves and brain were involved to a much lesser degree. The defect of thinly myelinated and naked axons was maximal at 20 days and largely resolved with time so that in the adult, most axons were myelinated. Myelin appeared structurally normal and immunocytochemistry indicated the presence of a panel of myelin proteins.

Although distribution of oligodendrocytes in the spinal cord was similar to normal, hypomyelination appeared to be due, at least in part, to a paucity of mature oligodendrocytes that was most profound in the spinal cord. The partial resolution of the myelin deficit was concomitant with an increase in the number of these cells. No ultrastructural abnormalities were found in *hsh* oligodendrocytes and *in vitro* studies failed to reveal any differences between the differentiation of O-2A progenitors obtained from *hsh* and control mice. No marked astrocytosis was apparent although a microgliosis was detected in older animals. Taken together, the evidence suggests that the *hsh* mutation does not involve a major structural protein but more probably perturbs an aspect of oligodendrocyte development.

The first stage of genetic mapping was undertaken using microsatellite markers and an intersubspecific (CAST/Ei) and two interstrain backcrosses (C57BL/6J and BALB/cJ). Incomplete penetrance and variation in the expression of the phenotype occurred on these genetic backgrounds due to the action of specific alleles at other non-disease loci. One such modifying locus was identified on proximal chromosome 17. The *hsh* gene was mapped to a 2cM interval in the middle of chromosome 3; three flanking and five intervening microsatellite markers were identified on a backcross population of 184 mice. There were no obvious candidate genes found on examination of composite genetic maps although *Cnp2* apparently lies 2cM proximal to the interval of interest and remains an interesting contender. Further fine mapping now awaits the generation of vital recombination breakpoints to delimit the *hsh* gene to a sufficiently small interval for positional cloning by contig construction.

To George and Mum

List of contents

List of figures

List of tables

Declaration

I, Helen Anne King, do hereby declare that the work carried out in this thesis is original, was carried out by myself or with due acknowledgement and has not been presented for the award of a degree at any other university.

Acknowledgements

First and foremost, I would like to thank my supervisor, Professor Ian Griffiths, for his support and enduring optimism. His apparent belief in my capabilities gave me inspiration even in the face of my own doubts. A special thanks also goes to the technical staff for their help, advice and friendship; Jenny Barrie, Nan Deary, Douglas Kirkham, Evangelos Kyriakides, Mailis McCulloch and Eilidh MacPhee.

My eternal gratitude to those colleagues and friends who have taught me techniques and given words of wisdom; Jim Anderson, Peter Dickinson, Monica Fanarraga, Paul Montague, Christine Thomson, Demitri Vouyiouklis.

Thanks to those people at the MRC Human Genetics Unit, Harwell who made time and effort to provide information, encouragement and mice; Mr Colin Beechey, Dr Yvonne Boyd, Dr Bruce Cattanach, Mr Roland Quinney and Ms Carol Rasberry.

I am grateful to the staff at the MRC Human Genetics Unit, Edinburgh, for letting me loose in their laboratory for a week; in particular, thanks to Mr Peter Budd and Dr Ian Jackson for all their subsequent help and advice.

Thanks to Allan May for photography and Prof Stuart Reid for statistical advice.

My thanks to the Wellcome trust for providing generous funding and fees during this period.

Finally I would like to thank George for his support and his unnerving ability to interpret my garbled scientific theorising.

1. Introduction

1.1 General introduction

The elaboration of the myelin sheath by the oligodendrocyte is one of the most complex and remarkable features of neural development. A vast amount of lipid must be produced by myelinating cells and a precise array of manifold proteins correctly inserted into the expanding membrane. The requirement for integration of these processes both in development and in subsequent maintenance of the myelin sheath is exemplified by inherited and acquired disorders of myelination. The failure of normal development or the ensuing loss of myelin lead to devastating neurological dysfunction and sometimes death of the organism. Mutant animals in which myelination in the central nervous system (CNS) is impaired provide one approach to the study of the normal process. The characterisation of the defect may shed light on the role of the normal protein in such processes as the division, maturation and survival of the oligodendrocyte. A major objective, however, is the identification and molecular cloning of the defective gene, to allow causal linkage between the gene product and the abnormal developmental process. Even then, the final conclusion may prove elusive, either because of complicated pleiotropic effects of the gene defect or functional redundancy in the system.

The goals of this project were the description of the phenotype of a novel myelin mutant mouse and the genetic mapping of the disease locus. An understanding of normal neural development, including the formation of the CNS, the developmental biology of the oligodendrocyte and the elaboration and biochemical structure of the myelin sheath, is a prerequisite for such a study. A description of these processes is therefore provided and a summary of other myelin mutants given. This is followed by an account of genetic mapping in the mouse.

1.2 Development in the central nervous system

The murine nervous system is evident at around day 7.5 of prenatal development as a thickened plate of ectoderm in the mid-dorsal region of the embryo. The plate invaginates to form the neural groove and then progressively closes, creating the neural tube (Figure 1, page 3). The broad cranial end of the tube develops three dilations destined to become the fore, mid and hindbrain whilst the narrower caudal part will constitute the spinal cord (Sadler, 1985).

Initially the neural tube consists of a single layer of germinal neuroepithelial cells. The subsequent mitotic activity of these cells gives rise first to progenitor neurons and then to glial progenitors which migrate out from the germinal zone. Ultimately,

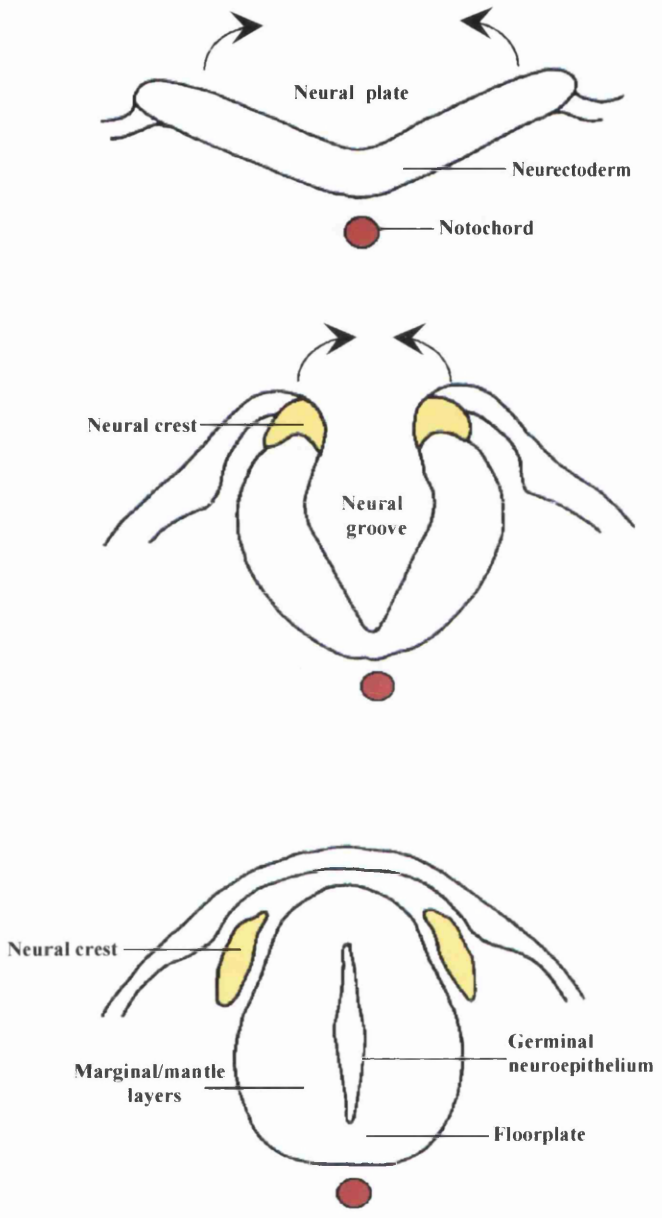

Figure 1: Development of the neural tube. The notochord can be identified lying ventral to the floorplate in the embryonic spinal cord.

when its proliferative function is exhausted, the germinal layer will form the ependymal lining of the ventricular system.

Neuronal development precedes that of glia with the exception of radial glia. For example, the formation of motor neurons in the ventral horns of the rat spinal cord occurs from embryonic day 11 (Nornes and Das, 1974) whereas the majority of oligodendrocytes appear postnatally (Warf *et al.*, 1991). As progenitor neurons, called neuroblasts, are generated, they migrate from the germinal layer to form a surrounding zone or mantle. The mantle will give rise to the grey matter of the spinal cord, the brain stem nuclei and the cerebral cortex. Axons that grow from the neuroblasts form the marginal layer, later to become the white matter of the brain and spinal cord. The scaffold for the developing CNS is provided by radial glia, a transient population of cells that subsequently disappears, perhaps by differentiating into another cell type (Choi *et al.*, 1983).

The neuroglia are divided into macroglia and microglia, with the macroglia being composed of astrocytes and oligodendrocytes. The macroglia develop from progenitor neuroepithelial cells in the late embryonic and early postnatal period of rodents, largely after the completion of neurogenesis. Although the precise genealogy of these cells is still poorly understood, it may be partly determined by the position of their precursors in relation to the notochord and floor plate. The notochord is a transient mesodermal structure located ventral to the developing neural tube (Placzek *et al.*, 1990) which ultimately gives rise to the nucleus pulposus of the intervertebral disc. Where the notochord is in contact with the neural tube, the floor plate develops as a midline specialisation of the neuroepithelium. Both appear to act as sources of signalling molecules in the embryo (Yamada *et al.*, 1991; Placzek, 1995), specifying the fate of ventral neuroepithelial cells. The other class of glial cell, the microglia, originates from a population of mononuclear leukocytes which penetrate the blood brain barrier in late foetal development (Ling and Wong, 1993).

Concurrent with early neural tube formation, paired columns of cells located at the dorsolateral margins of the neural tube separate to form the neural crests (Figure 1, page 3). Neural crest cells give rise to the neurons and glia of the peripheral nervous system (PNS), cells of the adrenal medulla and the melanocytes of the epidermis as well as contributing to craniofacial structures (Sadler, 1985).

Development in the CNS continues into the postnatal period. By the time of its completion, it will constitute the most complex organ in the body, containing many billions of neurons and some 10-50 times more glia. The huge cell numbers and

complexity of their arrangement mean that many features of neural development have yet to be elucidated.

1.3 Cells of the CNS

1.3.1 Oligodendrocytes

1.3.1.1 Introduction

The predominant function of the oligodendrocyte is the formation and maintenance of CNS myelin. In addition, perineuronal oligodendrocytes may serve to regulate the microenvironment around neurons and there is emerging evidence that oligodendrocytes have a role in axon growth and maintenance (Rubin *et al.*, 1994). Although first regarded as a relatively metabolically inactive cell with little capacity for reaction to injury, the oligodendrocyte is proving to be exceedingly varied with a complex developmental pattern, a wide range of proteins and lipids which are made in enormous quantities and a cell transport system to move these over considerable distances.

The origin, migration, proliferation and differentiation of neuroglia in the developing CNS are areas of intense study and some contention. Classical studies using ultrastructural analysis and autoradiography have shed some light on the development of these cells *in vivo* but cell lineages cannot be deduced from purely morphological evidence or from the sequential appearance of different cell types. In recent years investigation of oligodendrocyte development has been greatly facilitated by the availability of cell type-specific antibodies that can be used to identify progenitors, intermediate forms and terminally differentiated cells. Although much of this work has been performed *in vitro*, immunostaining and retroviral lineage tracing experiments suggest that a similar developmental progression does occur *in situ.* Some major discrepancies still exist, however, such as the *in vivo* existence of the type 2 astrocyte (see below).

1.3.1.2 Morphology and ultrastructure of the developing oligodendrocyte

The earliest classifications of oligodendrocytes date back to their description by the Spanish histologist Del Rio Hortega (Del Rio Hortega, 1921; Del Rio Hortega, 1922; Del Rio Hortega, 1924) using silver carbonate impregnation. Since that time, other techniques have confirmed and enlarged upon these findings (Friedman *et al.*, 1989; Butt and Ransom, 1989; Remahl and Hildebrand, 1990) but it is still unclear how the heterogeneous morphology of oligodendrocytes relates to function.

Del Rio Hortega grouped oligodendrocytes into four subtypes, which he numbered I through IV. Type I cells, the most abundant, possess a small cell body from which abundant fine processes emerge directed towards nerve fibres. These cells are found throughout the CNS. Type II have a larger soma and fewer, thicker processes and are found only in white matter. Type III cells, with three to four processes emanating from the cell body and directed towards axons, are localised in cerebral and cerebellar peduncles, the medulla oblongata and the spinal cord. Finally, type IV oligodendrocytes occur in association with large axons in the spinal cord and adhere to their fibre in a manner akin to the PNS Schwann cell. Several studies have since supported this classification (Stensaas and Stensaas, 1968; Remahl and Hildebrand, 1990).

Traditional *in situ* studies using microscopic examination and autoradiography have also classified oligodendrocytes, this time into three types according to their cytoplasmic density and extent of differentiation (Mori and Leblond, 1970). The relation between this and types I to IV is not clear. On EM examination, the light oligodendrocyte represents the most immature form, having a large pale cytoplasm and a light nucleus of 6 to 8.5μm diameter. This contains only slightly clumped chromatin and an obvious central nucleolus. Cytoplasmic organelles are abundant, particularly free ribosomes arranged as polysomes. The endoplasmic reticulum is scanty and usually not stacked and the Golgi apparatus consists of a few stacks of small saccules. Fine processes containing microtubules but no ribosomes and few mitochondria are characteristic.

These cells mature into medium oligodendrocytes with a smaller, denser nucleus of 4 to 7μm in diameter and less ample, darker cytoplasm. A few chromatin masses are apparent at the nuclear periphery and the nucleolus is less distinct. The rough endoplasmic reticulum tends to have longer, stacked cisternae and there are fewer free ribosomes. Golgi saccules are more prominent and distended. The fine processes now contain fewer microtubules.

Dark oligodendrocytes can be identified with the completion of myelination and full maturation of the cell. Cytoplasmic and nuclear volume are further reduced and there is rimming of the nuclear membrane by distinct clumps of chromatin. The typically dark, spherical nucleus has a diameter of 3.5 to 5.5μm with a small, paracentrally located nucleolus. The Golgi apparatus is usually perinuclear and has distended saccules. Stacks of long cisternae of rough endoplasmic reticulum often have a lumen and surround the Golgi apparatus. The remainder of the cytoplasm is filled with ribosomes and mitochondria in an electron-dense matrix. Lamellar

bodies can also be identified. Dark oligodendrocytes have only a few processes, usually of the same density as the cell cytoplasm.

Some of the criteria used to identify these types of oligodendrocytes can be applied to light microscopic examination of semi-thin resin sections (Mori and Leblond, 1970). The light oligodendrocyte has a large, pale, oval nucleus with few chromatin masses and a dark central nucleolus. The pale cytoplasm is voluminous and often distributed around the nucleus. As these cells mature into medium oligodendrocytes, the nucleus and cytoplasm stain more intensely. The smooth oval nucleus is now smaller and contains chromatin clumps around its periphery. The density of the cytoplasm may be equal to or darker than the nucleus. In dark oligodendrocytes, the nucleus is round or oval and very dark although occasional chromatin clumps can still be distinguished. The cytoplasm is even darker and now rather scanty, often being eccentrically located in relation to the nucleus.

1.3.1.3 Development of the oligodendrocyte lineage *in vitro*

Classical ultrastructural and autoradiographic studies were limited in their ability to demonstrate the progression of a cell along a particular lineage and relied on assumptions based on the sequential appearance of morphologically different cell types. The recent demonstration of cell type and stage-specific markers has opened up the study of many aspects of oligodendrocyte biology; the morphological development, the migration, proliferation and survival and the response to growth factors can all be examined and manipulated. This is more easily performed and therefore best characterised *in vitro*, usually using dissociated cultures of rat or mouse brain and rat optic nerve. A description of macroglial development in this system is given first and its application to the intact CNS discussed later.

In vitro studies have demonstrated three types of macroglial cells; type 1 astrocytes from an undefined precursor and type 2 astrocytes and oligodendrocytes from a common O-2A progenitor (Raff *et al.*, 1983; Miller *et al.*, 1985; Raff, 1989). The earliest precursor cells stain for the intermediate filament vimentin (Hardy and Reynolds, 1991; Gonye *et al.*, 1994) prior to differentiation into proliferative and migratory bipolar O-2A progenitors. These express gangliosides recognised by the antibodies against GD3 (Levi *et al.*, 1987) and the A2B5 antibody (Einsenbarth *et al.*, 1979) (Figure 2, page 9) and are bipotential in culture, generating either type 2 astrocytes or oligodendrocytes. The lineage selected depends on environmental signals (Raff *et al.*, 1983) but whether this bipotentiality is a feature of *in vivo* development is under debate (Fulton *et al.*, 1992). O-2A progenitors proliferate in response to a number of growth factors including insulin-like growth factor 1 (IGF-

1)(McMorris and Dubois-Dalcq, 1988), platelet derived growth factor (PDGF) and basic fibroblast growth factor (bFGF) (McKinnon *et al.*, 1990).

Vimentin and then A2B5 and GD3 staining are lost with progression along the oligodendrocyte lineage. Cells become multipolar, less migratory and lose their mitogenic response to PDGF (Gard and Pfeiffer, 1990; Warrington *et al.*, 1993) as they start to express the pre-oligodendrocyte antigen (POA) detected by O4/A007 (Bansal *et al.*, 1992b) (Figure 2, page 9). Cells at this stage may still be bipotential (Trotter and Schachner, 1989).

Later O4/A007 staining detects two sulphated glycolipids, sulphatide and seminolipid (Bansal *et al.*, 1989). This is followed by Ranscht monoclonal antibody (R-mAb) (Bansal and Pfeiffer, 1992a) which binds these two in conjunction with galactocerebroside (GalC). The onset of terminal differentiation and commitment to the oligodendrocyte lineage is characterised by a decline in proliferation, the appearance of O1 staining for GalC (Raff *et al.*, 1978) and the synthesis of 2', 3'-cyclic nucleotide 3'-phosphodiesterase (CNP). Continued maturation is marked by the regulated expression of terminal markers such as myelin basic protein (MBP), myelin associated glycoprotein (MAG), proteolipid protein (PLP), O10 and O11 and the elaboration of myelin membrane (Dubois-Dalcq *et al.*, 1986; Kuhlmann-Krieg *et al.*, 1988) (Figure 2, page 9).

O-2A progenitor cells have also been identified in adult as well as perinatal optic nerves (ffrench-Constant and Raff, 1986; Wolswijk and Noble, 1989). O-2A^{ADULT} progenitors have a different morphology, antigenic phenotype, cell cycle time, differentiation rate and migration rate from those in immature nerves (Wolswijk and Noble, 1989). They are thought to arise from a subset of perinatal O-2A progenitors and seem to have the capacity for self-renewal (Wren *et al.*, 1992).

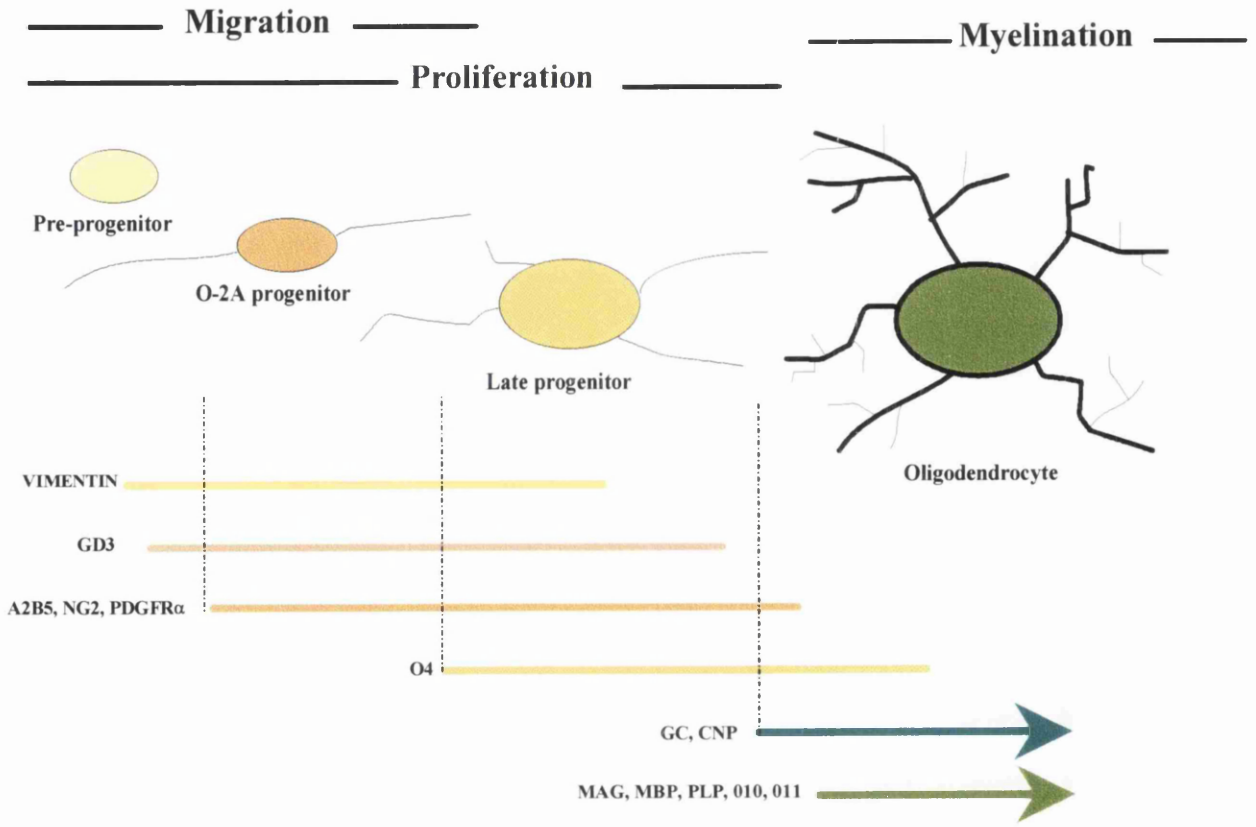

Figure 2: Antigenic and morphological development of O-2A progenitors *in vitro*. Migratory, proliferative and myelinating stages are indicated. The onset and loss of antigenic phenotypes are shown by the horizontal bars.

1.3.1.4 Comparison of *in vivo* and *in vitro* development

Although cell culture systems have facilitated characterisation and analysis of discrete populations of cells and modulation of their development by growth factors, these systems are inherently limited for several reasons. Cell culture lacks the framework of intact tissue and since many cellular interactions during development are dependent upon their position, they may not occur in culture. Furthermore, artifactual cellular processes may be produced instead. In contrast, a progenitor cell *in vivo* is exposed to a restricted sequence of signals in a local environment that is closely regulated temporally and spatially. This may lead to only one or a few developmental pathways being followed and hence the generation of a limited range of cell types from an individual precursor.

However, a major difficulty in the study of development *in vivo* has been the lack of definitive markers for distinguishing the different cell types and stages. Many markers useful in culture are not specific when applied to sections, for example A2B5 (Einsenbarth *et al.*, 1979) and GD3 (Wolswijk, 1995). A number of new markers appear to label cells in sections that correspond to the O-2A progenitor, such as NG2 glycoprotein (Levine *et al.*, 1993) and platelet-derived growth factor α receptor (PDGFRα) mRNA (Pringle *et al.*, 1992). Use of these markers combined with techniques such as retroviral tracing (Levison and Goldman, 1993b) suggests a pattern of development *in vivo* that is similar to that in culture but it has also highlighted important differences between the two systems. For example, there is still no definitive evidence for the *in vivo* bipotentiality of the O-2A progenitor or even the existence of type 2 astrocytes (Skoff, 1990; Fulton *et al.*, 1992). O-2A progenitors are therefore regarded as dedicated oligodendrocyte progenitors in normal development. Contradictory results have also been obtained when examining multipotentiality of early precursors *in vivo* and in culture; they are often multipotential in culture but appear committed to producing one cell type in the intact CNS (Luskin *et al.*, 1993; Levison *et al.*, 1993a).

Despite the caution with which *in vitro* results must be extrapolated to the *in vivo* situation, much of the information on oligodendrocyte biology has come from the former system and will doubtless continue to be central to its study.

1.3.1.5 Oligodendrocyte development *in vivo*

1.3.1.5.1 Origins of oligodendrocyte precursors

Ultimately the macroglia arise from the ventricular layer of the CNS. Two major questions posed relate to the precise locations in which the precursors are generated and whether they are multipotential at a late stage in the lineage. Early

morphological and immunocytochemical studies of the spinal cord resulted in several hypotheses to explain macroglial genealogy (Gilmore, 1971; Skoff *et al.*, 1976b; Choi *et al.*, 1983; Hirano and Goldman, 1988) but it is now generally accepted that oligodendrocytes initially arise in ventral subventricular regions of the neural tube from a specified precursor (Warf *et al.*, 1991; Noll and Miller, 1993; Pringle and Richardson, 1993; Ono *et al.*, 1995; Dickinson *et al.*, 1996). However, some recent studies have contradicted this (Williams and Price, 1995; Cameron-Curry and Le Douarin, 1995; Hardy and Friedrich, Jr., 1996) and the issue still requires resolution.

Several lines of evidence support the theory of a ventral origin of oligodendrocyte precursors. Indirect evidence is provided by the finding that ventral regions of the rat spinal cord develop the capacity for oligodendrogenesis *in vitro* prior to dorsal segments (Warf *et al.*, 1991). Also, labelled proliferating cell populations located in the ventral ventricular zone dorsal to the floorplate later appear to give rise to oligodendrocytes (Noll and Miller, 1993). Although early *in vivo* studies were hindered by the unreliability of markers in sections, the discovery of a number of new markers for putative O-2A progenitors has provided more direct evidence of their ventral origin. *In situ* hybridisation with a probe to *PDGFRα* mRNA (Pringle and Richardson, 1993), thought to be specific for oligodendrocyte precursors in the late embryonic rat CNS (Pringle *et al.*, 1992; Yu *et al.*, 1994) localises cells in the embryonic ventral spinal cord. Similar results have been obtained with a probe to mRNA for the myelin protein CNP. Immunolabelling with an antibody against PDGFRα (Hall *et al.*, 1996) and, in the chick, O4 antibody (Ono *et al.*, 1995) also identifies this ventral population. Under culture conditions, immunoselection with an antibody against PDGFRα confirms PDGFRα-labelled cells to be oligodendrocyte precursors whilst antibody-mediated complement lysis prevents the development of most oligodendrocytes (Hall *et al.*, 1996). *Dm20* mRNA and protein is also present in some oligodendrocyte precursors in the mouse (Timsit *et al.*, 1995; Dickinson *et al.*, 1996) but in the rat does not appear to colocalise with *PDGFRα* mRNA or *Cnp* mRNA although it does identify a population of cells in the ventral spinal cord. What is not clear is whether all oligodendrocyte precursors express detectable *PDFGRα* mRNA and whether *Dm20* mRNA expressing cells represent a separate subpopulation of precursors. In the brain, comparable localised sources of oligodendrocyte precursors have been identified in the ventral diencephalon using the same markers. These appear to migrate and populate more dorsal regions (Pringle *et al.*, 1992; Pringle and Richardson, 1993).

The notochord and floor plate appear to have an important regulatory role in the specification of the fates of ventral neuroepithelial cells. Signals from these have

been shown to induce the development of ventrally derived oligodendroglia (Pringle *et al.*, 1996). A strong candidate for the signalling molecule is the product of *Sonic hedgehog* (*Shh*), a vertebrate homologue of the *Drosophila* patterning gene *hedgehog (hh)* (Pringle *et al.*, 1996).

In contrast to studies indicating a ventral origin for oligodendrocyte precursors, others have produced evidence to the contrary. Chick-quail chimaeric transplant experiments seem to show the generation of oligodendrocytes all around the dorsoventral axis of the avian spinal cord (Cameron-Curry and Le Douarin, 1995). Studies involving the transplantation of labelled embryonic tissue indicate the development of oligodendrocytes from tissue obtained prior to the expression of *PDGFRα* mRNA (Hardy and Friedrich, Jr., 1996). It is suggested that *PDGFRα* mRNA expressing cells are not migrating dorsally but represent the temporal and spatial differentiation of earlier precursor cells already distributed throughout the neural tube (Hardy and Friedrich, Jr., 1996). In addition, retroviral experiments performed on cultures of rat cortical cells demonstrated oligodendrocyte clones from early embryonic tissue that contained no presumptive *PDGFRα*+ oligodendrocyte precursors (Williams and Price, 1995).

The question of the multipotential nature of early precursors has been studied largely using *in vivo* and culture retroviral technology and has yielded often contradictory results. In several studies, only one lineage was produced from a single clone (Luskin *et al.*, 1993; Luskin and McDermott, 1994) whereas others have shown various combinations of neural cell types being generated from a single precursor (Levison *et al.*, 1993a; Levison and Goldman, 1993b; Young and Levison, 1996). Generally, under culture conditions mixed clones are produced, whilst *in vivo* single clones produce only one cell type.

In summary, it seems likely that neuroepithelial cells throughout the entire neuraxis have the capacity to give rise to oligodendrocyte precursors during development but do so only in certain domains and at specified times. At what stages lineage restriction is operative and in which domains remains unclear, with different studies often giving contradictory results. The signals controlling the destiny of glial progenitors are largely unknown but probably involve factors inherent to the individual cell as well as extrinsic signals that are regulated both temporally and spatially.

1.3.1.5.2 Migration of oligodendrocyte precursors

Restricted induction of oligodendrocyte precursors necessitates the long range migration of cells to myelinate the CNS white matter. The nature of the migratory

cell and the signalling molecules have been investigated in culture and to some extent *in vivo*. Immature A2B5+ cells are significantly more motile than later O4+ cells *in vitro* (Small *et al.*, 1987) and migrate further in transplant studies (Warrington *et al.*, 1993). Little is known about the control of migration of these progenitors; in culture PDGF appears to promote migration (Armstrong *et al.*, 1990) as does bFGF (Milner *et al.*, 1997). Migratory roles for integrins which are expressed on oligodendrocyte precursors have also been suggested (Milner *et al.*, 1996). The *in vivo* migratory pathways and mechanisms are unknown.

1.3.1.5.3 Proliferation and differentiation of oligodendrocyte precursors

Once oligodendrocyte precursors have migrated into future white matter, their numbers must be matched to the number and length of axons requiring myelination. In addition, cells must be competent to myelinate fibres at the appropriate time. As oligodendrocytes are post-mitotic cells, their final number in a region will depend on the number of precursor cells that migrate into it, their proliferative capacity and the number of cells that undergo apoptosis (Barres *et al.*, 1992a). The subsequent differentiation into myelinating cells involves withdrawal from the cell cycle, the induction of myelin gene expression, formation of polarised cytoskeletal networks and transport pathways and the extension of cytoplasmic membrane. Co-ordinated control of proliferation and differentiation ensures the correct relationships between proficient myelinating cells and axons requiring sheaths. A number of mechanisms probably operate to regulate these processes, including the intrinsic properties of the precursor cells, extracellular signals from other cells and axon-oligodendrocyte interactions.

1.3.1.5.3.1 *Intrinsic properties controlling proliferation and differentiation*

Oligodendrocyte progenitors in culture continue to divide for a limited time only, even in the presence of mitogens. The progeny of an individual cell tend to cease dividing at around the same time, suggesting that an intrinsic clock mechanism is operating (Temple and Raff, 1986). It is thought this mechanism may consist of two elements, a counting component measuring the number of divisions and an effector part allowing differentiation. The latter component is dependent on signal transduction pathways involving hormones such as thyroid hormone, glucocorticoids and retinoic acid (Barres *et al.*, 1994) and without these differentiation does not occur although proliferation ceases. However, in the absence of mitogens, precursor cells undergo premature differentiation even when not supplied with the effector signals. This suggests these signals are not actually

necessary for differentiation but act to trigger it once the counting mechanism has reached time (Barres *et al.*, 1994).

1.3.1.5.3.2 *Extrinsic control of proliferation and differentiation*

If oligodendrocyte progenitors are cultured in the absence of mitogens, they promptly cease dividing and differentiate into oligodendrocytes (Temple and Raff, 1985; Barres *et al.*, 1992b), indicating that extrinsic substances are required for proliferation. At least four peptide growth factors have been shown to stimulate progenitor division *in vitro* and their presence has been demonstrated in the developing CNS. One of the best characterised is PDGF, and it is the only one which has been shown to promote DNA synthesis on its own. It triggers several divisions of rat optic nerve progenitors before they differentiate, despite the continued presence of the growth factor (Noble *et al.*, 1988; Raff *et al.*, 1988).

Basic fibroblast growth factor (bFGF)(McKinnon *et al.*, 1990) also acts as a mitogen for O-2A cells. In contrast to PDGF, bFGF blocks differentiation into oligodendrocytes and maintains progenitors in a proliferative state. The combination of bFGF and PDGF causes O-2A progenitors to proliferate for long periods without differentiating, apparently over-riding the "intrinsic clock"(Bögler *et al.*, 1990).

Insulin-like growth factors I and II may stimulate the proliferation, differentiation and survival of O-2A progenitors (McMorris and Dubois-Dalcq, 1988). Neurotrophin-3 (Barres *et al.*, 1994b) also affects precursor proliferation. Although no one of these factors used singly can stimulate sustained proliferation of purified precursors *in vitro*, they can do so in combination (Barres *et al.*, 1994b). NT-3 has been shown to have a role in stimulating precursor proliferation in the intact developing optic nerve. Antibodies to this peptide given at a critical time result in reduced numbers of oligodendrocytes (Barres *et al.*, 1994b).

The sources of these mitogenic substances *in vivo* is still uncertain although astrocytes and neurons are both likely candidates. Astrocyte cultures secrete factors that stimulate oligodendrocyte progenitor proliferation *in vitro* (Raff *et al.*, 1985) and produce all these four peptides (Noble and Murray, 1984; Temple and Raff, 1986; Pringle *et al.*, 1989). Neurons have been shown to produce PDGF *in vivo* (Yeh *et al.*, 1991; Ellison *et al.*, 1996) and could serve as another source of this mitogen.

As mentioned above, extrinsic factors likely to have influences on proliferation and differentiation of oligodendrocyte precursors include thyroid and steroid hormones and retinoic acid (Barres *et al.*, 1994).

Many signal transduction cascades using various second messenger systems are likely to be involved in the conveyance of extracellular signals across the oligodendrocyte cell membrane during development. Much still remains to be learned about these systems, but one of the best studied aspects to date is the role of the second messenger 3',5'-cyclic AMP (cAMP). The schedule of oligodendrocyte differentiation and the rate of progenitor cell proliferation *in vitro* are both modulated by cAMP. With increased levels of cAMP, differentiation is accelerated whereas proliferation is inhibited (Raible and McMorris, 1993). These appear to be independent events since the inhibitory effect of cAMP on proliferation is abolished by maximal levels of PDGF, while the stimulatory effect on differentiation remains (Raible and McMorris, 1993). The extracellular ligands that alter cAMP levels in developing oligodendrocytes and the cell type(s) that release those ligands are not yet known.

1.3.1.5.3.3 *Axonal control of oligodendrocyte proliferation*

Since oligodendrocyte numbers must be sufficient to myelinate the number and length of axons requiring sheaths, axons are likely to have a role in regulating precursor proliferation and survival. This appears to be the case *in vivo* as transection of the optic nerve results in a dramatic reduction in the number of mitotic precursors (Barres and Raff, 1993). This occurs even without axonal degeneration, inferring that electrical activity in axons is a requisite. It is suggested that electrical activity normally controls the production and/or release of mitogens and support for this comes from studies using tetrodotoxin, a blocker of voltage regulated sodium channels. Tetrodoxin has an inhibitory effect on precursor proliferation which is countered by the addition of PDGF, an oligodendrocyte precursor mitogen (Barres and Raff, 1993). Whether PDGF is normally released directly from axons or indirectly from astrocytes is unclear. An axonal role in the control of differentiation has also been suggested. It appears that axonal contact is necessary for the transformation of a premyelinating oligodendrocyte into a myelinating cell (Trapp *et al.*, 1997).

1.3.1.5.3.4 *Autocrine control of proliferation*

As well as being limited by an intrinsic clock mechanism and the absolute levels of growth factors and hormones, precursor proliferation may be altered by feedback

from cells of the same lineage. *In vitro* studies demonstrate the inhibition of precursor proliferation by cells of the same type at high plating densities. This appears to mediated either through contact or unidentified local-acting diffusible substances (Zhang and Miller, 1996). Transforming growth factor-β, produced by oligodendrocytes in culture, has a longer range of effect and also inhibits precursor proliferation (McKinnon *et al.*, 1993). On the other hand, differentiation is hastened by the presence of TGFβ (McKinnon *et al.*, 1993).

1.3.1.5.4 Survival of oligodendrocyte precursors

Oligodendrocyte numbers are not only dependent on the proliferative capacity of immigrant precursors but also on the survival of these and differentiated cells. At least 50% of the oligodendrocytes produced in the optic nerve will die within a few days of development (Barres *et al.*, 1992a), apparently undergoing apoptosis. Several factors affect survival rate, including growth factors from other cells and the presence of axons (Trapp *et al.*, 1997).

1.3.1.5.4.1 *Role of growth factors in survival*

Purified oligodendrocytes, or their precursors, rapidly undergo apoptosis if cultured in the absence of other cells or exogenous signalling molecules (Barres *et al.*, 1992a). Several such molecules have been shown to be survival factors, some with differing effects on the various developmental stages. *In vitro,* IGF-1 is a potent survival factor for both mature oligodendrocytes and their progenitors whereas PDGF only supports survival of progenitors and early oligodendrocytes (Barres *et al.*, 1992a). Increasing PDGF levels in the optic nerve through transplantation of secreting cells reduces cell death by about 80% (Barres *et al.*, 1992a), leading to a doubling of oligodendrocyte numbers with no change in astrocytes. This infers that normal oligodendrocyte death is caused by competition for limited trophic factors. Other factors that enhance oligodendrocyte survival *in vitro* include NT-3 (Barres *et al.*, 1994b), ciliary neurotrophic factor (CNTF) (Barres and Raff, 1993; Barres *et al.*, 1993), leukaemia inhibitory factor (LIF) (Barres and Raff, 1993) and interleukin-6 (IL6) (Barres and Raff, 1993; Barres *et al.*, 1993).

Optic nerve astrocytes produce PDGF, IGF-1, NT-3 and CNTF and therefore seem likely to have a part in supporting the survival of the oligodendrocyte lineage. However, axons also have a role to play.

1.3.1.5.4.2 *Axonal control of survival*

Axons appear to promote survival of oligodendrocyte precursors but by a different mechanism to that stimulating proliferation. Transection of the optic nerve followed by axonal degeneration results in oligodendrocyte death which can be prevented by elevating levels of IGF-1 or CNTF (Barres *et al.*, 1993). However, without axonal degeneration there is no death and nor does cell death result if tetrodotoxin is used to silence axons. Thus the ability of axons to promote survival is not dependent on electrical activity whereas stimulation of proliferation requires functionally active axons. Purified neurons, but not neuron conditioned medium, increase survival of purified oligodendrocytes *in vitro* (Barres and Raff, 1994a), which is again suggestive of an axonal role in the survival of these cells.

Eventually the elaborately interwoven processes of migration, proliferation and cell survival will culminate in a sufficient number of competent myelinating cells. This involves a huge increase in oligodendrocyte cell numbers that occurs largely in the postnatal period. It has been estimated that in the rat brain, the number of progenitors expands from about 5×10^5 at birth to a terminal population of 60×10^6 mature oligodendrocytes in adults (Pfeiffer *et al.*, 1993). Perturbation at any stage of this development may presumably lead to a deficit in cell numbers and, if this is severe enough, consequent hypomyelination.

1.3.2 Astrocytes

Approximately 50% of the glial cell population in the brain consists of astrocytes which are up to ten times more numerous than neurons in the mammalian CNS. Astrocytes constitute a heterogeneous class of cells in terms of structural and functional properties. Morphologically they are process-bearing stellate cells with a pale cytoplasm and a pale oval nucleus. Traditionally they are split into protoplasmic and fibrous types based on their morphology and distribution, with fibrous dominating in white matter and protoplasmic astrocytes largely in grey matter (Peters *et al.*, 1976). A second classification of astrocytes divides them into type 1 and type 2, thought to develop from different progenitors and proposed to be analogous to protoplasmic and fibrous classes respectively (Miller and Raff, 1984; Miller *et al.*, 1985). The progenitor cell for type 1 astrocytes is believed to be committed to this lineage, whereas the type 2 cell is thought to derive from the bipotential 0-2A cell although there is still much controversy regarding this. The most distinctive ultrastructural feature of astrocytes is the presence of intermediate filaments filling the cytoplasm. The major component of these is glial fibrillary acid protein (GFAP) which is relatively specific for astrocytes in the CNS and employed as an astrocyte marker (Bignami *et al.*, 1972). Organelles such as mitochondria,

endoplasmic reticulum and Golgi apparatus are sparse in mature astrocytes. Glycogen particles, dense inclusion bodies and fatty droplets are identified in the cytoplasm. Major astrocytic functions include guidance during neuronal migration in development, maintenance of the neural microenvironment and modulation of the immune response.

1.3.3 Microglia

This is the least frequent of the three classes of glial cells (Ling and Leblond, 1973). The outline of microglia is often irregular as the cells conform to the contours of the surrounding neuropil. The nucleus is electron-dense with large clumps of chromatin and the cytoplasm is light to moderate-staining, darker than astrocytes but less dense than oligodendrocytes. It contains no microtubules or filaments but includes dense core vesicles and large amounts of closely packed cisternae of the Golgi apparatus (Skoff *et al.*, 1976a; Skoff, 1990). It is considered to be a mobile phagocytic mesodermal cell that is activated in various pathological conditions (Perry and Gordon, 1988).

1.4 Formation and morphology of the myelin sheath

A major function of the mature oligodendrocyte is the production of vast amounts of membranous extension, the myelin sheath. The membrane forms multilamellar sheaths around neuronal axons, resulting in axons with high resistance and low capacitance. This dramatically increases nerve conduction velocities and reduces energy and space utilisation. At the onset of myelination, a newly differentiated oligodendrocyte gives rise to long, slender processes which associate with the surfaces of scattered axons. Each process elongates to form a cup around the axonal segment and then, with one lip insinuating under the other, spirally wraps this segment. Wrapping may occur in a clockwise or anticlockwise direction (Skoff *et al.*, 1980) and initally the layers remain separated by an extracellular space called the mesaxon. As further layers are added, compaction of the membrane occurs (Peters *et al.*, 1976). The major dense line (MDL) results from the extrusion of cytoplasm from the myelinating process and the fusion of the cytoplasmic surfaces. The intraperiod line (IPL) forms as the mesaxon compacts by the apposition of the extracellular membrane faces. In the spinal and cerebral white matter of the cat this transition from a simple cytoplasmic sheath to compact myelin occurs after formation of no more than 3 lamellae (Remahl and Hildebrand, 1990). When mature, the sheath will contain cytoplasm only within the inner and outer loops of the spiralling process and in connecting channels. Deposition of myelin starts at several discrete sites along the entire length of an axon (Skoff *et al.*, 1980) with internodes extending towards one another until only a small gap, the node of Ranvier, separates adjacent internodes. Some of the early short cytoplasmic sheaths will be eliminated as there is insufficient axonal space for them all to elongate (Remahl and Hildebrand, 1990). This conforms with the idea that some glial units shift from a polyaxonal to a monoaxonal relation before formation of compact myelin (Remahl and Hildebrand, 1990).

Axons in the CNS become myelinated within a diameter range of 0.2-0.8μm, with large diameter fibres acquiring a sheath first. The oligodendrocytes responsible for this form at an early developmental stage and produce just one or a few internodes (Remahl and Hildebrand, 1990). Cells destined to enwrap small axons appear later in development and produce up to 40 sheaths. The diameter range within which axons undergo primary ensheathment differs for prospective large and small CNS axons. Large axons must reach a greater diameter before ensheathment; as development proceeds and small fibres become myelinated, so the minimum diameter required decreases (Matthews and Duncan, 1971). There is, however,

considerable overlap in diameter ranges for unmyelinated, ensheathed and myelinated fibres at any one stage (Remahl and Hildebrand, 1982).

Both the radial and longitudinal dimensions of the mature myelin sheath are coupled to axon diameter (Murray and Blakemore, 1980; Friede and Bischhausen, 1982) although the precise relation varies between regions of the CNS and the species. The family of axons/sheaths related to an individual oligodendrocyte appears to be relatively uniform in terms of axon diameter and sheath thickness (Remahl and Hildebrand, 1990). Differences in the biochemical composition of thick and thin sheaths (Hartman *et al.*, 1982) make it unlikely that an individual oligodendrocyte would be capable of supporting sheaths of various sizes. It is unknown whether oligodendrocyte heterogeneity in terms of cell morphology, number of sheaths produced and the dimensions and structure of these is intrinsic or related to local factors such as axonal contact. Transplantation studies suggest the latter; optic nerve oligodendrocytes, which usually myelinate only small diameter axons, are capable of producing sheaths for much larger fibres in the spinal cord (Fanarraga *et al.*, 1997).

Eventually the majority of CNS axons, unlike those of the PNS, will acquire a myelin sheath (Remahl and Hildebrand, 1982). The fibres that remain unmyelinated are small diameter although the size spectra of myelinated and unmyelinated axons overlap considerably (Remahl and Hildebrand, 1982; Hildebrand and Waxman, 1984).

1.5 Myelinogenesis

The onset and completion of myelination varies between species and within different areas of the nervous system but several general trends exist. Myelination of the peripheral nervous system always precedes that of the CNS; in laboratory rodents this is by a period of several days. Within the CNS, the spinal cord myelinates before the brain (Langworthy, 1928; Langworthy, 1933; Fox *et al.*, 1967; Schwab and Schnell, 1989). The cervical spinal cord is the first area in which myelinated axons are detected prior to their appearance more caudally in the cord and rostrally in the hindbrain. Within the cord, there is a set pattern of myelination of tracts at any one level, with the ventral columns being myelinated first, followed by the cuneate, ventrolateral, gracile, rubrospinal and finally the corticospinal tracts (Langworthy, 1933; Matthews and Duncan, 1971; Baron *et al.*, 1993). In the brain, myelination spreads from the medulla to the pons, midbrain and then the telencephalon. Optic nerve myelination begins at several sites along the nerve and progresses in a general rostral to caudal direction from retina to the chiasm (Black *et al.*, 1982; Hildebrand and Waxman, 1984; Remahl and Hildebrand, 1990; Colello *et al.*, 1995). The time scale varies between species but in the rat, myelin sheaths can first be demonstrated in the ventral columns just before birth at E19, in the optic nerve by P6 but not until P12 in the corpus callosum (Bjartmar *et al.*, 1994). Myelination in this species is largely completed by 2 months of age.

Although these general statements can be made, the process of myelination is remarkably complex. There appear to be waves of rapid myelination (Ionasescu *et al.*, 1993) preceded by periods of oligodendrocyte proliferation (Matthews and Duncan, 1971; Skoff *et al.*, 1976a; Skoff *et al.*, 1976b) and rates of progression vary such that one system may be surpassed by another, later-starting, group (Ionasescu *et al.*, 1993). In individual early fibres, there may be a chaotic mixture of naked portions, portions invested by cytoplasmic sheaths, mixed uncompacted and compacted sheaths and compact myelin sheaths (Skoff *et al.*, 1980). Nodes may or may not be established. Apparently the move from a completely unmyelinated to myelinated state is gradual and non-uniform.

1.6 Molecular biology of the myelin sheath

1.6.1 Lipids

Lipids constitute about 70% of the dry weight of myelin and account for its insulating property but there is no known myelin-specific lipid. One distinguishing feature is a high content of the sphingolipids, galactocerebroside and sulphatide, which together account for about 65% of total lipid (Norton and Cammer, 1984). Galactocerebroside is restricted almost exclusively to myelin and oligodendrocytes and is used as an oligodendrocyte marker (Raff *et al.*, 1978). Myelin is also enriched in cholesterol and ethanolamine phosphoglycerides.

1.6.2 Proteins

The genes specific to myelination can be grouped according to their roles. Their protein products may be involved in the induction of myelination, in the contact and initial ensheathment of target axons or in the formation and compaction of the sheath. This last task requires structural myelin proteins as well as transport and assembly proteins. Although genes have been isolated in each of these categories, most progress has been made in terms of characterisation of the abundantly expressed genes of compact myelin and the axon-glial adhesion molecules.

1.6.2.1 Proteolipid protein (PLP)

Proteolipid protein (PLP) is the major integral membrane protein of myelin in the CNS and together with its isoform DM20, comprises 50% of the myelin protein mass (Nave and Milner, 1989). The gene is located on the X chromosome (Willard and Riordan, 1985) and contains 7 exons within 17kb. The open reading frame encodes for the PLP isoform of 276 amino acids. DM20 is generated by the use of an alternative splice site in exon 3 with deletion of exon 3B from the mature transcript. Consequently DM20 protein lacks 35 residues (amino acids 116 to 150) but is otherwise identical to PLP (Macklin *et al.*, 1987). Remarkable conservation of the gene across species is found with complete homology between man and mouse at the amino acid level. Sequence similarities with other molecules such as the neuron-specific M6 has led to the suggestion of the existence of a PLP/DM20 gene family (Yan *et al.*, 1993).

Both *Plp* and *Dm20* mRNAs are developmentally regulated, with *Plp* mRNA expression detected postnatally in the mouse CNS (Timsit *et al.*, 1992) where its levels parallel myelination. *Dm20* mRNA has been detected earlier in the developing CNS, prior to myelination (Timsit *et al.*, 1992; Yu *et al.*, 1994; Dickinson *et al.*, 1996). The ratio of PLP/DM20 changes during myelination with

DM20 as the major protein isoform prior to and during early myelination and PLP predominating in the adult (Van Dorsselaer *et al.*, 1987). The gene is also expressed at a lower level in Schwann cells but the products are barely detectable in PNS myelin (Puckett *et al.*, 1987). *Dm20* mRNA has also been localised in non-nervous tissue such as cardiac muscle and spleen (Campagnoni *et al.*, 1992).

Plp and *Dm20* mRNAs are translated on membrane bound ribosomes and undergo vesicular transport through the Golgi apparatus and on to the plasma membrane. Insertion into the membrane depends on correct association with lipids (Pasquini *et al.*, 1989) and in some cell lines also requires suitable proportions of DM20 and PLP (Sinoway *et al.*, 1994). PLP is a hydrophobic membrane protein consisting of a 276-residue polypeptide chain with four hydrophobic domains linked by highly charged hydrophilic regions. Several models for the membrane orientation of the proteins exist (Popot *et al.*, 1991; Weimbs and Stoffel, 1992) although most recent studies suggest that both the N- and C-termini lie on the cytoplasmic surface and the two loop regions of PLP are exposed to the extracellular surface (Weimbs and Stoffel, 1992; Gow *et al.*, 1997). The sequence deleted in DM20 is relatively hydrophilic and is likely to lie on the cytoplasmic side of the membrane.

The functions of PLP and DM20 are not known and there are a number of hypotheses, largely based on abnormalities seen in mutants. The abundance of PLP in the adult CNS, its localisation to compact myelin and the abnormal periodicity seen in the PLP-deficient mutants suggests a structural role in maintaining the closely apposed double intraperiod line (Duncan *et al.*, 1987). The strong conservation of the protein's primary sequence has led to the suggestion that PLP/DM20 are involved in either homotypic or heterotypic protein-protein interactions within the membrane (Helynck *et al.*, 1983; Sinoway *et al.*, 1994). Further evidence for a role in membrane adhesion comes from the accumulation of proteolipids at cell-cell interfaces in some cotransfected cells (Sinoway *et al.*, 1994). Possibly the proteolipids assemble into complexes in myelin, forming pores with adhesive properties between adjacent myelin lamellae (Sinoway *et al.*, 1994).

DM20 is present prior to PLP and not correlated with myelination, is distributed in central and peripheral glia (Griffiths *et al.*, 1995) and achieves higher levels than PLP in the least severe PLP mutants. These features have led to the proposition of a role in glial cell development for this isoform.

1.6.2.2 Myelin basic protein (MBP)

MBP refers to a group of small positively charged molecules, specific to myelin, that are derived by alternative patterns of mRNA splicing. MBPs are abundant in

compacted myelin (30-40% by mass in the CNS, 10-20% in PNS) in which they are membrane associated, presumably by electrostatic interactions with the negatively charged phosphate groups of the lipid bilayer. They are thought to be important in maintaining the fusion of the major dense line in the compact myelin sheath. The *Mbp* gene lies on mouse chromosome 18 and comprises 7 exons spanning 32 kb (Takahashi *et al.*, 1985). At least 6 isoforms, ranging in size from 14kDa to 21kDa, differ by the presence or absence of internal peptides which are encoded by exons 2, 5 and 6 (de Ferra *et al.*, 1985). A functional difference between the various MBP isoforms is not known but the evidence that the exon-2-containing proteins (17 kDa, 21kDa) appear earlier in development (Carson *et al.*, 1983) and are targeted to the nucleus at this time (Pedraza *et al.*, 1997) has led to the suggestion that they may subserve a regulatory function in implementing the myelination programme (Pedraza *et al.*, 1997). Once oligodendrocytes have differentiated into fully myelinating cells, however, *Mbp* mRNAs are selectively transported to intracellular regions where myelin compaction is occurring (Trapp *et al.*, 1987; Verity and Campagnoni, 1988). This spatial segregation of mRNA occurs in association with microtubules (Ainger *et al.*, 1993; Bassell and Singer, 1997) and presumably functions to target these reactive proteins precisely to myelin, preventing adhesion via electrostatic interaction to inappropriate intracellular components.

More recently it was shown that the organisation of the *Mbp* gene is even more complex. The *Mbp* transcripts active in myelinating cells (including the glial cell specific promoter) are contained within a larger gene, the gene-of-oligodendrocyte-lineage (*Golli-mbp*) (Pribyl *et al.*, 1993). This gene includes 5 additional exons and generates, by alternative RNA splicing, several MBP-related polypeptides, the functions of which are still unknown. *Golli-mbp* transcripts are expressed with a different developmental time course from myelin *Mbp* mRNA in glial cells. It is conceivable that the myelin-specific *Mbp* gene has evolved as a secondary transcription unit by acquisition of an intragenic transcription start site, thereby recruiting MBP as a novel structural protein.

1.6.2.3 Myelin-associated oligodendrocytic basic protein (MOBP)

MOBP, a recently characterised myelin protein specific to the CNS, appears to be a relatively abundant myelin component (Yamamoto *et al.*, 1994; Montague *et al.*, 1997). The protein shares several characteristics with MBP, being small, hydrophilic, basic and localised within compact myelin. Several isoforms, generated by alternative splicing, show different developmental expressions and associations with microtubules and the karyoplasm (Montague *et al.*, 1997). The late developmental expression of some of the isoforms and their localisation to

compact myelin suggest that MOBP acts at a late stage of myelin formation, perhaps in myelin compaction and sheath maintenance (Holz *et al.*, 1996). The *Mobp* gene maps to chromosome 9 in the mouse (McCallion *et al.*, 1996).

1.6.2.4 2', 3'-cyclic nucleotide 3'-phosphodiesterase (CNP)

CNP represents about 5% of the total CNS myelin protein and consists of two peptides with apparent molecular weights of 46kD and 48kD (Sprinkle *et al.*, 1978). Two genetic loci have been reported on mouse chromosomes 3 and 11 (Bernier *et al.*, 1988) but the locus on chromosome 11 appears to contain all the DNA sequences necessary to encode the alternatively spliced *Cnp* mRNAs (Monoh *et al.*, 1989; Kurihara *et al.*, 1990; Thompson, 1992). It is not yet clear whether the locus on chromosome 3 gives rise to *Cnp* mRNAs, perhaps in different tissues, or if it is a pseudogene. The gene on chromosome 11 is about 6kb in length and contains 4 exons. Two transcription sites are utilised, at the beginning of the first (exon 0) and second (exon 1) exons, that appear to give rise to the two mRNAs. The mRNA produced from the upstream transcription site is the smaller one (2.4kb) because the first exon splices into the interior of the second (Kurihara *et al.*, 1990). The additional splicing event adds 60 base pairs of coding sequence (Kurihara *et al.*, 1990; Thompson, 1992), resulting in the longer protein product. The larger protein, CNP2, is therefore identical to CNP1 except for an additional 20 amino acids at its N-terminus (Bernier *et al.*, 1987). CNP1 is generated from the longer mRNA of 2.8kb.

In the CNS, CNP is unique to oligodendrocytes. It is also found in the PNS in lower abundance and in a number of non-neural tissues at very low levels of activity. In the adult CNS, it is localised in the plasma membrane and processes, and in cytoplasm-containing compartments of the myelin sheath but is excluded from compact myelin (Trapp *et al.*, 1988). Embryonic expression in oligodendrocyte precursors has been reported *in vivo* (Yu *et al.*, 1994; Scherer *et al.*, 1994), and specifically *Cnp2* mRNA expression has been described in oligodendrocyte precursors *in vitro* (Scherer *et al.*, 1994). At the time of oligodendrocyte differentiation, both mRNAs are induced (Scherer *et al.*, 1994). The functional significance of the enzymatic activity displayed by CNP remains to be elucidated but since it appears to be the first myelin-related protein detected during development, it may have a crucial role in the early stages of myelination (Trapp, 1990). As well as possessing membrane-association properties, CNP binds to the actin-based cytoskeleton (Gillespie *et al.*, 1989; De Angelis and Braun, 1996) and it has been suggested that it may have a role in signal transduction cascades (Thompson, 1992). Isoprenylation of the protein at its C-terminal may have a role in

CNP function since transfection studies have shown that only isoprenlyated protein causes cells to extend filopodia and processes (De Angelis and Braun, 1994). Isoprenylation does not affect the ability of the protein to interact with the cytoskeleton (De Angelis and Braun, 1996).

1.6.2.5 Myelin associated glycoprotein (MAG)

MAG, a minor component of myelin, constitutes about 1% of CNS myelin protein. It is an integral membrane glycoprotein with an amino terminal extracellular domain, a single transmembrane region and a cytoplasmic carboxy terminal domain. The extracellular domain can be divided into 5 regions with structural features similar to immunoglobulin domains and MAG is therefore considered to be a member of the immununoglobulin gene superfamily (Salzer and Colman, 1989). The protein localises to the periaxonal regions in the CNS but is excluded from compact myelin (Trapp *et al.*, 1989), and it has been suggested that it is involved in contact between the myelin forming cell and the axon (Owens *et al.*, 1990; Trapp, 1990; Quarles *et al.*, 1992). The two isoforms, L-MAG and S-MAG, are generated by alternative splicing (Salzer *et al.*, 1987) of a single gene on mouse chromosome 7 and differ only in their C-termini. Their apparent molecular weights are 72 and 67kDa respectively before glycosylation, and 100kDa when glycosylated (Owens *et al.*, 1990; Quarles *et al.*, 1992). L-MAG is prominent during early CNS myelination whereas both forms are present in nearly equal amounts in mature CNS myelin (Trapp, 1990). Phosphorylation of L-MAG occurs on the cytoplasmic domain (Edwards *et al.*, 1989; Afar *et al.*, 1990; Bambrick and Braun, 1991) and may be related to the differential expression and possibly a different function from S-MAG. It has been proposed that the interaction of L-MAG with its ligand generates a signal involving activation of Fyn tyrosine kinase (Fyn) at the the beginning of myelination (Umemori *et al.*, 1994). Fyn apparently acts downstream of L-MAG as a signalling molecule, and indeed, *fyn*-knockout mice show impaired myelination (Umemori *et al.*, 1994).

1.6.2.6 Minor CNS proteins

Several other CNS myelin proteins have been documented including myelin/oligodendrocyte glycoprotein (MOG) (Linington *et al.*, 1984), mapping to chromosome 17, myelin oligodendrocyte specific protein (MOSP) (Dyer *et al.*, 1991), oligodendrocyte-myelin glycoprotein (OMgp) (Mikol *et al.*, 1993), myelin and lymphocyte protein (MAL) (Magyar *et al.*, 1997) and oligodendrocyte specific protein (OSP) which maps to chromosome 3 (Bronstein *et al.*, 1996). The functional significance of these proteins is not yet known.

1.7 Review of CNS myelin mutants

1.7.1 Introduction

Myelin mutants have contributed greatly to our understanding of the assembly and maintenance of the myelin sheath and its functional importance in the nervous system. A diverse group of spontaneous mutants in several species has recently been joined by engineered genetic variants characterised by defects of myelin formation. Both structural and regulatory genes may be altered, shedding light on the normal function of the gene through correlation with the resultant phenotype. Unfortunately, however, the pathogenesis of disease does not often appear as simple as lack of a functional protein. As well as yielding functional information, mutants may also be models for human neurological diseases or may act as recipients for glial cell transplantation studies. Most of the mutations involve genes encoding structural myelin proteins. Other genes encoding transcription factors, proteins for signal-transduction, enzymes of lipid metabolism, and cytoskeletal elements are as important as structural myelin proteins for myelin formation, but little genetic information is currently available. Although many of the spontaneous mutations still remain uncharacterised, the major developments in gene mapping and cloning make their future definition a real possibility. This will hopefully allow further access to the complex processes involved in the formation of the myelin sheath.

1.7.2 shiverer and myelin-deficient

The spontaneous shiverer *(Mbp^{shi})* mutant was the first myelin mutant characterised at the molecular-genetic level, arising from the deletion of exons 3-7 of the *Mbp* gene on chromosome 18 (Roach *et al.*, 1983; Roach *et al.*, 1985). Homozygous mice are unable to synthesise any of the MBP isoforms and thus provide a model system in which to investigate myelination in the complete absence of these proteins. Animals develop a generalised body tremor during the third postnatal week and adults suffer from tonic seizures, with most dying before 6 months of age (Chernoff, 1981).

Hypomyelination is most apparent in the CNS where axons are surrounded by very thin sheaths or remain naked (Rosenbluth, 1980; Carson *et al.*, 1983). Myelin compaction is variable and the intracellular surfaces of two myelin membranes frequently remain separated (Privat *et al.*, 1979). This absence of the major dense line suggests a role for MBP in its formation. However, occasional sheaths do demonstrate a MDL so it may be that other proteins can also contribute to this structure (Rosenbluth, 1980).

In contrast, PNS myelin shows very little alteration, with normal periodicity and only subtle alterations in thickness (Panagopoulos *et al.*, 1989; Gould *et al.*, 1995). The double mutant P_0-/MBP- confirms the suggestion that P_0 substitutes for MBP in the formation of the PNS major dense line (Martini *et al.*, 1995).

Transgenic complementation of *Mbp*^{shi} mice with a wild-type *Mbp* gene results in a partial phenotypic rescue (Readhead *et al.*, 1987) with restoration of the MDL, confirming the putative role of the protein in myelin compaction. The amount of myelin produced is gradually restored by increasing levels of MBP in mutant animals, which indicates that MBP synthesis is a rate-limiting step of myelin assembly (Readhead *et al.*, 1987; Popko *et al.*, 1987). Intriguingly, shiverer mice crossed with *Plp-/-* knock-out mice show amelioration of the phenotype and have a normal lifespan. They also produce more myelin than shiverer mice, although the myelin periodicity is abnormal (Stoffel *et al.*, 1997).

Allelic to shiverer is the mutant myelin deficient (*Mbp*$^{shi\text{-}mld}$), in which there is duplication of the entire *Mbp* gene and an inversion of the duplicated region between exon 2 and the 3′ end (Okano *et al.*, 1988). This results in the formation of endogenous antisense RNA (Tosic *et al.*, 1990; Fremeau, Jr. and Popko, 1990) which interferes with *Mbp* mRNA. The phenotype is slightly milder (Popko *et al.*, 1988), presumably because a small amount of residual MBP is incorporated into the myelin sheath.

1.7.3 quaking

The murine mutation quaking (*qk*) is inherited as an autosomal recessive trait. Homozygous mice show hypomyelination of the CNS and a less marked deficit in the PNS. Tonic seizures occur in these animals although they have a normal lifespan. Affected females breed normally but affected males are sterile. Oligodendrocyte density is increased and there are often vacuoles in the cytoplasm suggestive of defective incorporation (Greenfield *et al.*, 1977) and degradation of myelin proteins (Watanabe and Bingle, 1972). This mutation is associated with a deletion on chromosome 17 (Ebersole *et al.*, 1992). Initial characterisation of the locus indicates that several protein isoforms are produced, some abundant in brain, lung, heart and testis (Ebersole *et al.*, 1996). The gene product is predicted to have both signal-transducing and RNA-binding properties, perhaps having a role in the regulation of myelin gene expression (Ebersole *et al.*, 1996).

1.7.4 *Plp* mutants

The largest group of known myelin mutations involves the *Plp* gene and is inherited in an X-linked manner. The normal myelination process is impaired in these mutants, leading to severe neurological dysfunction and, in most cases, early death of the animal. Mutations occur in several species including mouse, man, rat, dog and pig and in some, several allelic forms are present. The majority of the mutations across the species are point mutations within the coding region, leading to amino acid substitutions (Gow *et al.*, 1994). The gene appears intolerant of any change so that even conservative substitutions result in gross phenotypic changes.

1.7.4.1 Plp^{jp}

The CNS of Plp^{jp} mice shows a severe reduction of myelin and a high rate of oligodendrocyte cell death. The resulting lack of mature oligodendrocytes is accompanied by an increase in the numbers of mitotic precursors (Skoff, 1982; Knapp *et al.*, 1986) which show an abnormal cell cycle (Knapp and Skoff, 1987). A small percentage of oligodendrocytes escape cell death and differentiate to a myelin-producing stage. Their myelin shows slightly reduced spacing of the intraperiod line, suggesting that PLP is not required for extracellular membrane adhesion but may act as a strut-like spacer (Duncan *et al.*, 1989). An astrocytosis is present and defects in astrocyte cell cycle and metabolism are reported (Knapp and Skoff, 1993).

The cellular mechanisms underlying oligodendrocyte death have not been determined. The two common hypotheses are the lack of a functional protein or the gain of a toxic function due to structural misfolding of the altered protein. There is evidence to support both theories. For example, knock-out and transgenic studies suggest that cell death is not due to a simple absence of PLP/DM20. Transgenic Plp^{jp}/Y mice are not successfully "rescued" (Nadon *et al.*, 1994; Schneider *et al.*, 1995) whilst knock-out mice deficient in both isoforms do not develop the lethal phenotype associated with *Plp* mutations (Boison and Stoffel, 1994; Boison *et al.*, 1995; Klugmann *et al.*, 1997). Conversely, evidence against a "toxic" theory includes the prolonged survival of Plp^{jp} oligodendrocytes when transplanted into shiverer tissue (Lachapelle, 1995) and their increased lifespan *in vitro* when cultured in astrocyte conditioned medium (Knapp *et al.*, 1996). If it is the case that loss of oligodendrocytes is due to abnormal conformations or toxic effects of mutant proteins, it is not clear whether this is a non-specific cytotoxicity or interference with a specific glial protein function. Arrest of transport of abnormal PLP/DM20 through the ER and secretory pathways may be involved (Gow *et al.*, 1994). Unexpectedly, transgenic mice over-expressing *Plp* and *Dm20* have been found to

develop a phenotype similar to *Plp*^{jp} (Readhead *et al.*, 1994; Kagawa *et al.*, 1994), indicating that myelination is very sensitive to any alteration in *Plp* gene dosage.

1.7.4.2 *Plp*$^{jp\text{-}rsh}$

The viable *Plp*$^{jp\text{-}rsh}$ mouse, characterised by a single amino acid substitution (isoleucine^{186} →threonine) in exon 4, differs from most other *Plp* mutants in that it shows dysmyelination associated with a normal complement of oligodendrocytes and little cell death (Schneider *et al.*, 1992). Also, affected males and homozygous females show normal fecundity and lifespan (Fanarraga *et al.*, 1991). Seizures are not a feature and the hindlimb tremor reduces with time (Griffiths *et al.*, 1990). Heterozygous females appear clinically normal.

Hypomyelination of the CNS is present but the deficit is not as severe as in other *Plp* mutants such as *Plp*^{jp}, the *md rat* or *sh pup*. Differences are identified between the pattern of myelination in the spinal cord and the optic nerve (Fanarraga *et al.*, 1992) such that many optic nerve axons remain unmyelinated whilst myelination continues to progress in the cord. Eventually many of the smaller spinal cord axons acquire almost normal myelin sheaths although larger ones remain hypomyelinated. Well-compacted sheaths of normal periodicity are not uncommon (Griffiths *et al.*, 1990). PLP protein levels are severely decreased but the amount of the DM20 isoprotein is normal (Mitchell *et al.*, 1992) and myelin sheaths stain intensely with antibodies recognising both isoproteins. A unique characteristic of *Plp*$^{jp\text{-}rsh}$ with respect to other *Plp* mutants is the presence of normal, or even increased, oligodendrocyte numbers at the time of myelination (Fanarraga *et al.*, 1992). Also, death of oligodendrocytes does not appear to be a major feature of this mutation (Griffiths *et al.*, 1990). This is intriguing in that it uncouples the two major phenotypic characteristics of *Plp* mutants, hypomyelination and cell death, and suggests a connection between DM20 and glial cell development and survival.

1.7.4.3 Other *Plp* mutants

1.7.4.3.1 *Plp*$^{jp\text{-}4j}$ and *Plp*$^{jp\text{-}msd}$

A new murine mutant, with a single nucleotide substitution in exon 2 of the *Plp* gene, has been identified and termed *Plp*$^{jp\text{-}4j}$ (Billings-Gagliardi *et al.*, 1995). Affected animals show a tremor, seizures and death before weaning. The number of myelin sheaths is even fewer than in *Plp*^{jp}, glial cell counts are increased and dead cells are prominent. *Plp*$^{jp\text{-}msd}$ is a lethal allele defined by the conservative

substitition alanine^{242}→valine in the last transmembrane domain of the PLP/DM20 (Gencic and Hudson, 1990; Macklin *et al.*, 1991).

1.7.4.3.2 Rat, dog, rabbit, pig and man

Other mutations in the *Plp* gene include the myelin deficient rat (*md-rat*) (Boison and Stoffel, 1989), shaking pup (*sh-pup*) (Nadon *et al.*, 1990), paralytic tremor rabbit (*pt*), type AIII Landrace pig (Blakemore *et al.*, 1974a) and Pelizaeus Merzbacher disease (PMD) and forms of spastic paraplegia in man (Seitelberger, 1995). Although there are differences in severity and age of onset between species and allelic forms, the general phenotype of the *Plp* mutants is similar with hypomyelination, generalised tremors, seizures and early death, prior to adulthood, in hemizygous males. The degree of hypomyelination varies, being very severe in the *md-rat* (Duncan *et al.*, 1987), for example, and less marked in the *sh-pup* (Griffiths *et al.*, 1981). Less severely hypomyelinated mutants, such as $Plp^{jp\text{-}rsh}$ and *sh pup*, tend to have longer lifespans. Any myelin which is formed is usually disproportionately thin, poorly compacted and fails to stain for PLP protein (Duncan *et al.*, 1987). Mitotic rates of immature glia are increased and in some mutants, oligodendrocytes show marked distension of the rough endoplasmic reticulum (Gow *et al.*, 1994). This swelling may indicate a failure of normal transport of proteins from the RER to the Golgi, perhaps due to abnormal protein folding. An astrocytosis is a common feature (Knapp and Skoff, 1993) and is most severe in the mutants with least myelin. Physiological abnormalities such as an increased pH have been seen in cultured mutant astrocytes (Knapp *et al.*, 1993). Microglia are increased, especially at the time of maximum oligodendrocyte death (Knapp *et al.*, 1993).

Female heterozygotes show a variable phenotype but the extent of hypomyelination is always considerably less than the 50% predicted by random X-inactivation (Duncan *et al.*, 1986; Duncan *et al.*, 1993). This suggests that there is either preferential inactivation of the mutant allele or increased survival of those cells with a wild type allele

1.7.4.4 Uncharacterised CNS dysmyelinating mutants

With advances in gene mapping and cloning being extended to other species, the possibility of cloning genes on the basis of mutant phenotypes is becoming more likely. Some of the myelin mutants will reveal novel genes or those with a previously unrecognised function in myelination. Several examples are given here although this is not exhaustive.

The taiep (tremor, ataxia, immobility, epilepsy, paralysis) rat is a CNS hypomyelinating and demyelinating mutation inherited in an autosomal recessive fashion. A unique feature is massive accumulations of microtubules in oligodendrocytes (Duncan *et al.*, 1992) so this mutation may offer insights into the role of the cytoskeleton in myelination. Another rat, the zitter rat (Kondo *et al.*, 1991; Kondo *et al.*, 1992), shows pronounced hypomyelination in the spinal cord and accumulation of abnormal membranous structures in oligodendrocytes, in conjunction with distension of the RER, perinuclear structures and Golgi apparatus. These changes may indicate a defect in membrane biosynthesis.

Two strains of Syrian hamsters have been reported with a hypomyelinating disorder of the CNS, inherited as an autosomal recessive trait. In the first strain (Nunoya *et al.*, 1985) there is persistence of the tremor throughout life, but the second shows recovery by 100 days (Kunishita *et al.*, 1986). The myelin, although reduced in amount, appears structurally normal and no qualitative or quantitative oligodendrocyte abnormalities were found (Nunoya *et al.*, 1985).

Two breeds of dog, the Chow Chow and Weimaraner, show an unusual distribution of CNS hypomyelination. Both conditions are autosomal recessive traits (Kornegay *et al.*, 1987; Lunn *et al.*, 1995) although it is not known if the same gene is involved in each. The hypomyelination, most marked in young dogs, involves mainly the peripheral margins of the spinal cord white matter and shows some recovery with age (Lunn *et al.*, 1995). The brains are only mildly affected. The susceptibility of the periphery of the spinal cord white matter may relate to the migration of oligodendrocyte precursors and the pattern of myelination.

Larger species may also suffer from CNS dysmyelination. For example, a dysmyelinating condition has been reported in Charolais cattle in which myelin compaction appears impaired, with hypertrophied tongues of oligodendrocyte cytoplasm surrounding axons at the paranodes (Palmer *et al.*, 1972; Blakemore *et al.*, 1974b).

1.7.4.5 Transgenic mice

As well as spontaneous mutants or those created in radiation/mutagenesis experiments, it is now possible to create mice with targeted null mutations or random transgene insertions for virtually any cloned gene. The phenotype resulting from complete loss of a gene can yield much information on the normal functioning of that gene. The over-expression of a particular protein can also shed light on its function as well as acting to "rescue" mutant phenotypes. The resultant phenotype of "knock-out" mice is often surprisingly mild, perhaps due to redundancy of

function of some genes. Several myelin genes have been studied in this way and some examples are given. This is not a comprehensive list, however, and new models are being created at a fast rate.

Null alleles have been created for several myelin genes including *Mag, Plp* and UDP-glucuronosyltransferase 8 (*Ugt8*). MAG-deficient mice are almost normally myelinated in the CNS and PNS with only subtle abnormalities of the periaxonal region and redundant myelin sheaths (Li *et al.*, 1994; Montag *et al.*, 1994). Targeted disruption of the *Plp/Dm20* gene results in surprisingly mild clinical signs and the production of large amounts of myelin, although this displays abnormal periodicity (Boison and Stoffel, 1994; Rosenbluth *et al.*, 1996; Klugmann *et al.*, 1997). Mice lacking UGT8 do not synthesise the major myelin glycolipids galactocerebroside and its sulfated derivative sulfatide, but instead substitute glucocerebroside into myelin. They form compact myelin with sheaths of virtually normal thickness but still exhibit severe generalised tremoring and mild ataxia. It seems likely that the compositional change in myelin lipids is responsible for the phenotype.

Transgenic *Plp* and *Cnp* mice with extra gene copies have also been created. Extra copies of *Cnp* lead to mild CNS hypomyelination, redundant myelin membrane with intramyelinic vacuoles and lack of cytoplasmic compaction. The oligodendrocytes appear to mature earlier in development, resulting in earlier maximum gene expression for *Mbp* and *Plp*, suggesting that CNP is an early regulator of cellular events leading to CNS myelination (Gravel *et al.*, 1996). Mice expressing *Plp* mRNA at only twice normal levels develop a dysmyelinating phenotype, demonstrating that the *Plp* gene is dosage sensitive (Readhead *et al.*, 1994; Kagawa *et al.*, 1994; Griffiths *et al.*, 1995).

1.8 Genetic mapping in the mouse

1.8.1 Introduction

Interest in mouse breeding began several hundred years ago when the Chinese and Japanese imperial courts were entertained by mice with unusual coat-colours or behaviour (Tokuda, 1935). Phenotypic variants continued to be of value to collectors throughout the centuries and in 1915, the genetic mapping of these mutants got underway with the reported linkage of two coat colour mutations, albino and pink-eyed dilution (Haldane *et al.*, 1915). Conceptually mouse mapping altered little until the 1970s and consisted primarily of linkage analysis of phenotypic deviants. This changed with the advent of recombinant DNA technology and the discoveries of polymorphic genetic markers (Botstein *et al.*, 1980) and interspecific crosses (Avner *et al.*, 1988) which gave tremendous impetus to the production of mouse genetic maps. Amongst mammalian species, the mouse genetic map is now the second most sophisticated and serves many functions, from studies on genome evolution to the analysis of disease models and complex traits that may be applicable to man. As the only species where it is possible to rapidly perform high resolution mapping, positional cloning and genetic engineering leading to targeted alterations, it is obvious that the mouse has no equivalent as a mammalian model.

1.8.2 Mouse taxonomy

1.8.2.1 Systematics of the *Mus* species

Since genetic mapping in the mouse often exploits allelic differences between strains and species of mice, an understanding of the taxonomy is vital to any mapping project. Mouse systematics are complex and as more information is gained, so the classification of and within species may alter. Currently, within the subgenus *Mus* there are nine species of mice including the house mouse *Mus musculus*, some of which can be bred to produce fertile hybrids (Figure 3, page 36). The house mouse is made up of four populations or subspecies, namely *M. musculus musculus*, *M. musculus domesticus*, *M. musculus castaneus* and *M. musculus bactrianus* (Bonhomme and Guenet, 1989). These groups can be distinguished morphologically and genetically and inhabit non-overlapping ranges but can interbreed readily. A question still remains about whether they are simply subspecies or in fact should be classified as separate species (Bonhomme and Guenet, 1989).

The three closest relatives of *Mus musculus* are the species *Mus spretus*, *Mus spicilegus* and *Mus macedonicus*. These do not breed with *Mus musculus* in the

wild although they can be induced to do so in the laboratory (Bonhomme *et al.*, 1984). The genetic divergence between the *Mus* species and subspecies, and their ability to interbreed with laboratory strains to produce fertile offspring have been exploited to great effect, playing an important role in the development of genetic maps. In particular, crosses between inbred laboratory strains and *Mus spretus* or *Mus musculus castaneus* have proved invaluable.

1.8.2.2 Origin of inbred laboratory strains

Mice that result from the process of at least 20 sequential brother-sister matings are considered to be inbred. There are now hundreds of inbred laboratory strains and substrains available to the researcher but the recent common ancestry of many of the traditional strains has limited their genetic diversity. Their history dates back to the 19th century, when the house mouse became an object of fancy in Europe and many variant strains were imported, particularly from the Far East. By the beginning of this century, European and American fanciers were familiar with numerous phenotypically distinct lines (Morse, 1981). A critical connection between these mouse fanciers and early geneticists was Miss Abbie Lathrop, a retired schoolteacher in Massechussetts who began to breed mice for sale as pets in the early part of this century (Morse, 1978). She supplied the geneticists with a constant source of variant mice obtained from fanciers and many of the common inbred strains used today such as C57BL/6 and C57BL/10 are derived entirely from her mice. Their mixed origins mean that none of the traditional inbred strains are truly representative of any one *Mus musculus* subspecies, but it is suggested that the most prominent component of the mosaic is *Mus musculus domesticus* (Bonhomme *et al.*, 1987). Despite this multi-faceted origin, limited polymorphism exists between the strains due to their shared recent ancestry. In fact, all the classical inbred strains have been found to carry the same *domesticus* mitochondrial DNA derived from a single female (Ferris *et al.*, 1982; Ferris *et al.*, 1983) and many carry an indistinguishable *musculus* Y chromosome (Tucker *et al.*, 1992). The absence of sufficient interstrain variation has limited mapping using DNA polymorphisms and brought about the shift to interspecific and intersubspecific crosses (see Interspecific crosses, page 41). In this situation, inbred laboratory strains are bred with *Mus spretus* or *Mus musculus castaneus* to exploit the much larger genetic divergence and more frequent occurrence of DNA polymorphisms. However, the great variation in microsatellite markers, even between inbred strains, has reversed this somewhat, enabling the use of interstrain crosses for linkage analysis.

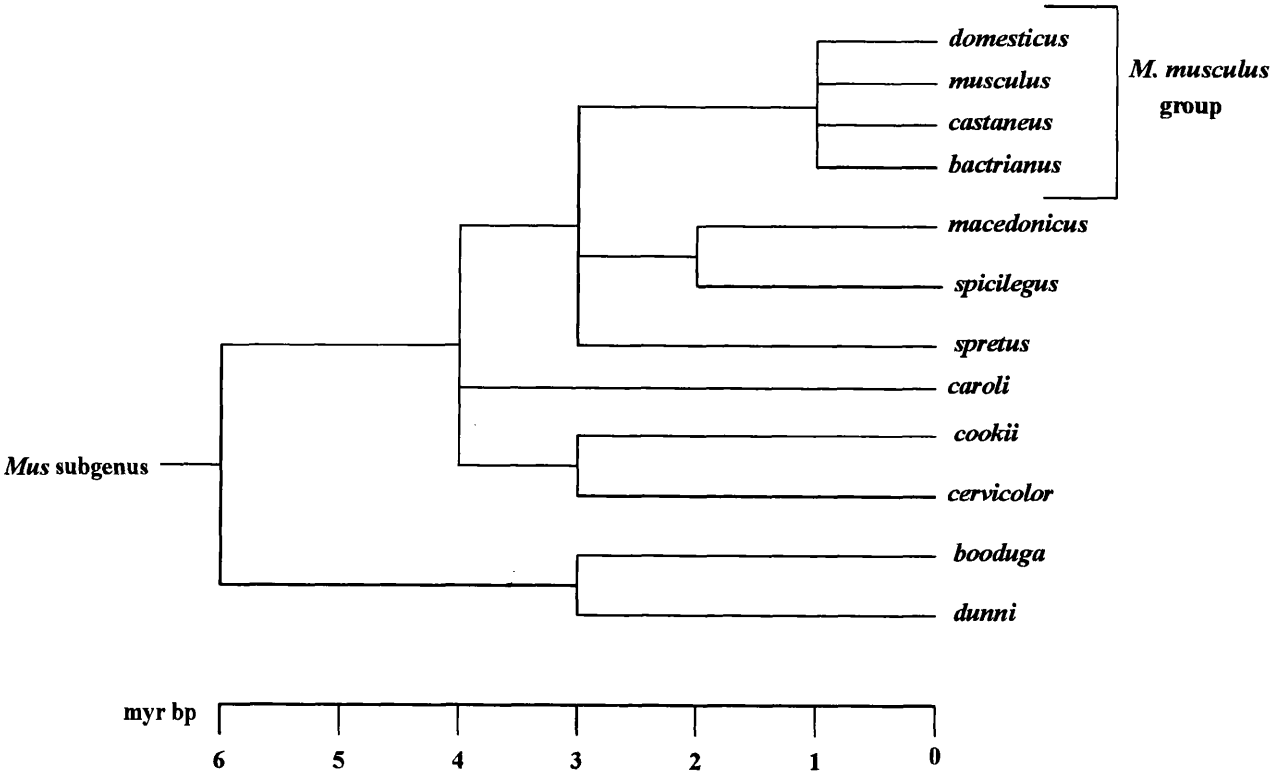

Figure 3: Systematics of the *Mus* subgenus. *Domesticus, musculus, castaneus* and *bactrianus* are all subspecies within the *M. musculus* group. Other lines represent well-defined species. The indicated times of divergence between subspecies are in millions of years before present (myr bp).

1.8.3 The mouse genome and mutant loci

The mouse genome represents a total haploid length of three billion base pairs spanning 20 chromosomes. Large genomic sequences have been conserved between mice and humans and it has been suggested that by simply breaking the mouse genome into about 180 pieces and re-ordering them, the human genome could be reproduced (Copeland *et al.*, 1993). Currently, about 2/3 of the mouse map is made up of such segments where both synteny and gene order have been conserved. At the time of writing, over 6000 microsatellites (see Microsatellite markers, page 40 for definition) and 5554 genes have been mapped in the mouse with 1900 genes common to both man and mouse.

There have been 958 deleterious murine mutations recorded, of which more than 700 have been localised on the genetic map. The spontaneous mutation rate in mice is about 5×10^{-6} to 10^{-5} for recessive alleles although some loci are highly mutable compared to others. About two thirds of mutations are in a previously unknown locus and one third define an already known locus. Variant mice carrying mutations provide a vital means of accessing the genome. With the recent technological advances in mapping, it should be possible to clone virtually any mouse mutation on the basis of its phenotype and its position in the genome. This should permit identification of the gene and the study of its protein product, its normal biological function and its role in disease states. The large number of conserved linkage groups also enables the identification of homologous human genetic disorders and the use of the mouse as a disease model.

1.8.4 Linkage mapping in the mouse

1.8.4.1 Types of genetic maps

A genetic map is a representation of the distribution of a set of loci within the genome. Mapping can be accomplished at many different levels of resolution and several types of maps exist. The linkage map was the first to be developed and can be constructed only for those loci that occur in two or more heritable alleles. Offspring are counted that receive either parental or recombinant allele combinations from a parent heterozygous at two or more loci. Linkage between loci can be determined and the relative distances between them calculated on the basis of recombination rates. Distances are measured in centimorgans (cM), where one centimorgan is equivalent to a recombination rate of 1%, ie. one in a hundred offspring has the non-parental combination of alleles. In the mouse, the genome is considered to be 1600cM in length.

The chromosome map is based on the number and banding pattern of mouse chromosomes and is defined by microscopic examination. Resolution is therefore not high compared to linkage and physical maps. Somatic cell hybrid analysis and *in situ* hybridisation, techniques used to develop chromosome maps, have been limited in their application to the mouse genome (see Historical perspectives of linkage mapping in the mouse, page 38) and mapping in this species has tended to rely on classical linkage analysis.

Physical maps involve the direct analysis of DNA and distances between loci are measured in base pairs. Eventually, the goal of the mouse genome project is the development of a complete physical map where the entire DNA sequence is known. In theory, linkage, chromosomal and physical maps should all provide the same information on chromosomal assignment and order of loci but in fact, the relative distances within each map can be quite different. Only the physical map provides an accurate measurement of the actual length of DNA between two loci. Chromosomal maps are modified according to the packing of DNA molecules in different chromosomal regions and linkage distances are influenced by the bias of different DNA regions to undergo recombination. Genetic maps tend to be a combination of all these map types although the greatest bulk of information comes from linkage analysis. Thus, the centimorgan is the genetic unit of measurement at present but it is likely that accumulation of physical mapping data will lead to the megabase becoming the established unit.

1.8.4.2 Historical perspectives of linkage mapping in the mouse

The mouse has appealed to geneticists for far longer than the relatively recent leaps in mapping technology. Early geneticists found the mouse attractive for the investigation of Mendel's laws of inheritance for several reasons. A short generation time, large litter sizes and an immediate post-partum oestrus permitted the breeding of large numbers of mice relatively quickly. The availability of inbred and wild-derived strains, the existence of naturally occurring variants and the ability to perform controlled matings meant that the inheritance of phenotypically obvious traits could be followed (Avner *et al.*, 1988; Côté *et al.*, 1994). Vaginal plugs allowing accurate identification of mating times, the male's tolerance of young offspring and the ease of handling were also advantageous. Despite these inherent advantages, studies in other species such as *Drosophila* and *Caenorhabditis* greatly overshadowed early mouse genetics. It took the recent discoveries of interspecific crosses (Avner *et al.*, 1988), new types of genetic markers (Botstein *et al.*, 1980) and large numbers of conserved regions between human and mouse genomes (Côté *et al.*, 1994) to move mouse genetics from backwater to forefront. It is now a vital

model for the Human Genome Project and substantial emphasis has been placed on the genetic and physical mapping of the mouse genome worldwide (Brown, 1992).

Early classical linkage mapping was founded on localising the genes responsible for phenotypic variants and until the 1980s, the vast majority of mapped loci were defined by mutations that had been painstakingly incorporated into the genome map. Progress was slow because it was technically difficult to arrange crosses in which more than a few visible markers were segregating. Each new mutation had to be bred into a strain with other phenotypic markers and then further breeding pursued to test for linkage to any of these other markers. This had to be repeated with different groups of phenotypic markers until linkage was established. Chromosomal mapping using *in situ* hybridisation and somatic cell hybrids, powerful tools in the mapping of human disorders, were less successful in the mouse. In the case of *in situ* hybridisation, this was due to the acrocentric nature of mouse chromosomes which makes it difficult to differentiate cytologically between individual chromosomes. Somatic cell hybrids carrying single mouse chromosomes, or chromosomes with deletions or translocations, were not as widely available in mouse genetics as in the human field (Copeland *et al.*, 1993). Also, it was usually possible in mice to find a variant that could be used for linkage mapping, obviating the need for other techniques.

Genetic mapping in the mouse was revolutionised by DNA cloning technology, the interspecific backcross and new DNA markers. Recombinant DNA techniques allowed the identification of numerous restriction fragment length polymorphisms (RFLPs) between strains of mice. RFLPs are DNA variations that affect the distance between restriction sites, usually as a result of a nucleotide change that creates or eliminates a site. The different fragment sizes generated after enzyme digestion can then be detected with labelled cloned probes on Southern blots. Theoretically, thousands of cloned loci could be mapped in a single cross. However, attempts to identify RFLPs between different inbred laboratory strains often met with limited success even after testing with large numbers of enzymes. In one study, RFLPs were identified at only 30% of the single copy loci tested with 22 different restriction enzymes (Knight and Dyson, 1990). The use of interspecific crosses overcame the limitations imposed by the low degree of allelic variation among traditional strains. RFLPs could be identified for nearly every cloned locus tested on the *spretus* backcross (LeRoy *et al.*, 1992). This breeding strategy was incredibly important because it provided the first complete linkage map of the mouse genome based on DNA markers and because it created mapping panels that

could be used to rapidly map essentially any new locus that was defined at the DNA level.

However, although the capacity to type RFLPs changed the face of genetics, it was not a panacea. Limitations included the difficulty in finding polymorphism in a cloned region, the often di-allelic nature of the polymorphism and the labour-intensive nature of typing large numbers of RFLP loci by Southern blotting. More recently, highly polymorphic microsatellite markers distinguishable by PCR have been developed which are technically easier and faster to map than RFLPs. There is no need for these loci to represent actual genes because their only purpose is to mark particular points along each chromosome, acting as anchor loci. Most new loci are now mapped in interspecific or intersubspecific crosses using microsatellite markers as positional anchors to establish linkage.

1.8.4.3 Microsatellite markers

Microsatellite markers, also termed simple sequence length polymorphisms (SSLPs), are now the most abundant class of marker on the mouse map. These are di-, tri- and tetranucleotide sequences repeated multiple times in series and were first developed as human genetic markers (Weber and May, 1989) before being applied to the mouse (Love *et al.*, 1990; Cornall *et al.*, 1991). The commonest microsatellites in the mouse genome are dinucleotide repeats, the most frequent being $(CA)_n$ which occurs in about 100,000 locations (Hamada *et al.*, 1982). Perfect microsatellites are those with a single uninterrupted repeat element whilst imperfect loci contain two or more runs of the same sequence broken up by short stretches of other sequences. Many microsatellites are imperfect and also a mixture of distinct runs of two or more different repeat units. The length of the repeat run varies among individuals in a species and between different inbred strains of mice, apparently due to slippage during replication with a mutation rate estimated to be around 10^{-4} per locus per generation (Dietrich *et al.*, 1992). Microsatellite markers can be easily typed by PCR using unique sequences on each side for primer production and show polymorphism rates of about 50% among inbred laboratory mouse strains (Dietrich *et al.*, 1992). The vast majority have been developed by the Whitehead Institute/Massachusetts Institute of Technology Centre for Genome Research (Copeland *et al.*, 1993), from which the term Mit, used in naming individual markers, is derived. Each marker has been analysed for polymorphism on a panel of 12 commonly used laboratory strains. At the time of writing, there are over 6500 microsatellite markers spread across the genome, allowing fine mapping to a very small interval.

1.8.4.4 Interspecific crosses

Until the mid 1980s, mouse gene assignment relied on two- or three-point crosses between laboratory strains or recombinant inbred strains. This was limited by the low degree of allelic variation among laboratory strains and as only a small number of genes were informative in each cross, a composite map could only be deduced indirectly. The introduction of the interspecific cross overcame this limitation, initially using *Mus spretus* and inbred laboratory strains to produce fertile F1 hybrid females (Avner *et al.*, 1988). The genetic divergence that exists between these two species is such that RFLPs can be identified for nearly every locus that is tested. There are, however, disadvantages in using *Mus spretus* as the wild mouse species in an interspecific cross, the main one being that the F1 males are infertile, thus preventing the study of male meiosis and slowing down the generation of sufficient backcross progeny. Also, the wide divergence may have permitted the accumulation of chromosomal inversions that could suppress recombination and hamper fine mapping (Hammer *et al.*, 1989). For these reasons, *Mus musculus castaneus* is often used instead and although more closely related, the degree of polymorphism is still high and both sexes of the F1 generation are fertile. With the advent of microsatellite markers, the need to use highly divergent mice in backcrosses has diminished and it is in fact possible, although more difficult, to map genes in crosses between laboratory strains.

1.8.4.5 Approach to mapping of a novel mutation

In mouse genetics, the search for a gene responsible for a mutant phenotype with an unknown basis begins with consideration of potentially related, previously characterised loci. These candidates may be genes in which mutations cause a similar phenotype or those suggested by biochemical or molecular analysis of the phenotype. If efforts to map the novel phenotype by association fail, it is necessary to move to a positional cloning exercise where the cloning of a gene is based solely on pinpointing its position in the genome (Collins, 1992; Collins, 1995). This is a two stage process that involves the identification of close flanking DNA markers followed by cloning across the region and characterisation of the mutated gene. For the first stage, a new mapping cross must be established in which DNA markers from across the genome can be tested for linkage. A detailed linkage map is accomplished by following the segregation of the mutant locus, defined by the phenotype, and the DNA markers, usually microsatellite markers. For recessive genes, an interspecific or intersubspecific backcross is utilised to generate the progeny for mapping. Markers that have been finely mapped and ordered via the backcross serve as a scaffold onto which overlapping clones from large insert genomic libraries can be positioned relative to each other and the mutant locus.

This set of contiguous clones covering the region of interest is termed a "contig". The generation of a contig is achieved by using the ends of previously obtained clones to rescreen the library in a technique known as "chromosome walking". A number of systems for generating large insert libraries have been described including, most importantly, the yeast artificial chromosome (YAC) (Kusumi *et al.*, 1993), but also the bacterial artificial chromosome (BAC) (Collins, 1995) and phage 1 (P1) (Pierce and Sternberg, 1992a; Pierce *et al.*, 1992b). Once clones covering the critical region have been obtained, the gene of interest must be identified apart from all other genes and non-genic sequences within this region.

However, to some extent, high resolution mapping can reduce the guesswork involved in the candidate gene approach and expedite the search since genes that recombine outwith a defined interval can be excluded. This combination of positional cloning and candidate gene identification (the "positional candidate" approach) is increasingly successful as the genetic map becomes ever denser, and will soon become the predominant approach to identification of a novel mutant locus (Collins, 1995).

1.8.5 Modifiers of spontaneous mutants

It has long been known that mouse mutants can show considerable variation in both penetrance and expressivity despite a common genotype. Incomplete penetrance describes the failure of some animals with a mutant genotype to express the associated mutant phenotype. Variable expressivity occurs when multiple individuals all express a particular trait but in a quantitatively distinguishable manner. Both phenomena may become apparent when the mutation is crossed onto different genetic backgrounds and are due to the influence of alleles at other non-disease (modifier) loci. For example, curly tail (*ct*), a murine model for human neural tube defects, shows incomplete penetrance and variable expressivity on several different backgrounds. The disease locus has been mapped to distal chromosome 4 and several strong candidates for modifier loci have been identified by backcrosses to recombinant and inbred strains (Neumann *et al.*, 1994; Letts *et al.*, 1995). It is likely that modifiers achieve alteration of the phenotype by suppressing or enhancing the expression of other involved genes. Several possible mechanisms have been suggested. They may alter transcription rates, mRNA stability or modify the degree of DNA methylation (Wilkins, 1990). Alternatively they may change the phenotype by increasing or decreasing the activity of a redundant gene as occurs with the mouse model for cystic fibrosis on the C57BL/6J background (Rozmahel, 1996). Exploring modifying genes is particularly attractive, allowing the identification of further genes involved in the pathophysiological pathway. They

may also provide an expanded array of potential therapeutic targets in complex and polygenic traits.

1.9 Aims of thesis

Myelination within the CNS depends on a successful series of interactions between oligodendrocytes and their target axons. Oligodendrocytes develop from precursors through a complex differentiation pathway, including proliferation and migration, under the influence of various growth factors, cell to cell interactions and soluble molecules. The regulation of this sequence of events is poorly understood. Natural myelin mutants provide one method of studying the processes involved; correlation of a particular phenotype with mutation in a specific gene may provide clues as to the normal function of that gene.

It was the aim of this study to evaluate a new myelin mutant mouse, hindshaker (*hsh*), in which there was CNS hypomyelination which gradually reduced with age. Initial studies had shown that the myelin deficit was most marked in the spinal cord and in mice up to two months of age. No obvious oligodendrocyte pathology had been observed. Preliminary immunostaining demonstrated the presence of major myelin proteins. The mutation was inherited in an autosomal recessive manner and linkage tests showed it was not an allele of quaking. The genetic and morphological studies therefore indicated that this was a novel mutation not involving a major structural gene but more probably affecting the biology of the oligodendrocytes. The postulated defect could have perturbed cell migration, proliferation, differentiation or the ability to elaborate membrane. The goals of the study were twofold. Firstly, the effect of the mutation on glial cell development and myelin formation was to be further evaluated using established histological and molecular techniques including morphometry, glial cell quantification, immunostaining and *in situ* hybridisation. The ability of oligodendrocytes to undergo differentiation *in vitro* was to be assessed with cell culture techniques. Secondly, genetic mapping of the mutant locus was to be carried out. Initial mapping using visible phenotypic markers was to be undertaken at Harwell to establish a chromosomal assignment. Fine mapping of the chromosomal locus with microsatellite markers and an interspecific backcross would be initiated as part of the project if this was successful. Evaluation of candidate genes using techniques such as immunostaining, Western blotting and *in situ* hybridisation would be undertaken as appropriate. Definition of the *hsh* phenotype and identification of the gene may provide new information on the complex process of myelination, defining the role of another critical factor in oligodendrocyte biology.

2. Materials and Methods

The details of the preparation of solutions etc, and of processing and staining techniques are given in the appendix. The page reference is provided as necessary.

2.1 Tissue fixation

2.1.1 Fixatives

2.1.1.1 Buffered neutral formaldehyde (BNF) (4%)

BNF was the fixative employed for tissues destined for paraffin-embedding (see Buffered neutral formaldehyde, 4% (BNF), page 213). Sections were cut for haematoxylin and eosin staining (H&E) and immunocytochemistry.

2.1.1.2 Strong fixative (paraformaldehyde/glutaraldehyde 4%/5%)

Tissues removed from mice perfused with "strong fix" were resin-embedded and sections used for light and electron microscopy and immunocytochemistry (see "Strong fix" (paraformaldehyde/glutaraldehyde 4%/5%), page 213).

2.1.1.3 Periodate-lysine-paraformaldehyde (PLP) fixative

This fixative was used for preservation of tissue to be stained with the macrophage specific F4/80 antibody (see Periodate-lysine-paraformaldehyde, page 213).

2.1.2 Fixation techniques

2.1.2.1 Intracardiac perfusion

2.1.2.1.1 Technique

All perfusions were performed in a fume hood. Mice were euthanased with either carbon dioxide or halothane overdose and then pinned in dorsal recumbency. Following creation of a thoracotomy site, the right auricle was identified and a nick made through the full thickness of its wall. A 23-27 gauge needle, depending on the size of animal, was placed through the wall of the left ventricle to lie within its lumen. After initial exsanguination by flushing with 0.85% sodium chloride (NaCl), perfusion was initiated with either BNF, strong fix or PLP fix. The amount of fixative required depended on the weight of the animal and varied from 10 to 120 ml; rigidity was used to assess fixation. In the case of BNF and strong fix, animals were then wrapped in fixative-soaked tissue and stored in containers at 4°C for 24 hours prior to dissection. Tissue not immediately processed following dissection was stored in the appropriate fixative at 4°C. Tissue perfused with PLP fix was dissected immediately and placed in the same fix for 4-6 hours before transfer to

20% sucrose in 0.1M phosphate buffer overnight. Blocks were then frozen in OTC as described (Cryopreservation and sectioning, page 47).

2.1.2.1.2 Dissection of tissue

Tissues were dissected using a low power microscope and microsurgical instruments. Skin and muscle overlying the head and dorsum was incised longitudinally and reflected to reveal the skull and spine. Starting rostrally, the calvarium was elevated with forceps, exposing the cerebral hemispheres and cerebellum. Individual vertebral arches were removed until the cord was visible; meninges and nerve roots were severed at this point, allowing elevation of the cord from the caudal end forward. The entire brain was freed by cutting the cranial nerves except for the optic nerves, which were sectioned only if required for resin-embedding. Other samples such as sciatic nerve were obtained by dissection of overlying skin and muscle and careful excision of the tissue.

2.2 Tissue processing and cutting

2.2.1 Paraffin processing and sectioning

Following their removal from mice perfused with BNF, whole brains and spinal cords were wrapped in filter paper, placed in processing biopsy cassettes and loaded in a basket of a Shandon Elliot automatic processor (Histokinette). Passage through dehydrating solutions and infiltration with wax (Paraffin wax processing, page 214) was followed by embedding in wax at 60°C. Paraffin sections for routine staining and immunostaining were cut at 6μm using a Biocut 2035 microtome (Leica) and left overnight in a 56°C oven to ensure adherence to the slide.

2.2.2 Resin processing and sectioning

Tissue required for resin embedding was obtained from mice which had been perfused with strong fix. Samples were processed using a Lynx microscopy tissue processor (Leica) (Resin processing, page 214) and placed in resin filled rubber moulds for polymerisation at 60°C overnight. Blocks were cut on a Reichert-Jung E ultratome at 1μm (thick sections) for light microscopy and 70 nm (thin sections) for electron microscopy. Thick sections were cut using a glass knife and those for immunostaining were placed on APES coated slides (see *In situ* hybridisation, page 60 for preparation). The 70 nm sections were cut with a diamond knife and mounted on 200 mesh-3.06 mm diameter copper grids.

2.2.3 Cryopreservation and sectioning

Cryopreservation was used for tissues destined for immunofluoresent immunocytochemistry, *in situ* hybridisation and F4/80 staining for microglia. Fresh tissue was dissected immediately following euthanasia and suspended in "Tissue-Tek" OCT compound (Miles Inc.) in small foil boats. These were held in isopentane cooled to below -70°C in liquid nitrogen until the OCT was completely frozen. The foil was rapidly removed, the frozen block wrapped twice in "Sealon film" (Fuji) to limit dehydration and stored at -20°C. Spinal cords from animals perfused with periodate-lysine-paraformaldehyde were also cryopreserved after cryoprotection in 20% sucrose. All sections were cut at 15μm using an OTF cryostat (Bright Instrument Company) and mounted on APES coated slides.

2.3 Staining techniques

2.3.1 Light microscopy

2.3.1.1 Haematoxylin and eosin stain for paraffin sections

Sections were routinely stained with H&E (Haematoxylin and eosin, page 216) to assess tissue quality and to give an overview of tissue morphology in various organs at the onset of the study. Counterstaining with haematoxylin alone for nuclear detail was carried on sections used for *in situ* hybridisation and F4/80 staining.

2.3.1.2 Methylene blue/azur II for resin sections

Resin sections for light microscopy were routinely stained with methylene blue/azur II (Methylene blue/azur II, page 218). Slides were heated on a hot plate to 60°C and flooded with stain for 10-30 secs followed by rinsing in running tap water. After drying overnight on the hot plate, they were mounted in DPX (BDH).

2.3.2 Electron microscopy

Thin sections of resin embedded tissue destined for EM examination were stained with uranyl acetate and lead citrate using standard techniques (Staining of tissues for electron microscopy, page 217).

2.4 Morphological studies

2.4.1 Quantification of glia

Quantification of glia was performed on 1μm resin sections of cervical cord (C2-C3) stained with methylene blue/azur II. Cells were counted within an area of the white matter adjacent to the ventromedian fissure and along the ventral aspect of the cord. A 6.3x eyepiece with a 100x oil immersion lens were used to visualise cells within a 100 square graticule (Graticules Ltd.). Four fields, 2 to each side of the fissure, were examined and the glial cell nuclei identified as oligodendrocytes, astrocytes, microglia or unclassifiable using morphological criteria. Endothelial cells were excluded. A second section, 12μm caudal to the first to ensure nuclei did not appear twice, was counted in a similar manner. A total of 400 to 600 cells, depending on age and status, were examined per animal.

The length of glial cell nuclei was measured in longitudinal thoracic cord sections using a calibrated eyepiece. Both astrocytes and oligodendrocytes were measured and the mean length of 30 nuclei was calculated. This figure was used in calculations of glial cell numbers and density.

Areas of whole spinal cord and spinal grey matter were calculated from Polaroid micrographs using Sigma Scan/Image measurement software (Jandel Scientific Software) and SummaSketch III graphics tablet (Summagraphics). Corrected total glial cell counts and densities were calculated using Abercrombie`s formula as discussed by Sturrock (Sturrock, 1983) and from these the specific glial cell numbers were estimated. Three to six animals of mutant and wild type genotype were counted at each age and the results were plotted using Graphpad Prism software (Graphpad Software Inc.).

2.4.2 Dead cell density

The dead cell density was estimated by counting pyknotic nuclei distributed throughout dorsal, lateral and ventral white matter of the same cord sections used for counting. Although the cell type cannot be ascertained, it is recognised that during development of the CNS a large proportion of such dead cells represent glial cells of which the majority are oligodendrocytes (Barres *et al.*, 1992b).

2.4.3 Myelin volume

Thin resin sections were obtained from the cervical spinal cord and optic nerves of at least three mutant and three wild type mice at several ages. These were photographed at approximately 5000 and 7500 times magnification for cord and

optic nerve respectively and printed at two times magnification. A diffraction grating with 2160 lines per mm was photographed at the same time for calibration.

Myelin volume was measured using a method described by Williams (1977). A ruled transparency with squares 2 cm by 2 cm was placed over each micrograph and intercepts coincident with either axon or myelin were recorded. At least ten to twelve photographs were counted for each area per animal. Results were expressed as a ratio of actual to possible contacts to give an arbitrary measure of myelin volume.

2.4.4 Morphometry

The same electron micrographs were used for morphometric analysis of a smaller range of ages. Using a graphics pad, about 150 myelinated fibres were outlined for each cord to generate the total areas of axon plus myelin and axon alone (software/hardware as above). In younger mutant mice, all myelinated axons were measured if this totalled fewer than 150. Results were used to derive diameters of circles with equivalent areas and the notional myelin thickness (Excel 5, Microsoft). The derived myelin thickness and equivalent axonal diameter allowed the calculation of the *g* ratio, which is defined as the ratio of axon diameter to that of the axon plus sheath.

Axon diameter ranges for both myelinated and unmyelinated fibres were calculated with the same software in younger mutant animals and compared to axonal diameters in normal mice.

2.4.5 Classification of fibre type

The spinal cord sections of 30 day old mutant animals were rephotographed at 7000 times magnification to permit easier identification of the stage of myelination. Fibres were then classified as unmyelinated, ensheathed or myelinated. At least one lamella of compacted myelin constituted a myelinated fibre. Percentages of each group were calculated for each animal.

2.4.6 Statistical analysis

In general, the results for experimental groups were demonstrated graphically by separate data points. In some cases, the small group size limited the applicability of complex statistical analyses but by presenting individual data points, general trends can be illustrated. Experimental groups with sufficient data points were compared using the non-parametric two tailed Mann-Whitney test. This ranks the data points and makes a statement on the significance of the mixing of the distributions of

ranked values from the two groups. Statistical significance was set at the 5% level ($P<0.05$). In some areas of the study, sample sizes were large enough for the illustration of the mean values for mutant and wild type animals.

2.5 Immunocytochemistry

2.5.1 Peroxidase-anti-peroxidase (PAP) immunostaining

2.5.1.1 Description of antibodies

The PAP technique was performed on paraffin and/or resin-embedded sections of spinal cord, brain, optic and sciatic nerves of mutant and wild type animals. Staining for PLP and MBP, the two major CNS myelin proteins, was used to examine their assembly into the myelin sheath and the degree of myelination. Anti-PLP 226 antiserum (Prof N.P. Groome, Oxford) was used at 1:600 with a goat-anti-rabbit link (1:10) and a rabbit PAP complex (1:400). Anti-MBP (Dr J.M. Matthieu, Lausanne) was used at 1:1000 (paraffin sections) and 1:750 (resin sections) with the same link and PAP complex as for PLP.

GFAP, an astrocyte-specific marker in the CNS, was used to investigate numbers of these cells as an astrocytosis is commonly observed in the spontaneous myelin mutants (Baumann *et al.*, 1986). GFAP was detected using a polyclonal antibody (1:750) from DAKO. The same link and PAP complex was used as above. Negative controls with the primary antibody omitted were included for each experiment. Non-specific immunoreactivity was never detected.

2.5.1.2 Technique

Paraffin-embedded sections were first passed through the following hydration solutions;

1. Xylene 2 min;
2. Absolute alcohol 2 min;
3. Methylene 2 min;
4. Water 2 min;
5. Iodine 1 min;
6. Water 2 min;
7. Sodium thiosulphate 1 min;
8. Water 2 min.

Resin embedded tissue was treated by immersion in sodium ethoxide solution for 30 min using a basket rotor, washing 6 times in absolute alcohol over a 30 min period and washing in running water for 30 min. Removal of resin was checked microscopically before proceeding to the wash stages.

Endogenous peroxidase activity was blocked by the submergence of the slides in a 3% hydrogen peroxide solution for 30 min. This was made up in absolute alcohol for paraffin sections and in water for resin sections. The slides were next washed in running water for 30 min. A 10% solution of normal goat serum made up in PBS was pipetted onto the sections to block non-specific binding sites. This was tapped off after 2 hrs and the slides dried around the sections with tissue. Primary antibodies were made in 1% normal goat serum/PBS and placed over the sections. These were incubated overnight at 4°C in a moisture chamber. Control sections had normal rabbit serum applied at the same dilutions as the test sections.

The following day, the slides were brought to room temperature over 30 min before being washed in PBS 6x. The secondary antibody was diluted to 1:10 with 1% normal goat serum/PBS and incubated with the sections for 1 hour. After washing 6x with PBS, the excess liquid was wiped off and sections were covered with PAP complex diluted with 1% normal goat serum/PBS. The slides were again washed 6x in PBS and then with 0.2M phosphate buffer for 2 min. A 100 ml solution of 3,4,3',4'-tetramino-biphenyl hydrochloride (DAB) was made with 50mg of DAB in 50 ml of distilled water, made up to 100ml with 0.1M phosphate buffer. 330µl of 30% aqueous hydrogen peroxide was added to the DAB solution and the sections placed in it until the required colour intensity had been achieved (30s to 5 min). Slides were then washed in 0.2M phosphate buffer for 2 min and running water for 5 min before counterstaining. Paraffin sections were counterstained with haemalum (Haematoxylin, page 216) whilst resin sections were immersed in 1% osmium/caccodylate buffer for 2 min before washing. All sections were then cleared and mounted in DPX.

2.5.2 Immunofluorescence

2.5.2.1 Description of antibodies

A number of oligodendrocyte-specific antibodies were tested on cryosections of cervical spinal cord of 10 and 20 day old mutant and wild type animals. This was both to examine the absolute presence of protein in the search for a candidate gene prior to molecular mapping, and/or to correlate levels of each protein in normal and mutant mice. Methods of fixation and antibody binding times varied but each was used as a single label and detected with a fluoroscein isothiocyanate (FITC) or

Texas Red (TXR)-labelled secondary. FITC absorbs light of wavelength 495nm and emits at 525nm and can therefore be visualised as green light using a blue filter. The Texas red labelled conjugate absorbs light at 596nm and emits at 620nm and can be viewed as red light with a green filter.

Primary antibody	Dilution	Source	Secondary
anti-MOG clone Y10	1:50	S. Piddledson	Goat-anti-mouse IgG1 FITC 1:80
anti-MAG 253	1:500	N. Groome (Oxford, UK)	Goat-anti-rabbit IgG FITC 1:80
anti-MOBP clone 32	1:80	N. Groome	Goat-anti-mouse IgG1 FITC 1:80
anti-CNP	1:300	Sigma	Goat-anti-mouse IgG1 FITC 1:80
anti-GFAP	1:1000	Dako	Goat-anti-rabbit IgG TXR 1:200

Table 1: Antibodies, secondaries, dilutions and sources used in immunofluorescence on cryosections. All secondaries were obtained from Southern Biotech.

2.5.2.2 Techniques

2.5.2.2.1 CNP, MOG, MAG and GFAP.

Sections were first thawed and dried before washing in PBS for 10 min. Those for MOG and CNP staining were fixed with 4% paraformaldehyde at room temperature for 20 min, washed in PBS for 5 min 3x and covered in primary antibody for 1 hour in a humidity chamber on the bench. MAG and GFAP sections were treated likewise but also received a 10 min fixation in methanol at -20°C after paraformaldehyde. The primaries were removed by washing 3x in PBS and secondary antibodies applied for about 30 min. Sections were washed in PBS for 5 min 3x, water for 5 min and then mounted in Citifluor antifade mountant (UKC Chem Lab). Negative controls with the primary omitted were run with each experiment.

2.5.2.2.2 MOBP

Cryosections to be stained for MOBP were fixed in 5% acetic acid/95% ethanol for 5 min at room temperature. After washing, the primary antibody was applied overnight at 4°C. The following day, sections were washed in PBS for 5 min 3x and covered in secondary antibody for 30 min. Washing and mounting were as described.

2.5.3 F4/80 immunocytochemistry

F4/80 staining for microglia was performed using the ABC technique (Vector Labs Ltd) on 15μm cryosections of spinal cord fixed in periodate-lysine-paraformaldehyde. The antibody binds to an unknown macrophage antigen and is used as a microglial-specific antibody in the CNS. Sections were allowed to air dry before washing in PBS for 10 min to remove embedding medium. All subsequent incubations were carried out in a humidity chamber and at room temperature. Firstly, sections were incubated with 1% normal rabbit serum for 30 min and then covered in F4/80 antibody (Serotec) at 1:20 in PBS for 1 hr after removal of excess serum. Two 10 min washes in PBS were followed by incubation in biotinylated rabbit anti-rat IgG (Vector Labs Ltd) at 1:100 in PBS. After two further washes, endogenous peroxidase activity was quenched by placing sections in 0.3% hydrogen peroxide in 96% alcohol for 20 min. Slides were again washed and then incubated for 45 min with Elite ABC, made up according to manufacturer's instructions. Post-washing, peroxidase was visualised with the chromagen 3'-3'-diaminobenzamine (DAB) by dissolving 125mg DAB in 250ml 0.1M phosphate buffer and adding 125μl 30% hydrogen peroxide just before use. The DAB reaction was intensified by incubation in 0.01% osmium tetroxide in 0.1M phosphate buffer for about 30 sec, followed by careful washing. Counterstaining with haematoxylin was performed (Haematoxylin, page 216) and slides mounted in DPX (BDH).

2.6 Preparation of DNA for riboprobe production

2.6.1 Core techniques

2.6.1.1 Nucleic acid electrophoresis

Electrophoresis of DNA was performed using 1-1.5% regular agarose gels of ultra pure electrophoresis grade agarose (Gibco BRL). Gels were cast by melting the agarose in the presence of 1x Tris acetate EDTA (TAE) buffer (see Tris acetate EDTA buffer x10, page 219) with a final concentration of 0.04M Tris acetate and 0.001M EDTA. Ethidium bromide (10mg/ml) was added after cooling of the agarose to 60°C, at a concentration of 0.5μg/ml. Samples were loaded with 6x TAE gel loading buffer (see Loading dye, page 219) and the gels then run in 1x TAE buffer. A "Fotoprep I" ultraviolet transilluminator (Fotodyne Inc) was used to view gels which were then photographed using a Polaroid MP4 land camera (Polaroid), a T2201 transilluminator (Sigma), a Wratten 22A filter (Kodak) and Polaroid 667 (ASA 3000) film.

2.6.1.2 Restriction enzymes

Restriction enzymes were supplied by Gibco BRL, Promega and New England Biolabs and used with the appropriate buffer according to manufacturer's instructions. Linearised vectors containing sequence for proteolipid protein (*PLP*) and UDP-glucuronosyltransferase 8 (*UGT8*) were generated by digesting the appropriate plasmid in the presence of suitable enzyme. Plasmid details are given in Figure 4, page 56 and the following digests performed;

Insert	Vector	Digest	Promoter	Probe
PLP	pGEM-4	*Eco*R I	T7	antisense
		Hind III	SP6	sense
UGT8	pGEM-3Z	*Eco*R I	SP6	antisense
		Hind III	T7	sense

Table 2: Restriction digests carried out to linearise vectors containing inserts. Sense probes were generated as negative controls.

10μg digests were usually performed for about 2 hours and a small aliquot run on a 1% gel to ensure complete digest. Samples were then stored at -20°C prior to probe production.

2.6.1.3 Ethanol precipitation

DNA was routinely precipitated in the presence of 0.3M sodium acetate pH5.2 and 3x ice cold ethanol. Amounts of less than 1μg were precipitated at -70°C overnight while larger amounts were precipitated at -20°C for not less than 2 hours. RNA probes were precipitated in the presence of 0.75M ammonium acetate. Samples were centrifuged at 4°C and 12000 rpm for 15-30 min to pellet the nucleic acid. After removal of the supernatant, the pellet was washed in 70% ethanol/sterile distilled water (SDW) for DNA or 75% ethanol/DEPC SDW (see *In situ* hybridisation, page 60 for preparation of DEPC/SDW) for RNA and air dried for 5-10 min. DNA was reconstituted in the appropriate amount of SDW and RNA in DEPC SDW.

2.6.1.4 Phenol:chloroform extraction

Removal of protein from samples containing nucleic acid was performed using phenol:chloroform:isoamyl alcohol in a ratio of 25:24:1. The combination of two organic solvents is more efficient than one used individually. An equal volume of phenol:chloroform was added to the nucleic acid sample, mixed thoroughly and centrifuged at 12000 rpm for 2 min. The aqueous phase, containing the nucleic acid, was harvested and ethanol precipitation performed as described.

2.6.2 Subcloning for riboprobe production

2.6.2.1 DNA fragment isolation

DNA fragment isolation was made from a 1% agarose gel following enzymatic liberation from the original vector. A gel slice containing the fragment was excised whilst viewed with a UV transilluminator and the fragment then isolated using a Qiaex gel extraction kit (Qiagen). The gel slice was incubated in 3x its volume in buffer QX1 at 50°C in the presence of 10μl of QiaexII silica beads for 10 min, with frequent vortexing. Nucleic acids are selectively absorbed onto the QiaexII beads whilst the agarose melts. The beads were pelleted by centrifugation and the supernatant removed. The beads were then vortexed for 30 sec in a further 500μl of QX1 to remove any remaining agarose. Two washes in 500μl buffer PE, a high salt/ethanol buffer, were performed to remove final traces of salts. The beads were then pelleted, air dried for 10 min and the DNA eluted by vortexing in SDW for 30

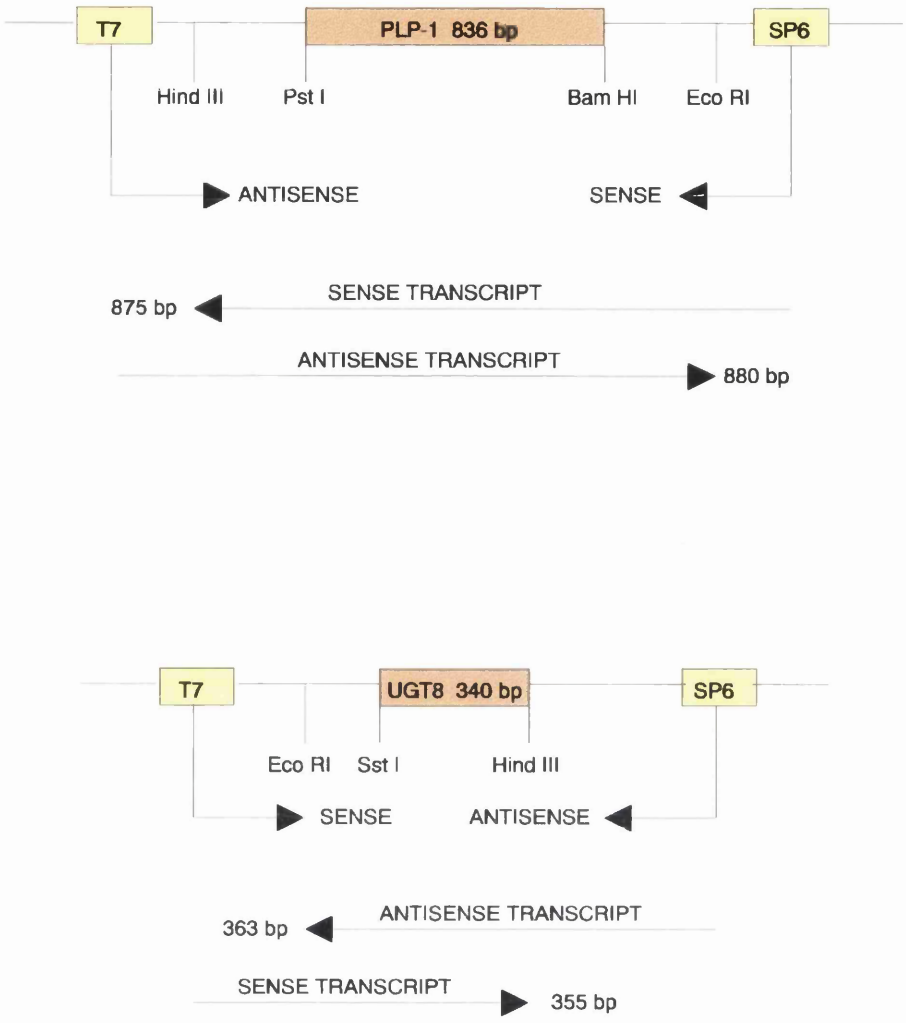

Figure 4: Schematic diagram of vectors, inserts, insertion and restriction sites used in riboprobe production.

sec. After the beads were once again pelleted, the supernatant containing the nucleic acid was harvested.

The yield was calculated by comparison of aliquots of isolated fragment with parallel fragment digests of known amounts.

2.6.2.2 Enzymatic manipulation

2.6.2.2.1 Alkaline Phosphatase

The vector to be used for riboprobe production was dephosphorylated (CIP treated) prior to insert ligation. This was to prevent reannealing of the linearised plasmid and was performed using calf intestinal alkaline phosphatase (CIAP) (Gibco BRL). 5μg of linearised vector was dephosphorylated in the presence of 50mM Tris-HCl pH8.5 and 0.1mM EDTA using 0.1U CIAP at 37°C for 30 min. This was followed by the addition of a further 0.1U CIAP and another 30 min incubation. The enzyme was inactivated by heating at 75°C for 15 min and denatured by two phenol/chloroform extractions. The remaining CIP-treated vector was precipated and reconstitution in SDW was at 250μg/ml.

2.6.2.2.2 Ligase

Ligation was catalysed by T4 DNA ligase (Gibco BRL) at 15°C overnight in a 20μl volume in the presence of 0.25U enzyme, 0.05mM Tris-HCl pH7.6, 10mM $MgCl_2$, 1mM ATP, 1mMDTT, 25% (w/v) polyethylene glycol-800 and 250ng (1μl) CIAP treated linearised vector. Reactions containing vector:fragment ratios of 1:1, 2:1 and 1:2 were established and the following control reactions were also set up;

a) pGEM4z + ligase	- to assess transformation efficiency
b) Linearised vector (non-CIP) - ligase	- to assess efficiency of vector digest
c) Linearised vector (non-CIP) + ligase	- to assess ligation efficiency
d) Linearised vector (CIP) + ligase	- to assess CIP efficiency

2.6.2.3 Transformations

Transformations were performed in sterile 40ml polypropylene tubes pre-chilled on ice. About 150ng of DNA from each ligase reaction was taken and made up to a final volume of 100µl with Tris EDTA buffer pH8.0. Available competent cells (JM101 Escherichia coli) were thawed and a 100µl aliquot added to the DNA, mixed gently and incubated on ice for 30 min. The mixture was then heat-shocked at 42°C for 45 sec and transferred to ice for 2 min. After the addition of 800µl of SOC medium (SOC medium, page 220), cultures were incubated at 37°C and 100 rpm for 1 hour in an orbital incubator. Duplicate plates of each culture were made by plating out 200µl aliquots onto Luria-Bertrani agar indicator plates using a sterile bent glass rod. Once all the liquid had been absorbed, the plates were inverted and incubated at 37°C overnight. Colonies on test and control plates were counted to gauge the efficiency of ligation and transformation. A number of single white colonies were then selected from the test plates for individual small scale culture prior to miniprep plasmid DNA extraction. These cultures were performed at 37°C in an orbital incubator overnight, in 5ml Luria Bertrani medium (Luria-Bertani medium, page 219) in the presence of 100µg/ml ampicillin.

2.6.2.4 Plasmid preparation

2.6.2.4.1 Minipreps

Plasmid DNA was isolated from bacterial cells from 1.5ml of each culture using the Wizard™ miniprep DNA purification system (Promega). The remainder (3.5ml of broth) was retained. The miniprep system is based on the alkaline lysis procedure with lysis of bacteria using sodium dodecyl sulphate (SDS) and sodium hydroxide (NaOH). SDS denatures bacterial proteins whilst NaOH denatures both chromosomal and plasmid DNA. Neutralisation with potassium acetate causes the covalently closed plasmid DNA to reanneal rapidly but most of the chromosomal DNA precipitates with bacterial proteins and is removed by centrifugation. Further purification of plasmid DNA is achieved by passage through a proprietary chromatography column before elution with Tris EDTA buffer. Test digests were performed and run on a 1% agarose gel to check for the presence of fragment before setting up a large scale culture.

2.6.2.4.2 Maxipreps

One of the cultures was selected to start a 200ml culture. 100µl of the retained broth was added to 200ml LB broth and cultured as described for the smaller

preparations. The Wizard^{TM} maxiprep DNA purification system was used to isolate plasmid DNA according to manufacturer's instructions.

2.6.2.5 DNA quantification

DNA samples were quantified using a GeneQuant RNA/DNA calculator (Pharmacia Biotech). A spectrophotometer cell with a minimum volume of 70µl was used to ensure the minumum amount of nucleic acid was discarded during quantification.

2.7 *In situ* hybridisation

2.7.1 Materials and solutions

To minimise RNase activity, all solutions were made using diethyl pyrocarbonate (DEPC) treated SDW. This was prepared by treating distilled water with 0.01% DEPC overnight and sterilising by autoclaving at 15lb/in^2 for 15 min. Glassware was cleaned by soaking in 6% sulphuric acid/6% potassium dichromate overnight before soaking in DEPC SDW and sterilisation by baking at 180°C. Plastics were treated by soaking in DEPC SDW and autoclaving at 15lb/in^2 for 15 min. Sections were cut onto 3-aminopropyltriethoxy-silane (APES) coated slides to ensure adherence. Slides were prepared by soaking in 5% Decon 90 (Decon Labs Ltd) overnight, washing and oven drying. They were then soaked in 0.25% APES (Sigma) in methylated spirit for 2 min in a fume hood, rinsed in DEPC SDW for the same time and oven-dried wrapped in foil. The coverslips used to cover sections during hybridisation were soaked in 1M hydrochloric acid for 30 min, rinsed 3x in distilled water and air dried. Cleaned coverslips were immersed in Repelcot (BDH) for 20 min, rinsed 2x in distilled water and baked at 130°C for 90 min. The siliconisation with Repelcot was included to reduce non-specific probe binding.

2.7.2 Preparation of ^{35}S labelled riboprobes

Sense and antisense ^{35}S riboprobes were generated using an SP6/T7 transcription kit (Boehringer Mannheim). The reaction was carried out on 2µg of linearised plasmid DNA in a 20µl reaction volume containing 0.5mM ATP, 0.5mM GTP, 0.5mM UTP, 50µCi ^{35}S-CTP (specific activity 37TBq/mM; <1000Ci/mM; Amersham), 20U RNase inhibitior, 20U SP6 or T7 RNA polymerase, transcription buffer and DEPC SDW. The mixture was incubated at 37°C for 30 min before the addition of a further 20U of enzyme and incubation for the same period. The DNA template was removed by incubating for 15 min at 37°C with 20U of RNase free DNase. To remove contaminating protein, an equal volume of phenol/chloroform was added to the sample and vortexed for 10 sec, centrifuged at 13000 rpm for 3 min and the aqueous layer removed to a fresh DEPC treated eppendorf. The solvent was then back extracted by adding an equal volume of DEPC SDW, repeating centrifugation and adding the aqueous layer to that previously harvested. RNA was precipated from this aqueous solution with 0.75M ammonium acetate and 2.5x volume of cold ethanol for 3 hr at -20°C. A 5µl aliquot was removed prior to centrifugation and placed in 5ml "Ecoscint" in a scintillation vial. This represented the total amount of isotope present.

Following precipitation, RNA was spun at 13000 rpm for 30 min at 4°C and 5µl of the supernatant removed as before; this represented unincorporated isotope. The remaining supernatant was discarded and the pellet resuspended in 100µl of DEPC SDW. A final 5µl was removed and added to "Ecoscint" as a measure of incorporated isotope. The three scintillation vials were counted on a Beckman LS 1801 scintillation counter and the percentage of incorporated isotope calculated.

RNA was reprecipitated overnight as described. The solution was then centrifuged at 13000 rpm at 4°C for 30 min, the pellet washed with 70% ethanol/DEPC SDW, briefly air dried and resuspended in DEPC SDW with 10mM DTT at 1ng/µl/kb. Probes were stored at -20°C and used within 6-8 weeks.

2.7.3 *In situ* hybridisation technique

2.7.3.1 Pretreatment of sections

The procedure was performed as described by Cox *et al* (1984) and modified by Wilkinson *et al* (1987). Pretreatment of the tissue rendered the target mRNA accessible to the probe without disrupting the morphology of the tissue. Hybridisation was undertaken in low stringency conditions to favour hybrid formation with the unbound probe removed by the higher stringency washes. An RNase step was included to remove single stranded RNA.

Frozen cord and brain sections on APES slides were allowed to air dry before rinsing in PBS and fixation in 4% paraformaldehyde for 20 min. After rinsing in PBS, sections were placed in a solution of 0.1M triethanolamine and 0.25% acetic anhydride for 5 min. A further addition of 0.25% acetic anhydride was made and solutions left for another 5 min. This acetylation step reduces the non-specific binding of probe to the proteins via electrostatic interactions. Sections were next passed through 5 min washes in PBS, 0.85% saline and methylated spirits and dehydrated in absolute alcohol (2 x 5 min).

2.7.3.2 Hybridisation

The required volume of probe was calculated on the basis of number and size of sections and the dilution factor of the probe. Brain sections took 6 ul and spinal cord half as much. Generally probe dilution was 1:10 and was made up in hybridisation buffer (50% formamide, 10% dextran sulphate, 1X Denhardt's, 20mM Tris Hcl pH8, 0.3M NaCl, 5mM EDTA, 10mM $NaPO_4$, pH8 and 0.5mg/ml yeast tRNA) with 1% 1M dithiothreitol added to the final mixture.

After denaturation of the diluted probe by heating at 80°C for 2 min and cooling on ice, it was applied to the sections and covered with siliconised coverslips. Slides were placed horizontally into a holding box containing tissue paper soaked in 50% formamide and 5 x SSC. This was sealed with tape and placed inside three vacuum sealed bags before immersion in a 50°C waterbath for overnight hybridisation.

2.7.3.3 Post hybridisation treatment

After removal of the slides from the bags and container, the following washes were performed to remove unbound or non-specifically hybridised probe:

1)	wash 1	5xSSC/0.01M DTT	50°C	30 min
2)	wash 2	2xSSC in 50% formamide/ 0.1M DTT	65°C	20 min
3)	wash 3	0.5M sodium chloride/ 0.005M EDTA/0.01M Tris-HCL (pH7.5)	37°C	10 min (x3)
4)	wash 3	0.02mg/ml RNaseA in 10mM sodium acetate	37°C	30 min
5)	wash3		37°C	30 min
6)	wash 2		65°C	20min
7)	wash 4	2xSSC	room temperature	15 min
8)	wash 5	0.1xSSC	room temperature	15 min

followed by dehydration in the following solutions:

1)	75ml ethanol, 162.5ml DW, 12.5ml 6M ammonium acetate	2 min
2)	150ml ethanol, 87.5ml DW, 12.5ml 6M ammonium acetate	2 min
3)	200ml ethanol, 37.5ml DW, 12.5ml 6M ammonium acetate	2 min
4)	237.5ml ethanol, 12.5ml 6M ammonium acetate	2 min

Slides were rinsed in absolute alcohol for 2 min, air dried and positioned in a radiographic cassette for overnight exposure. This was to give an indication of exposure times after dipping.

2.8 Autoradiography

2.8.1 Slide dipping

Slides were dipped in a solution of Ilford emulsion K5 mixed in a 1:1 ratio with distilled water containing 1% glycerol to provide a thin layer over the specimen. Emulsion temperature was 42°C. After wiping the backs of the slides, they were placed in a plastic box with silica gel to air dry for 4 to 6 hours. They were then transferred to a light tight box containing a sachet of silica gel; the box was tape-sealed and wrapped in a black plastic bag prior to storage at 4°C for a time determined by the exposure against the radiographic film.

2.8.2 Developing

This was carried out in undiluted Kodak D19 developer at room temperature under safelight conditions. Slides were immersed for between 3 and 4 min and then placed for 1 min in a 1% acetic acid/1% glycerol solution in water to halt development. Next they were transferred to a 30% sodium thiosulphate solution for 3 min to fix the autoradiograms before final washing in water in the dark for 30 min. After air drying, sections were counterstained with haematoxylin and mounted using DPX mountant.

2.9 Cell culture

2.9.1 Tissue preparation

2.9.1.1 Spinal cord cell dissociation

Mutant and wild type mice of the same age were selected from litters of similar sizes to ensure that they were at a similar developmental stage. Test and control cultures were set up within 24 hours of one another using the same media, and antibody staining was carried out simultaneously where possible, with the same antibody batches. Spinal cords were obtained from 2 mice for each culture. All manipulations were carried out in a tissue culture hood except for the initial dissection. The cords were dissected into Hanks Balanced Salt Solution (HBSS)(Ca^{2+}/Mg^{2+} free to prevent enzyme inactivation) and the meninges and nerve roots stripped. Cords were then minced on the inside of a petri dish lid using a No.10 scalpel blade and transferred into a sterile bijou by adding and sucking back about 1ml of antibiotic enriched HBSS. The same volume of trypsin 0.25% and 100 µl of 1% collagenase (10mg/ml) were added to this and incubated at 37°C for 30 min. The addition of the same amount of each solution was repeated and a further 30 min incubation performed. 1 ml of SD solution (SD solution, page 220) was added and the solution allowed to stand for about 5 min to halt enzymatic activity and reduce cell clumping.

Mechanical dissociation was performed by very slowly triturating through a 21G needle (5x) and a 23G (3x). The suspension was transferred to a centrifuge tube, about 5 ml of Dulbecco's modified eagle medium (DMEM)/10% foetal calf serum (FCS) added and then spun at 1000 rpm for 10 min. The supernatant was removed and the pellet reconstituted in 1.4 ml of DMEM/10% FCS.

2.9.1.2 Plating out

Cell density was calculated using a regular Levy counting chamber with a Neubauer ruling by counting the four large ruled squares in the corners ($1mm^2$ = 16 squares). Cell numbers were adjusted to 2-300,000/ml with the same medium. Plating of 50µl per poly-L-lysine coated coverslip (Poly-L lysine coverslips, page 221) ensured about 15,000 cells per coverslip. The coverslips had previously been placed in FLOW 24 well plates which were now put in an incubator at 37°C, 5% CO_2 for 30-40 min to permit cell attachment. After this, the cultures were fed with 500µl of SATO/0.1% FCS (SATO medium, page 220) and maintained in the incubator until immunofluorescence was carried out.

All solutions used in cell dissociation were warmed to 37°C prior to use.

2.9.2 Immunofluorescent staining

2.9.2.1 Antibodies

All antibodies were diluted in DMEM unless otherwise stated. Immunostaining was performed to assess the *in vitro* antigenic development and the morphology of mutant oligodendrocytes. Several antibodies were tested on both wild type and mutant cultures; counts were carried out on those that gave strong fluorescence without high background. Details are given below. CNP and MOG did not give a strong enough signal to be confident of identifying positive staining above background.

Primary	Dilution	Source	Secondary
anti-PLP 226	1:600	N.P. Groome (Oxford, UK)	Goat anti-rabbit IgG FITC 1:80
anti-MBP	1:1000	N.P. Groome	Goat anti-rat IgG FITC 1:50
O4	1:5	I. Sommer (Glasgow, UK)	Goat anti-mouse IgM TXR 1:50
O1	1:5	I. Sommer	Goat anti-mouse IgM FITC 1:50

Table 3: Details of antibodies used for immunostaining in cell culture.

2.9.2.2 Technique

All coverslips were used for double immunostaining. For surface markers, coverslips were incubated with 20µl of the primary antibody for 20 min at room temperature, washed for 5 min in DMEM and then incubated with the secondary for the same length of time. The same procedure was repeated if the second immunostain was also a surface marker. After washing for 5 min in DMEM, cells were fixed with 2% paraformaldehyde in DMEM applied for 30 min at room temperature. Nuclear staining was achieved with 4',6-diamidino-2-phenylindole (DAPI) (6µg/ml) for 30 sec and coverslips mounted in Citifluor antifade mountant (UKC Chem Lab).

For immunostaining with a cytoplasmic marker following a surface marker, Gow's technique was instituted post-fixation. Blocking buffer (Blocking buffer, page 221) was applied for at least 30 min before being removed with a tissue without washing.

The primary antibody was applied overnight at 4°C in the same blocking buffer but with 0.02% saponin. The following day, sections were washed in TBS for 20 min (3x) and the secondary antibody, diluted as detailed, applied for 20 min. Coverslips were then washed, stained and mounted as described above.

An Olympus IX70 inverted microscope was used to view and photograph coverslips. Three coverslips were counted for each antibody combination at 24, 48 and 72 hours for both mutant and wild type animals. About 300 cells were counted per coverslip. The experiment was repeated three times.

2.10 Western blotting

2.10.1.1 Isolation of protein from tissue

Protein was isolated from whole spinal cords by homogenisation in 0.1M Tris (pH 6.8) and 1mM Nα-p- tosyl-l-lysine chloro-methyl ketone (TLCK) to which 2% SDS was added and the samples then boiled for 5 min. After centrifugation at 13000 rpm for 5 min at 4°C, the supernatant was harvested and stored at -20°C. Total protein concentration was measured using the BCA assay (Pierce). DTT was added to give a final concentration of 40mM.

2.10.1.2 SDS-polyacrylamide gel electrophoresis

Protein analysis was performed using a vertical sodium dodecyl sulphate polyacrylamide gel electrophoresis (SDS-PAGE) gel produced by polymerisation of the acrylamide polymer cross-linked by N,N'-methylene bisacrylamide. The accelerator for the reaction was N,N,N,N',-tetramethylethylenediamine (TEMED) and the catalyst was ammonium persulphate.

To prepare the gel, a 5% solution of acrylamide-bisacrylamide (Acrylamide/bisacrylamide solution, page 221) was placed in one well of a Biorad mode 385 gradient former and a 20% solution (Acrylamide/bisacrylamide solution, page 222) in the other well which also contained a magnetic stirrer. The outlet from the gradient former passed through a peristaltic pump (LKB Bromma 2120 Varioperpex II pump) and into the glass plate sandwich. The gradient former delivered the most concentrated acrylamide into the sandwich first and as the level of this rose, then the concentration of the acrylamide decreased. The rate of delivery was 3.0 ml/min. This produced a gel that was 17.5% at the bottom and 5% at the top. A 2.5% bis-acrylamide stacking gel (Stacking gel, page 222) was layered over the resolving gel once this had polymerised. The stacking gel had minimal

sieving effect on the proteins because of its large pore size. It thereby concentrated them into a relatively narrow band at the stacking/resolving gel interface.

Aliquots of protein samples were prepared for electrophoresis by adding 100µl of SDS-PAGE sample buffer (Sample buffer, page 222) and boiling for 5 min to denature the polypeptides. The SDS bound to the denatued polypeptides in a constant weight ratio so that they had an essentially similar charge and migrated through the gel according to size. Samples were cooled and electrophoresed through a vertical LKB electrophoresis apparatus at 35mA for about 4 hours.

A discontinuous buffer system was used such that the gel buffer and the tank buffer were different (Discontinuous buffers, page 222). This helped to concentrate the proteins prior to their entry into the resolving gel.

2.10.1.3 Immunodetection

Electrophoretic transfer of the separated proteins onto Hybond ECL nitrocellulose membrane (Amersham Life Sciences) was performed at 200mA for 4 hours at 4°C in a transblot cell (Bio-Rad). Immunodetection was carried out using enhanced chemiluminescence (ECL). Non-specific binding was blocked by overnight treatment with Tris buffered saline (pH 7.6) containing 5% dried milk, 0.2% gelatin and 0.1% Tween 20. The ECL nitrocellulose membrane was treated with the primary antibody, polyclonal CNP (Prof P.J. Brophy) at 1:300 for 1 hour at room temperature followed by extensive washing in the blocking buffer. The membrane was incubated in the secondary antibody, anti-rabbit IgG conjugated with peroxidase, at 1:80 for 1 hour followed by thorough washing with blocking buffer and a final TBS rinse. The membrane was incubated in equal volumes of luminol enhancer solution and stable peroxide solution (Pierce Chemical Co.) for 5 min at room temperature. The membrane was wrapped in Saran wrap and exposed to X-omat imaging film (Kodak) in a cassette for 30 sec. The film was developed using an automatic processor (Dupont Cronex CX-130).

2.11 Mouse breeding

2.11.1 Homozygous stock

2.11.1.1 Breeding

Homozygous *hsh* stock was donated by the MRC Mammalian Genetics Unit, Harwell for establishment of breeding stock at the Parasitology Mouse House, part of the Veterinary Research Facility, Glasgow. Individual males were permanently housed with one or two females and a variable number of litters, usually in the region of 6-8, obtained from each pair. Brother-sister matings were avoided. Only severely affected mice were used in the phenotypic studies or retained as parents for subsequent generations. Wild type C3H/101 mice were already maintained at Glasgow and were housed under the same conditions.

2.11.1.2 Phenotypic measurements

Mice were aged taking the day of birth as P1. Phenotypic severity was classified at several ages by assessment of the tremor. The body weight of at least 50 wild type and 50 mutant mice was measured at several time points during development and mean values calculated. Small litters and very large litters were excluded from this study and those litters from which pups were removed prior to weaning were eliminated after that time. This was to ensure a representative growth pattern for the two phenotypes. Litter sizes were also recorded for both wild type and mutants.

2.11.2 Intersubspecific backcross

2.11.2.1 Choice of breeding strategy

To map a mutationally defined locus, it is necessary to generate a special panel of samples in which segregation of the mutant and wild type alleles can be followed phenotypically prior to DNA preparation for marker locus typing. For hindshaker, a two generation cross, the outcross-backcross, was adopted. In the outcross, *hsh* mice were bred with non-mutant mice from a different genetic background to generate first generation offspring (F1). F1 mice, heterozygous at all loci and therefore phenotypically normal, were backcrossed to homozygous *hsh* mice. The resultant F2 offspring were either homozygous or heterozygous at any given locus (Figure 5, page 69). Mice were typed phenotypically for homo- or heterozygosity at the *hsh* locus and then DNA extracted for typing with a number of microsatellite markers.

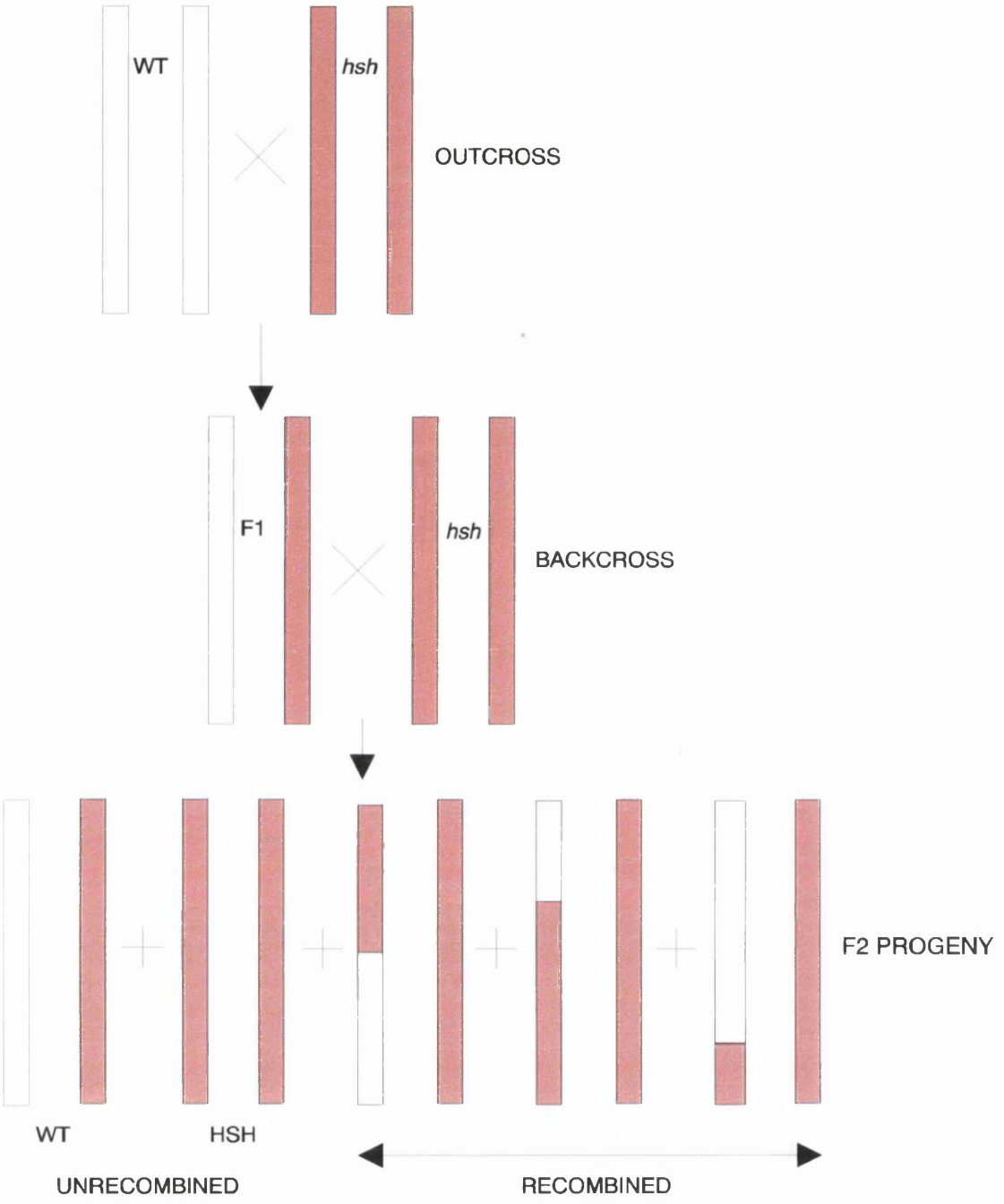

Figure 5: Generation of F2 mice in outcross-backcross. WT mice from a different genetic background are outcrossed to *hsh* to generate F1 mice, heterozygous at all loci. Recombination may occur during formation of gametes in these mice. F2 mice are produced by backcrossing with *hsh*. All F2 mice inherit one chromosome in a pair from the C3H/101 *hsh* parent, and one from the F1 parent. This F1 chromosome may be intact (WT or hsh) or recombinant. The closer a marker is positioned to the *hsh* locus, the less probability of recombination between the two loci. Mice with a tremor will therefore tend to be homozygous for microsatellite markers close to that locus.

2.11.2.2 Choice of parental strain

The parental strain carrying the mutant locus was on a mixed C3H/101 background. The choice of the second parental strain for use in the outcross was based on considerations of genetic distance (the more distant the strain, the greater chance of polymorphisms at DNA marker loci) and the ability to generate offspring in which segregation of the mutant allele could be observed. As *Mus spretus* is the most distant species from *Mus musculus* that still allows the production of fertile F1 hybrids (females only), outcrosses with this will provide the highest level of polymorphism that is theoretically obtainable for the purpose of mapping (about 90%) (Love *et al.*, 1990; Dietrich *et al.*, 1992). For this reason, the original mapping was initiated with two *M. spretus* males (B and K Universal) individually paired with C3H/101 mutant females. These failed to breed over a period of several weeks despite careful management and so an intersubspecific cross using *Mus musculus castaneus* was begun. Although the degree of polymorphism is less than that with *M. spretus* (about 77%) (Dietrich *et al.*, 1992), it is still much greater than that between laboratory strains, and offspring of both sexes are fertile. The first 17 *hsh* x *M. m. castaneus* F1 mice were generated at Harwell until *M. m. castaneus* (CAST/Ei) stock was available commercially. F1 mice were then bred on site. C3H/101 females were mated to *M. m. castaneus* males for the production of larger and more frequent litters from the hybrid female. All F2 backcross mice were generated on site. Both male and female F1 parents were backcrossed to C3H/101 mutants. Breeding stock were kept in permanent groups of one male with one or two females and generally produced 7-10 litters before being replaced with young stock. The F2 offspring were phenotypically graded at about twenty days and were classified as *hsh* or unaffected.

2.11.3 Interstrain backcross

In order to examine the penetrance of the *hsh* mutation on different genetic backgrounds, two interstrain outcross-backcross breeding regimes were established. C57BL/6J and BALB/cJ inbred strains were obtained (B and K Universal) as a male and female of each, and outcrossed to *hsh* C3H/101 mice as for *M. m. castaneus.* The F1 mice of both sexes were backcrossed to *hsh* stock and the offspring classified as *hsh* or unaffected. Although there is even less polymorphism between classical inbred laboratory strains, which are largely derived from *M. m. domesticus*, it is estimated that about 50% of microsatellite markers show interstrain polymorphisms (Dietrich *et al.*, 1992). It was therefore possible to utilise the phenotypically affected mice for DNA marker analysis in addition to the F2 mice from the *M. m. castaneus cross.*

2.12 General principles of linkage analysis

The fundamental principle underlying linkage analysis is recombination in the F1 parent. Closely linked genes or markers will tend to undergo few recombination events in F1 mice and will be inherited together. Unlinked loci will assort randomly and hence have a recombination rate of 50%. The method for analysing the frequency of recombination is the examination of the inheritance of polymorphic genes and markers in the F2 offspring. However, it must be remembered that F2 mice are only a means to analyse recombination and it is genetic events in F1 parents that are pivotal to linkage detection.

In an outcross-backcross using C3H/101 *hsh* mice, F1 hybrid mice are heterozygous at all loci, inheriting one chromosome in a pair from the *hsh* parent and the other from the tester strain. Thus, all F1 mice carry only a single *hsh* allele and are phenotypically wild type. F2 mice inherit one intact C3H/101 chromosome in a pair from the *hsh* backcross parent. The other chromosome in the pair comes from the F1 hybrid and may be intact wild type or *hsh*, or may represent a combination of genetic material from both strains (Figure 5, page 69). Half of the F2 mice will carry two *hsh* alleles and should express a shaky phenotype. The other half inherit the wild type allele from the F1 hybrid and are heterozygous for *hsh*. These mice will be phenotypically normal.

Similarly, for any other locus, half of all mice will be heterozygous, inheriting the tester strain allele from the F1 parent, and half will be homozygous, having received the C3H/101 allele. A C3H/101 allele is always inherited from the *hsh* parent. If a particular marker locus shows no linkage to *hsh*, random assortment occurs and half of the homozygous *hsh* F2 mice will be heterozygous and half homozygous for the marker locus. This gives a recombination rate of 50% between the marker and *hsh*. The same proportions will be derived for the wild type group, which are all heterozygous at the *hsh* locus. With a linked marker (*i.e.* in close physical proximity to *hsh*), few recombination events will have occurred between *hsh* and the marker in the F1 parent, such that a greater proportion of phenotypic *hsh* F2 mice will inherit the C3H/101 allele for the marker and hence be homozygous. Similarly, more wild type mice will be heterozygous for the marker, having inherited a tester strain allele at both loci. The recombination rate thus reduces from 50%. For a marker positioned very close to *hsh,* few recombination events will occur and the vast majority of shaky mice will be homozygous for the marker, with the reciprocal change in the wild type population. The aim in linkage analysis is the identification

of those marker loci which fail to recombine with *hsh;* since the positions of the markers are known, the map location of the *hsh* locus can be inferred.

2.13 Genome-wide linkage analysis

Markers were chosen on the basis that the typing of 50 mice for a marker permits detection of linkage in a region extending 15cM proximally and distally from this marker (Silver, 1995a). Coverage of the genome using these criteria necessitates 2-4 markers, appropriately spaced, per chromosome. As described above, an unlinked marker will recombine with *hsh* at a rate of 50% *i.e.* half of the mice will be homozygous for the marker and half will be heterozygous. With markers closer to *hsh,* this rate will reduce as more mice become homozygous. Eventually complete concordance will be found with very close markers. Under the conditions of 50 mice being typed for markers detecting linkage within a radius of 15cM, a recombination fraction of less than 26% demonstrates linkage at $p<0.001$. Therefore 26% was taken as the value below which linkage had been identified.

Once a recombination fraction of less than 26% for a marker had been found, tighter linkage was sought to other markers on that chromosome. Markers showing tight linkage, called flanking markers, were next tested against all available samples. Only the recombinant mice were then typed for intervening markers and haplotypes for these mice were created. New samples were run against the flanking markers and only further tested if recombinant for one of these.

2.14 Statistical analysis

Map distances were measured in centimorgans (cM) where a centimorgan is the distance between two genes that will recombine with a frequency of 1%, *i.e.* 1 mouse in 100 will have a recombination event between those two genes. In the mouse, this is roughly equivalent to 2000 kb pairs. Standard errors were calculated with the following formula;

$$S.E. = \sqrt{RF[(100-RF)/n]}$$

where RF = recombination fraction
and n = total number of samples

The cut-off values for statistical significance of recombination rates between *hsh* and microsatellite markers were derived from a Bayesian corrected χ^2 test (Silver, 1995a) and $p<0.001$ was taken as demonstration of linkage. This ensures that only 1 in 20 cases of positive demonstration of linkage is likely to be false. With a p value of 0.05, one will conclude that linkage exists in 1 of every 20 experiments conducted on loci that are in fact unlinked. Since true linkage exists only for a very small number of microsatellite markers (about 3/100 with the strategy employed here), the expected number of false positives would exceed the number of truly linked markers. Thus, the probability of linkage would actually be considerably less than 95% (about 40% in this case). A p value of 0.001 sets a limit for accepting less than 1 false positive for every 20 true positives, *i.e.* demonstration of linkage with a 95% probability.

Logarithm of odds (LOD) scores were calculated where necessary using the Map Manager programme available at http://mcbio.med.buffalo.edu/mapmgr.html and an Apple Mac computer. A LOD score of 3 or greater was taken as significant, as discussed by previous authors (Lander and Kruglyak, 1995).

2.15 Genetic maps

About 12 different mouse genetic maps can be accessed through the World Wide Web (WWW), either directly or through the Mouse Genome Database (MGD) at the Jackson Laboratory. The uniform resource locator (URL) for this resource is http://www.informatics.jax.org. Two of the maps are microsatellite linkage maps that serve only to indicate the position of microsatellite markers across the genome. The Whitehead/MIT map (http://www-genome.wi.mit.edu) shows the position of over 6000 microsatellite markers based on their results from an intersubspecific intercross using C57BL/6J-ob and CAST/Ei mice. Since only 98 meiotic events have been typed, markers have only been mapped to about 1.1cM and many are listed together in linkage groups called "bins". About 3200 of these markers have been mapped more precisely by the European Collaborative Interspecific Backcross (EUCIB) mapping project (European Backcross Collaborative Group, 1994) on a C57BL/6 x *Mus spretus* backcross of 983 mice (http://www.hgmp.mrc.ac.uk/MBx/MBxHomepage.html), which has allowed mapping to an interval of 0.1cM. Genetic distances for markers differ between the two maps due recombination frequency differences in the strains of mice used for the crosses.

In an attempt to combine data from all maps, two integrated maps, the Mouse Genome Database (MGD) and the Chromosome Committee maps can be accessed at the MGD. Data of mouse/man gene homology were accessed through the MGD (http://WWW.informatics.jax.org/homology.html) to allow examination of the syntenic regions in man. The human gene maps were accessed through the WWW server maintained by the National Center for Biotechnology (NCBI) which is the location of the GenBank database. The URL for this is http://www.ncbi.nlm.nih.gov/.

2.16 Preparation of genomic DNA

2.16.1 Collection of tissue

After identification of *hsh* and wild type phenotypes, F2 mice from the mapping backcross were euthanased with carbon dioxide and their tails and spleens harvested. Fresh gloves and scalpel blades were used for each mouse to minimise the possibility of sample contamination. Spleens were placed in cryotubes and tails in eppendorfs before both were frozen in liquid nitrogen. Splenic samples were then transferred to liquid nitrogen for long term storage while tails were kept at -70°C. Tails were used for extraction of genomic DNA in the first instance; spleens were utilised if tail tissue became exhausted.

2.16.2 Technique

The procedure adopted for routine gDNA extraction was influenced by throughput, reproducibility and ease of performance. At the onset of mapping using the intersubspecific backcross, only small numbers of samples were being processed simultaneously. The traditional method of cell lysis and deproteination by phenol/chloroform extraction was used. About 0.5cm of tail was incubated at 55°C in 700µl of buffer based on sodium dodecyl sulphate (SDS), which causes lysis of cell membranes. Proteinase K (0.4mg/ml) was included to denature protein. After 3 hours, 20µl of RNaseA (0.35µg/ml) was added and the mixture incubated for a further 2 hours. Debris was removed by centrifugation at 13000 rpm for 5 min and an equal volume of phenol/chloroform added to the supernatant. After shaking for 3 min, the cloudy solution was spun for 5 min at 13000 rpm and the upper aqueous layer harvested. This was repeated a total of 3 times. The gDNA was precipitated routinely, air dried for no more than 10 min and dissolved in 100µl of SDW overnight. Yields of about 20µg were achieved. Samples were stored at 4°C.

A commercial kit, the QIAamp Tissue kit (Qiagen), was assessed later in the study and was found to give consistently high yields with reduced manipulations. This technique was therefore sometimes used for ease and reliability when large numbers of samples were being processed simultaneously. The system is based on a patented spin column system in which gDNA is first absorbed onto a membrane, allowing the removal of protein in the flow-through. The gDNA is then eluted by the addition of a different buffer. Manufacturer's instructions were followed. Yields, when quantified, were generally in excess of 40µg.

Quantification of DNA was necessary for the preparation of "pooled" samples for use as described by Ben Taylor (Taylor *et al.*, 1994). This is described in DNA

quantification, page 59. These samples were also run on 0.7% agarose gels to check both the integrity and the quantification of DNA. Samples extracted using the Qiagen kit were not usually quantified or run on a gel and gave very satisfactory PCR results when used directly.

2.16.3 Preparation of pooled DNA samples

DNA samples were standardised to 0.5 mg/ml in SDW or TE and aliquots of 3µl were mixed and diluted 10-fold to give a final concentration of 50µg/ml.

2.17 Microsatellite primer pairs

Primer pairs were obtained from Research Genetics Inc, Huntsville, Alabama at a concentration of 6.6µM. Selection of an individual primer pair was based on the position of the microsatellite marker in the genome and polymorphism between C3H and the subspecies or strain (test strain) used in the backcross. At least a 10 base pair difference was required, depending on the size of the PCR product. The 101 strain fragment lengths had not been characterised by the Whitehead Institute/Massachusetts Institute of Technology (Whitehead/MIT), and as this constituted part of the hybrid *hsh* background, it was necessary to test each new primer pair with DNA from C3H, 101 and the test strain to ensure all were polymorphic. If the 101 band was too close to the test strain, that primer pair was abandoned. A pooled sample of C3H/test strain was also tested to check for preferential priming of one strand over the other. Again, the markers that showed this phenomenon were not used.

2.18 Polymerase chain reaction

Several PCR programmes were tested but there proved to be little difference in terms of intensity and specificity of product. In light of this, the final choice was largely based on duration of PCR reaction time and the fastest programme was adopted. If a primer pair failed to give satisfactory product with this programme, other protocols were attempted that used a different annealing temperature or cycle number. However, this was found to make no substantial difference in the majority of cases. A Perkin-Elmer or Hybaid Omnigene DNA thermal cycler was used for the amplification.

1) **Initial cycle**	94°C	2 min
	55°C	40 sec
	72°C	2 min
2) **Step cycle (35 cycles)**	93°C	20 sec
	55°C	40 sec
	72°C	15 sec
3) **Final cycle**	93°C	2 min
	55°C	40 sec
	72°C	1 min

Reactions were carried out in 0.5ml eppendorfs in a 25µl volume containing 1.5µl of target (approximately 100ng) and 1 unit of Taq DNA polymerase (Bioline). Manufacturer's buffer was used with 1mM dNTP (Bioline), 2.25mM $MgCl_2$ and 0.2µM each primer. Formamide was added at 0.2µl per reaction to reduce non-specific primer binding if a large number of spurious bands were produced. Q solution (Qiagen) was tried with primer pairs that gave very weak or no product. Both these are reported to decrease the melting temperature of DNA and therefore reduce the tendency for non-specific priming by disrupting these weaker bonds. Reagents were covered with 25µl mineral oil to prevent evaporation.

2.19 Analysis of PCR products

2.19.1 Agarose gel electrophoresis

Most PCR products could be separated on 3% Nusieve GTG agarose gels. This is a high resolution agarose that challenges polyacrylamide and can be used to separate fragments that differ by as little as 2%. To prepare gels, agarose was sprinkled on top of the appropriate volume of 0.5x TBE (Tris borate EDTA buffer x5, page 219), mixed well and left for 15 min. The solution was microwaved on "medium" for 1-2 min, mixed again and left to rest for 2 min. It was then microwaved on high for 1 min whilst the agarose boiled. After allowing to cool to about 60°C, ethidium bromide (10mg/ml) was added to a concentration of 0.5ng/ml and the gel cast. Once set, it was placed at 4°C for 20 min prior to use to obtain the optimum resolving and handling qualities.

6x TAE loading dye was added to each sample prior to loading. Samples were loaded onto a dry gel which was then placed in an Electro-4 gel tank containing 0.5x TBE. Gels were run at 75-100V for at least 45 min, depending on the size of the fragments and the degree of polymorphism between them.

2.19.2 Gel photography

Gels were photographed using one of the following camera set-ups;

a) Polaroid MP4 land camera (Polaroid), a T2201 transilluminator (Sigma), a Wratten 22A filter (Kodak) and Polaroid 667 (ASA 3000) film).

b) Kaiser RA1 CCD camera, a Herolab UVT-28M transilluminator and a Sony UP-890CE video graphic printer.

3. Study of the hindshaker phenotype

3.1 Background to the *hsh* mutation

The spontaneous hindshaker (*hsh)* mutation was first recognised at the MRC Mammalian Genetics Unit, Harwell in 1992. The original *hsh* mouse was a single male in a litter of mice carrying the downless (*dl*) and Steel contrasted (*Mgf*$^{sl\text{-}con}$) mutations (see below). The phenotype was described as a marked quivering of the hindquarters that occurred during locomotion and was less evident at rest (Beechey, 1993). The behaviour was very reminiscent of rumpshaker (Cattanach and Beechey, 1991) but differed in that the quivering decreased rapidly with age in *hsh* and disappeared by 50 days of age. Homozygous *hsh* stock was established at the MRC Mammalian Genetics Unit by breeding the mutation onto the C3H/101 hybrid background for several generations; hybrid mice were created by crossing C3H/HEH females with 101/H males. This background gives improved vigour and fecundity and is routinely used for maintenance of mutant stocks at Harwell. Breeding studies conducted at this time indicated an autosomal recessive inheritance and proved that *hsh* was not an allele of quaking (Beechey, 1993)

Fifteen homozygous *hsh* mice were donated to Prof I.R. Griffiths at the Applied Neurobiology Group, Glasgow in 1994 to set up a breeding colony for investigation of the phenotype. All mice were heterozygous for the *dl* mutation and 8 were known to be heterozygous for *Mgf*$^{sl\text{-}con}$. The recessive *dl* mutation, found on chromosome 10, is a spontaneous coat variant first recognised in 1958 in the A/H strain. Mice are characterised by a thin haircoat with shiny, bald patches behind the ears and a bald tail. Incisor teeth may be abnormal or absent and molars are abnormal. *Mgf*$^{sl\text{-}con}$, also on chromosome 10, is a semidominant mutation that gives a silver haircoat and resulted from a neutron irradiation experiment in 1963; the original mice used in this experiment were on C3H/101 (female) and SN (male) backgrounds. The A/H and SN strains are no longer in existence. It is not known what contribution the founding strains made to the genetic makeup of the original *hsh* male. Since the stock maintaining the *dl* and *Mgf*$^{sl\text{-}con}$ mutations has been crossed several times with C3H/101 hybrids in the last three decades (C. Beechey, personal communication) and one original parent was also C3H/101, these two strains must have made a sizeable contribution. Presumably there may also have been some genetic material from the A/H and SN strains still present in the stock.

Preliminary morphological studies carried out by I.R. Griffiths showed that the most obvious feature of *hsh* mice was hypomyelination in the CNS, most prominently in the spinal cord of young animals. Numerous naked and thinly sheathed axons were present in spinal cord white matter of immature mice; myelin debris and macrophages were absent and axons appeared normal. Immunostaining

demonstrated the presence of the major myelin proteins in these sheaths. No obvious glial cell abnormalities were found. By 4 months of age, the majority of axons were myelinated, although many sheaths appeared disproportionately thin.

3.2 Aims of the *hsh* phenotypic studies

The description of the phenotypic consequences of a mutation in a specific gene is an important part in elucidating its role in the normal animal. The aim of the *hsh* phenotypic study was to develop a detailed account of the effects of the *hsh* mutation and thus to shed light on the putative role of the gene in normal myelination. This chapter will present the account in four separate sections; the behavioural phenotype, the nature and development of the myelin defect, glial cell analyses and *in vitro* development of *hsh* oligodendrocytes.

Genetic mapping of the disease locus was also initiated as part of my project, the findings of which are presented in the subsequent chapter (Linkage mapping of the *hsh* mutation, page 162). On the basis of the results, a small number of candidate genes were suggested for further investigation. For continuity, these studies will be presented in the final section of this chapter as part of the phenotypic results.

3.3 Phenotypic studies

3.3.1 Introduction

The most obvious aspect of a mutation is usually its effect on the physical or behavioural characteristics of the organism. These changes may indicate the body system that is involved and therefore direct subsequent detailed analyses of the phenotype. Although the tremor exhibited by *hsh* mice had suggested neurological dysfunction, the behavioural phenotype had not been fully characterised in our laboratory. Also, it had not been established whether other physiological functions were impaired. Thus, a study of the behavioural signs, growth rate and fecundity was undertaken to investigate the phenotype more fully.

3.3.2 Methods

3.3.2.1 Tremor study

To describe the development of the phenotype, twenty-six litters of mutant animals were examined daily for the presence of a tremor between P10 and P25 and then at P30, 35, 40, 50, 60, 75 and P100. Mice were assigned one of four grades; "0" for mice with no tremor, "1" for animals with a slight gait abnormality and straight tail, "2" for those with an obvious tremor when ambulating and "3" for mice with a tremor at rest. The general behaviour and viability of these mice was also observed.

3.3.2.2 Weight study

To evaluate growth, at least 50 mutant and 50 wild type animals were weighed at P1, 5, 10, 15, 20, 30, 50, 75 and P100 and the mean weight at each age calculated as described in Phenotypic measurements, page 68. Mice homozygous for the *dl* mutation were smaller than their littermates from about P10 and were not used for phenotypic studies or breeding. Mice with silver haircoats were also rejected from the study.

3.3.2.3 Litter sizes

Fecundity was assessed by recording the number of newborn pups in *hsh* and wild type litters and evaluating the percentage distribution of mice per litter.

3.3.3 Results

3.3.3.1 General phenotypic description

Homozygous mice of both sexes developed a tremor of the rump (lumbar region and hindlegs) and tail at about P12, at the onset of ambulation. In general, this was apparent only during locomotion and disappeared at rest. Shaking increased in intensity over the next 1-2 weeks, reaching maximum severity between P20 and P30. After this time, mice gradually improved and few exhibited a shake beyond P40, although an abnormal tail carriage persisted in some older mice.

Notwithstanding this general pattern, the severity of the shake and rate of its disappearance varied quite considerably. This was most evident at the start of the project when some mice were grade 3 by P20 and remained so for 10-14 days before slowly improving, others reached only grade 1 and appeared normal by P25, and a small number of mice (about 10%) did not shake at all. Even the most severely affected mice exhibited a gradual improvement to grade 1 by P50. As the study continued, deliberate selection of only markedly shaky mice (grade 3 at P20) for breeding stock led to the majority of offspring exhibiting a grade 2 to 3 tremor by P20, remaining markedly shaky for about 10 days and slowly improving to grade 0 or 1 by P40 to P50. Littermates appeared to develop a similar degree of tremor, although this was not always the case. The very occasional severely affected animal suffered spontaneous seizures but this was a rare occurrence.

Viability of mice appeared to be normal; the number of mice born in a particular litter was generally equivalent to the number weaned at P20 and the longevity of adult mice did not appear different from wild type animals. The activity and agility of mutants also appeared unaltered.

3.3.3.2 Weight study

No observable differences were found between the body weights of *hsh* and wild type animals at any age (Figure 6, page 86).

3.3.3.3 Breeding study

In total, the numbers of newborn pups were recorded for 156 *hsh* and 189 wild type litters. No marked differences were found in the distributions of the numbers of pups per litter (Figure 7, page 87).

3.3.3.4 Discussion

At the beginning of the study, the *hsh* mutation was known to result in a tremor of the hindquarters and tail in young homozygous mice that reduced with age (Beechey, 1993). However, the detailed study of the behavioural phenotype presented here demonstrated that there was a marked variation in the expression of the tremor, with some mice exhibiting a marked shake for several weeks and others having only a slight tremor for a short period of time. It is also became apparent early in this work that there was incomplete penetrance of the mutation, with 10% of homozygous animals appearing phenotypically normal throughout development. It is known that the phenotype resulting from a mutation in a specific gene can vary markedly on different genetic backgrounds due to modifying genes at other non-disease loci (see (Erickson, 1996) for review). Since the *hsh* mutation was not maintained on an inbred background but instead represented a combination of C3H, 101 and original background genetic material, mice were not genetically identical. Since they were maintained under the same environmental conditions, the variation seen in the *hsh* phenotype, in terms of both penetrance and expressivity, was likely to result from these genetic differences. In other words, the presence or absence of specific alleles at loci separate to *hsh* was influential on the appearance and the severity of the phenotype. Support for this came from the apparent heritability of the intensity of the shake; selection for only the markedly shaky mice as breeding stock appeared to lead to a more homogeneous population and a more predictable phenotype. At the time of writing, non-shaky homozygous mice have not been identified for about 1 year and the vast majority of mice develop a shake of at least grade 2 at P20. Presumably most mice now carry a complement of modifier alleles that is compatible with penetrance and greater expression of the *hsh* phenotype.

When the study was initiated, the homozygous stock carried the *dl* and *Mgf*$^{sl\text{-}con}$ mutations. Mice homozygous for *dl* grew poorly, probably due to dental abnormalities related to *dl*. These mice were not used for breeding or phenotypic studies and the mutation may well have been eliminated. Silver-coated mice were also rejected for breeding and the *Mgf*$^{sl\text{-}con}$ mutation also appears to have disappeared from the stock.

The growth rate and/or viability of mice carrying a particular mutation can be affected either directly as a consequence of the altered gene product, or indirectly, for example, due to behavioural abnormalities that interfere with feeding. No marked differences were found in the body weights of *hsh* or wild type animals at any age. This suggested that the *hsh* gene product was unlikely to have a significant role in the growth of mice and that their ability to feed was not affected by their

tremor. The viability of mice into adulthood also appeared to be unaffected by the mutation.

Mutations involving myelin genes or genes in their vicinity can affect fertility of one or both sexes, for example, in quaking mice where the deletion of a neighbouring gene is responsible for sterility in homozygous males (Ebersole *et al.*, 1992). Deleterious mutations may also lead to embryonic or perinatal death, resulting in small litter sizes. Although it was known that homozygous *hsh* mice of both sexes were fertile (Beechey, 1993), the consequences of the mutation, if any, on litter size had not been closely studied. The results presented here suggested that the mutation had no deleterious effect on the number of pups born.

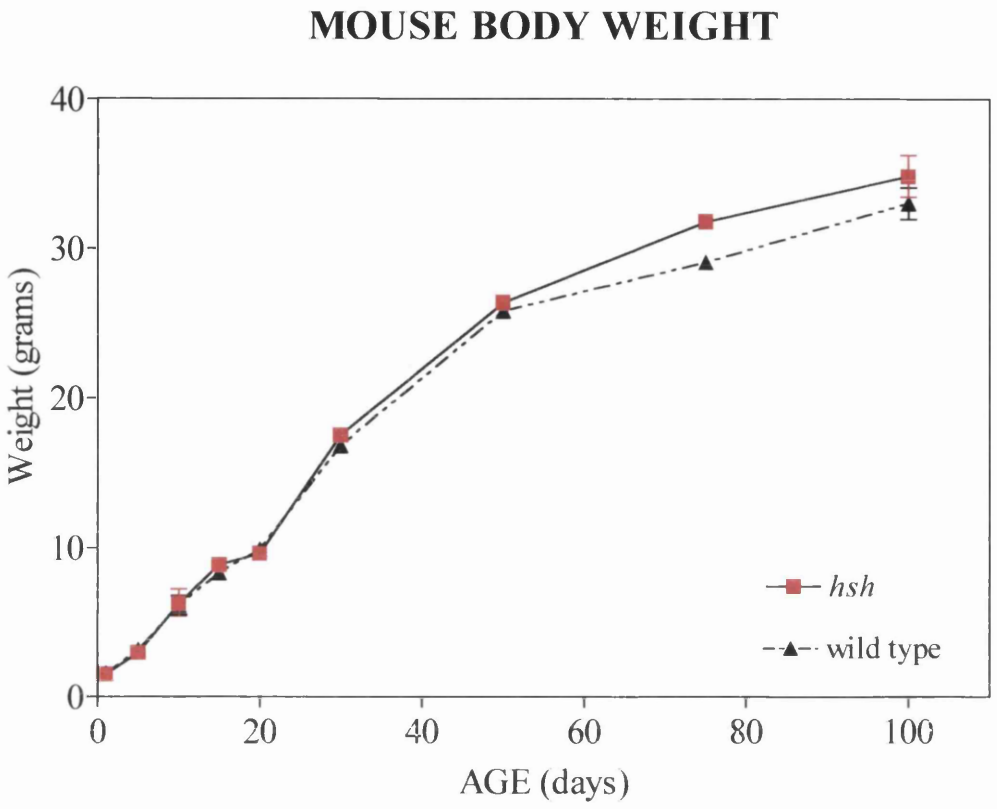

Figure 6: Age-related weight gains for wild type and *hsh* animals. Between 50 and 100 animals of each phenotype were weighed at each time point (Mean ± SEM). No marked differences are seen.

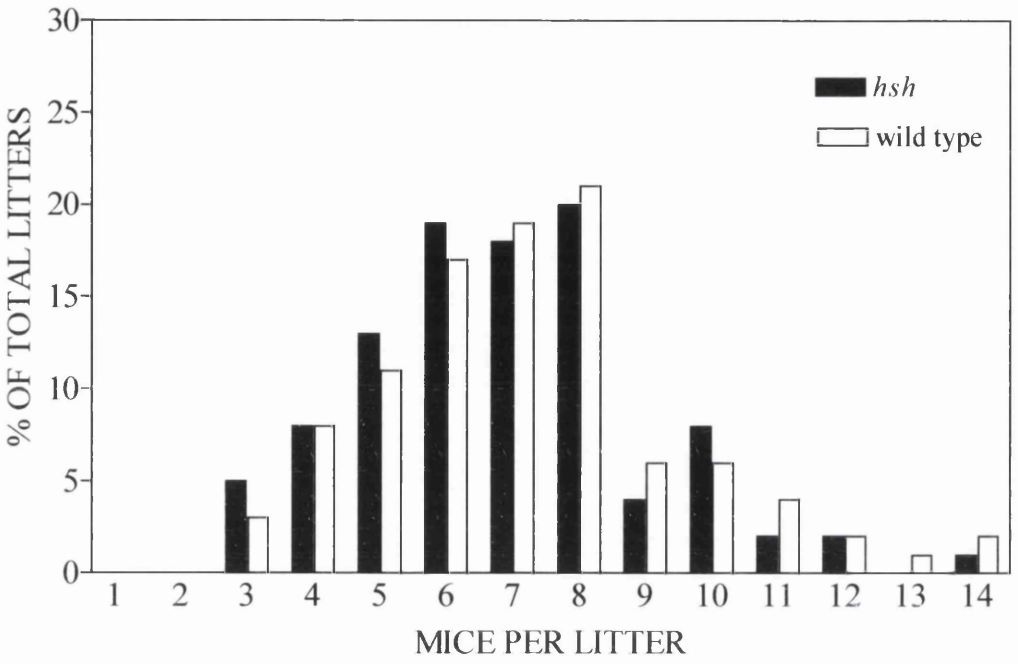

Figure 7: Results of the breeding study. The number of litters of each size is shown as a percentage of the total number of litters (156 mutant and 189 wild type litters). No marked differences are seen.

3.4 Characterisation of the myelin defect

3.4.1 Introduction and aims

At the inception of the project, there was limited information concerning the effects of the *hsh* mutation on myelination. It was known that young homozygous animals exhibited hypomyelination of the CNS, with the spinal cord being more prominently affected than the brain. The PNS appeared unaffected (Prof I.R. Griffiths, personal communication). Thus, the initial aim of this work was to further define the affected areas and to describe the nature and severity of the myelin defect in these regions. An indepth study of the development and resolution of the myelin abnormality over time was performed on a selected area of the CNS. Assessment of the presence of a panel of myelin proteins was also undertaken, both to further characterise the phenotype and to identify any putative candidate genes. The results presented here encompass the myelin defect specifically; analysis of glial cell biology is given in the following section (Glial cell morphology and quantification, page 119).

3.4.2 Materials and Methods

3.4.2.1 Mouse breeding

Mutant and wild type mice were maintained and bred as described in Breeding, page 67. Unless stated otherwise, only *hsh* mice that exhibited a marked tremor at P20 were used for analysis. Younger mice were obtained from parents that had been shown to consistently produce markedly affected offspring.

3.4.2.2 Preparation of tissue

Tissue was prepared for resin and paraffin wax embedding and cryosections as described in Tissue processing and cutting, page 46. Wild type and mutant mice at P10, 20, 30, 50, and P100 were used. Blocks were obtained from cervical, thoracic and lumbar cord, cerebellum, midbrain, forebrain, optic nerve and sciatic nerve. In addition, tissues were removed from thymus, heart, lungs, liver, kidney, testis, intestine and muscle.

3.4.2.3 Histopathology

To define the distribution, nature and severity of the hypomyelination, a survey of the nervous system was undertaken on 1μm resin sections stained with methylene blue/azur II and on paraffin sections stained with H&E. To search for any other

abnormalities resulting from the mutation, the non-neural tissues were examined on paraffin sections after H&E staining.

3.4.2.4 Immunocytochemistry

This was performed for a number of purposes. PLP/DM20 and MBP PAP immunostaining was employed to further characterise the phenotype, illustrating the extent of the myelin deficit in various regions of the CNS. Staining for a panel of myelin proteins was assessed in *hsh* spinal cord white matter to establish the relative effects of the mutation on the levels of these proteins. Immunostaining was also used to confirm the presence of specific myelin proteins in *hsh* myelin to aid in excluding their encoding genes as likely candidates for the mutation.

PAP immunostaining for PLP/DM20 and MBP was performed on resin and paraffin sections from spinal cord, forebrain and optic nerve at P10, 20, 30 and P50. This technique can give a clearer assessment of the extent of myelination than methylene blue/azur II stained sections since detail of the myelin sheaths is not obscured by surrounding cell bodies. Also, large areas such as the forebrain are more easily processed for PAPs than for resin sections. The technique is described in Peroxidase-anti-peroxidase (PAP) immunostaining, page 50. CNP, MAG, MOBP and MOG immunostaining was carried out on frozen sections of cervical cord from P10 and P20 animals. The protocols and details of the antibodies, fluorescent conjugates and their sources are given in Immunofluorescence, page 51.

GFAP PAP and immunofluorescent immunostaining was performed on spinal cord resin sections to assess the astrocyte population in mutants. The techniques are given in Immunofluorescence, page 51.

3.4.2.5 Myelin volume

The cervical cord ventral white matter was selected for measurement of myelin volume on the basis of the initial histopathological observations. Myelin volume was determined at P10, 20, 30, 50 and P100 as described in Myelin volume, page 48. It was also measured at P20 in the optic nerve.

3.4.2.6 Morphometric analysis

Axon and myelin morphometry to assess axonal size and myelin sheath thickness was performed on cervical cord ventral columns of P30 and P100 wild type and mutant mice (see Morphometry, page 49). These ages were selected to describe the maximal defect in young mice and the extent of resolution with age, based on the results from the myelin volume study. G ratios were calculated for individual fibres

to allow comparison of sheath thickness for equivalent axon sizes in mutant and wild type animals. The mean *g* ratio for all fibres was also evaluated for both phenotypes at the two ages. Frequency distributions of axon diameter for myelinated and unmyelinated axons were calculated for P30 mutant animals (Morphometry, page 49) to assess any effect of the mutation on axon populations of different sizes. The number of myelinated axons was also determined for these mice and expressed as a percentage of the total number of axons analysed (Classification of fibre type, page 49).

3.4.3 Results

3.4.3.1 Distribution of the lesion

The most obvious abnormality at all ages was a myelin deficit, which was due to a combination of naked and thinly sheathed axons. This was confined to the CNS, with the sciatic nerves and dorsal and ventral nerve roots appearing normal by light microscopy (data not shown). The most marked changes were found in the spinal cord whilst the brain appeared considerably less affected. In the spinal cord, there was generalised hypomyelination with no predilection for any tract or cord segment (Figure 8, page 97). Ventral and dorsal columns appeared equally affected and changes extended from the cervical to lumbar segments. No abnormalities were detected on paraffin sections of fore, mid or hindbrain stained with H&E and little difference was seen in *hsh* and wild type forebrain sections immunostained for PLP/DM20 (Figure 9, page 98). The majority of optic nerves at all ages appeared adequately myelinated on examination of resin sections and by PLP/DM20 immunocytochemistry (Figure 10, page 99). There was, however, evidence of hypomyelination on EM (Figure 11, page 100). Non-neural tissues were examined grossly and on paraffin sections stained with H&E; no abnormalities were evident.

3.4.3.2 General morphological features of the cervical cord

Since the spinal cord was the most severely affected area and the changes were uniformly distributed, the cervical cord (approximately C2) was selected for a detailed developmental study of the pathology. Hypomyelination was grossly visible during dissection of mice up to P30, with the spinal cord white matter forming a thinner rim than in equivalent control animals. The number of myelinated fibres in the ventral white matter was already lower in *hsh* by P10 but these differences were most obvious at P20-P30; the larger, more peripheral axons were thinly myelinated and were interspersed with groups of naked smaller axons (Figure 12, page 101 and Figure 13, page 102). With advancing age, an increasing proportion of small axons were myelinated and by P100, most axons were

myelinated although the sheaths tended to remain abnormally thin (Figure 14, page 103). Dorsal columns exhibited a similar degree of hypomyelination in younger mice that showed partial resolution with age.

The structure and periodicity of myelin in *hsh* was comparable to normal mice (data not shown) and no obvious axonal degeneration or ultrastructural abnormalities were seen. Glial cell development will be described in the subsequent section (Glial cell morphology and quantification, page 119), but initial observations suggested an increase in white matter total glial cell density. Morphological abnormalities of the oligodendrocytes were not detected and a marked astrocytosis was not observed on visual inspection of sections. Cells with an LM appearance typical of microglia seemed more numerous in the white matter. Myelin breakdown and debris was not observed at any age, and pyknotic nuclei were not more frequent than in corresponding wild type tissue.

3.4.3.3 Phenotypic variation

In the morphological study of *hsh*, only those mice which had demonstrated an obvious tremor when young, or came from affected parents in the case of P10 mice, were selected. However, to assess the variation in phenotypic expression, a single litter, all homozygous for the mutant allele but showing markedly different severities of tremor, was perfused at P20. The degree of hypomyelination in the spinal cord varied considerably (Figure 15, page 104) and reflected the intensity of tremor.

3.4.3.4 Immunostaining of the cervical cord

All myelin proteins assessed were present in *hsh* tissue although the amounts were reduced in comparison to wild type. On PAP sections of cervical cord stained for PLP and MBP, there was a reduction in the amount of myelin due to thin and absent sheaths (Figure 8, page 97). The majority of myelin sheaths were associated with the larger, peripherally located axons (Figure 16, page 106) and the myelin deficit partially resolved in older mice. Immunofluorescent staining for MAG, MOG, MOBP and CNP was reduced in all cases. MAG immunostaining (Figure 17, page 107) and MOBP (Figure 18, page 108) at P20 revealed an obvious reduction in the number of positive sheaths in the white matter of *hsh*. On the MAG section, the majority of positive sheaths were within the peripheral white matter of the ventral cervical spinal cord. MOG staining was bright in *hsh* white matter although this was clearly reduced in area compared to wild type and staining in the grey matter

was reduced (Figure 19, page 109). Immunostaining for CNP was reduced (Figure 20, page 110).

GFAP PAP and immunofluorescent staining did not demonstrate a marked difference between *hsh* and wild type (Figure 21, page 111).

3.4.3.5 Myelin volume

Measurements of *hsh* total cord and white matter areas were reduced in comparison to wild type animals at all ages (Figure 22, page 112). Significant differences were found at P10, P20 and P30 ($p = 0.0286$ at all these ages). A decrease in myelin volume was already detectable at P10, with the greatest disparity between mutant and wild type animals occurring at P20-P30 ($p = 0.0286$ at P10 and P20, $p = 0.05$ at P30)(Figure 23, page 113). At P20 and P30, myelin volume was approximately 40-45% of normal. A marked improvement occurred between 30 and 50 days of age so that by P50, myelin volume had reached approximately 75% of normal. There was no further improvement beyond this and mice remained hypomyelinated in comparison to wild type.

3.4.3.6 Axon and myelin morphometry

Axon/myelin sheath relationships were examined and quantified in the ventral white matter of the cervical spinal cords of P30 and P100 mutant and wild type animals.

General observations

On visual examination, many axons in mutant mice were unmyelinated at P30 whereas virtually all fibres in wild type animals had myelin sheaths at this age. A few ensheathed but unmyelinated fibres were apparent in mutants. There was a tendency for small diameter axons to be unmyelinated, with larger fibres being surrounded by disproportionately thin sheaths. There was an impression that small axons made up a larger proportion of the total axon population in *hsh* compared to control animals. There was no evidence of excessively abundant astrocytic processes in contact with naked axons.

At P100, most axons in mutant animals were myelinated. No degenerating axons were identified at either age and qualitatively the density of neurofilaments appeared comparable to control fibres. Relationships between myelinated axons and their surrounding sheaths were unremarkable and no instances of interposition of astrocytic processes between myelin lamellae or axon and sheath were identified.

Axonal diameter distributions

The axonal diameter frequency distributions for total axons were similar in mutant and wild type mice at P30 (Figure 24, page 114). The proportions of myelinated, ensheathed and unmyelinated fibres in mutants varied considerably between animals despite a similar phenotype; in the 4 mice studied, the percentage of myelinated fibres ranged from 27% to 66% whilst the majority of remaining axons were unmyelinated. No greater than 2% of total axons were ensheathed in any of the mutant animals. The calculation of axonal frequency distributions for myelinated and unmyelinated axons in *hsh* confirmed the impression that the majority of unmyelinated fibres were of small diameter (Figure 25, page 115).

Myelin sheath thickness

The majority of sheaths that were present in mutant animals at P30 were disproportionately thin (Figure 26, page 116) and hence the *g* ratios were increased (Figure 27, page 117). By P100 the sheaths were thicker, and although many remained thin compared with wild type, a proportion of the smaller axons were now surrounded by sheaths of normal dimensions (Figure 26, page 116). Thus, the *g* ratios were lower than at P30 but still tended to be greater than wild type figures, particularly for large axons (Figure 27, page 117). The mean *g* ratios at P30 and P100 illustrate the accumulation of myelin between these two time points and the deficit still present at the older age (Figure 28, page 118).

3.4.3.7 Myelin volume in the optic nerve

At the level of light microscopy, *hsh* optic nerves were of comparable diameter to wild type, and myelin sheaths appeared to be of similar dimensions to those in normal nerves. However, when examined by EM, a mild degree of hypomyelination was identified by the presence of thin sheaths and some naked axons (Figure 11, page 100). These changes were not as marked as in the spinal cord and when the myelin volume was assessed in two animals of each phenotype at P20, the value in mutant nerves was 74% of wild type versus 40-45% in the spinal cord.

3.4.4 Discussion

The hindshaker mouse is a hypomyelinating mutant exhibiting a delay in myelination of the CNS but no obvious pathology in the PNS. Interestingly, the spinal cord is more severely affected than the forebrain and optic nerve. A partial resolution of the myelin deficit occurs with increasing age of mice. The severity of hypomyelination in the cords of young animals is reflected in the intensity of tremor. No segmental or tract selectivity is observed within the cord; dorsal and ventral

columns are both hypomyelinated and changes extend from the cervical to lumbar regions. Myelin sheaths appear structurally normal despite their attenuation, as do axons, and there is no evidence of degenerative change in either. PLP, MBP, CNP, MAG, MOG and MOBP are all present in *hsh* myelin although they are reduced in amount. Overall, the impression is of retardation of an otherwise essentially normal myelination process.

In contrast to *hsh,* the best characterised murine myelin mutants Mbp^{shi} and the *Plp* mutants such as Plp^{jp} and its various alleles, generally show persistence of the behavioural phenotype and myelin defect. Both Mbp^{shi} and Plp^{jp} have much less myelin than *hsh* and the most severe reductions are seen in the brain rather than in the spinal cord, (for reviews, see (Duncan, 1990; Nave, 1994; Lunn *et al.*, 1995; Griffiths, 1996)). Additionally, any myelin formed in Mbp^{shi} and the *Plp* mutants is structurally abnormal. Affected mice also die prematurely. Quaking mice have normal longevity but the brain is severely affected (Friedrich, Jr., 1974) and the PNS is also involved (Suzuki and Zagoren, 1977; Suzuki and Nagara, 1982). Two uncharacterised canine mutations show some similarities to *hsh* in terms of inheritance and the preferential susceptibility of the spinal cord to hypomyelination. In Chow Chow and Weimaraner dogs, autosomal recessive mutations cause hypomyelination principally of the peripheral spinal cord white matter and some resolution of the defect with time (Duncan, 1987; Kornegay *et al.*, 1987; Lunn *et al.*, 1995).

Assessment of myelin volume in the cervical cord at several ages suggests that greatest myelin production in *hsh* occurs between P30 and P50, in contrast to wild type mice in which the biggest increase in myelin volume is seen between P10 and P20. This results in the most marked myelin deficit occurring at P20-P30 and partially resolving between P30 and P50 as mutants "catch up". The early tendency for small axons to be unmyelinated probably reflects the normal pattern of myelination, in which oligodendrocytes associate with larger axons prior to smaller ones (Lord and Duncan, 1987; Remahl and Hildebrand, 1990; Butt *et al.*, 1997). The delay in this process in *hsh* leads to small fibres remaining unmyelinated for a extended period of time. By P50, the majority of axons are myelinated although many sheaths remain disproportionately thin. This is particularly obvious for large fibres whilst a greater proportion of small axons acquire sheaths of normal thickness. This may be related to the fact that more myelin is required for the single internode of a large axon than for multiple internodes of smaller axons (Smith *et al.*, 1982; Remahl and Hildebrand, 1990). Oligodendrocytes in mutant mice may be

able to meet the lesser demands of a number of small fibres but unable to elaborate sufficient myelin for single large axons.

The total axonal diameter distribution reveals no differences between mutant and wild type animals at P30. This is surprising in light of studies showing that myelin influences the calibre of axons and their radial growth during development (De Waegh *et al.*, 1992; Colello *et al.*, 1994; Hsieh *et al.*, 1994; Sánchez *et al.*, 1996). In shiverer, quaking and myelin synthesis deficiency (*Plp$^{jp\text{-}msd}$*) mice, even the prolonged ensheathment stage that occurs in these mutants is sufficient to induce full calibre growth and neurofilament accumulation (Sánchez *et al.*, 1996). There is no increase in the proportion of ensheathed axons in *hsh* to account for the apparently normal axonal size distribution in the face of a large population of unmyelinated fibres. Also, there is a conflicting visual impression that small axons actually do make up a greater proportion of the total axonal population compared to wild type. It may be that any presumptive difference could not be detected by the method of measurement used in this study; perhaps a higher magnification, the analysis of a greater number of fibres or the use of electron micrograph montages to include more large fibres which often spanned the photographic borders and were therefore excluded, would highlight a difference.

Optic nerves in *hsh* are relatively less severely hypomyelinated than spinal cord ventral columns. The reason for this is open to conjecture but could possibly relate to differences in axonal size or times of myelination between the two regions. The optic nerve is composed mainly of small, late myelinating axons, while the spinal cord comprises fibres of various diameters which myelinate at different times. However, comparison with spinal cord dorsal columns makes these explanations unlikely; optic nerves and dorsal column corticospinal tracts both contain a similar population of small axons that myelinate relatively late in development, yet the corticospinal tracts appear to be as severely hypomyelinated as the ventral columns on visual examination at appropriate ages. An alternative explanation is that the *hsh* mutation involves a gene which is more significant in the function of oligodendrocytes in the spinal cord than in other CNS regions, regardless of size of glial unit or time of active myelination. The characterisation of the *hsh* product may therefore provide further information on intrinsic and/or environmental factors determining cell heterogeneity, particularly in relation to location within the CNS.

Immunostaining of *hsh* CNS tissue was performed as a quick and straightforward way to assess the presence, location and amount of several known myelin proteins. This served both to further characterise the myelin deficit and to test known myelin genes as candidates prior to identification of a chromosomal locus for the *hsh*

mutation. The complete absence or dramatic reduction of a protein might suggest a causative role for the gene encoding that protein. It has been shown that this is the case in some myelin mutants; for example, *Plp*^{jp} has undetectable PLP/DM-20 (Sorg *et al.*, 1987), as does *md* rat (Yanagisawa *et al.*, 1986) whilst shiverer and its allele do not stain for MBP (Sorg *et al.*, 1987). Often, however, the pleiotropic effects of a mutation mean that the expression of other proteins is also altered as a consequence of the abnormal myelination process (Nave, 1995). In addition, a mutation may not result in lack or absence of a protein but rather, production of an abnormal protein. Therefore reduced protein levels cannot be taken as definitive proof of a mutation in the encoding gene and near normal protein levels do not necessarily indicate a normal gene, although these may be useful gauges. A further reason for performing MOG immunostaining in particular was the suggestion of genetic linkage of *hsh* to genetic markers on chromosome 17, made early in the study by workers at Harwell (Beechey and Cattanach, 1996). *Mog* lies in the region of apparent linkage (Daubas *et al.*, 1994) and, being the only known myelin gene in the vicinity, was a logical candidate to assess. The positive immunostaining in the cervical cord did not strongly implicate this gene, although *in situ* studies were carried out concomitantly (see *In situ* hybridisation study of myelin-oligodendrocyte glycoprotein, page 146) to investigate gene expression. Later in the mapping study, chromosome 17 was shown not to harbour the *hsh* gene and complete concordance was detected between *hsh* and a region of chromosome 3. This lay close to the map position of one of the two reported *Cnp* genes (Bernier *et al.*, 1988), *Cnp2,* casting this a candidate. The presence of CNP in *hsh* myelin was confirmed using immunostaining, although the two protein isoforms could not be differentiated using the antibody employed. Hence, western blotting was carried out to investigate this further and is discussed in Western blotting for CNP, page 153.

(A)

(B)

Figure 8: PLP/DM20 peroxidase-antiperoxidase immunostaining of paraffin sections from the cervical cord of (A) wild type and (B) *hsh* at P20. There is a reduction in immunoreactivity due to hypomyelination which appears to involve all white matter tracts. (Approx. magnification x50).

(A)

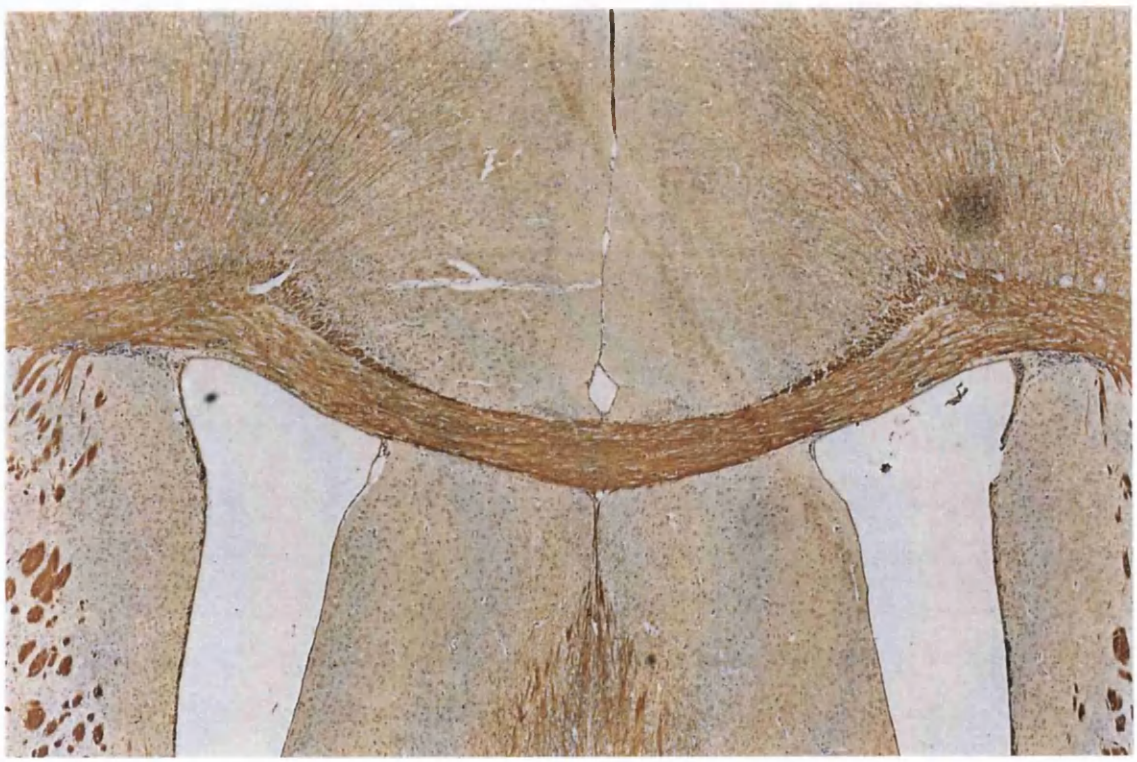

(B)

Figure 9: PLP/DM20 peroxidase-antiperoxidase immunostaining of paraffin sections of the corpus callosum and cingulate gyrus of (A) wild type and (B) *hsh* mice at P20. There is little detectable difference in staining intensity between the two. (Approx. magnification x60).

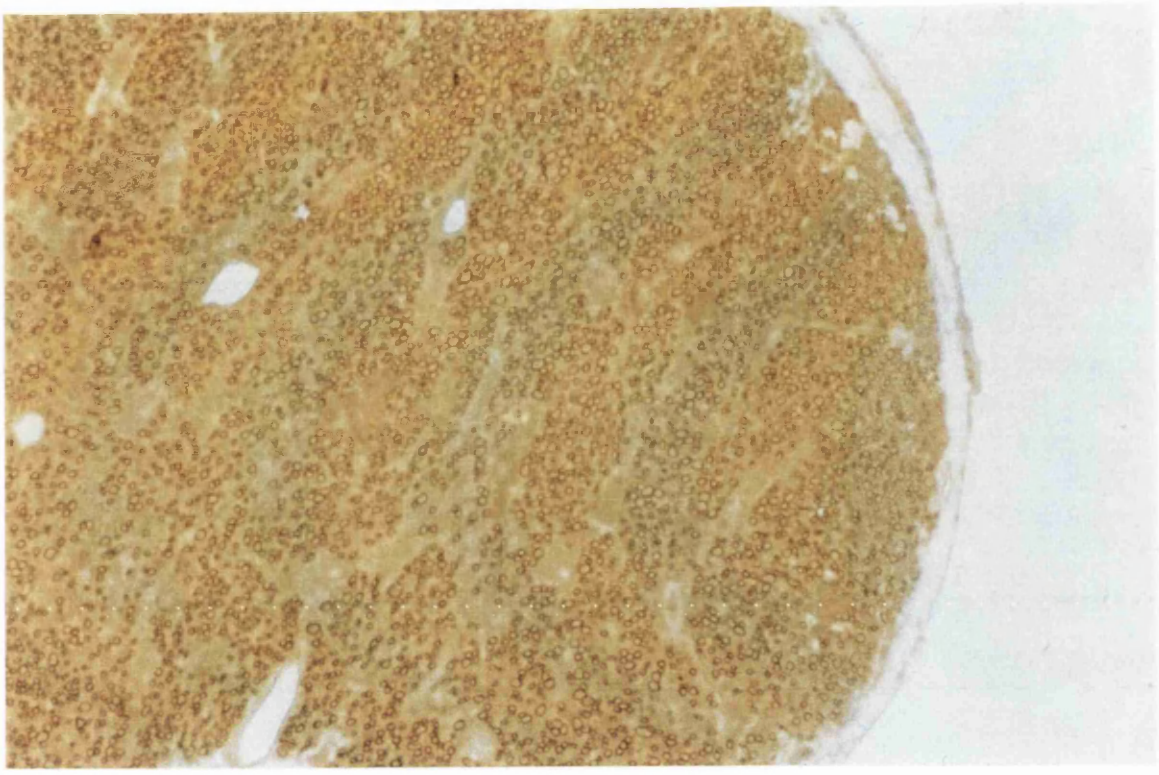

Figure 10: PLP/DM20 peroxidase-antiperoxidase immunostaining of a paraffin section of the optic nerve of a P20 *hsh* animal. Most axons are surrounded by adequate sheaths compared with the spinal cord (Approx. magnification x990).

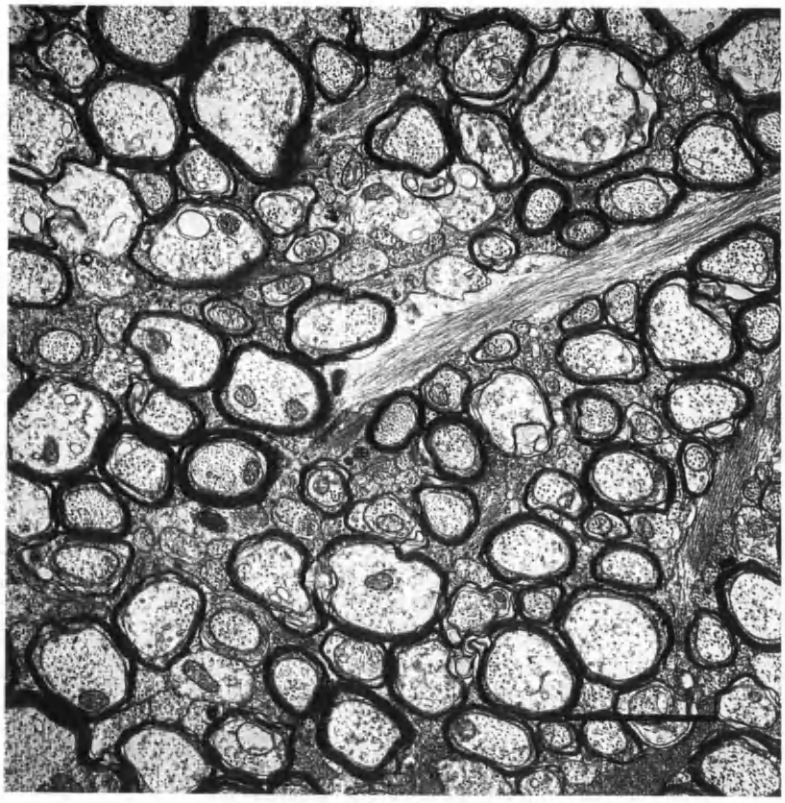

(A)

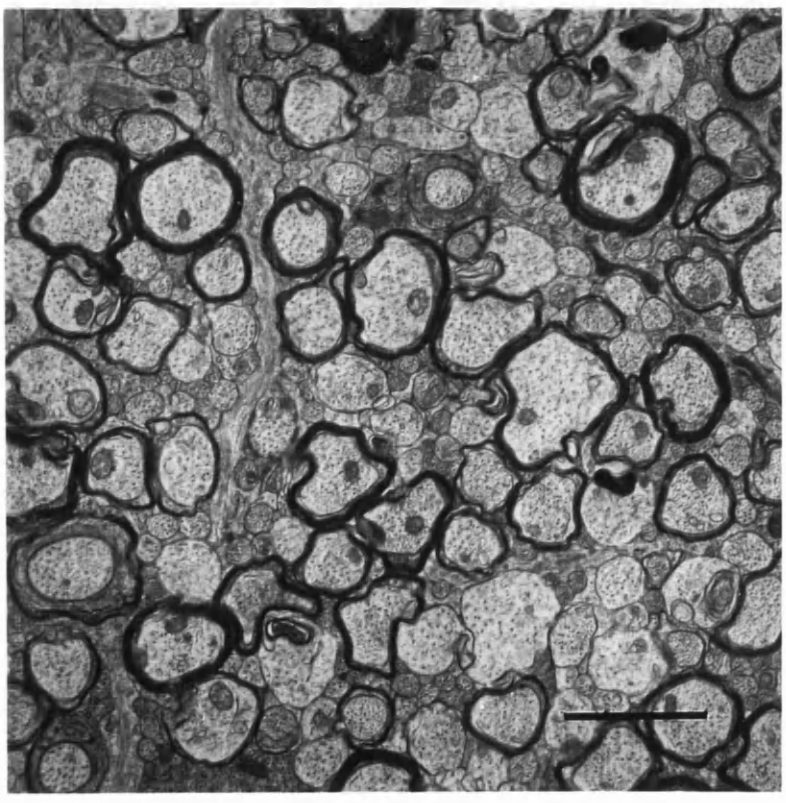

(B)

Figure 11: Optic nerves from (A) wild type and (B) *hsh* mice at P20. This example represents the most marked hypomyelination seen in the optic nerve at this age. Bar = 2μm.

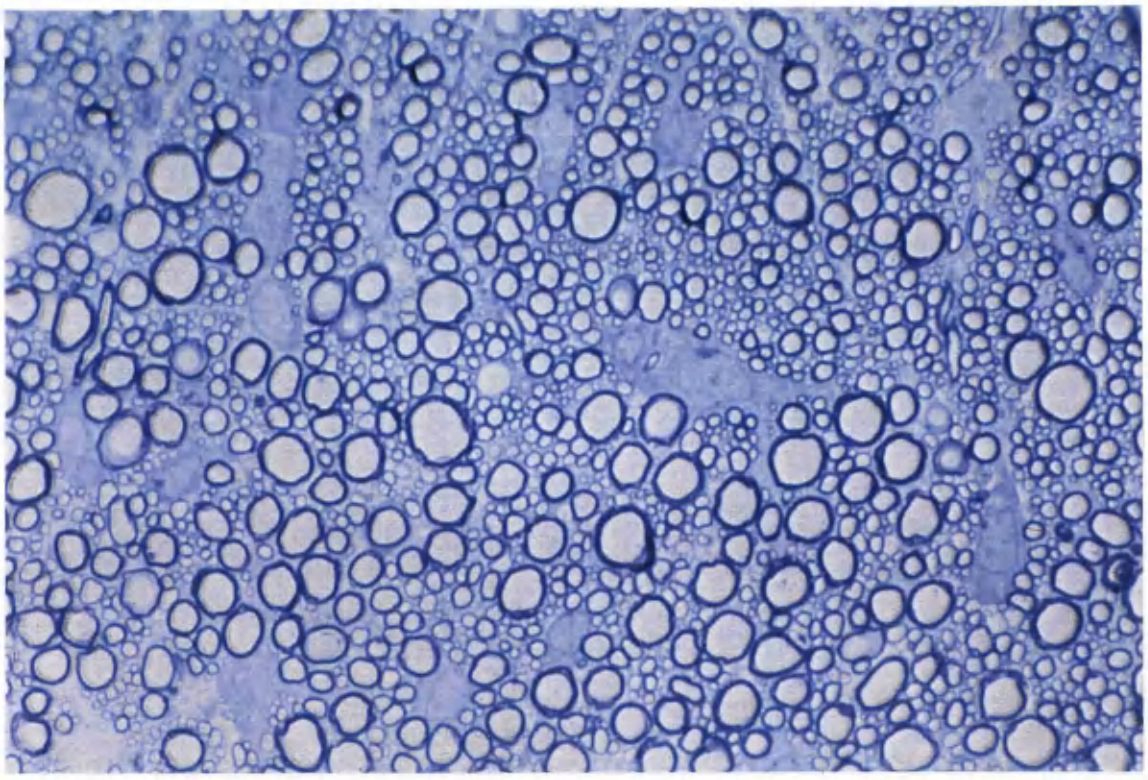

(A)

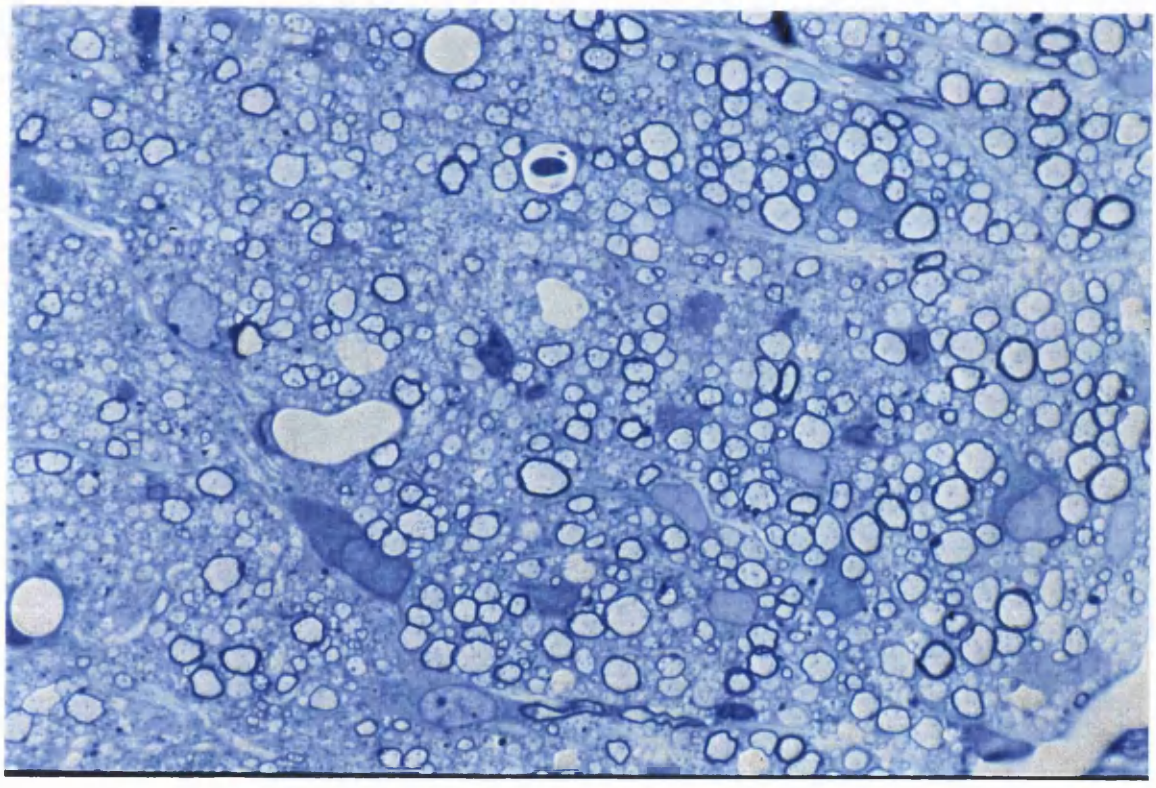

(B)

Figure 12: Areas of ventral spinal cord from P20 (A) wild type and (B) *hsh* mice showing typical hypomyelination with a mixture of thinly myelinated and amyelinated axons. (Approx. magnification x1500).

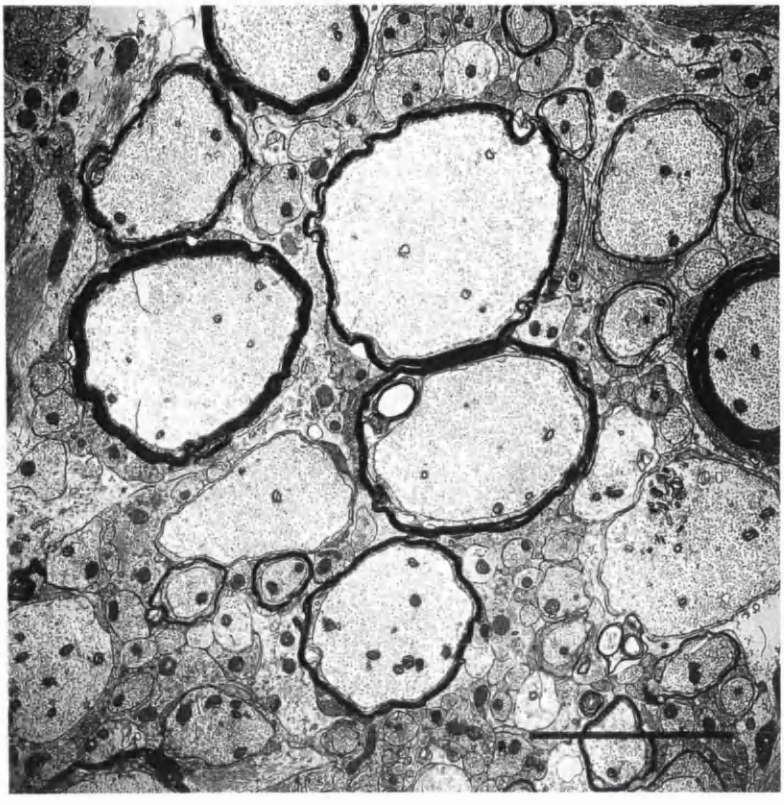

Figure 13: Area of ventral spinal cord from P20 *hsh* mouse showing hypomyelination with a mixture of thinly myelinated and amyelinated axons. The myelin present is well compacted. Bar = 4μm.

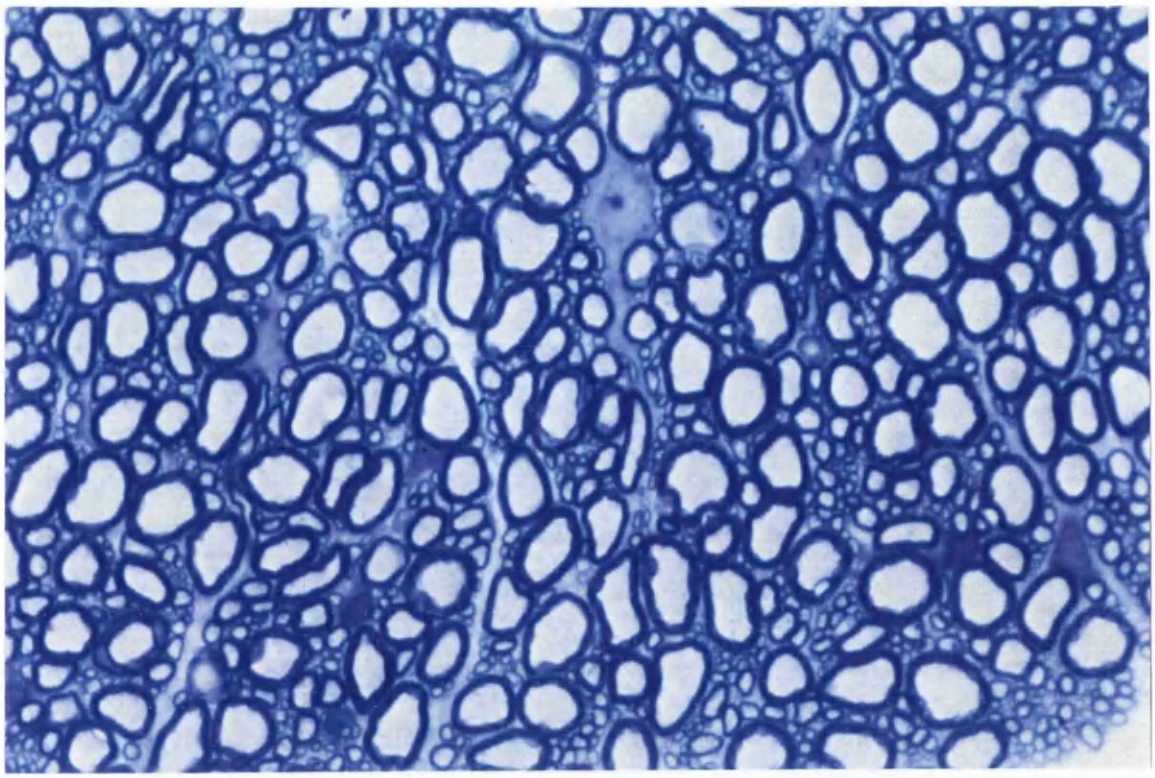

(A)

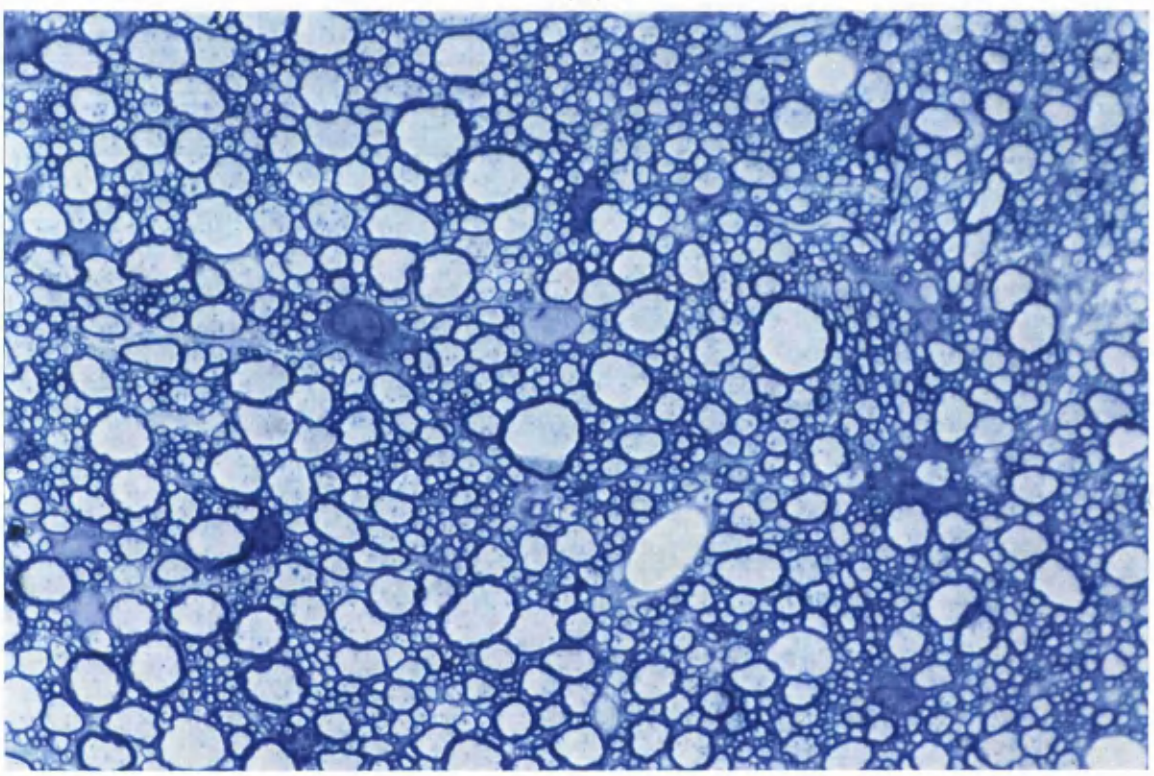

(B)

Figure 14: Area of ventral cervical spinal cord from P100 (A) wild type and (B) *hsh* showing that although most axons are now myelinated, the sheaths of both large and small axons are disproportionately thin. (Approx. magnification x1500).

(A)

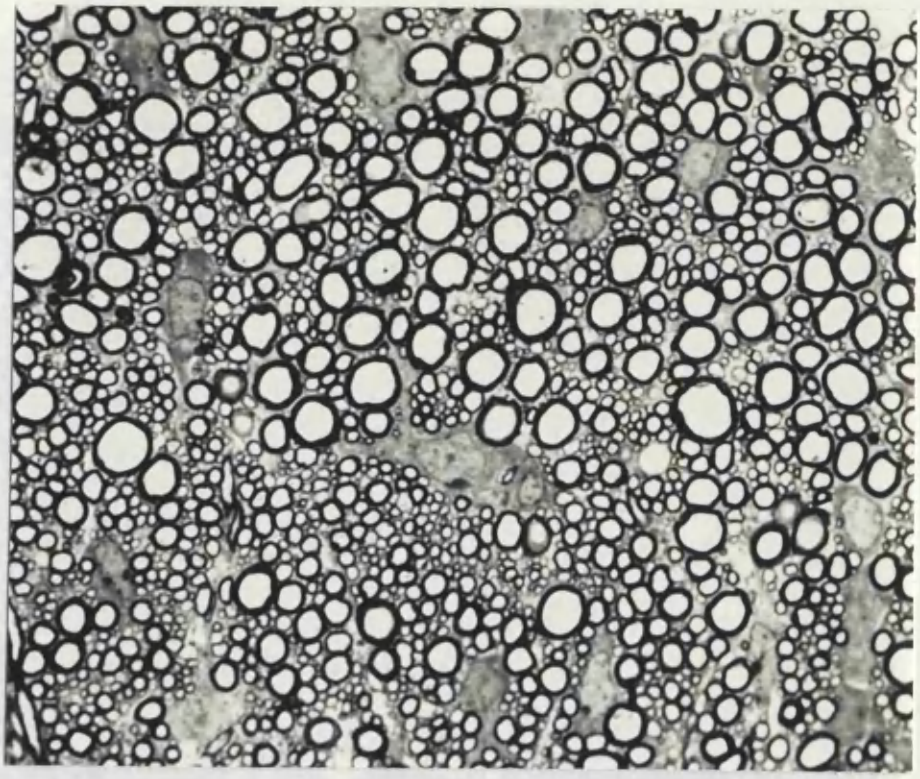

(B)

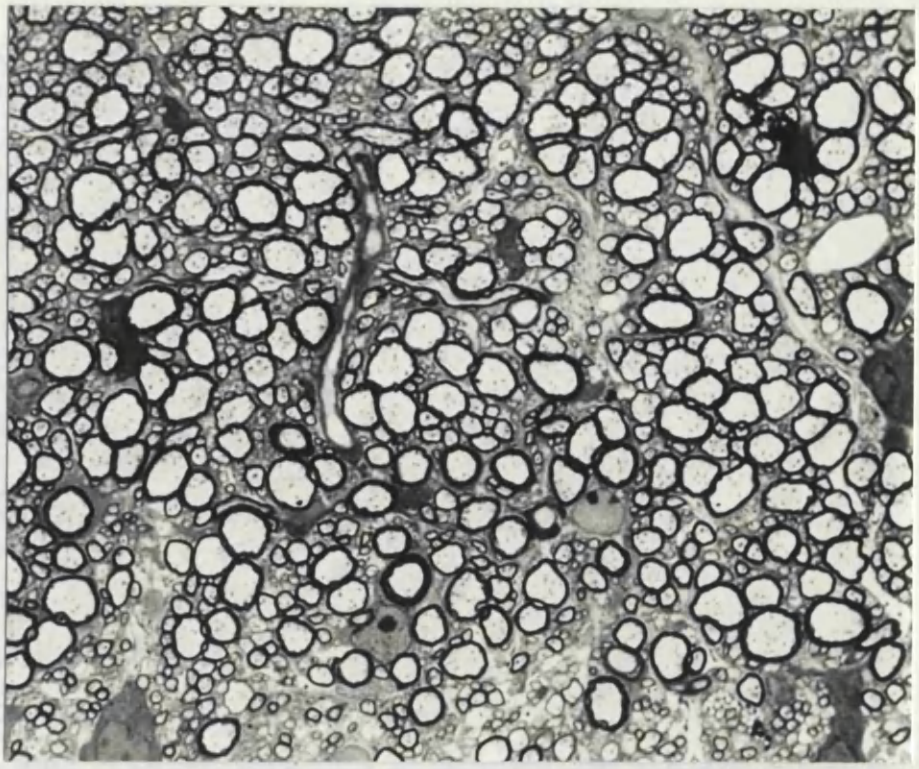

Figure 15: Areas from the ventral cervical cord of P20 (A) wild type and (B-D) *hsh* mice to show variation in phenotype. B-D are littermates and show a progressive increase in the myelin defect which reflected the intensity of the tremor. The mouse in B was phenotypically virtually normal, having only a slightly stilted gait, and shows slightly thinner sheaths than wild type with only an occasional naked axon. (Approx. magnification x1100).

(C)

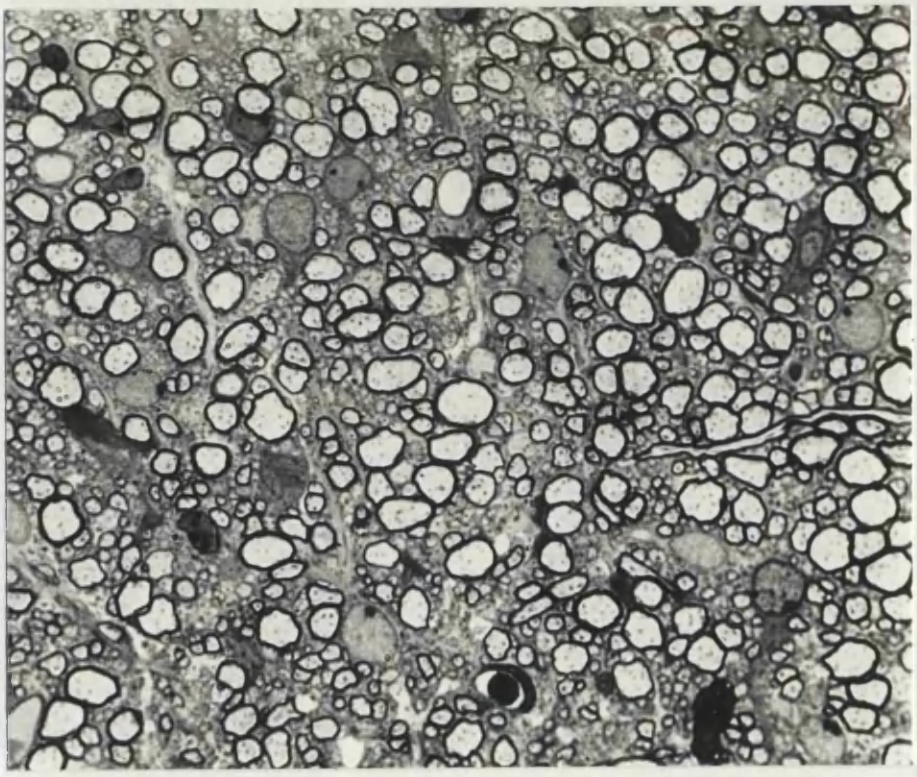

(D)

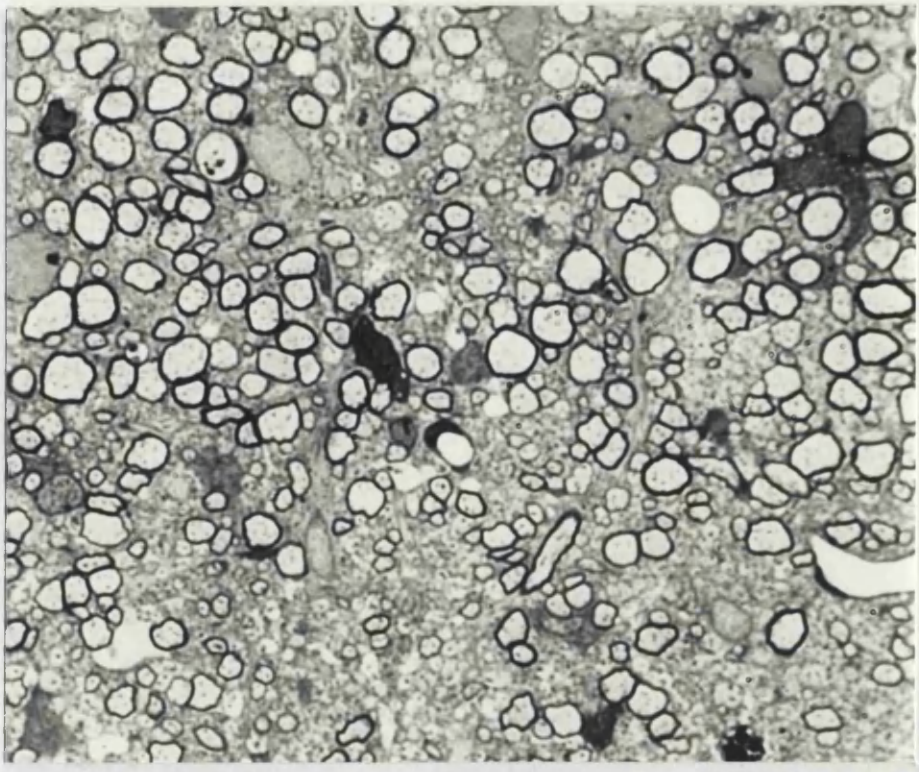

Figure 15 (cont.) Areas from the ventral cervical cord of P20 *hsh* mice to show variation in phenotype. The mouse in C showed a tremor when ambulating and has more naked axons. The most severe phenotype, with a tremor at rest, is seen in D where many axons lack a myelin sheath. (Approx. magnification x1100).

(A)

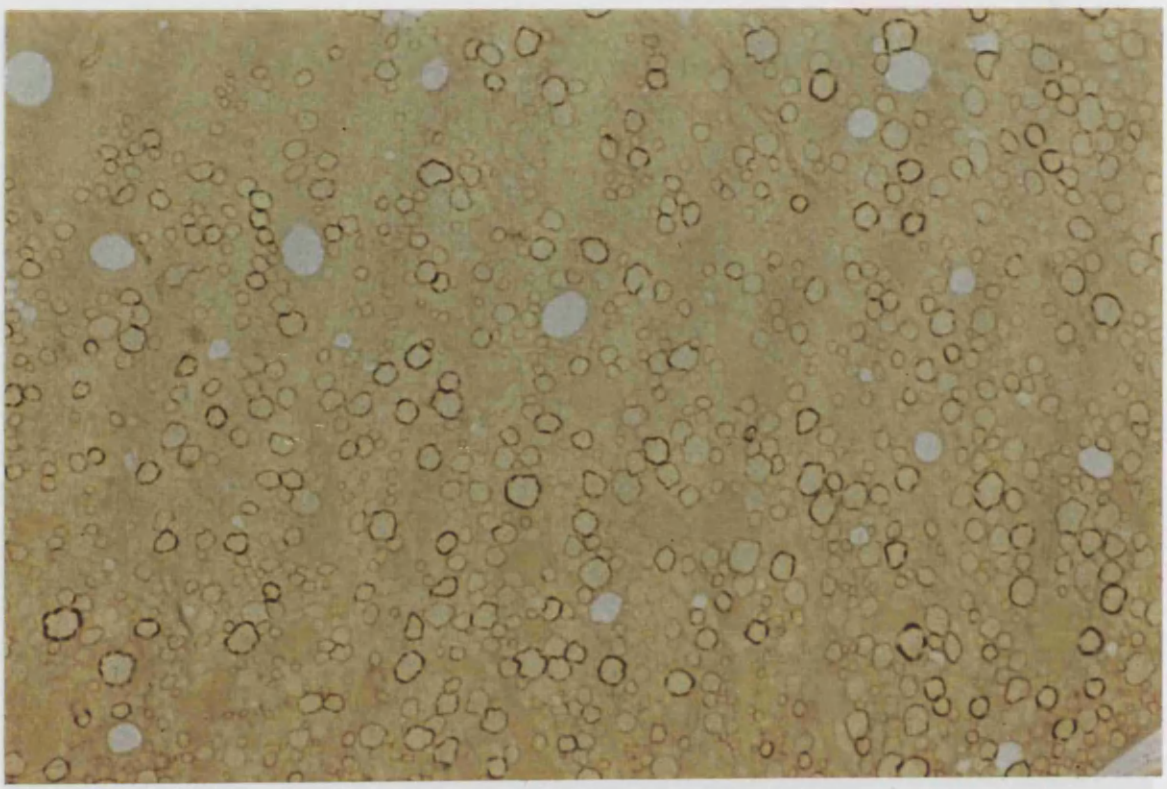

(B)

Figure 16: PLP/DM20 peroxidase antiperoxidase immunostaining of the cervical spinal cord ventral white matter of a P20 mutant animal. The majority of the myelin sheaths are associated with larger fibres. (Approx. magnifications (A) x110. (B) x990).

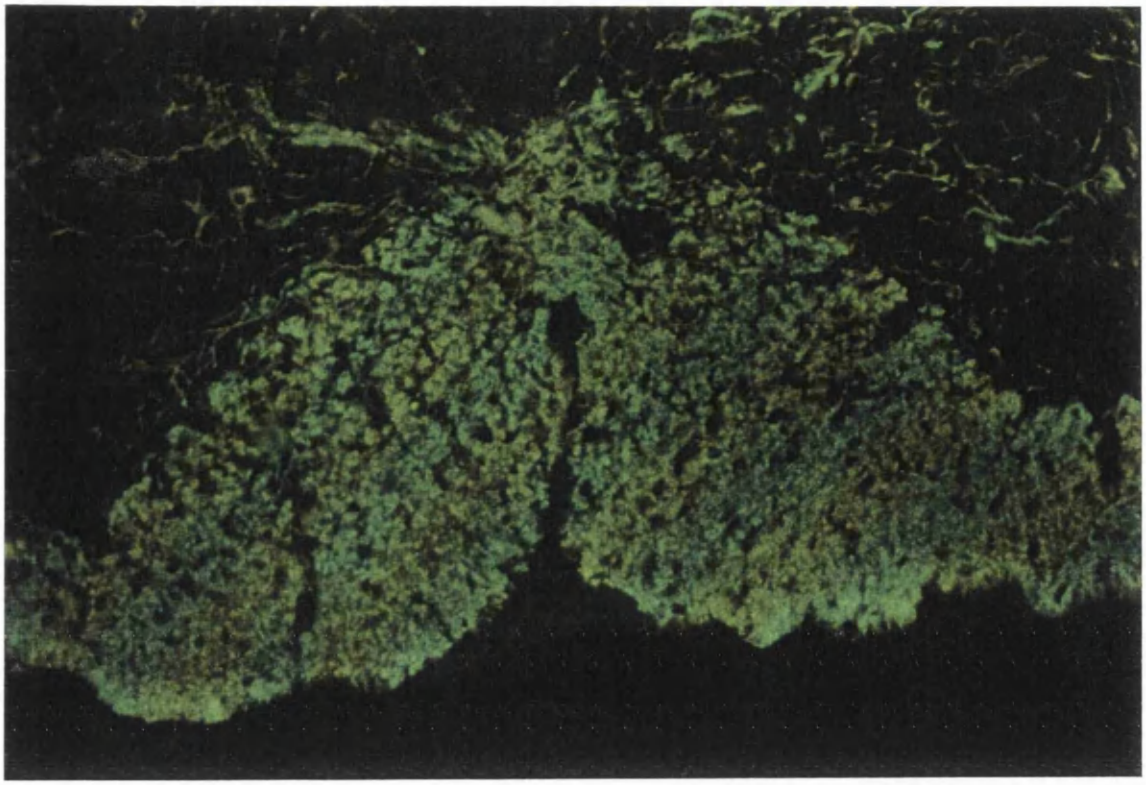

(A)

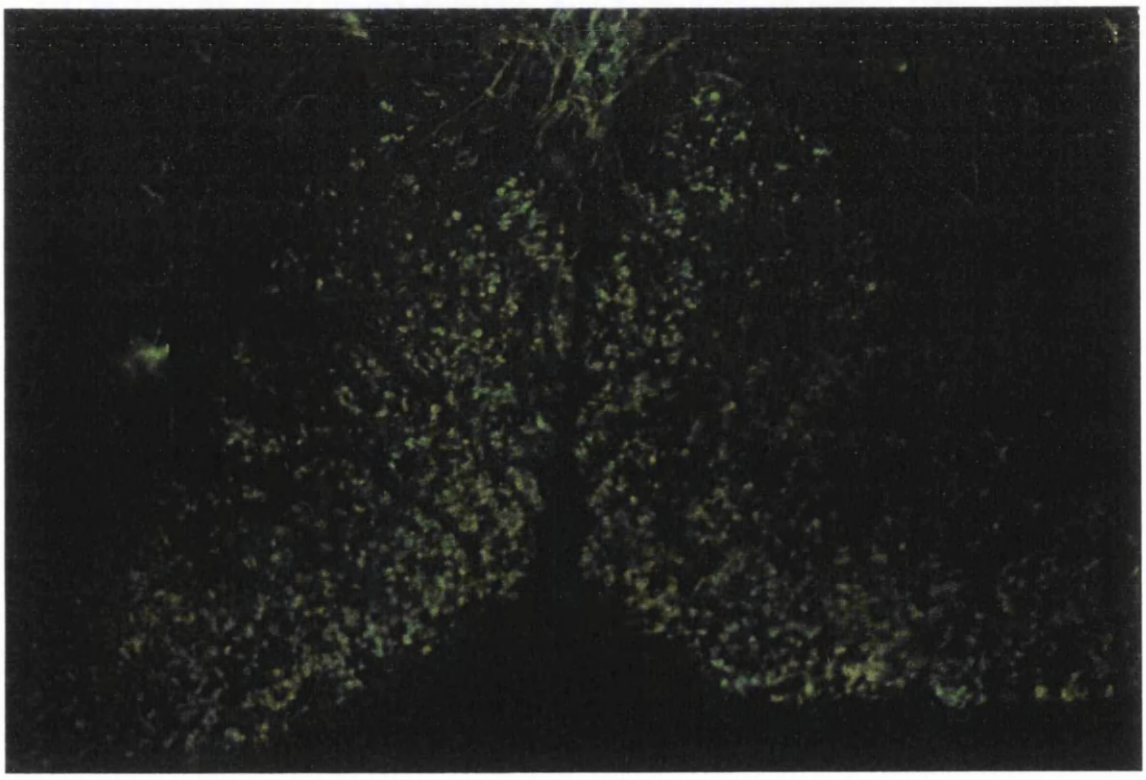

(B)

Figure 17: Immunofluorescent staining for MAG on cryosections from the cervical spinal cord ventral white matter of P20 (A) wild type and (B) *hsh* animals. There is an obvious reduction in the number of positive staining sheaths. (Approx. magnification x400).

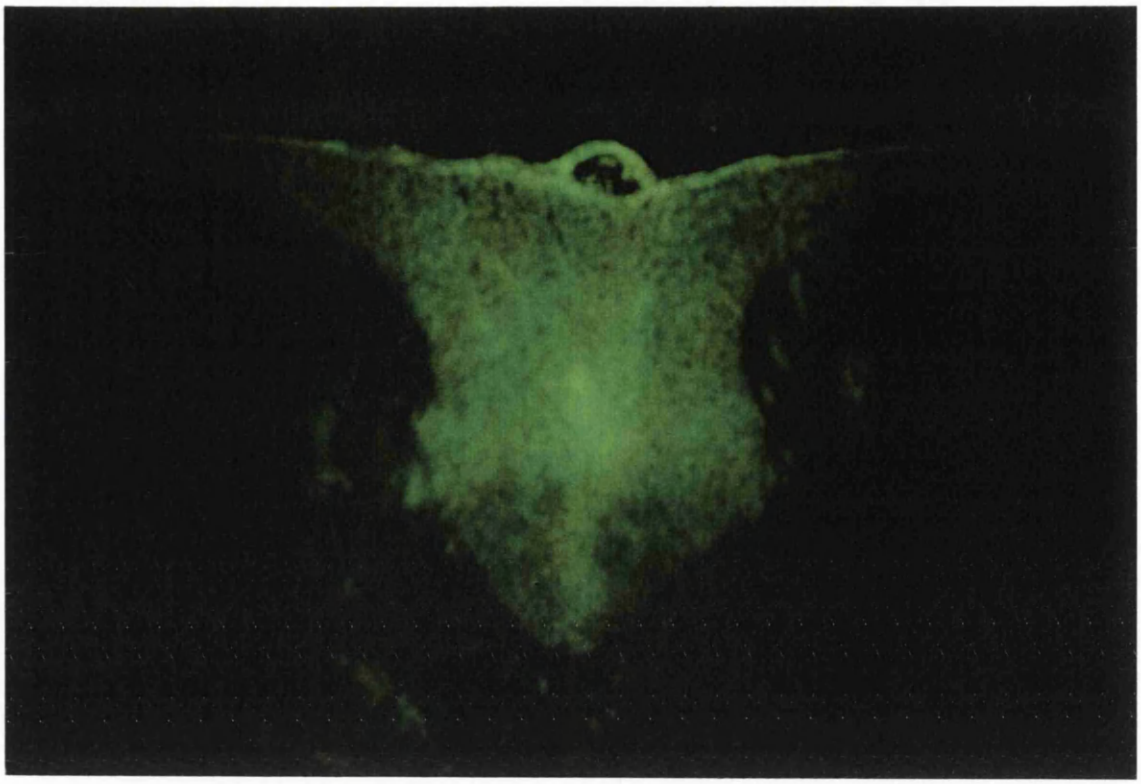

(A)

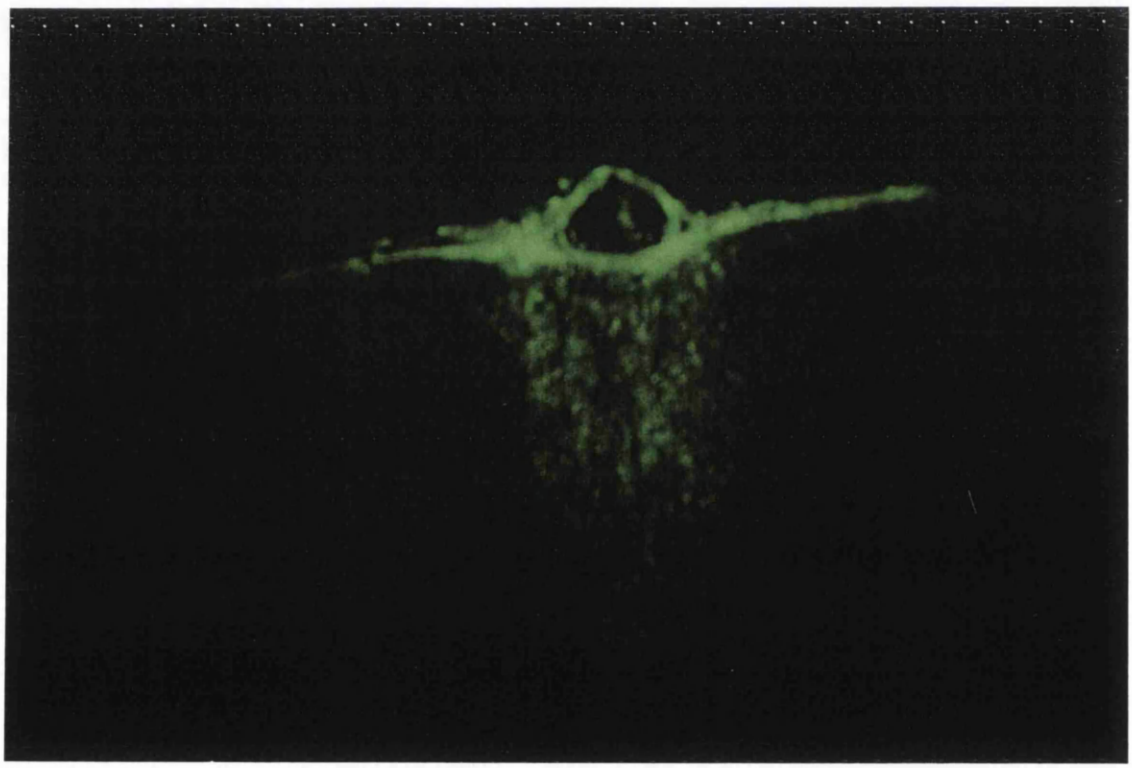

(B)

Figure 18: Immunofluorescent staining for MOBP on cryosections from the cervical spinal cord dorsal columns of P20 (A) wild type and (B) *hsh* animals. There is a marked reduction in the intensity of staining in the mutant. (Approx. magnification x400).

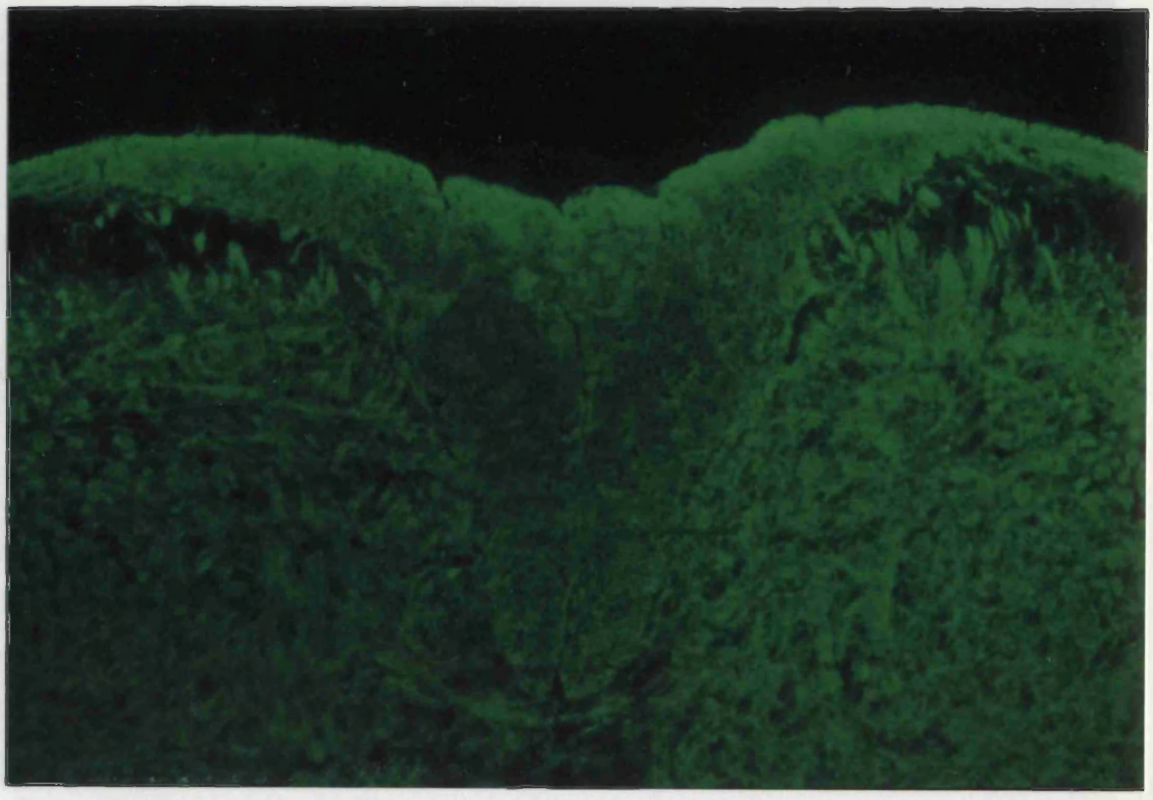

(A)

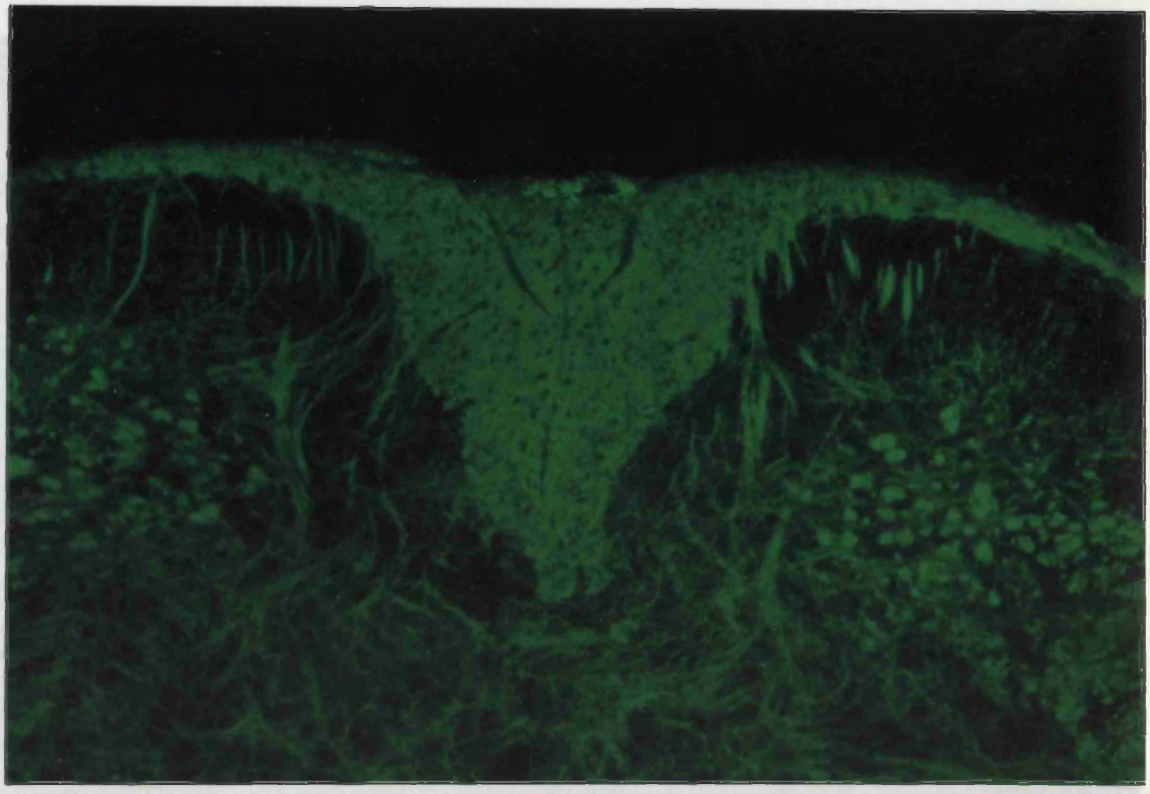

(B)

Figure 19: Immunofluorescent staining for MOG on cryosections from the cervical spinal cord dorsal columns of P20 (A) wild type and (B) *hsh* animals. Staining intensity is bright in the mutant. The area of reduced staining intensity in wild type is probably an artefact. (Approx. magnification x400).

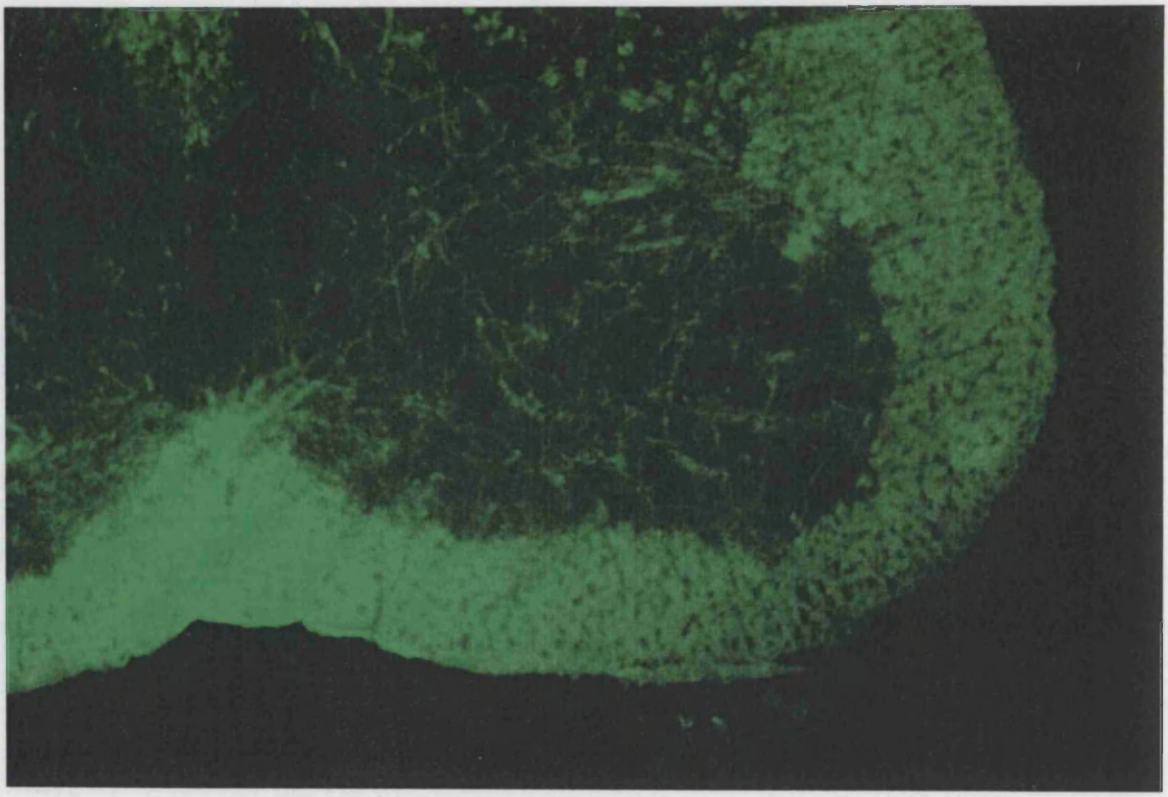

(A)

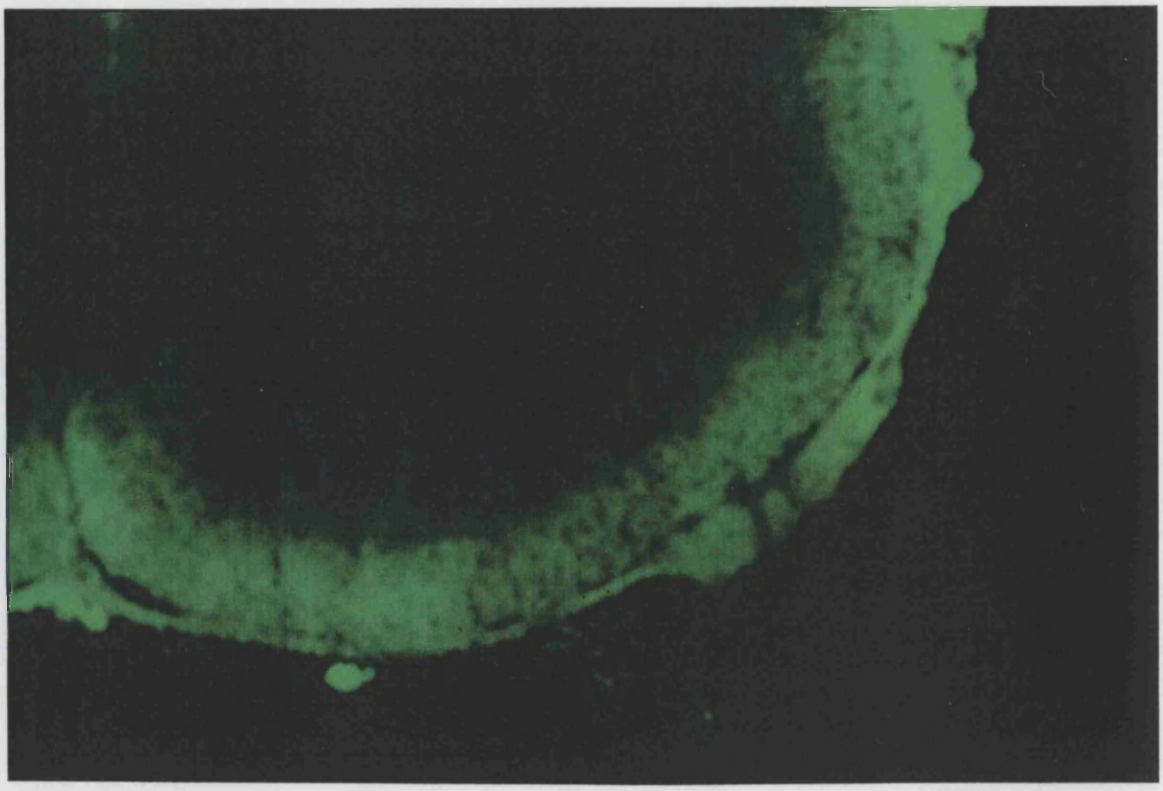

(B)

Figure 20: Immunofluorescent staining for CNP on cryosections from the cervical spinal cord ventral white matter of P20 (A) wild type and (B) *hsh* animals. Staining is reduced in the white and grey matter of the mutant. (Approx. magnification x400).

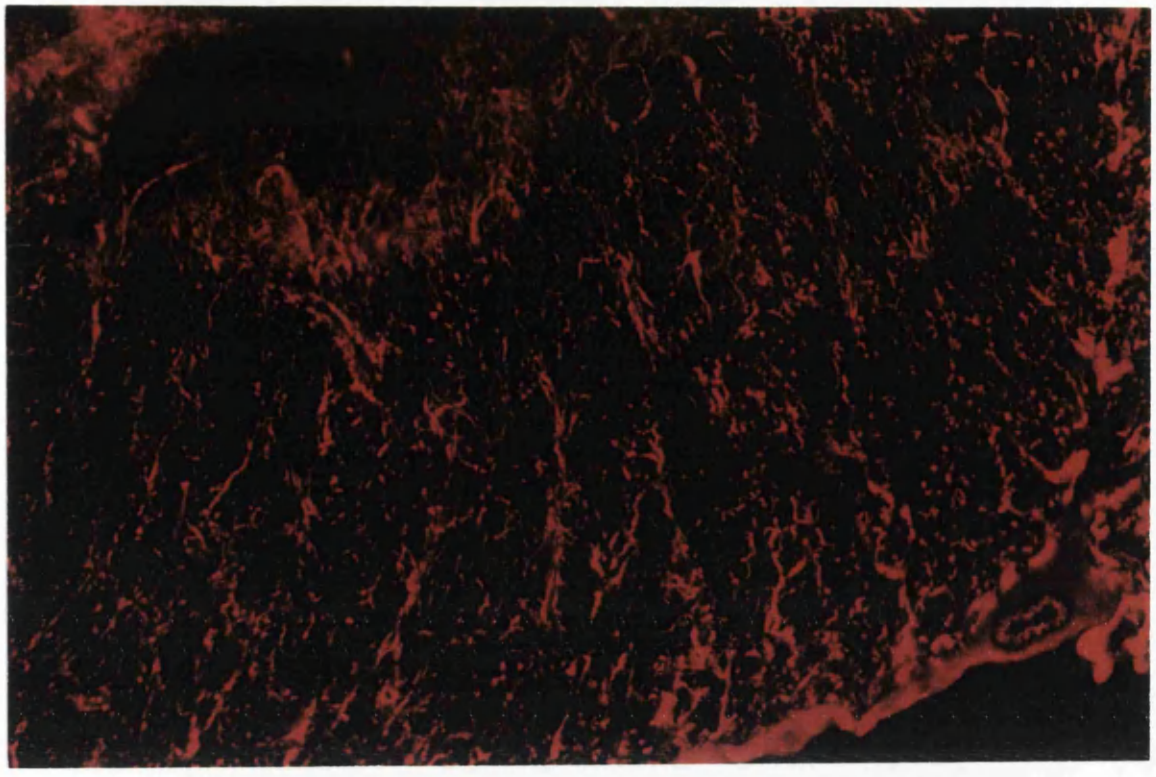

(A)

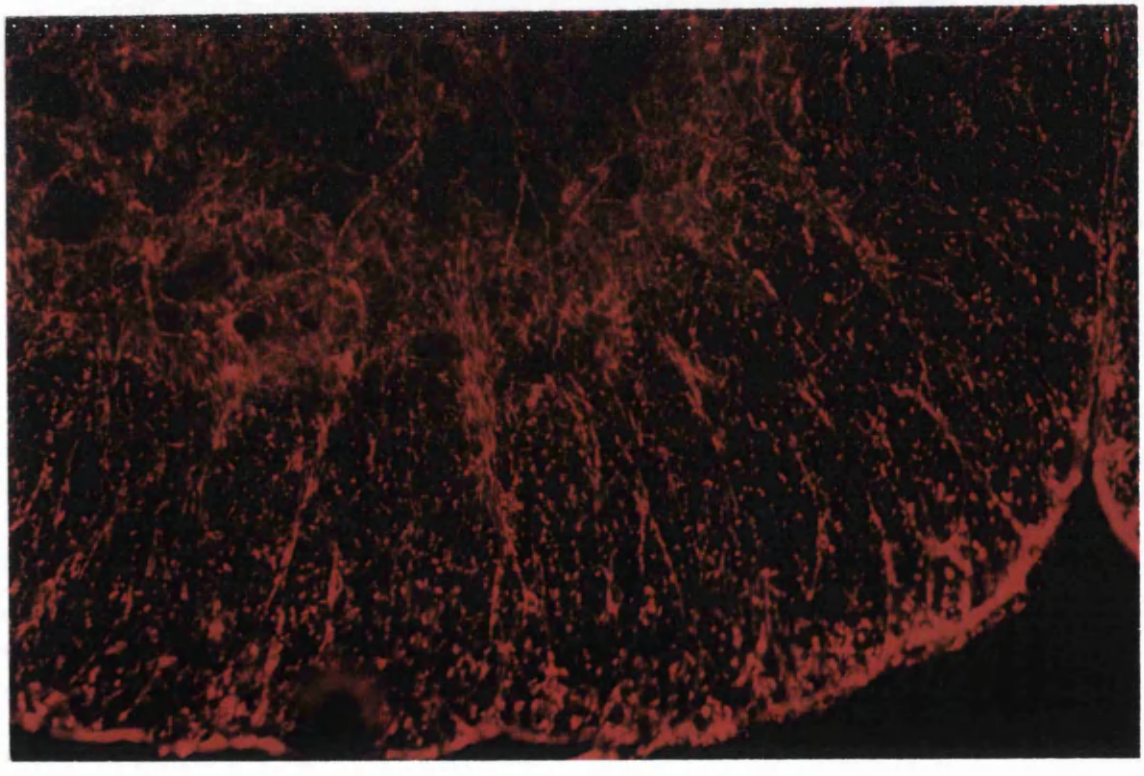

(B)

Figure 21: Immunofluorescent staining for GFAP on cryosections from the cervical spinal cord ventral white matter of P20 (A) wild type and (B) *hsh* animals. There is a reduced amount of white matter in the mutant with an increased intensity of staining. (Approx. magnification x500).

A)

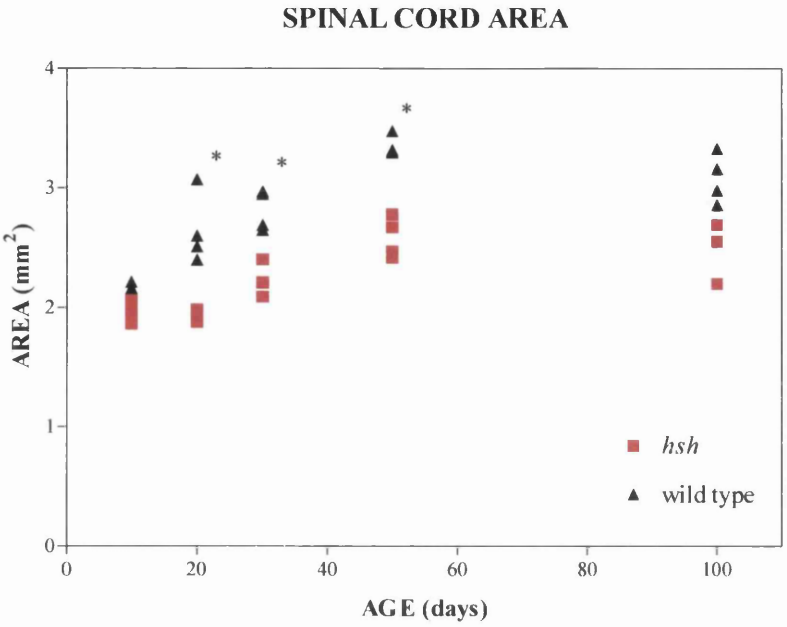

B)

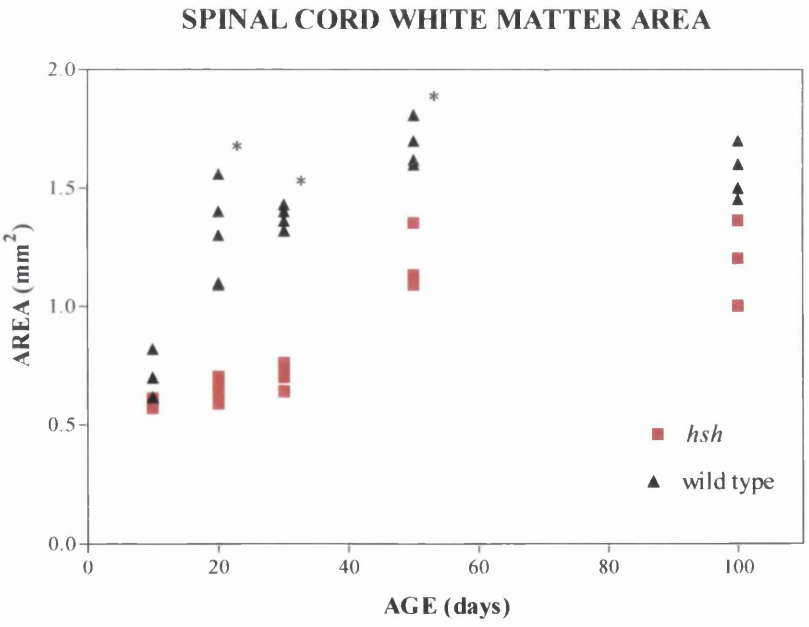

Figure 22: Graphs showing (A) Total areas of transverse sections of cervical spinal cord of wild type and mutant animals and (B) Areas of white matter only from the same sections. The deficit in white matter, a consequence of hypomyelination, is evident in *hsh* animals. Significant differences are marked with *.

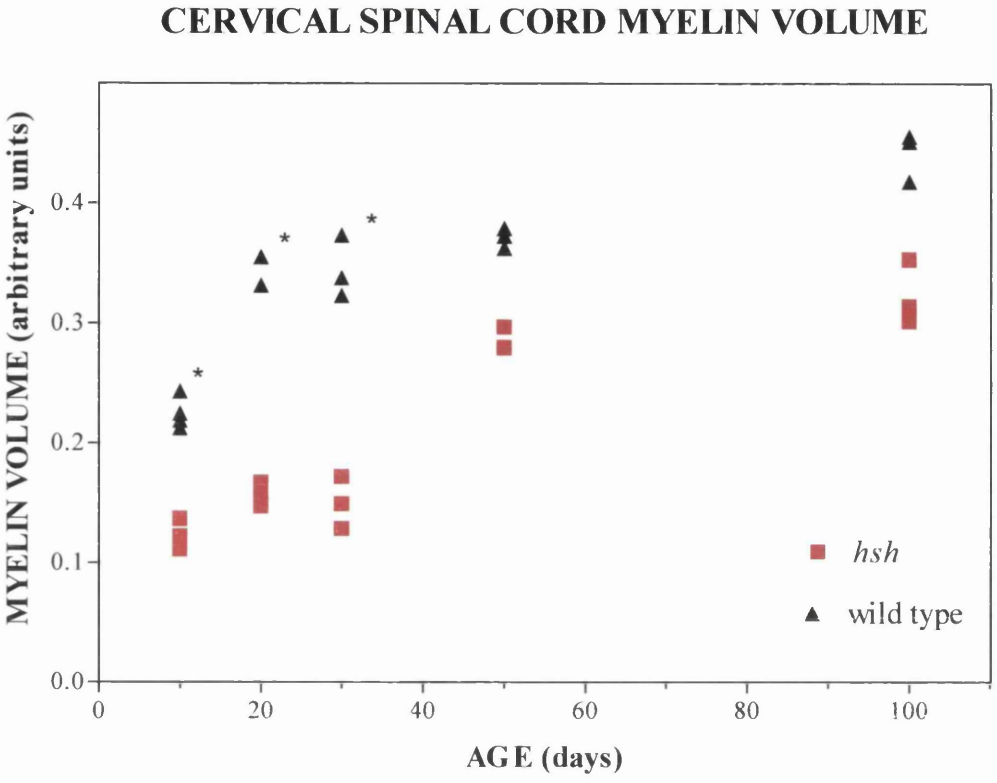

Figure 23: Myelin volumes in ventral columns of cervical spinal cord of wild type and mutant mice. Three to four mice were recorded for both groups at each age and shown as individual points. The myelin deficit is maximal at P20-P30 and partially resolves in the older animals. Significant differences are indicated by *.

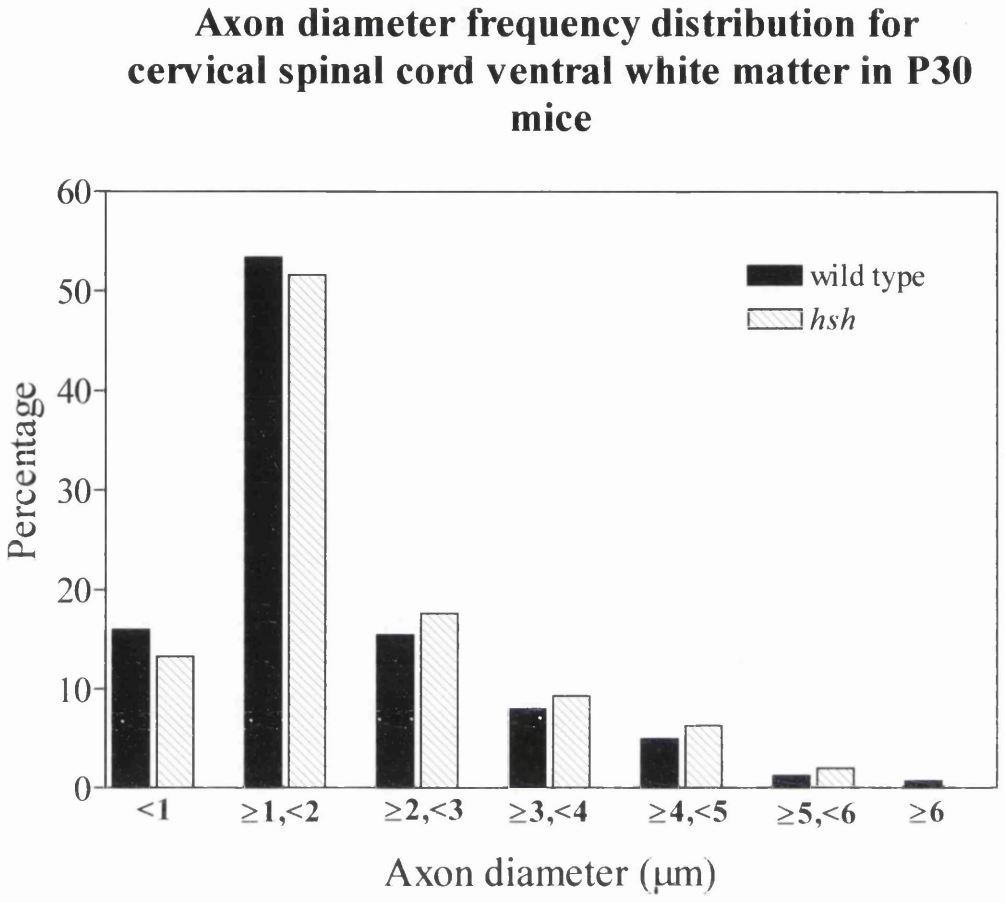

Figure 24: Axon diameter frequency distributions for cervical spinal cord ventral white matter in P30 wild type (n = 2) and *hsh* (n = 3) mice. Measurements from mice in each group were pooled. Both myelinated and unmyelinated axons are included. The distribution is similar.

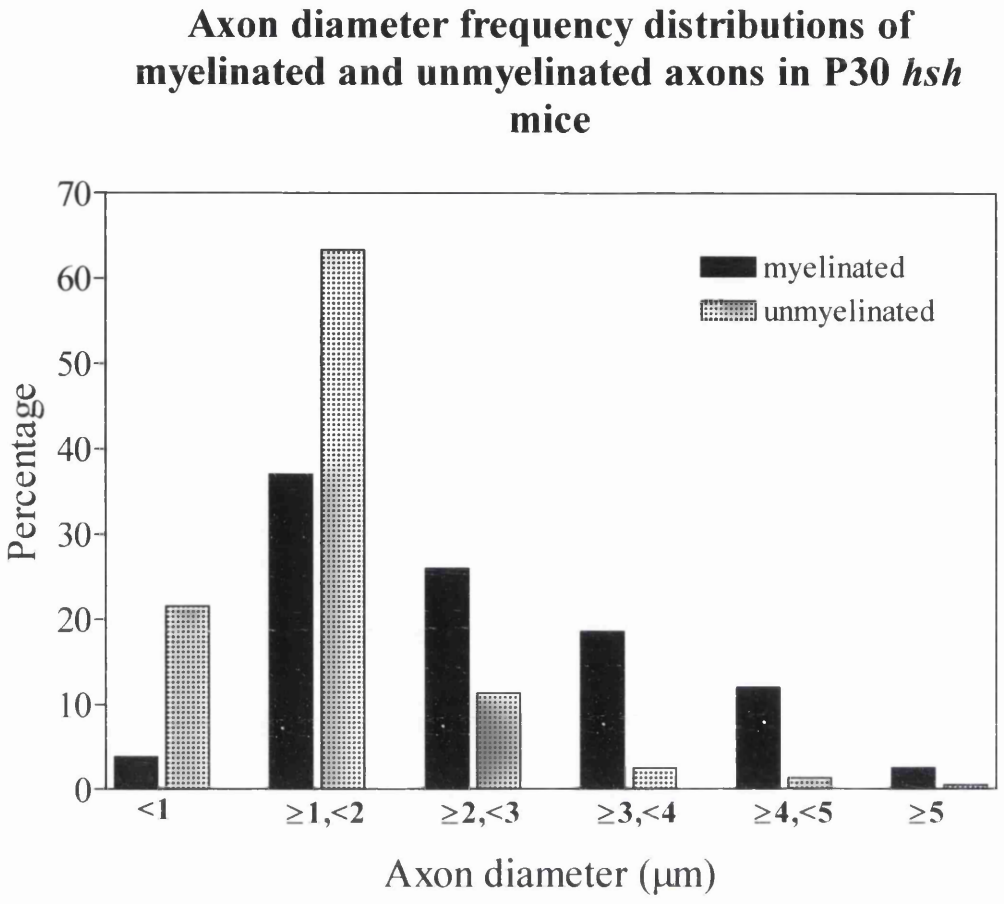

Figure 25: Axon diameter frequency distributions of myelinated and unmyelinated axons in the cervical spinal cord ventral columns of P30 *hsh* mice (n = 3). A larger proportion of small diameter axons are unmyelinated compared with bigger fibres.

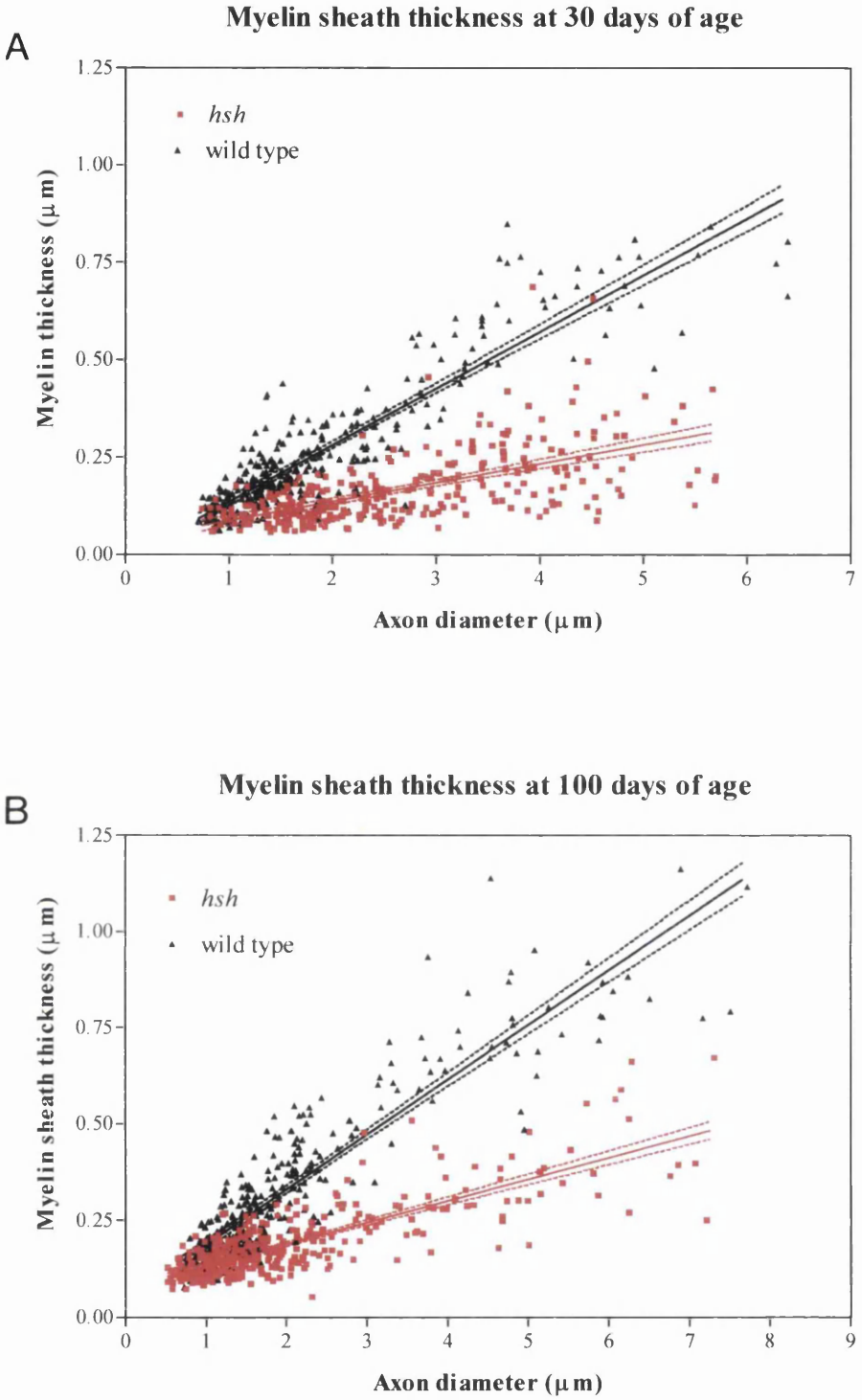

Figure 26: Myelin sheath thickness in wild type and *hsh* mice at (A) P30 and (B) P100. Most axons in mutant animals possess a disproportionately thin sheath compared with wild type animals. Sheaths are thicker by P100. Fibres are plotted as individual points and the linear regression line for each group is shown.

A)

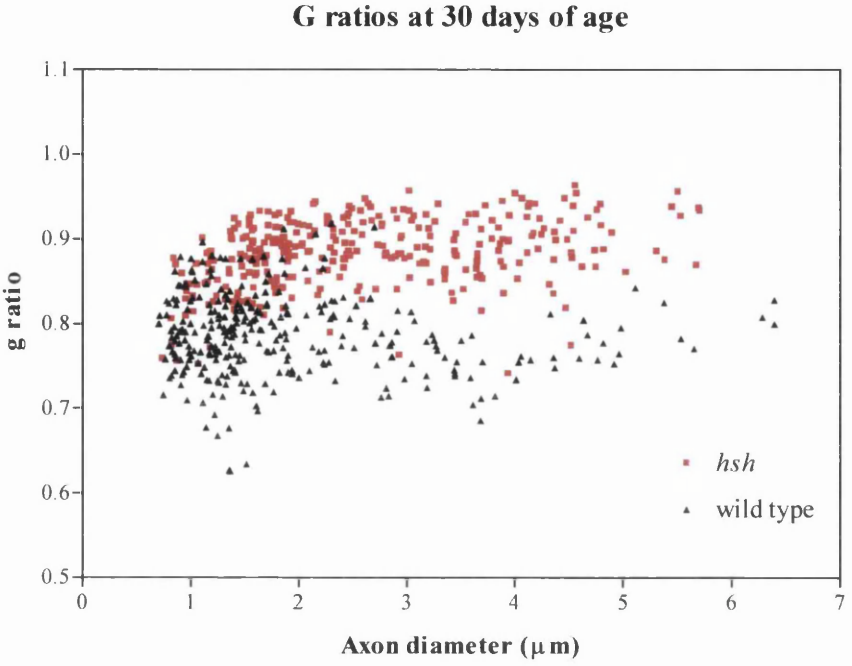

B)

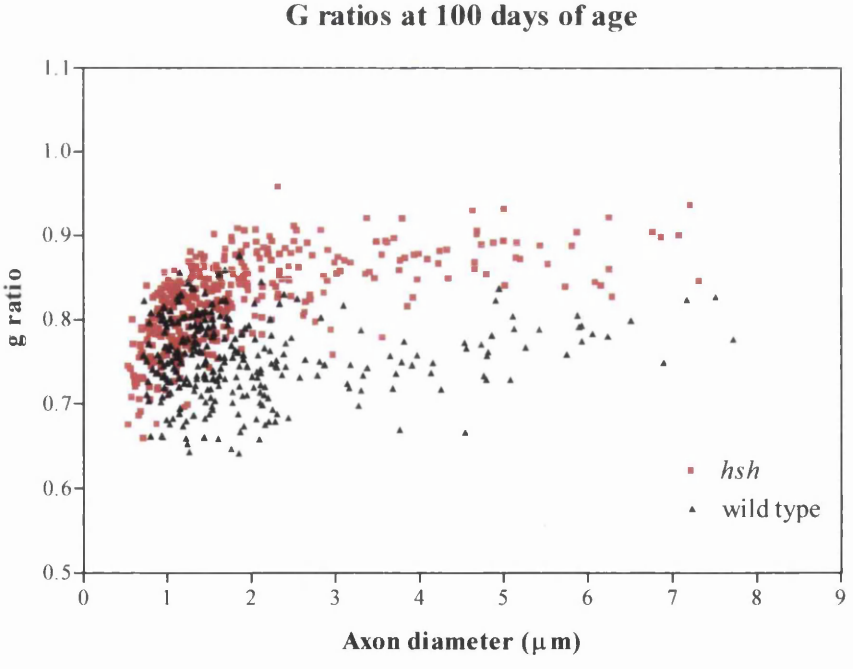

Figure 27: G ratios for wild type and *hsh* mice at (A) P30 and (B) P100. At P30, the higher *g* ratios for the majority of axons in mutant mice indicates that most sheaths are disproportionately thin. By P100, *g* ratios are reduced in mutants. Many small fibres now have *g* ratios comparable to fibres of the same diameter in wild type mice.

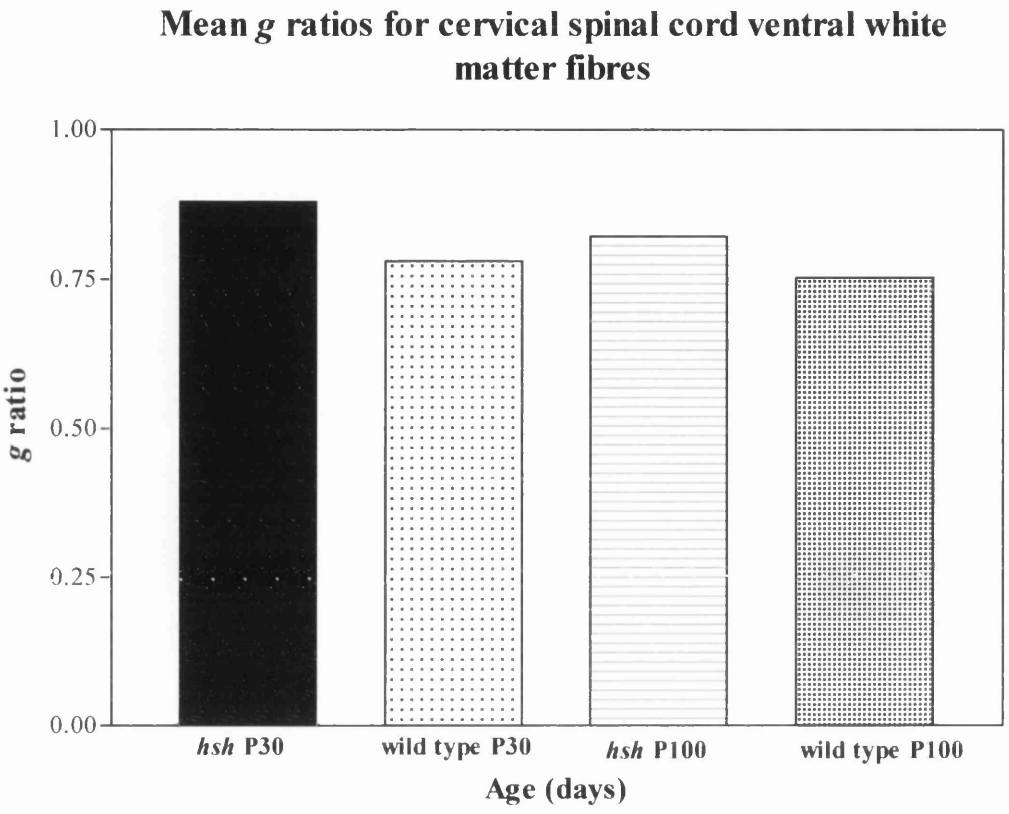

Figure 28: Mean *g* ratios for wild type and mutant mice at P30 and P100. The higher ratio in *hsh* indicates the sheaths are disproportionately thin. An improvement occurs with age and by P100, the *g* ratio is reduced, although still greater than in the equivalent wild type.

3.5 Glial cell morphology and quantification

3.5.1 Introduction and aims

Hypomyelination may be due to the presence of inadequate numbers of oligodendrocytes, appropriate numbers but insufficient myelinating function of these cells or a combination of both. Quantification and scrutiny of oligodendrocytes in affected regions may infer which of these is the basis of the myelin defect. Gross deficits in cell numbers can be measured and ultrastructural abnormalities may suggest a functional impairment. Mutations may also have effects on other glial cells, either directly or as a response to abnormal myelination. Thus, analysis of astrocytes and microglia may shed further light on the basis and consequences of the mutation. The aim in this part of the study was to investigate the effect of the *hsh* mutation on glial cell biology in terms of their distribution, absolute and relative numbers and their ultrastructural appearance.

3.5.2 Materials and Methods

3.5.2.1 Preparation of tissue

Tissue was resin embedded for glial cell quantification and ultrastructural analysis (Resin processing and sectioning, page 46). Cryosections were prepared as described in Cryopreservation and sectioning, page 47 for ISH while sections for F4/80 microglial specific staining were prepared as described in Periodate-lysine-paraformaldehyde (PLP) fixative, page 45.

3.5.2.2 Glial cell quantification

Total and differential glial cell counts were performed on ventral white matter in cervical cord sections from mutant and wild type mice at P10, 20, 30, 50 and P100 as described (Quantification of glia, page 48). Three mice of each phenotype were used at P10 and P100 whilst 4 to 6 mice were used at the intervening ages. Classification of cell types was based on nuclear and cytoplasmic morphology with cells being categorised as oligodendrocytes, astrocytes or 'other', which included microglia and cells of indeterminate class. The Mann Whitney t test was used for statistical analysis. The methodology for dead cell quantification is given in Dead cell density, page 48.

3.5.2.3 Immunostaining for microglia

The microglial population was further investigated qualitatively in the cervical cord at P20 and P50 using immunostaining for F4/80. The protocol is given in F4/80 immunocytochemistry, page 53.

3.5.2.4 Ultrastructure of glial cells

Ultrastructural analysis of glial cells was performed on EM photographs of the cervical cord ventral columns from P10, 20, 30, 50 and P100 mice at 7500 to 15000 times magnification.

3.5.2.5 *In situ* hybridisation

In situ hybridisation was employed in this study as an independent technique for qualitative assessment of the numbers and distribution of oligodendrocytes that did not rely on morphological critera. Experiments were performed using a probe for *Plp-1* on sections of cervical, thoracic and lumbar cord, forebrain and cerebellum at P5, 10, 15, 20, 30 and P50. This recognises both *Plp* and *Dm20.* A probe for *Ugt8* was used on cervical cord sections at P5, P10 and P20. The ISH technique is described in *In situ* hybridisation, page 60.

3.5.3 Results

3.5.3.1 Histological studies

The observed distribution of *hsh* oligodendrocytes in the spinal cord white matter appeared identical to wild type. There was a significant increase in total glial cell density at P20 ($p = 0.0043$), P30 ($p = 0.0079$) and P50 ($p = 0.0286$) in comparison with wild type, but by P100 values were very similar ($p = 0.2286$) (Figure 29, page 126). With compensation for the reduced amount of white matter, there was actually a slight decrease in total glial numbers up to P50 (Figure 29, page 126). Significant differences were found at P20 and P30 ($p = 0.0043$ for both).

The reduction in total glial numbers appeared to be due to a decrease in the number of oligodendrocytes which showed significant differences between *hsh* and wild type at P20 and P30 ($p = 0.0043$ for both). There was little alteration in astrocyte numbers (Figure 30, page 127) or 'other' cell types (Figure 31, page 128). The maximum cell deficit occurred at P20 when oligodendrocyte numbers were about 60% of wild type values. Between P30 and P50, oligodendrocyte numbers increased so that by P50, they were virtually identical to wild type .

No obvious morphological abnormalities were found in *hsh* glial cells on resin sections but there was the impression of a greater proportion of "light" oligodendrocytes at P10 and P20, implying a delay in maturation. Examination of EM photographs revealed ultrastructurally unremarkable oligodendrocytes with no obvious maturational delay (Figure 32, page 129). No astrocytic abnormalities were apparent.

On visual examination of spinal cord ventral white matter on thick resin sections, microglial cells appeared subjectively more numerous in mutant animals of all ages than in wild type. Immunostaining with F4/80 at P20 (Figure 33, page 130) and P50 (Figure 34, page 131) confirmed the increased microglial cell density. Morphological quantification indicated no increase in the total number of microglia and unclassified cells at P20 but at P50, elevated cell numbers were detected (Figure 31, page 128) with about twice as many cells in *hsh* sections. On EM photographs, the majority of cells classified as microglia were unremarkable, although the occasional cell contained multiple cytoplasmic vacuoles with wispy membranous inclusions (Figure 35, page 132).

There was no increase in the number of pyknotic nuclei in *hsh* white matter, with only 2-3 cells identified in each section up to P20-P30. After this time, very few pyknotic nuclei were seen in either *hsh* or wild type cords.

3.5.3.2 *In situ* studies

A probe for *Plp/Dm20* message isoforms suggested the distribution of hybridising cells was similar to wild type in all the CNS regions and ages examined (P5-P50). However, the number of positive cells was dramatically reduced in the spinal cord compared to normal, even when exposure times were increased (Figure 36, page 133). This difference was most prominent in mice up to P30 but was still apparent at P50. The intensity of signal per cell in the mutant was comparable to that in wild type. A marked difference was also found in the number of *Plp/Dm20* positive cells in the cerebellum (Figure 37, page 135) but in contrast, little difference was observed between *hsh* and wild type mice in the hybridisation pattern of the forebrain (Figure 38, page 136). ISH for *Ugt8* demonstrated a similar paucity of oligodendrocytes in *hsh* cervical spinal cord at all ages examined (P5-P20) (Figure 39, page 137). A difference in intensity of signal in individual cells was difficult to assess as hybridisation was more diffuse than for *Plp/Dm20*, even in wild type.

3.5.4 Discussion

The distribution of oligodendrocytes in *hsh* spinal cord is identical to wild type, suggesting that cells are able to migrate normally. Using morphological criteria, a deficit in total glial numbers is found in younger mice, and is apparently due to a lack of oligodendrocytes. An increase in oligodendrocyte numbers between P30 and P50 leads to complete resolution of this difference. Interestingly, this matches the period of maximum myelin production in the mutant as measured by point counting (see Myelin volume, page 92). A more profound paucity of oligodendrocytes is found using ISH for *Plp* and *Ugt8.* No astrocytosis is detected but microglial cell numbers appear increased from P50. Cell death does not apparently exceed control results, although this was assessed only by counting pyknotic nuclei.

Quantification of cells was carried out primarily in 1μm resin sections using morphological criteria to enable the sampling of a large number of cells from several animals at each time point, a task which is not easily undertaken using ultrastructural identification. However, this technique is complicated by the difficulty in unambiguously assigning cells to a particular lineage at younger ages and there is a potential for misidentifying cells (Skoff, 1990). Thus, ISH was employed to provide an alternative means of assessing the apparent reduction in oligodendrocyte numbers in younger mice.

ISH was carried out with two oligodendrocyte-specific probes, *Plp-1* and *Ugt8*; although this resolves the problems of morphological identification, its limitations lie in the ability to clearly distinguish positively hybridising cells and hence, to quantify cell numbers precisely. Thus, it cannot be easily used as the sole method for enumeration. Although the *Plp-1* probe hybridises with both *Plp* and *Dm20* mRNA, positive cells are likely to be mature *Plp* expressing oligodendrocytes based on the age of mice tested, the distribution of cells and the intensity of signal. *Ugt8* is expressed earlier than *Plp* (Kagawa *et al.*, 1996) and serves as a marker of less mature oligodendrocytes.

There is a dramatic reduction in the number of *Plp/Dm20* expressing cells in the cervical spinal cord at P20 that appears subjectively greater than the difference detected using morphological criteria; with that technique, oligodendrocyte numbers are approximately two thirds of control values at P20. At P50, the paucity of cells is still apparent with ISH for *Plp* whereas morphological assessment suggests a resolution of the deficit has occurred. The disparity between the two results may imply a delay in maturation, which is supported by the impression of more "light" oligodendrocytes on resin sections from young mice. Interestingly, the *Plp* signal

intensity per cell is not reduced and in fact, in many cells it appears comparable to the most strongly expressing wild type oligodendrocytes. However, high signal intensity does not always correlate with the final protein levels and the ability to form myelin, as has been demonstrated for other mutations, for example some of the *Plp* mutants (Gardinier and Macklin, 1988; Boison and Stoffel, 1989; Nadon *et al.*, 1990; Fremeau, Jr. and Popko, 1990) and Mbp^{shi} together with its allele, $Mbp^{shi\text{-}mld}$ (Popko *et al.*, 1987).

The deficit in *Plp/DM20* expressing cells is also obvious in the cerebellum, but is hardly detectable in the forebrain. This correlates with the more mild degree of hypomyelination in the forebrain (see Distribution of the lesion, page 90) and suggests that hypomyelination is indeed related to a paucity of mature oligodendrocytes. It also demonstrates that the *hsh* factor is not only important in myelination in the spinal cord but also in the hindbrain, whilst it is of less significance in the forebrain.

Ugt8 is considered to be a key enzyme in the biosynthesis of galactocerebroside and has been shown to be a good marker for localising oligodendrocytes (Kagawa *et al.*, 1996). It is expressed a short time prior to myelination and is therefore an earlier marker than *Plp* (Kagawa *et al.*, 1996). The dearth of *Ugt8* expressing oligodendrocytes seen in *hsh* indicates that the cellular defect involves not just the most mature myelin forming stages but also cells preparing to myelinate nearby axons.

Other CNS myelin mutants in which oligodendrocytes have been quantified exhibit disparate changes. A paucity of oligodendrocytes is seen many of the *Plp* mutants where it is associated with cell death (Skoff, 1976; Dentinger *et al.*, 1982; Duncan *et al.*, 1983). In these animals, hypomyelination is presumably due partly to inadequate cell numbers. However, one *Plp* mutant, rumpshaker, does not suffer from increased cell death and in fact has increased numbers of oligodendrocytes (Schneider *et al.*, 1992), but is still hypomyelinated albeit less severely. The other well-studied mutants shiverer and quaking have also been reported to have more oligodendrocytes than normal (Friedrich, Jr., 1975; Nagara and Suzuki, 1981). Hypomyelination in these cases results from inadequate myelin production by individual cells rather than too few cells. A report of a tremor/hypomyelinating syndrome in Samoyed dogs quantified glial cell numbers in the ventral funiculus of the spinal cord and found a marked decrease in oligodendrocytes (Cummings *et al.*, 1986). There appeared to be a preponderance of light and medium oligodendrocytes with few dark cells being identified, leading the authors to conclude that there was a deficit in stem cell division with a delay in maturation. A definite hereditary basis

was lost. Weimaraner dogs with an inherited hypomyelinating condition also demonstrate reduced numbers of oligodendrocytes in the affected white matter (Kornegay *et al.*, 1987), which is largely the peripheral portion of the lateral and ventral columns. Possibly cell migration is impaired in these animals.

The basis of the reduced *hsh* oligodendrocyte population in young animals is not obvious but any hypothesis must explain both the histological findings and the more profound paucity of *Plp* and *Ugt8* expressing cells. Also interesting is the apparent increase in oligodendrocyte numbers between P30 and P50. Abnormal cell death does not appear to be involved, although a slight increase might pass undetected. This could be further assessed using a terminal deoxynucleotidyltransferase-mediated incorporation of biotinylated nucleotides (TdT-mediated dUTP biotin nick end labelling; TUNEL) technique to label apoptotic cells that may be missed using morphological criteria. In the absence of perturbed cell death, perhaps some aspect of the proliferative capacity of precursors is disrupted by the mutation, with reduced proliferation in early myelination but a compensatory extension of the proliferative period to generate adequate numbers later. Cell mitosis studies using tritiated thymidine labelling as an index of DNA synthesis could be carried out to shed light on this. There may also be a delay in differentiation, resulting in the disproportionate reduction in mature *Plp* gene expressing cells. It was this hypothesis that stimulated the *in vitro* culture study of oligodendrocyte development presented in the following section. In addition, it would be interesting to know how far back in the oligodendrocyte lineage the cell deficit extends and whether the precursor population is also affected; ISH for *PDGFRα*, a marker of oligodendrocyte precursors (Pringle *et al.*, 1992), could be employed investigate this.

No astrocytosis is found in *hsh* and in general, a marked astrocytic response is not a feature of other autosomal recessive mutants (Duncan, 1995). In contrast, *Plp* mutants exhibit an astrocytosis that is more marked in the most severely hypomyelinated animals. Defects in astrocyte cell cycle and metabolism have also been reported in *Plp* mutants and may be a direct effect of the mutation (Knapp *et al.*, 1993; Knapp and Skoff, 1993) rather than a consequence of hypomyelination.

There appears to be an increased density of microglia in spinal cord white matter at all ages. In younger animals this can be ascribed to the increased total glial cell density, but in older animals it seems disproportionately elevated on visual examination of immunostained sections, a finding supported by quantification using morphological criteria. Cytoplasmic vacuoles are present in a small proportion of *hsh* microglia but were not found in equivalent wild type cells, implying that these

occur as a consequence of the *hsh* mutation. Microglia are numerous in Plp^{jp} (Vela *et al.*, 1996) and the *md* rat (Jackson and Duncan, 1988), and seem related to the time of maximum cell death. The single report on hypomyelination in Samoyed dogs also described an increase in microglia but cell death was not an obvious feature of this disease on morphological assessment (Cummings *et al.*, 1986). A similar increase in microglia has not been reported in quaking or shiverer mice. Since cell death is not prominent in *hsh,* the stimulus for the apparent expansion of the microglial population in older mice is obscure. It may be, however, that any increase in cell death escaped detection using only quantification of pyknotic nuclei and a higher rate of death may be identified using the TUNEL technique. The basis of the cytoplasmic vacuoles in the absence of apparent cell death or myelin breakdown is also puzzling, but perhaps it is a consequence of more rapid turnover of myelin products.

A)

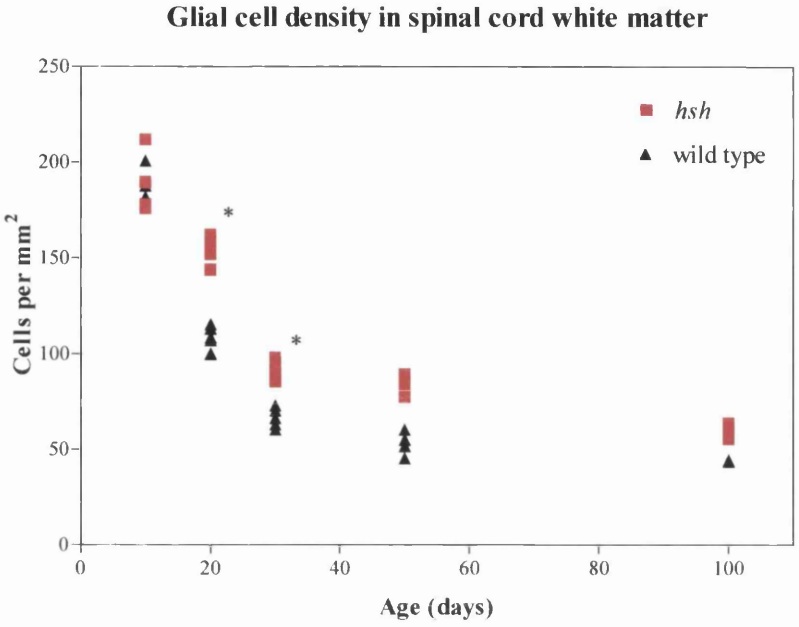

B)

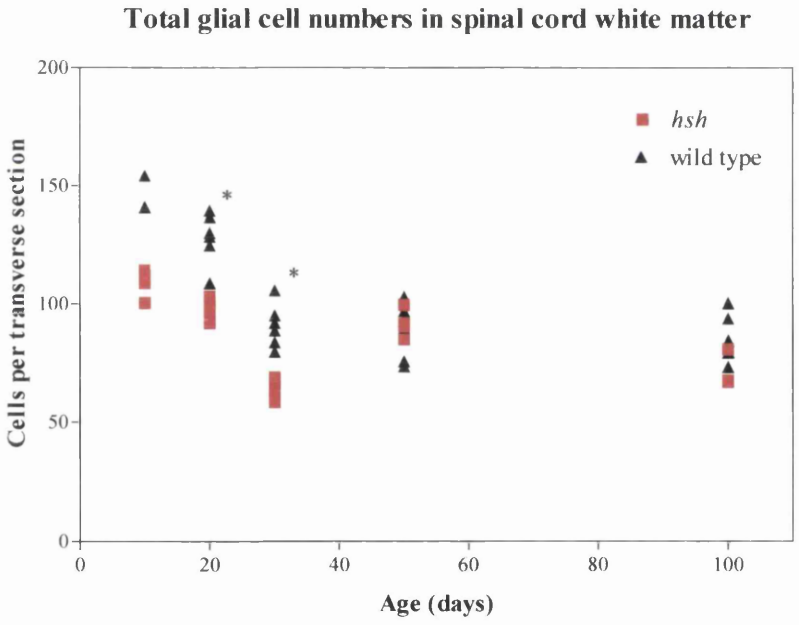

Figure 29: A) Glial cell density in the cervical cord ventral column white matter in wild type and *hsh* animals. Values are increased and P20, P30 and P50. B) Total glial cell numbers for the same animals. A slight reduction in total glial numbers is evident up to P30. Significant differences are marked with *.

A)

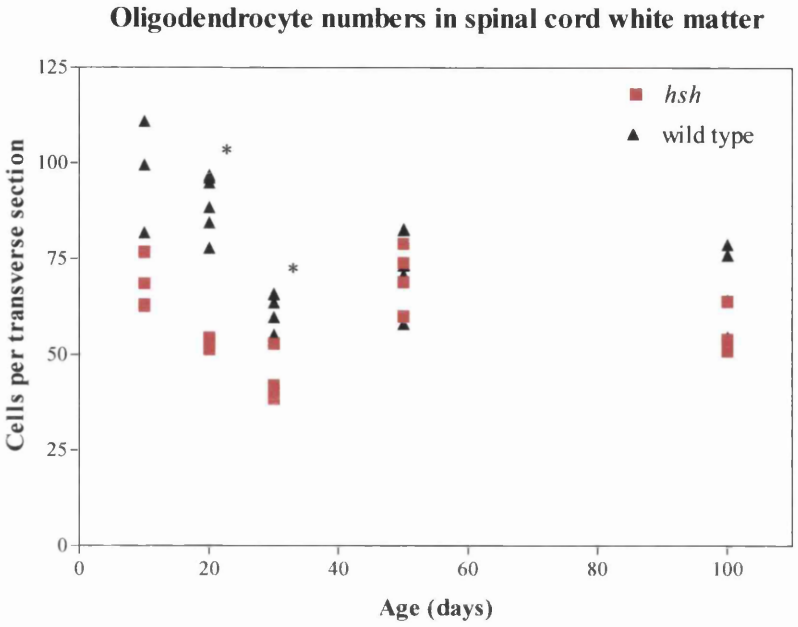

B)

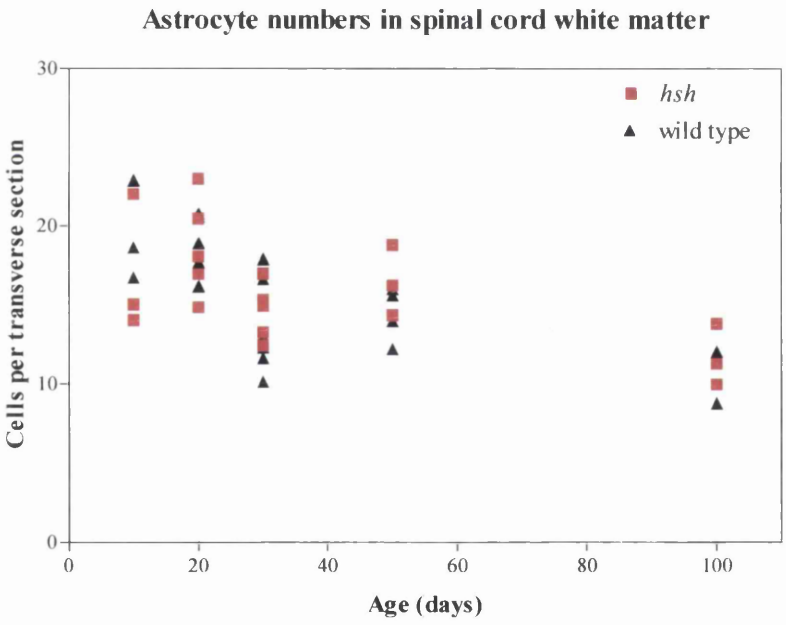

Figure 30: A) Oligodendrocyte numbers in the cervical cord white matter in wild type and *hsh* animals. Values are reduced at P10, P20 and P30. Significant differences are marked with *. B) Astrocyte numbers in the same sections. No differences are seen.

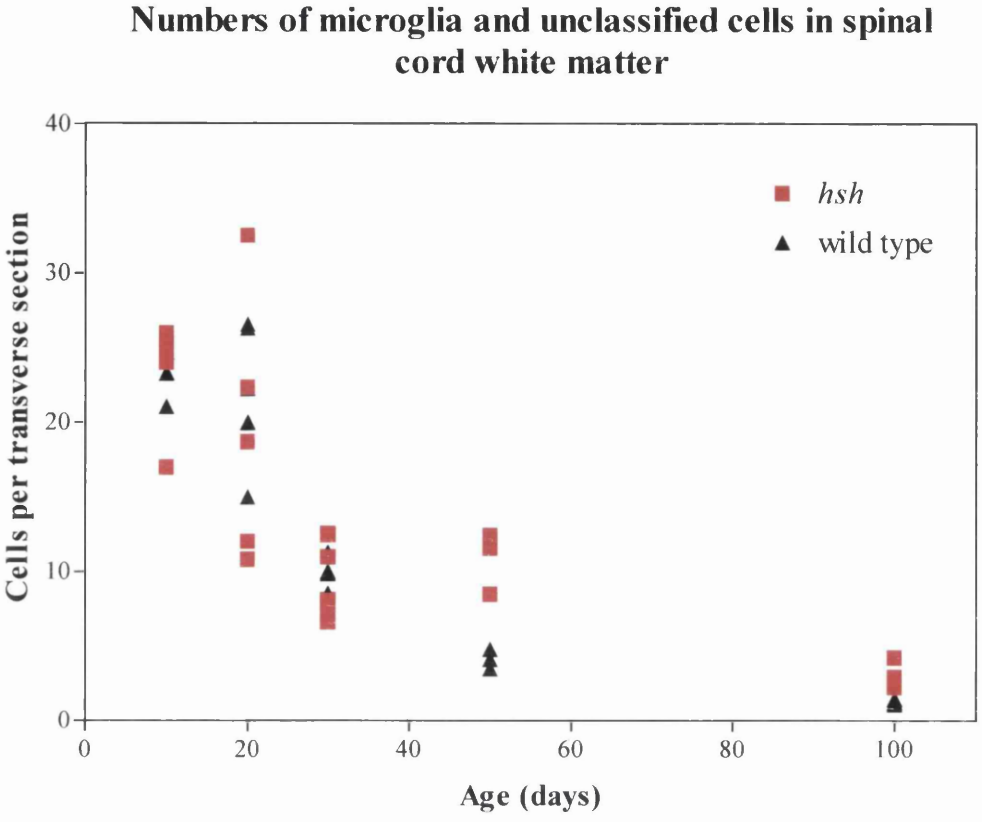

Figure 31: Numbers of microglia and unclassified cells in the cervical cord white matter in wild type and *hsh* animals. No consistent differences are seen before P50. At P50 and P100, an elevated cell count was obtained in mutants; at these ages very few cells have ambiguous morphology so the difference is almost entirely due to an increase in microglia. The numbers of cells involved are nevertheless small in comparison to total cell numbers.

A)

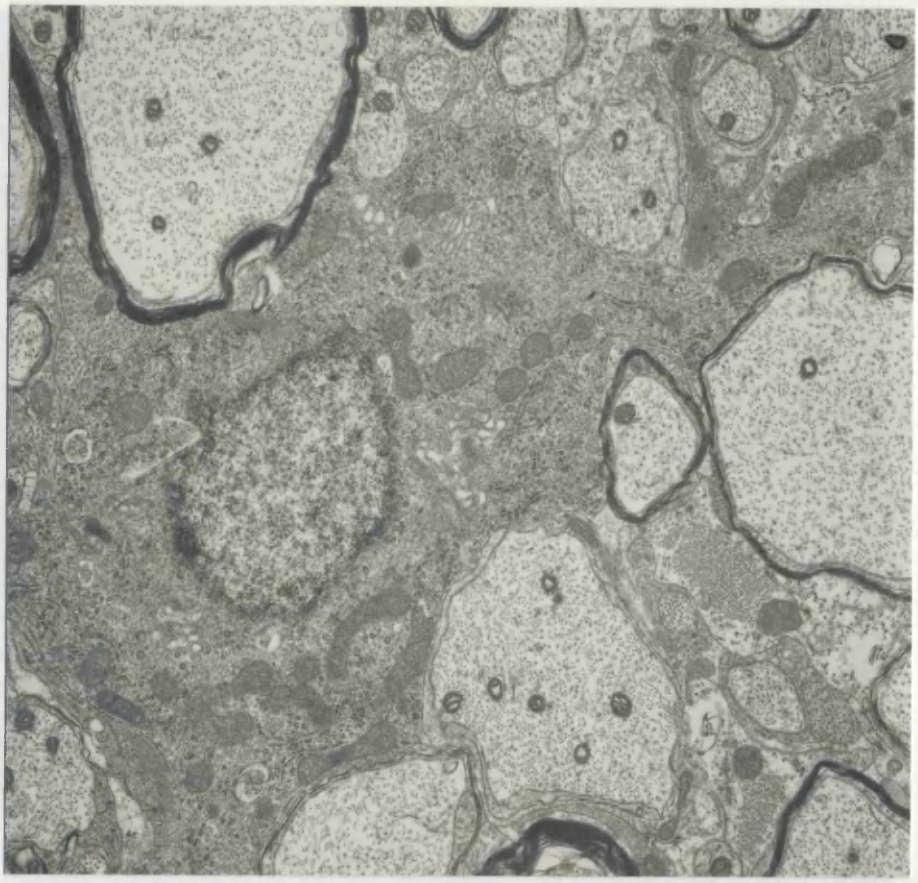

B)

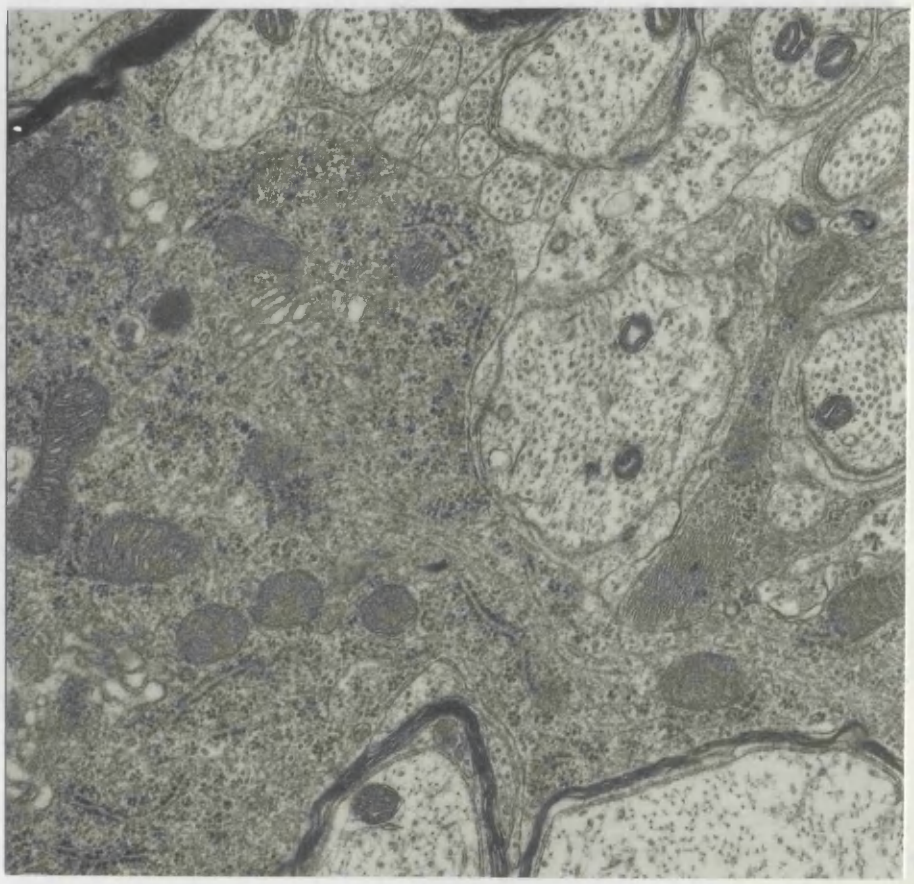

Figure 32: Ultrastructure of a typical *hsh* oligodendrocyte from a P20 animal. No abnormal features can be seen. A) x7500 and B) x15000

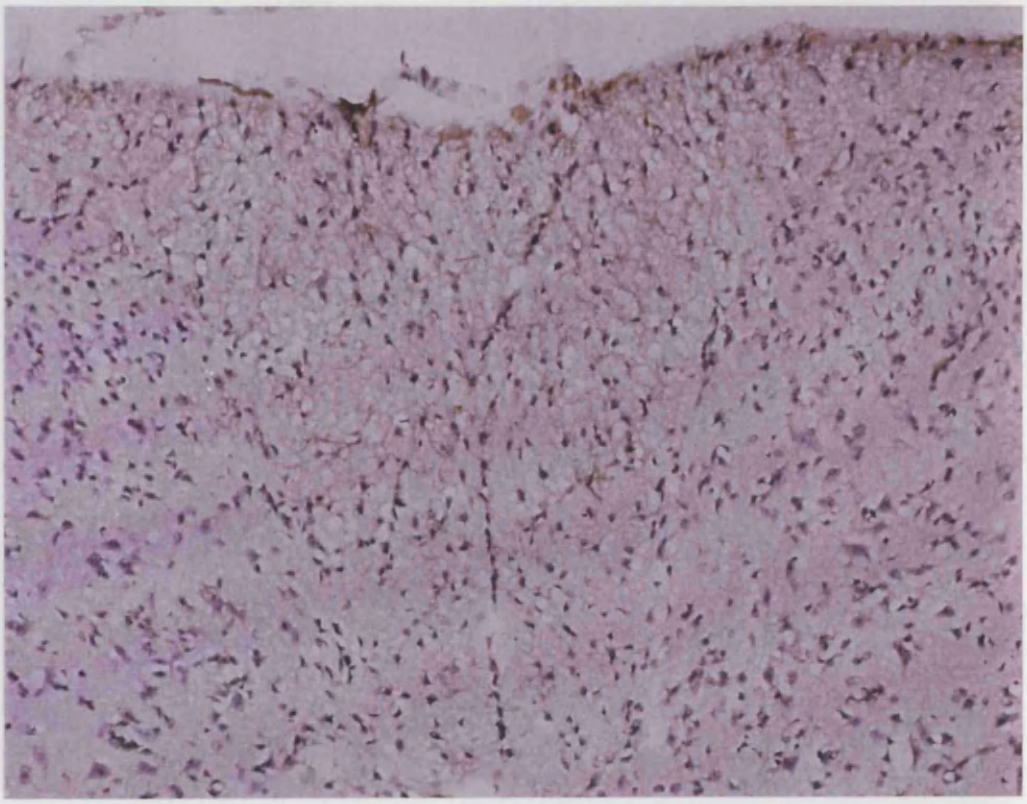

(A)

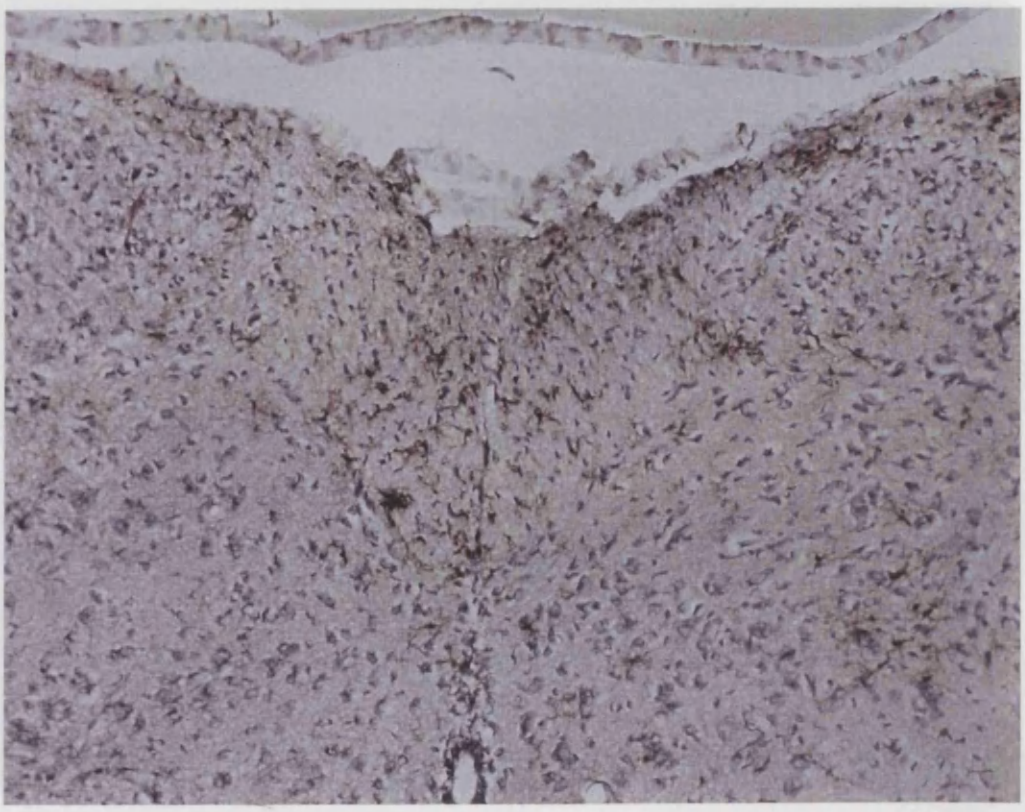

(B)

Figure 33: Dorsal columns of P20 (A) wild type and (B) *hsh* cervical cord stained for F4/80, a microglial antigen. An increase in cell density is seen in mutant tissue but quantification showed no increase in absolute numbers. (Approx. magnification x400).

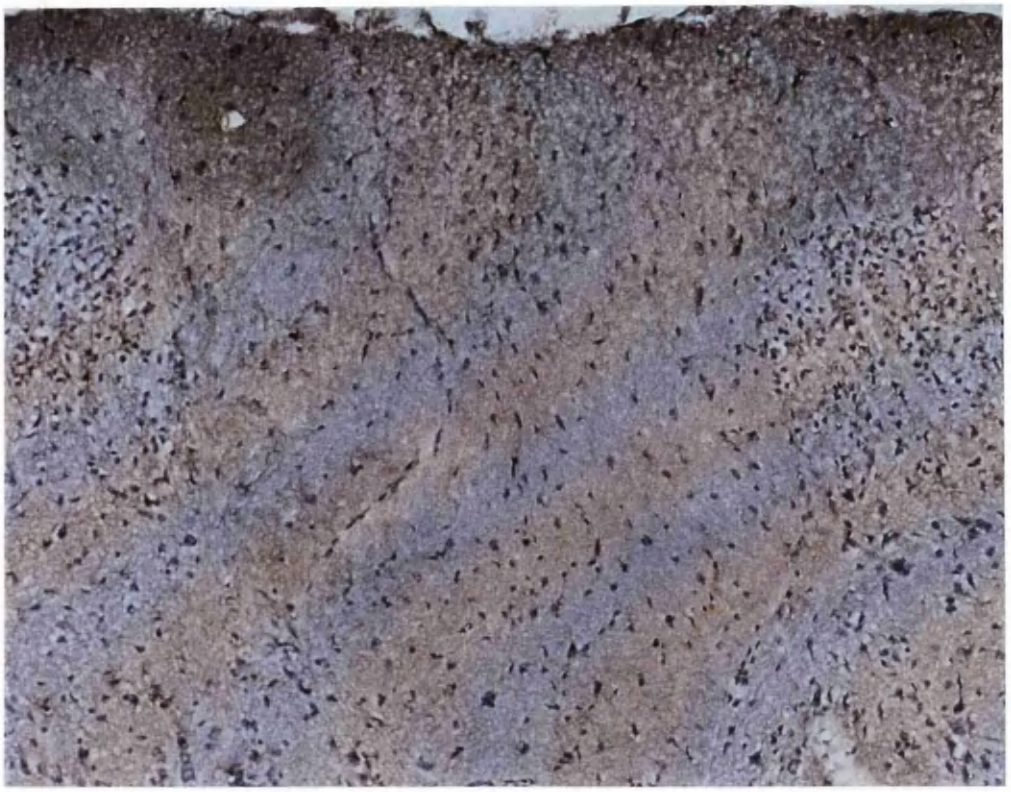

(A)

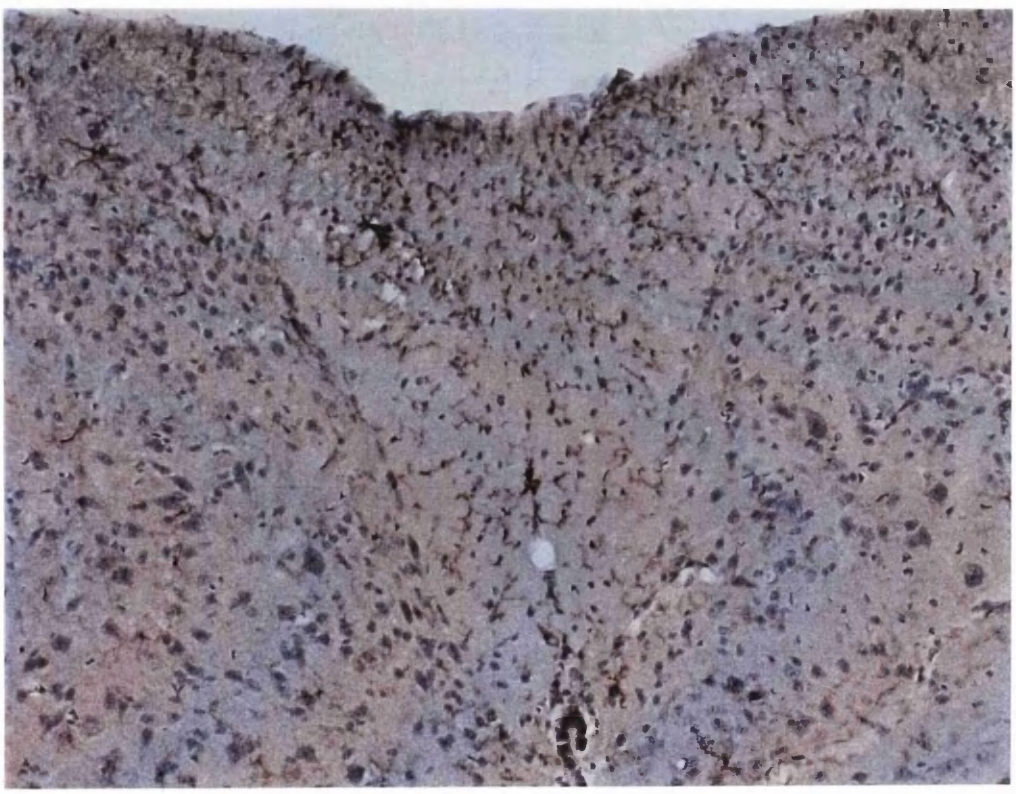

(B)

Figure 34: Dorsal columns of P50 (A) wild type and (B) *hsh* cervical cord stained for F4/80. There is an increase in microglial cell density in the mutant. (Approx. magnification x400).

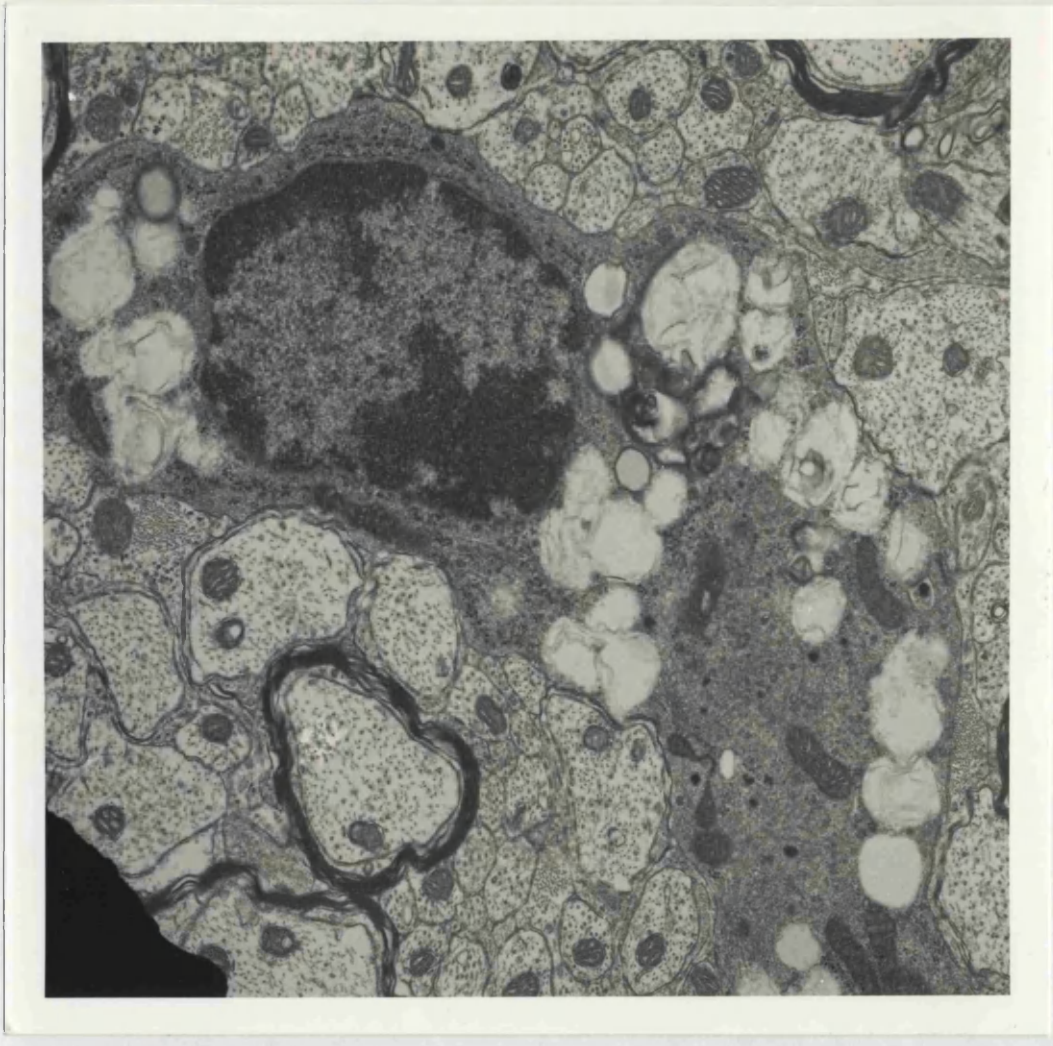

Figure 35: A P20 *hsh* microglial cell containing multiple lucent cytoplasmic inclusions. (Approx. magnification x10000).

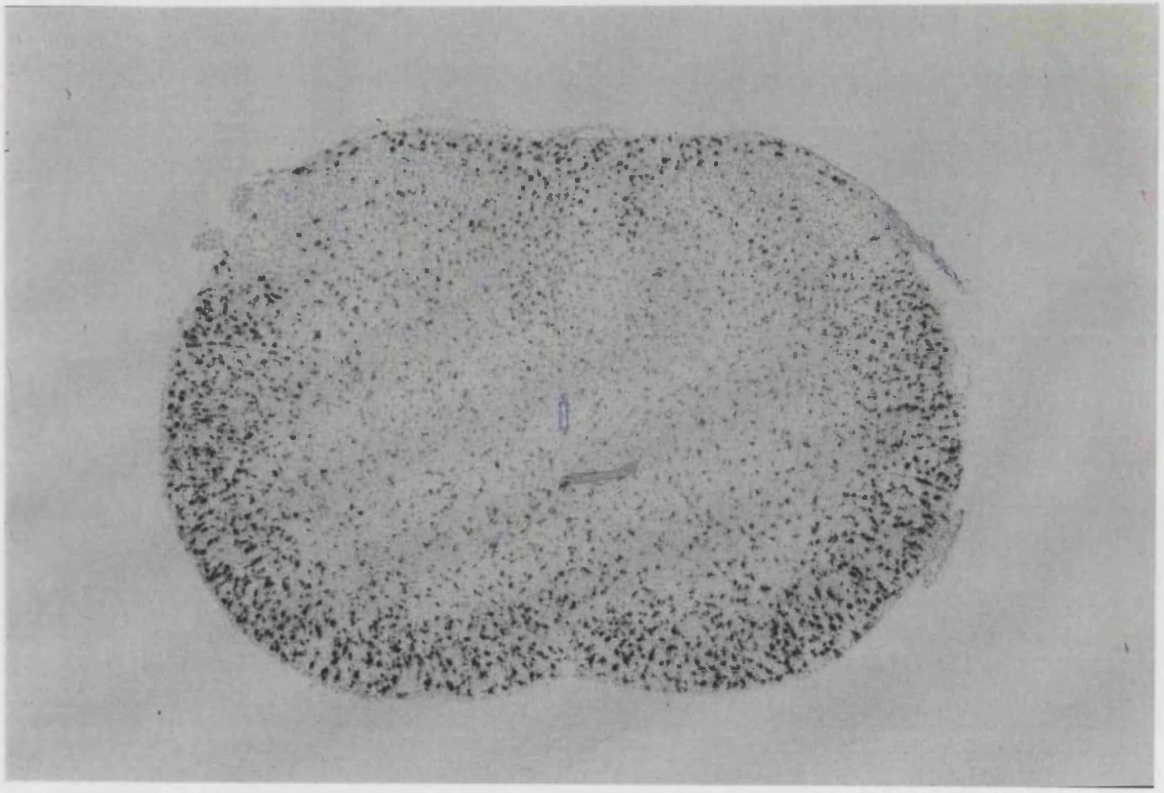

(A)

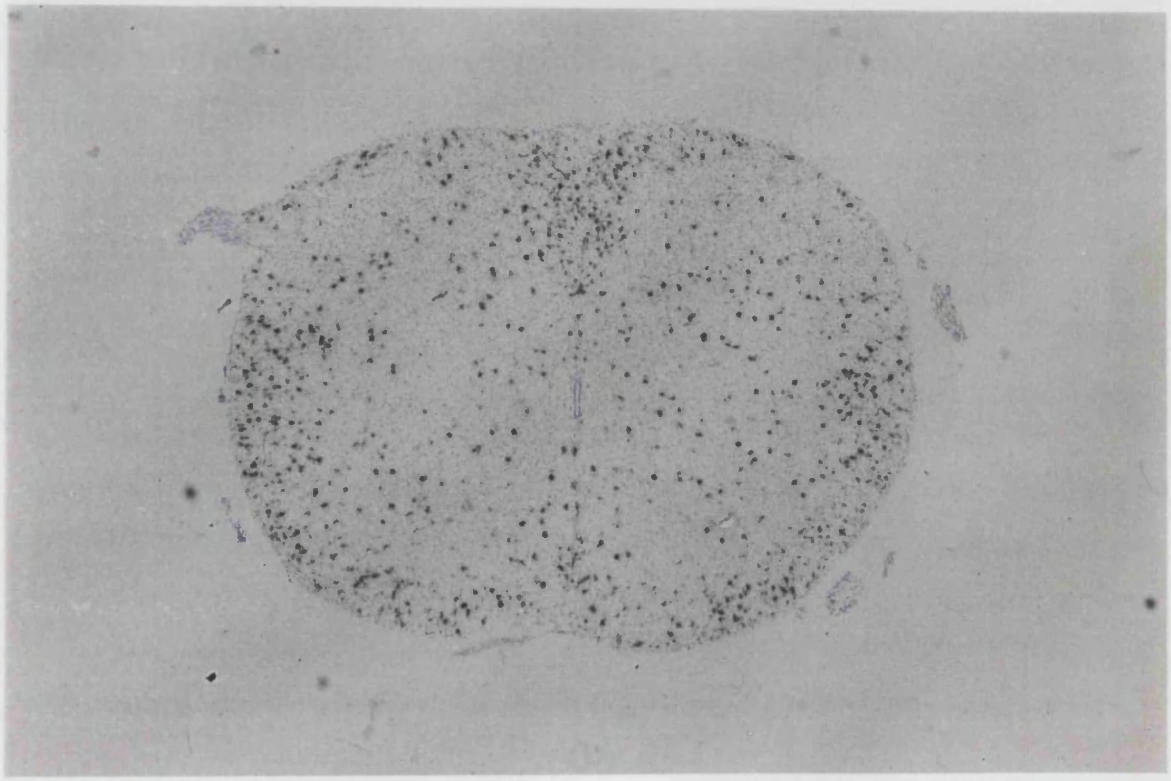

(B)

Figure 36: Autoradiograms of P20 (A,C) wild type and (B,D) *hsh* cervical spinal cord hybridised for *Plp/Dm20* and counterstained with haematoxylin. Fewer positive oligodendrocytes are seen in *hsh* although the distribution throughout the cord is similar. (Approx. magnification A, B x40, C, D x90).

(C)

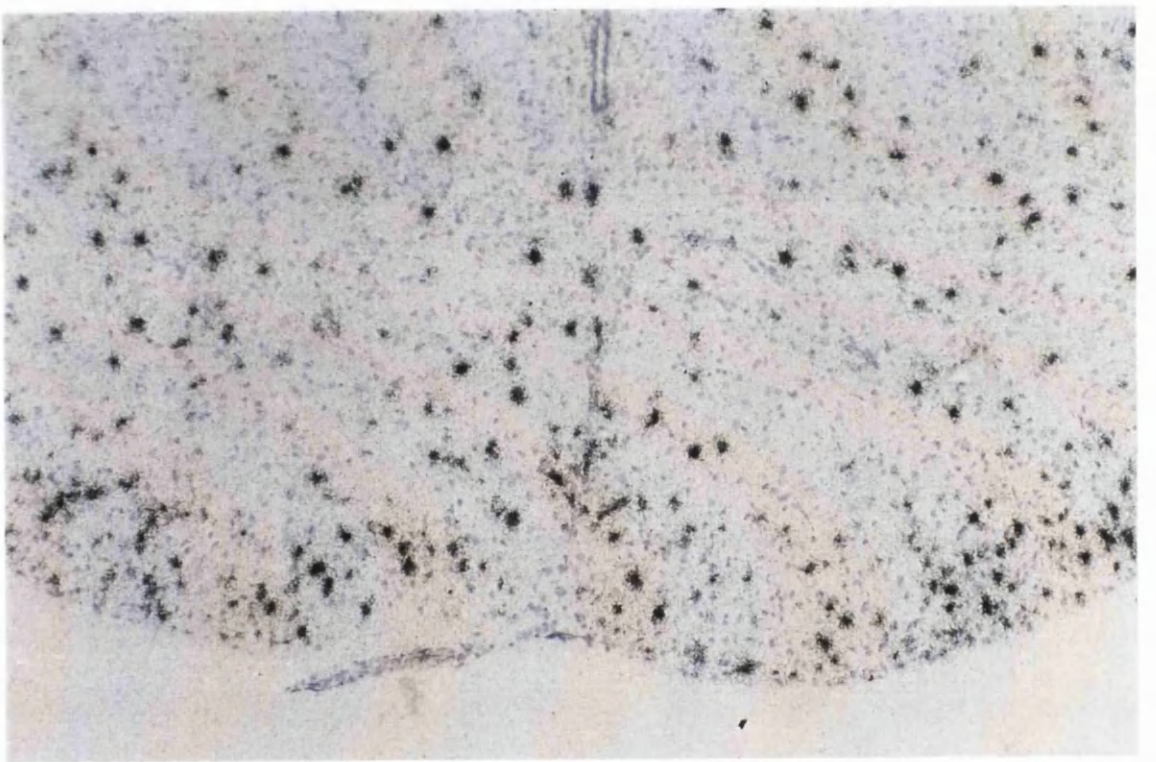

(D)

Figure 36 (cont).: Autoradiograms of P20 (C) wild type and (D) *hsh* cervical spinal cord hybridised for *Plp/Dm20* and counterstained with haematoxylin. The comparable intensity of signal per cell in the mutant can be seen. (Approx. magnification x90).

(A)

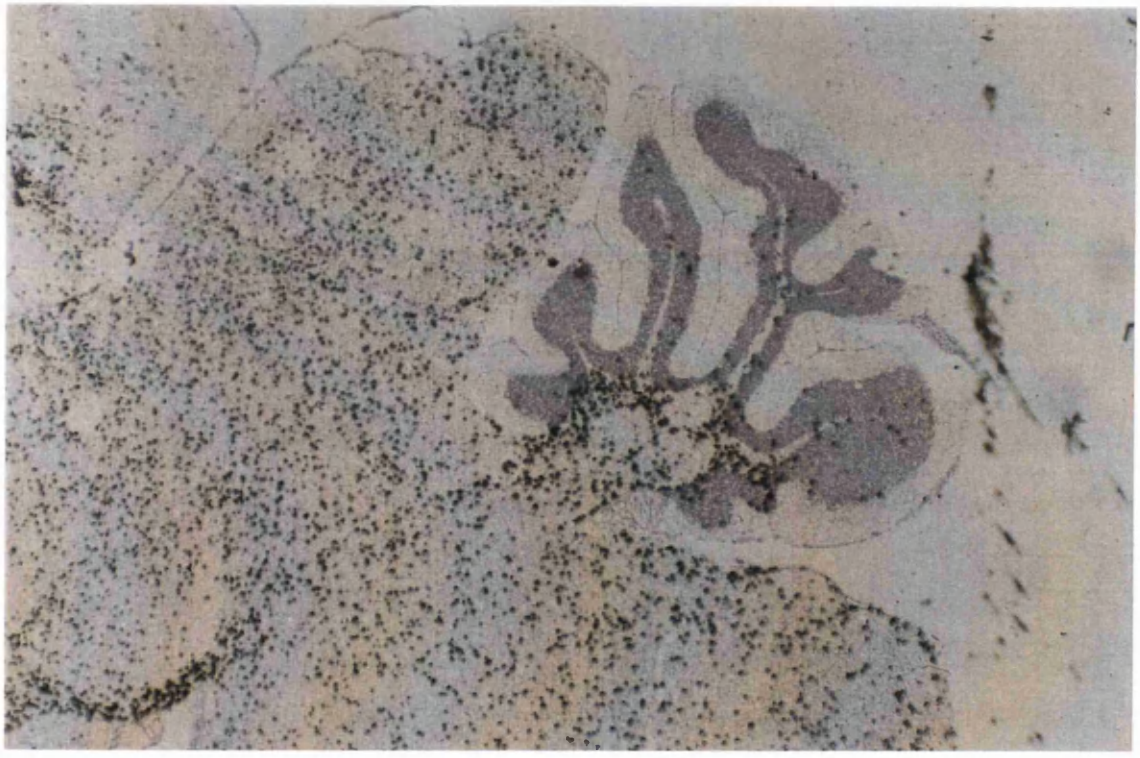

(B)

Figure 37: Autoradiograms of P20 (A) wild type and (B) *hsh* cerebella hybridised for *Plp/Dm20* and counterstained with haematoxylin. The *hsh* cerebellum contains fewer hybridising cells than the age matched wild type although a similar distribution is seen. (Approx. magnification x50).

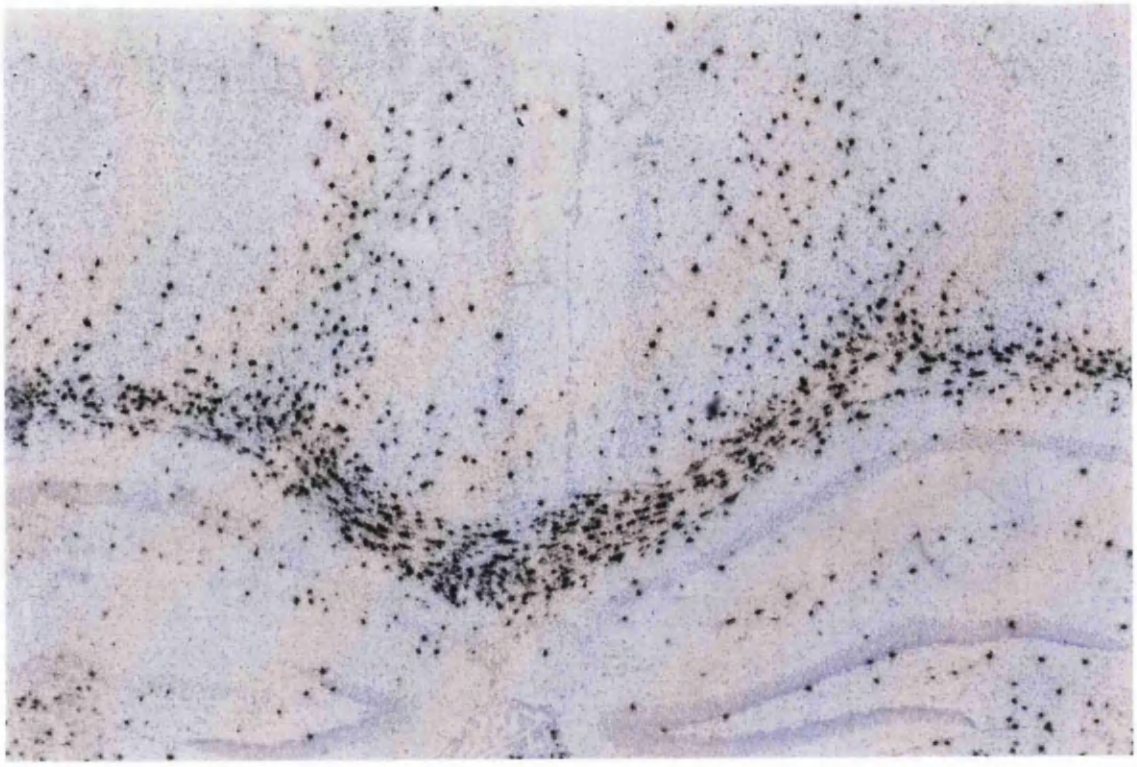

(A)

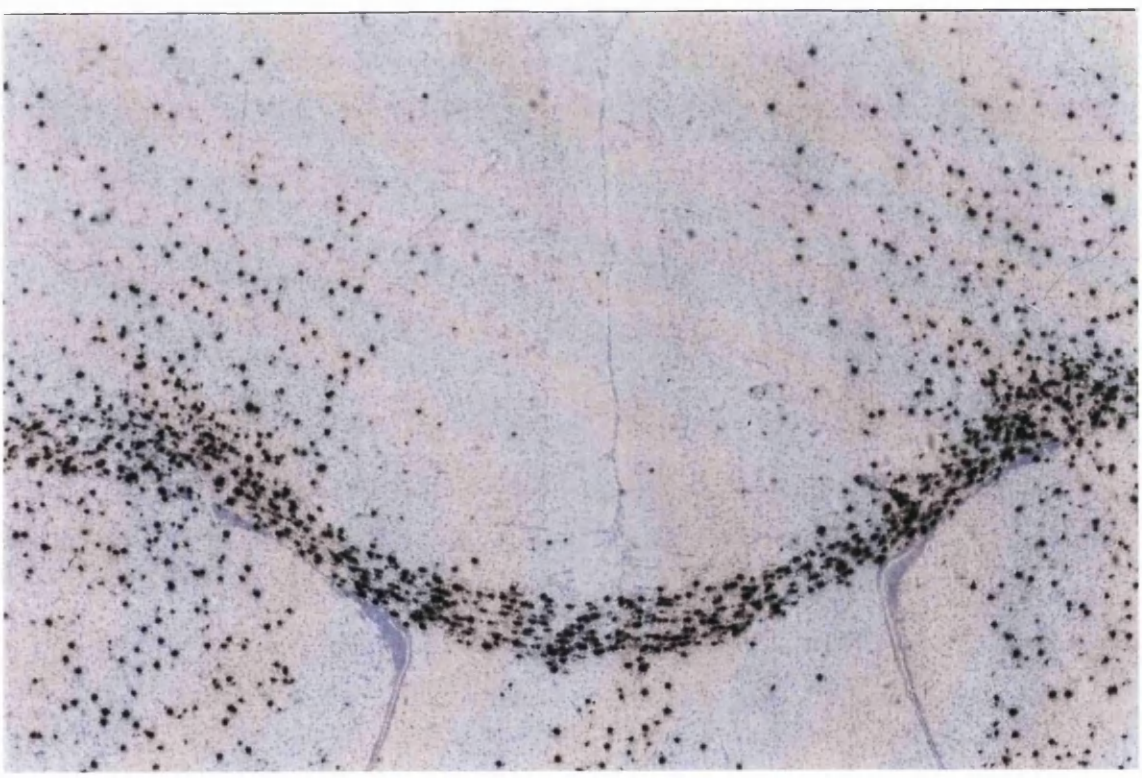

(B)

Figure 38: Autoradiograms of the forebrain of P20 (A) wild type and (B) *hsh* mice hybridised for *Plp/Dm20* and counterstained with haematoxylin. In the corpus callosum and cingulate gyrus, there is less difference in cell numbers than the spinal cord and cerebellum. (Approx. magnification x50).

(A)

(B)

Figure 39: Darkfield autoradiograms of P20 cervical spinal cord from (A) wild type and (B) *hsh* mice hybridised for *Ugt8* and counterstained with haematoxylin. Fewer positive cells are seen in the mutant animal compared with wild type. (Approx. magnification x50).

3.6 *In vitro* development of *hsh* oligodendrocytes

3.6.1 Introduction

Without question, the most convenient means of studying oligodendrocyte differentiation is in tissue culture. Cells in culture are more accessible, can be observed directly during development and most importantly, their environment can be controlled in a way that is impossible *in vivo*. Dissociated cells undergo a complex pattern of antigenic and morphological development that appears similar to the *in vivo* situation, culminating in the formation of myelin membrane. However, because cell culture lacks the framework of intact tissue, many intercellular interactions that occur during development may not occur in culture; this limits the extent to which results can be extrapolated to development of oligodendrocytes *in situ*.

3.6.2 Aim

These experiments were stimulated by the finding of a deficit of mature oligodendrocytes in areas of hypomyelination in *hsh* mice. The aim was to observe the effects of the mutation on oligodendrocyte survival and differentiation *in vitro* with the hope of correlating this to the *in vivo* findings. The study was performed on cells from dissociated spinal cord because this region was known to be the most severely affected by the mutation. A small range of markers was tested at a limited number of time points to provide an overview of the developmental profile of *hsh* oligodendrocytes in relation to wild type cells. Any further experiments were to be decided on the basis of results from these preliminary studies.

3.6.3 Materials and Methods

3.6.3.1 Cell culture technique

Cultures were established from spinal cords of P5 *hsh* and wild type mice; this age was selected to provide a suitable balance between the ease of establishing cultures whilst being sufficiently mature for the presumptive developmental delay in *hsh* to be apparent. Pups were obtained only from *hsh* mice that were known to reliably produce offspring with a marked phenotype. Control and mutant cultures were set up from similar sized litters within a close time interval and with the same batches of solutions and antibodies The technique has been described in Cell culture, page 64 and was closely adhered to for consistency of results. Cultures that had obvious variation in cell density between mutant and control coverslips after plating were not used.

3.6.3.2 Immunostaining

O4 staining for sulfatide and related glycolipids was taken as the marker of commitment to the oligodendrocyte lineage and considering this as 100%, the percentage of cells positive for other antibodies was obtained from double immunofluorescent immunostaining. O1 staining was used to identify more mature cells, and MBP and PLP detected the most mature stages of the lineage. The PLP antibody detected an antigen common to both PLP and DM20. R-mAb, an antibody for sulfatide and GalC, was used in the first set of experiments but as there was virtually no difference between that and O1, it was abandoned. Immunostaining was performed as described in Immunofluorescent staining, page 65 after 24, 48 and 72 hours in culture with 3 coverslips being used for each antibody combination at each time point. Three hundred cells were counted for each coverslip. The experiment was repeated three times and the results were pooled.

3.6.4 Results

The yield of oligodendrocytes from *hsh* spinal cord was comparable to that from wild type tissue and survival in culture was good. Mutant oligodendrocytes did not show obvious morphological differences from controls. Staining for O4 was bright and a similar number of cells were stained in relation to the total number of nuclei as was estimated in wild type (Figure 40 page 143). They produced processes in a similar fashion to wild type and eventually developed myelin membranes of comparable dimensions at the expected time (Figure 41, page 144). Quantification of percentages of O4+ cells that were also stained for either O1, MBP or PLP showed no difference between *hsh* and wild type cultures (Table 4, page 140). The only remarkable difference between mutant and control cells was a subjective reduction in intensity of staining for MBP and PLP in mutant cells at all time points. This was identified as less bright fluorescence and more localised staining; fluorescence appeared to be more likely to be perinuclear in *hsh* whereas membranes also stained brightly in differentiated wild type cells.

Only small increases in the percentages of double-stained cells occurred over the 72 hour time period in cultures of both phenotypes. It was noted that there appeared to be a wave of O4+/O1- cells appearing between 48 and 72 hours, both in wild type and *hsh*. These were multipolar, had not yet started to form membrane sheets and appeared to boost the population of cells stained for O4 at 24 hours.

Phenotype	Wild type	*hsh*	Wild type	*hsh*	Wild type	*hsh*
Hours in culture	**24 hours**		**48 hours**		**72 hours**	
O4/O1	15	13	16	14	17	16
O4/MBP	8.6	6	9	8.5	11	10.3
O4/PLP	7	6	9	8.5	10	9.4

Table 4: A table showing the percentages of O4 positive cells that stain for O1, MBP and PLP at 24 hours, 48 hours and 72 hours. Results are the mean of three experiments (a total of about 2700 cells per test). Minimal difference is seen between the values obtained for mutant and wild type cells.

3.6.5 Discussion

In culture, the differentiation of O-2A cells, the precursors to oligodendrocytes and type 2 astrocytes, is controlled by both intrinsic and extrinsic factors. In this study, a low concentration of foetal calf serum allowed differentiation of O-2A cells into oligodendrocytes rather than type 2 astrocytes. By placing cells from mutant and wild type animals in a similar environment that was permissive for rapid differentiation, it was hoped that intrinsic differences in their survival and/or differentiation and maturation would become apparent. Great care was taken to ensure that wild type and mutant cultures were obtained from similar sized litters and were of comparable densities to minimise extraneous influences on oligodendrocyte development. Obviously mice from smaller litters may be developmentally more advanced in comparison to those from very large litters, which could be reflected in the population of oligodendrocytes and precursors obtained from them. Cell density has been shown to influence proliferation and differentiation of oligodendrocytes in culture, with low density increasing proliferation (Zhang and Miller, 1996) and high density favouring progression of O-2A progenitors along the oligodendrocyte lineage (Levi *et al.*, 1991; Agresti *et al.*, 1991). No mitogens other than insulin and any present in the FCS were added, to facilitate the immediate differentiation of precursors (Temple and Raff, 1985; Barres *et al.*, 1992b). High concentrations of insulin have been shown to have a major beneficial effect on cell survival and differentiation (Barres *et al.*, 1992a; Barres *et al.*, 1993), for which it was used here. However, it has also been shown to stimulate proliferation of O-2A progenitors (McMorris and Dubois-Dalcq, 1988) so it is possible that some precursors did undergo divisions before differentiating.

Cultures established from *hsh* cords yield a large population of cells and in fact, it is subjectively easier to obtain good cell density than from normal cords. This may be related to the more advanced stage of axonal ensheathment/myelination of many of the normal oligodendrocytes, which thus sustain greater mechanical trauma and subsequent cell death upon dissociation. No morphological differences are observed at any stage, with *hsh* oligodendrocytes surviving and developing similar features to cells in control cultures. However, in view of the preceding phenotypic studies, it was anticipated that a developmental delay would be described, so it is a little surprising that no quantifiable variance is found in the expression of stage specific markers. Even PLP and MBP, late markers in oligodendrocyte maturation that are expressed at high levels in myelinating cells, show no quantifiable differences. This suggests that *in vitro* at least, *hsh* oligodendrocyte precursors are capable of regulated differentiation to mature myelinating cells over a temporal period comparable to wild type. How this correlates to the *in vivo* finding of a disproportionate reduction in the number of mature oligodendrocytes is not clear; perhaps extrinsic signals triggering differentiation are absent or not responded to *in vivo* but are provided or not required *in vitro.* Whether these differentiated cells are functionally normal and capable of producing adequate myelin, is not known. The subjective finding in the culture experiments of reduced intensity of fluorescent staining for MBP and PLP and its persistent perinuclear localisation would suggest that they are not. It is also not clear if this apparently reduced ability to form normally stained sheaths is due to an intrinsic defect in oligodendrocytes or if it is because extrinsic signals are not forthcoming. It has to be borne in mind that cultures of this nature are mixed glial cultures, containing microglia, oliogodendrocytes and heterogeneous astrocytes, so the effects of other glial cells on oligodendrocyte development cannot be eliminated. It has been shown for *Plp/P,* culturing oligodendrocytes in the presence of medium conditioned by astrocytes from wild type mice can significantly improve survival, suggestive of a role for a specific astrocytic abnormality in the oligodendrocyte cell death seen in this mutant (Bartlett *et al.*, 1988). Therefore, although the present study has tried to remove the majority of potential environmental differences between *hsh* and wild type to allow investigation of intrinsic oligodendrocyte properities, the presence of other glial cell types could still be influential.

The absence of mitogens other than insulin led to the expectation that differentiation would be rapid and that by 72 hours, many cells would have reached MBP and PLP positive stages. In fact, very little increase in percentages of O4+ cells stained for these later markers is found. Instead, there appears to be a wave of O4+/O1- cells appearing in cultures derived from both phenotypes between 48 and 72 hours. Thus, although there are subjectively more O1+, MBP+ and PLP+ cells, judging by their

density on coverslips, the increase is partly disguised by newly appearing O4+ cells. Such findings have been found by other workers performing cell culture in our laboratory (Dr C. Thomson, personal communication). Whether this wave is due to differentiation of pre-O4+ cells in the cultures, or to proliferation of O4+ precursors already present is still under investigation by other workers in our laboratory. Labelling with bromodeoxyridine would identify cells replicating DNA and thus clarify to what extent proliferation versus differentiation is occurring under our culture conditions.

Antibody to CNP was originally tested on cultures but staining was too weak with my technique to be unequivocal in identification of positive cells. Instead, immunostaining of cryosections and western blotting were carried out to investigate this protein. Other late markers, such as MOG and MOBP, were not thought to be likely to yield further information in the first instance and were omitted from the study.

Taken together, it has to be concluded that cell culture has not greatly illuminated the nature of the mechanism underlying the *hsh* mutation. No explanation for the lack of mature oligodendrocytes identified *in situ* has been found and it remains unclear whether oligodendrocytes in *hsh* are inherently defective or whether they lack the correct extrinsic signals *in vivo.* What can be said is that there is little difference in the ability of oligodendrocytes to differentiate on schedule *in vitro.* However, their intrinsic ability to produce normal amounts of myelin is still under debate with the finding of reduced intensity of staining for major structural myelin proteins.

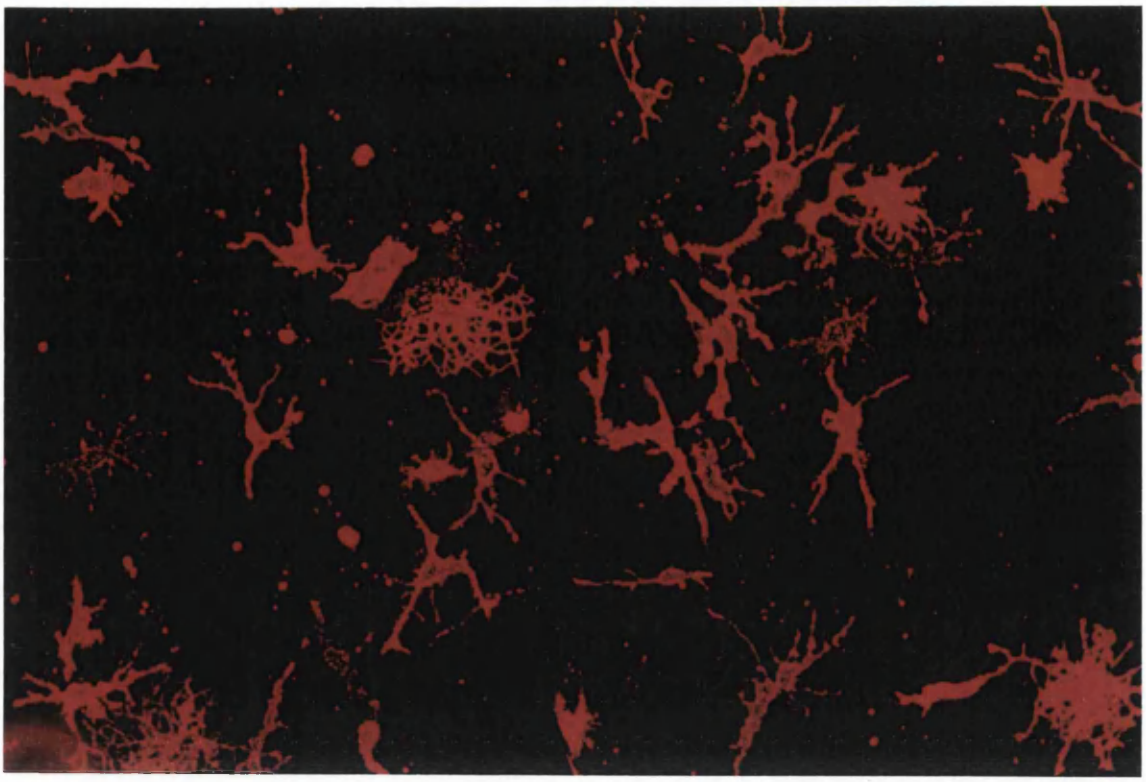

(A)

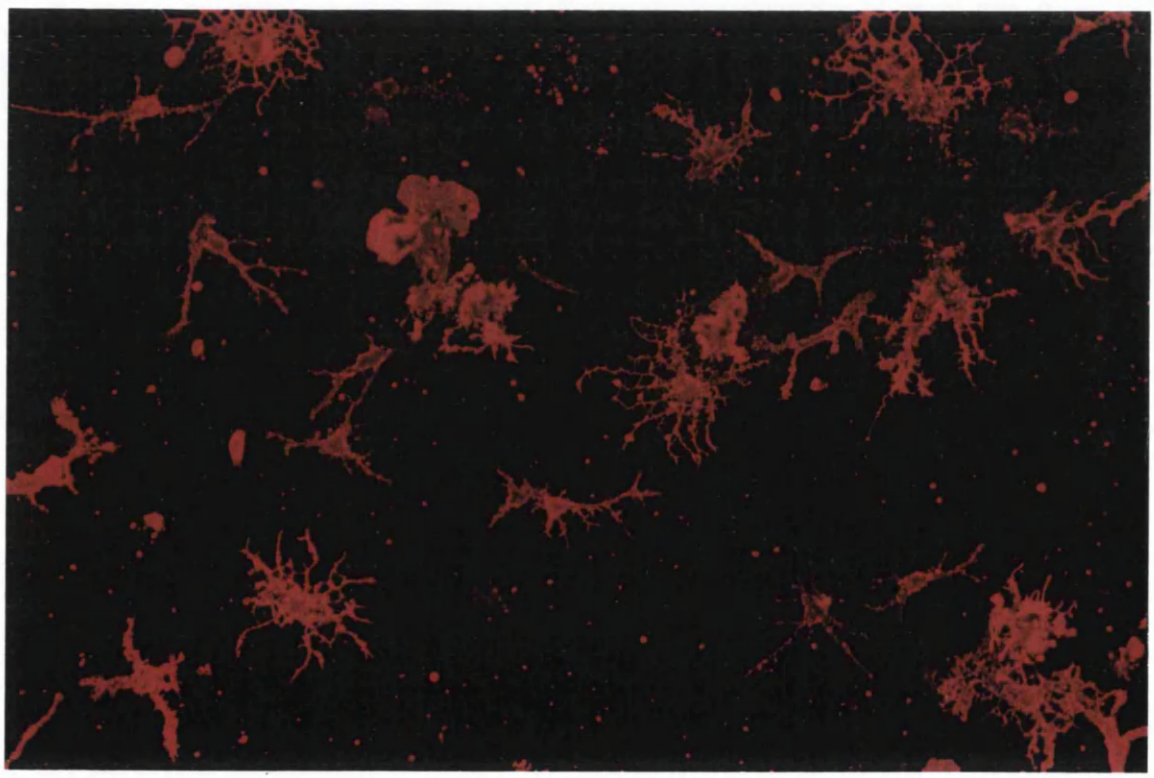

(B)

Figure 40: Immunofluorescent staining with O4 antibody on 24 hour cultures of (A) wild type and (B) *hsh* spinal cord cultures obtained from P5 animals. No morphological differences can be seen between oligodendrocytes in the two cultures. (Approx. magnification x400).

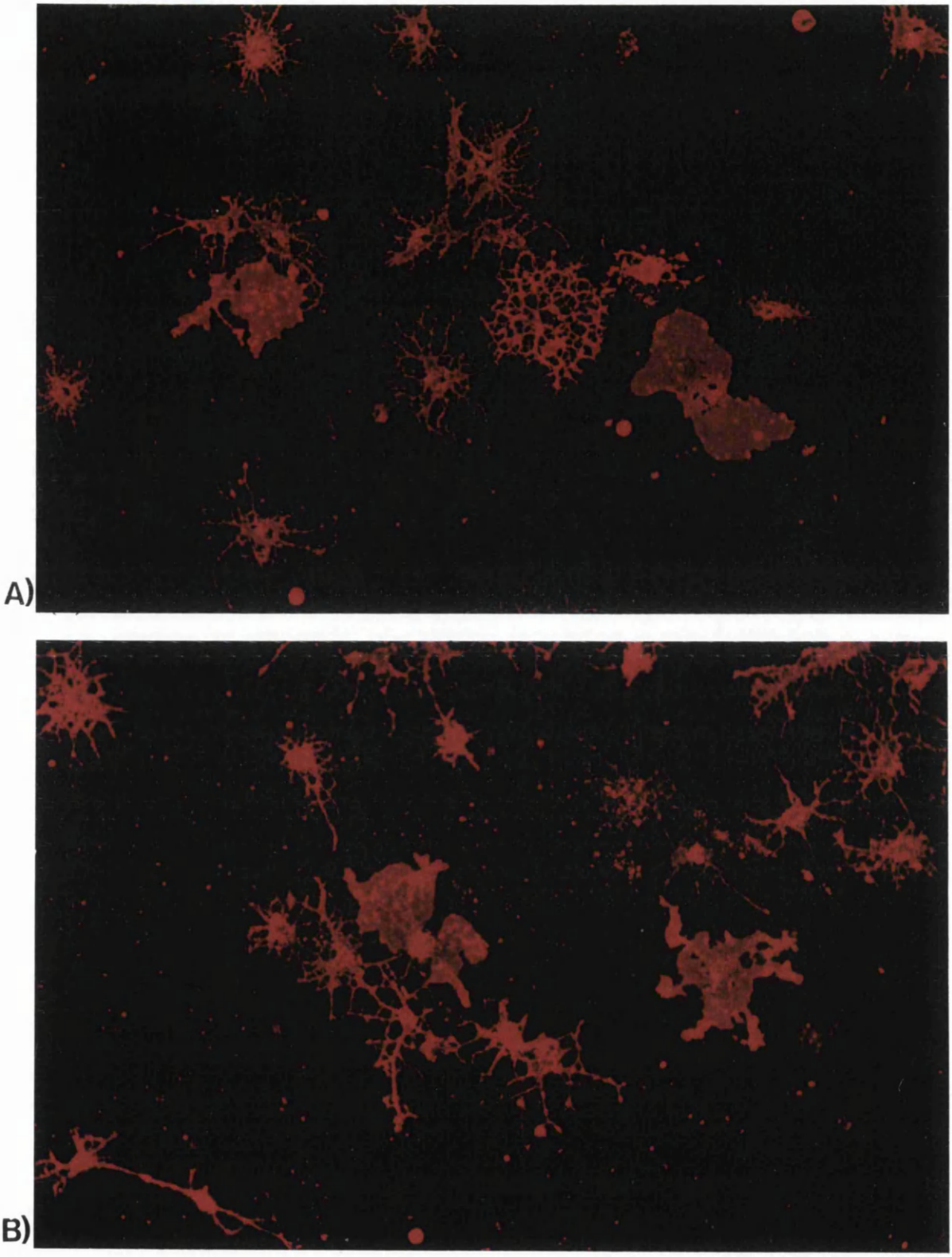

Figure 41: Immunofluorescent staining with O4 (this page) and PLP (next page) antibodies on 72 hour cultures of (A,C) wild type and (B,D) *hsh* spinal cord cultures from P5 mice. Using O4 staining, mutant cells have developed similar morphological features to wild type, producing processes and membranes in a comparable fashion on schedule. (Approx. magnification x400).

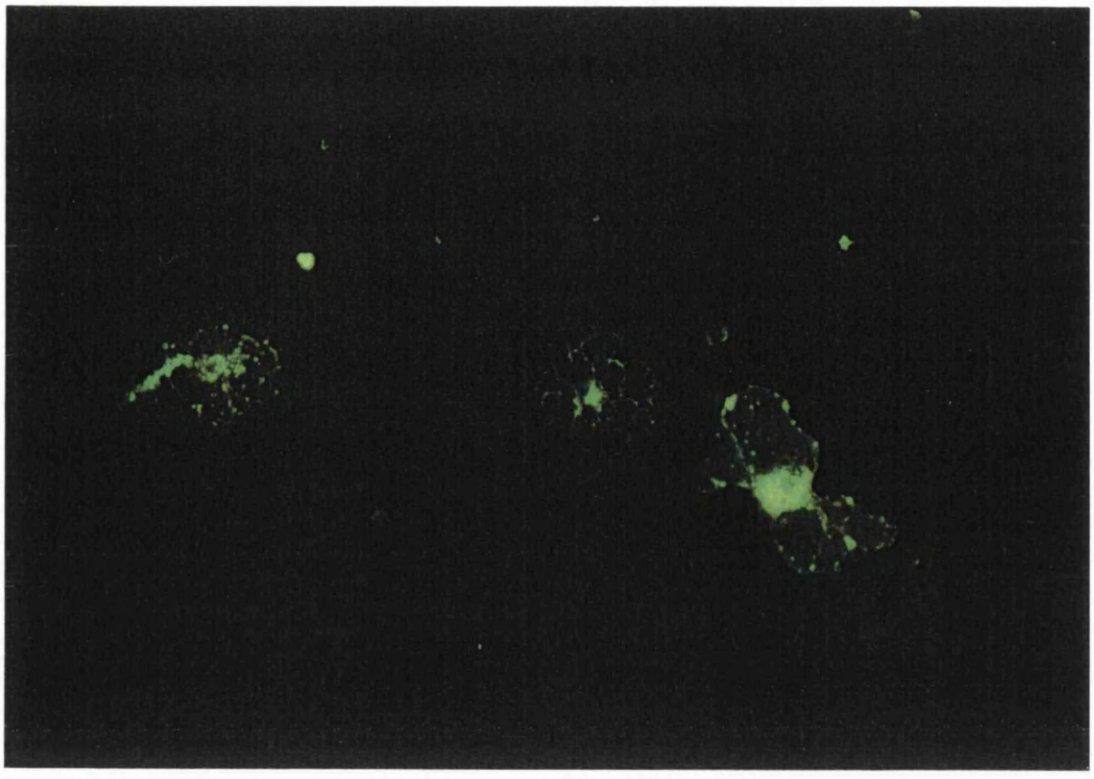

(C)

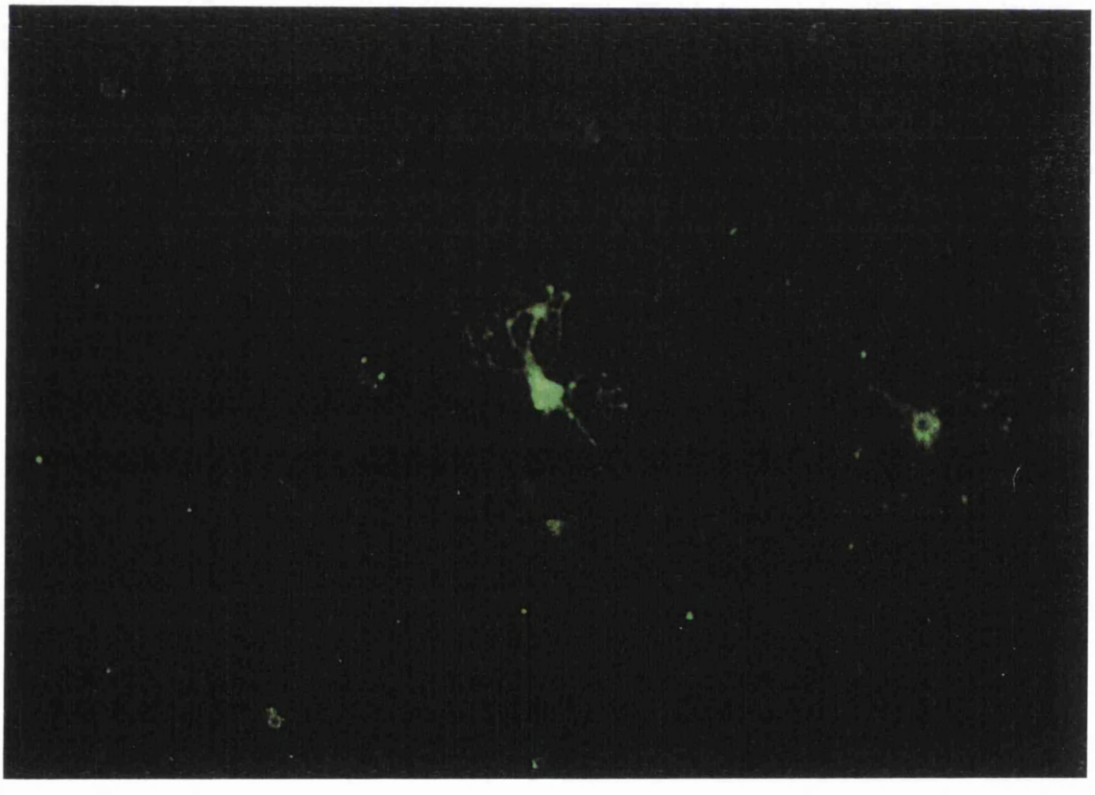

(D)

Figure 41 (cont.): Immunofluorescent staining with PLP antibody on 72 hour cultures of (C) wild type and (D) *hsh* spinal cord cultures from P5 mice. Less intense PLP staining is apparent in oligodendrocytes from *hsh* mice. (Approx. magnification x400).

3.7 Analysis of candidate genes

3.7.1 Background

The characterisation of a phenotype due to a mutation in a particular gene can be valuable in defining the function of the gene product, even if the gene is unidentified. However, without knowledge of the molecular basis of the mutation, the ultimate goal of correlating the phenotype with the precise genetic alteration cannot be achieved. Thus, an integral part of the *hsh* study was the endeavour to identify the mutated gene. This was approached by recombinational linkage analysis using an intersubspecific backcross and by immunohistochemical studies of a panel of myelin proteins, the results of which are described in Immunostaining of the cervical cord, page 91. The absence of a particular protein in the *hsh* CNS might have implicated its encoding gene, although it may also be possible to have normal immunostaining in the presence of altered protein. In addition, two specific myelin genes were highlighted as candidates during the genetic mapping of the *hsh* locus; the *Mog* gene on chromosome 17 and *Cnp2* on chromosome 3. The results of immunostaining for MOG and CNP have been presented previously in Immunostaining of the cervical cord, page 91. Additional studies performed to further examine the expression of these genes are described here. The genetic mapping data that led to the emergence of these genes as candidates are presented in the following chapter.

3.7.2 *In situ* hybridisation study of myelin-oligodendrocyte glycoprotein

3.7.2.1 Background and aims

Initial mapping studies performed at Harwell suggested linkage of *hsh* to distal chromosome 17 (Beechey and Cattanach, 1996). Since *Mog* is mapped to this region (Daubas *et al.*, 1994), it was manifestly a candidate gene at that time. Immunostaining of cervical cord at P10 and P20 was positive although reduced in comparison to wild type tissue (see Immunostaining of the cervical cord, page 91). Concomitant with immunostaining, ISH with a *Mog* probe was undertaken to examine the distribution and amount of mRNA. The aim was to investigate the expression of the *Mog* gene in *hsh* animals at appropriate ages.

3.7.2.2 Experimental procedure for subcloning of the mouse *Mog* sequence

A *Mog* cDNA was provided by André Dautigny (Institut des Neurosciences, Paris Cedex) as purified pCL642 plasmid and JM109 cells containing vector in 50% glycerol. The insert was a 780bp RT-PCR fragment amplified from mouse brain RNA and included all eight exons (Daubas *et al.*, 1994). This had been inserted at an *Eco*R V site in a 5/ to 3/ direction. Directional subcloning into the pGEM-4Z vector was necessary for generation of an antisense riboprobe using the T7 promoter. Digests of the original plasmid were carried out using *Bam*H I and *Sal* I to check the insert. The only restriction site for each enzyme was in the multiple cloning site so separate digests linearised the plasmid whilst a fragment of approximately 780bp was liberated with a joint digest. A fragment for subcloning was obtained with a *Bam*H I and *Sal* I digest followed by gel extraction using a QIAEX kit (see DNA fragment isolation, page 55) (Figure 43, page 150).

The fragment was ligated into pGEM-4Z following *Bam*H I/*Sal* I digest and CIP treatment of the plasmid (see Subcloning for riboprobe production, page 55). To generate sufficient plasmid DNA for analysis of fragment incorporation, transformation of JM101 competent cells and plasmid minipreps were performed as described (Subcloning for riboprobe production, page 55). Correct orientation of the fragment in a 5/ to 3/ direction was assessed for a number of clones using a *Pvu* II digest, exploiting the asymmetric restriction site in the insert (Figure 42, page 149). The fragment sizes yielded for these were consistent with correct orientation (Figure 44, page 151) so one clone was selected for a maxiprep (see Maxipreps, page 58) and the plasmid was termed pG4MOG.

Separate *Eco*R I and *Hin*d III digests were carried out to linearise pG4MOG for sense and antisense riboprobe production respectively. Sense probe was generated from the SP6 promotor and antisense from the T7 promoter (Preparation of ^{35}S labelled riboprobes, page 60).

3.7.2.3 *In situ* hybridisation study

3.7.2.3.1 Methods

The technique was carried out on cryosections of cervical spinal cord from mice of 10, 20 and 50 days as described in *In situ* hybridisation, page 60.

3.7.2.3.2 Results

The distribution of positive cells and qualitative assessment of their numbers was indistinguishable from that of *Plp* expressing cells at the same age (Figure 45, page 152).

3.7.2.4 Discussion

This study shows that oligodendrocytes in *hsh* were transcribing the *Mog* gene and taken in conjunction with the immunostaining, were capable of producing a considerable amount of protein. The number of *Mog* expressing cells was comparable to those positive for *Plp,* an unsurprising finding in light of expression of both proteins relatively late in myelination (Coffey and McDermott, 1997). Although these findings do not necessarily exonerate the *Mog* gene as a candidate, it does appear to reduce the likelihood. Later work in the genetic study actually excluded chromosome 17 as harbouring the *hsh* gene, substantiating these observations.

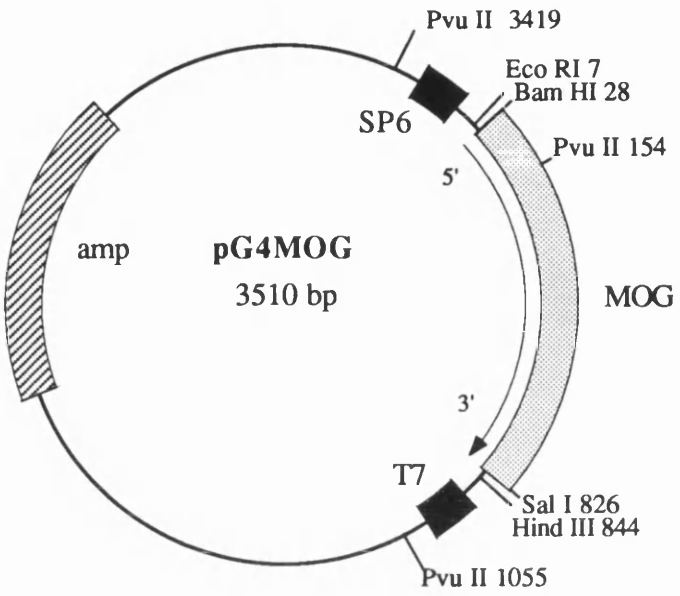

<u>*Pvu* II restriction profile</u>

MOG insert 5′-3′	*MOG* insert 3′-5′
2364/901/**245**	2364/791/**355**

Figure 42: pG4MOG plasmid map showing restriction sites utilised in the study. Diagnostic *Pvu* II restriction profile is shown below. The diagnostic fragment sizes used in identification are shown in bold.

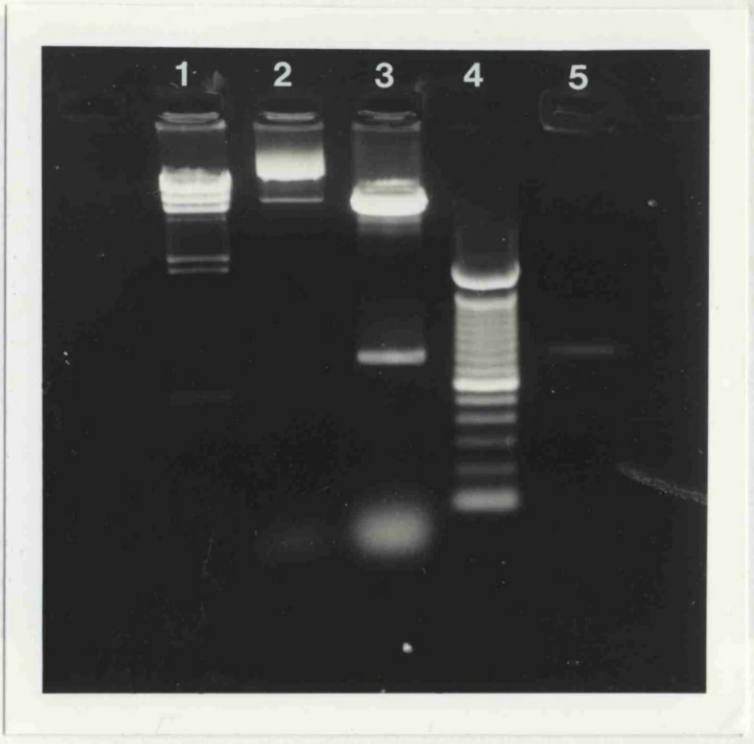

Figure 43: pCL642 digests; Lane 1 λ*Hin*d III marker, Lane 2 undigested pCL642 with insert, Lane 3 *Bam*H I/*Sal* I digest showing liberated fragment, Lane 4 100bp calibration ladder, Lane 5 isolated fragment.

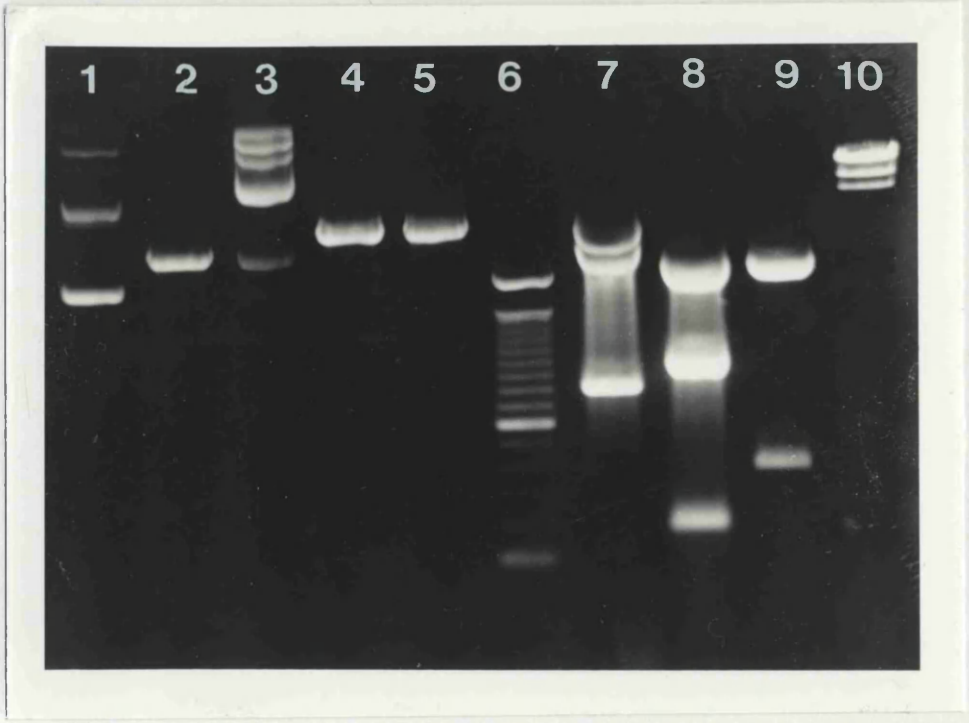

Figure 44: pG4MOG orientation digests. Lane 1 undigested pGEM4Z, Lane 2 pGEM4Z *Bam*H I/*Sal* I digest, Lane 3 undigested pG4MOG, Lane 4 pG4MOG linearised with *Hin*d III, Lane 5 pG4MOG linearised with *Eco*R I, Lane 6 100 bp calibration ladder, Lane 7 pG4MOG *Bam*H I/*Sal* I digest to show insert, Lane 8 pG4MOG *Pvu* II digest to liberated a fragment of about 250 bp, Lane 9 PGEM4Z *Pvu* II digest and Lane 10 λ*Hin*d III marker.

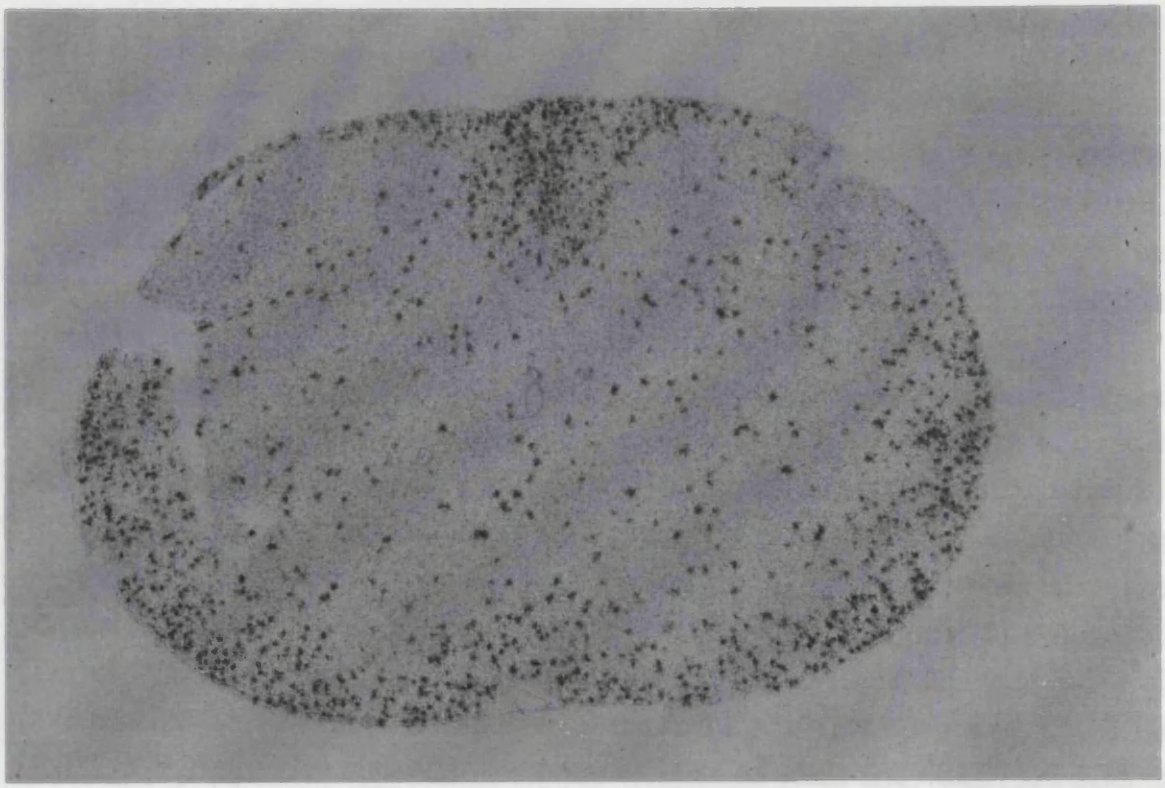

Figure 45: Autoradiogram from a 20 day old *hsh* spinal cord hybridised for *Mog* and counterstained with haematoxylin. The distribution and number of positive cells is similar to that seen with *Plp*. (Approx. magnification x50).

3.7.3 Western blotting for CNP

3.7.3.1 Introduction and aims

Linkage of the *hsh* gene to the middle third of chromosome 3 was identified towards the end of the study period. One of two reported *Cnp* genes, *Cnp2,* has been mapped to chromosome 3 (Bernier *et al.*, 1988), at a position about 3cM proximal to the region of the *hsh* locus on the Chromosome Committee map (http://www.informatics.jax.org). However, different mapping techniques mean that precise distances and positioning of markers and genes cannot always be relied on in combined maps (see Genetic maps, page 74 for discussion of genetic maps) so *Cnp2* was still considered as a candidate. The protein product for *Cnp2* remains to be elucidated (see 2', 3'-cyclic nucleotide 3'-phosphodiesterase (CNP), page 25), although it has been suggested that it may generate a particular CNP protein isoform or exhibit activity in specific tissues (Bernier *et al.*, 1988). It has also been suggested that it may be a pseuodgene or encode for a CNP-related polypeptide (Bernier *et al.*, 1988). The most logical initial strategy thus appeared to be the investigation of CNP protein isoforms in the *hsh* CNS. Two peptides, CNP1 and CNP2, with respective apparent molecular weights of 46kD and 48kD, are detected in the mouse (Sprinkle *et al.*, 1978). Western blotting was undertaken with the assistance of Mr Douglas Kirkham to study total protein and relative isoform levels in *hsh.*

3.7.3.2 Materials and Methods

Spinal cords were obtained from P20 *hsh* and wild type animals and processed for protein extraction (Isolation of protein from tissue, page 66). These were analysed by western blot and immunostained for CNP using polyclonal CNP antibody (P. Brophy) (SDS-polyacrylamide gel electrophoresis, page 66).

3.7.3.3 Results

There is a marked reduction in the level of CNP protein in *hsh* spinal cord. However, both isoproteins are present, with the 46kDa form predominating as in the control sample.

3.7.3.4 Discussion

Genetic mapping of the *hsh* mutation identified a region on chromosome 3 that was likely to contain the mutated gene (Fine mapping of chromosome 3, page 187). The interval was examined for candidate genes on integrated mouse genetic maps (http://www.informatics.jax.org) and was found to be about 3cM distal to the map position of one of the two reported *Cnp* genes, *Cnp2.* The precise role of CNP in

myelination is not yet entirely elucidated (2', 3'-cyclic nucleotide 3'-phosphodiesterase (CNP), page 25) but it appears to be the first myelin-related protein detected during development (Trapp, 1990), and has postulated roles in signal transduction (Thompson, 1992) and in the formation of cell processes that contact and envelop axons (Gravel *et al.*, 1996). The suggestion has therefore been made for a role in early myelination. Interestingly, oligodendrocytes in transgenic mice with extra copies of *Cnp* appear to mature earlier in development, resulting in premature maximum gene expression for *Mbp* and *Plp* (Gravel *et al.*, 1996). This contrasts to the retardation of myelination and the reduction in numbers of mature oligodendrocytes that is identified in *hsh.* Taken with the putative functions for CNP, this made *Cnp2* a potentially interesting candidate gene. CNP is also found at lower levels in the PNS and a number of non-neural tissues but since no abnormalities were detected in the *hsh* PNS or in other body systems, it is not clear how this would relate to a mutation in *Cnp2.*

However, a complication in the analysis of *Cnp2* as a candidate arose from the putative identification of two *Cnp* loci in the mouse, on chromosomes 3 and 11. No function has yet been ascribed to the gene on chromosome 3 and in fact it has been reported that both mRNA isoforms (*Cnp1* and *Cnp2*) are transcribed from the single gene on chromosome 11 (Monoh *et al.*, 1989; Kurihara *et al.*, 1990). *Cnp1* mRNA gives rise to the smaller CNP1 protein (46 kDa) while *Cnp2* mRNA generates the larger CNP2 protein (48 kDa). In man only the homologue to the mouse chromosome 11 gene has been described (Sprinkle *et al.*, 1992), although two protein isoforms and mRNAs have been identified (Douglas and Thompson, 1993). Nevertheless, it seems ostensible that one isoform may be preferentially generated from each of the two genes in the mouse, perhaps at different stages of development and/or in different tissues. Interestingly, it has been shown that one mRNA isoform, *Cnp2*, is specifically expressed in oligodendrocyte precursors *in vitro* (Scherer *et al.*, 1994). The absence of abnormalities in other *hsh* tissues might also be explained if these utilise an isoform from the *Cnp* gene on chromosome 11. If isoform or tissue-specific expression from the two genes is the case and *Cnp2* is the affected gene, it could be hypothesised that an absence or marked reduction in one protein isoform might be found in *hsh* CNS tissue. Immunostaining for CNP had previously shown a reduction in the intensity of staining (Immunostaining of the cervical cord, page 91) but did not distinguish between isoforms. It was therefore considered a useful undertaking to establish the presence and proportions of the protein isoforms using western blotting.

The data presented here demonstrates that both isoforms are present in *hsh* spinal cord, although markedly reduced in amount. In normal mice, the ratios of the

46kDa and 48kDa isoforms are about 10:1 (Thompson, 1992) and as an approximation, no marked deviation from this appears to occur in *hsh*. It must therefore be concluded that, if *Cnp2* does encode for a CNP isoform, there is no convincing evidence that a mutation of this gene is responsible for the *hsh* phenotype. The reason for the rather marked reduction in protein levels remains obscure. *Cnp* mRNA and protein expression have been studied in some myelin mutants and do not seem to correlate with the amount of myelin present; virtually normal CNP protein and mRNA levels have been reported, for example, in shiverer mice (Mikoshiba *et al.*, 1980) whilst others, including quaking and shaking pup, show reduced expression (Kurihara *et al.*, 1989; Nadon and Duncan, 1996). None of these mutations involves *Cnp*, and the significance of the CNP levels has not been explained.

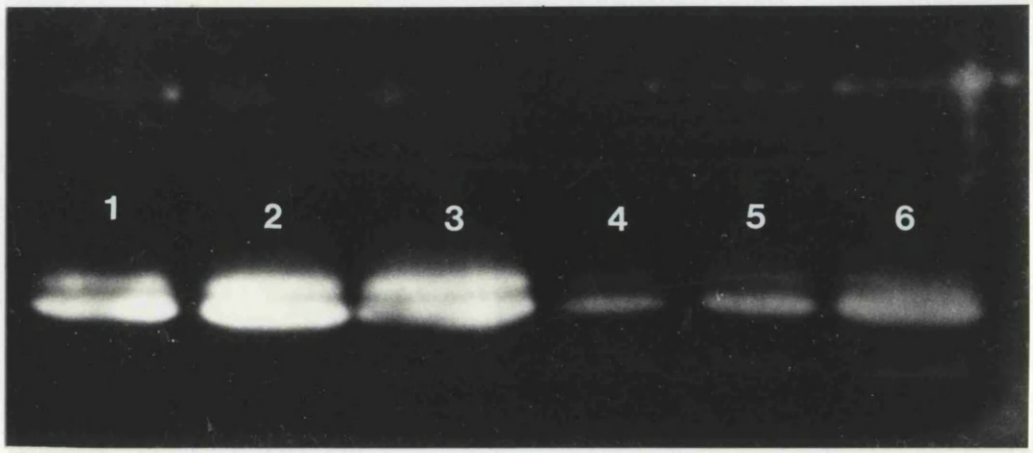

Figure 46: Western blot for CNP in wild type and *hsh* spinal cord. Lanes 1,2,3 aliquots of wild type protein, Lanes 4,5,6 equivalent aliquots of *hsh* protein. A marked reduction is seen in the mutant and although the 48kDa band is faint, both isoforms can be detected.

4. Discussion of the *hsh* phenotype

The pathway from spontaneous mutant phenotype to gene function has been successfully employed in the deciphering of several myelin genes. Particularly profitable has been the analysis of those genes coding for structural proteins of CNS and PNS myelin, such as MBP, PLP and P_0 (Nave, 1995). Few regulatory genes have yielded spontaneous phenotypic mutants, with the exception of quaking, although several mutants remain uncharacterised (see (Lunn *et al.*, 1995; Griffiths, 1996) for reviews). It is likely that, in the absence of mutant phenotypes, the existence or function of many of these genes would not have come to light for some time and new mutations resulting in impaired myelination are obviously extremely valuable. The novel spontaneous hindshaker mutation represents a unique opportunity to identify and study a previously unrecognised function of a known protein or an entirely novel protein involved in the synthesis of CNS myelin. A description of the phenotype that results from abnormal *hsh* gene product has been provided in an attempt to shed some light on the putative function(s) of the protein in normal myelination and a number of candidate genes have been excluded.

Within the *hsh* CNS, the spinal cord is the most severely affected area, whilst the brain shows a caudal to rostral gradient of hypomyelination. In contrast, many of the CNS mutants exhibit the reverse pattern of hypomyelination, for example, shiverer, quaking and the *Plp* mutants (for example, see (Friedrich, Jr., 1974; Duncan, 1990; Nave, 1994; Lunn *et al.*, 1995; Griffiths, 1996)), although a similar distribution is seen in some uncharacterised canine mutations (Duncan, 1987; Kornegay *et al.*, 1987; Lunn *et al.*, 1995). In addition, the myelin sheaths of all diameters of axons are affected within a region, so it appears that the *hsh* gene product relates to oligodendrocyte heterogeneity in terms of location rather than the diameter of target axons or time of myelination. A partial resolution of the myelin defect occurs between 30 and 50 days of age, the time of peak myelin formation in the spinal cord of mutant mice.

A moderate reduction in total cell numbers is found in conjunction with hypomyelination and appears to be due to a paucity of oligodendrocytes. *In situ* studies using *Plp-1* as a marker for mature oligodendrocytes show a more dramatic reduction in cell numbers throughout the CNS that reflects the extent of the hypomyelination. This suggests there is an overall reduction in the total oligodendrocyte population with a more profound decrease in the numbers of fully differentiated cells in young mice. It appears very likely that hypomyelination is at least partly a consequence of insufficient myelinating oligodendrocytes but it remains to be answered at what precise stage(s) oligodendrocyte development is

impaired. It is therefore difficult to conjecture about the putative function(s) of the *hsh* gene at this stage.

As oligodendrocytes are post-mitotic cells, the total population size in a region depends on the number of precursors that migrate into it, their proliferative capacity and the proportion that undergo apoptosis (Barres *et al.*, 1992a). The final stages of differentiation will determine the number of mature cells. A hypothesis of dysfunction of one or more of these developmental process(es) in *hsh* must be able to account for the findings of a moderately reduced total oligodendrocyte population and a greatly decreased number of fully differentiated cells, and explain the regional effects of the mutation. The normal distribution of oligodendrocytes in all areas of the *hsh* CNS examined suggests that it is unlikely that impaired migration of precursor cells is the basis of the reduced oligodendrocyte population. Other aspects of oligodendrocyte development must therefore be considered in relation to the *hsh* mutation.

Oligodendrocytes appear to originate in discrete regions of the developing CNS (Warf *et al.*, 1991; Noll and Miller, 1993; Pringle and Richardson, 1993; Ono *et al.*, 1995; Dickinson *et al.*, 1996). The correct environmental cues and subsequent mechanisms for mediating the choice of cell fate are likely to be important in the establishment of an appropriate founding population for this lineage. The induction of an inadequate precursor population could result in a dearth of mature cells if proliferation and survival were not compensatory. It has been shown that the induction of oligodendrocyte precursors in the spinal cord and hindbrain is influenced by the dorsoventral axis of the developing neural tube, in particular, signals from the notochord and the floorplate (Orentas and Miller, 1996; Pringle *et al.*, 1996). In more rostral regions of the developing CNS, oligodendrocyte precursors appear to be generated both from the ventral diencephalon (Pringle and Richardson, 1993) and the subventricular zones surrounding the lateral ventricles (Levison *et al.*, 1993a; Levison and Goldman, 1993b). It is not known whether this is specified by signals from an organising centre equivalent to the notochord/floorplate of the more caudal hindbrain and spinal cord and if so, the nature and location of this putative centre remains unknown. Since different structures appear critical for oligodendrocyte induction in distinct regions of the CNS, it is feasible that a mutation may impair induction in one region exclusively or more profoundly than in another. However, it might be expected that precursor proliferation and survival would compensate to a large extent for a paucity in founding cells, particularly as it seems likely that the regulation of proliferation and survival is dominated by local environmental signals and competition for growth factors. With fewer precursors, one would surmise that greater stimulation of

proliferation might occur and that less cell death would result from reduced competition for limiting growth factors. An initial approach to the study of precursor induction could be made using ISH with a probe to *PDGFRα*, a marker that appears to be specific for oligodendroycte precursors at the time of their development (Pringle and Richardson, 1993); this would provide an assessment of oligodendrocyte precursor numbers in various CNS regions and their proliferation rate could then be subjected to investigation.

Alternatively, increased cell death, perhaps due to an absence of, or an inability to respond to, survival factors, or a reduction in precursor proliferation would explain the decrease in *hsh* oligodendrocyte numbers. However, cell death is not a feature of the mutation on resin or EM sections, although clearance of apoptotic cells is very rapid (Raff, 1992; Barres *et al.*, 1992a) and it is possible that some increase could pass undetected. Cell proliferation has not yet been studied in *hsh* but should certainly be regarded as one of the next avenues for investigation.

Differentiation and/or formation of myelin sheaths may also be impaired in *hsh* oligodendrocytes. A defect in the late stages of maturation is suggested by the finding of a relative decrease in the number of *Plp* expressing cells that is apparently greater than the reduction in total oligodendrocyte numbers. However, if a delay in maturation is the sole basis for the deficit in mature oligodendrocytes, the total number of oligodendrocytes should remain unaltered, which does not appear to be the case. It therefore seems likely that there is both impaired generation of cells, for whatever reason, and a defect in their differentiation to fully mature oligodendrocytes. Interestingly, there is no evidence for slower differentiation of *hsh* oligodendrocytes in culture, suggesting *in vitro* development can proceed normally.

The ability of individual mature *hsh* oligodendrocytes to produce myelin has not yet been investigated. Since very few axons acquire sheaths of normal thickness, it is possible that individual oligodendrocytes generate less myelin that their wild type counterparts. However, it is also conceivable that these cells are in fact compensating for the cellular paucity by producing longer internodes and/or more of them; therefore, although individual sheaths are abnormally thin on cross-section, the amount of myelin produced by each oligodendrocyte would be normal or even increased. Increased production of myelin by individual oligodendrocytes has apparently been demonstrated in female carriers of the jimpy gene, suggesting flexibility in the amount of myelin that individual oligodendrocytes can produce (Skoff and Ghandour, 1995).

The environmental signals regulating oligodendrocyte lineage induction and development and the cellular mechanisms mediating the responses are complex and poorly understood, and with the current knowledge of the *hsh* phenotype, lengthy conjecture on the specific function of the mutated gene is difficult. As discussed, the gene could be involved in any or all of the stages of oligodendrocyte development, and it could be expressed either by oligodendrocytes or by signalling cells such as neurons or astrocytes in the environment. It must also be remembered that with a mutant phenotype, one is studying the whole response of a system to the absence or dysfunction of a specific protein, and not purely the removal of the culprit protein. To extricate from a complex phenotype the function of one single component can be a monumental task.

In summary, it appears that retarded myelination in the *hsh* mouse is at least partly due to a paucity of myelinating cells. The partial resolution of the myelin defect is related to increasing numbers of oligodendrocytes. Defective function of the *hsh* gene product retards oligodendrocyte development more profoundly in the spinal cord and hindbrain than forebrain, which suggests regulation of different oligodendrocyte populations that is dependent on their location. The reason for the cellular deficit is not yet known but could involve oligodendrocyte precursor induction, proliferation and/or survival. Differentiation of post-mitotic cells and formation of myelin sheaths may also be impaired. Much work remains to be done on characterising this phenotype, the most pressing of which must include cell mitosis studies to examine cell proliferation and *in situ* hybridisation for *PDGFRα* to quantify precursor numbers. Although the study is far from complete, it has laid the foundations for further analysis of the *hsh* phenotype. Characterisation of the gene and its protein product should elucidate another aspect of the complex network of pathways and interactions involved in CNS myelination.

5. Linkage mapping of the *hsh* mutation

5.1 General introduction and aims

The fundamental goal of molecular biology is to understand, at the molecular level, how genotype is translated into phenotype. One pathway in the analysis of gene function begins with a mutant phenotype and follows this back to a clone of the altered gene. The process of moving from a phenotypic difference to the causative gene is referred to as positional cloning and can be divided into two distinct stages. Firstly, linkage analysis is performed to find flanking DNA markers that lie very close to the gene of interest. The second stage involves cloning across the region that must contain the gene responsible for the phenotype, and then separating the desired sequence from other genes and non-genic sequences within this interval. It was the first stage that formed the basis of the *hsh* study.

Breeding studies carried out at Harwell had established the mode of inheritance as autosomal recessive and disproved the possibility of mutation at the previously characterised quaking locus (Beechey, 1993). Immunostaining had confirmed the qualitative presence and distribution of the major myelin proteins. Since no other known myelin genes or dysmyelinating mutants appeared to be possible candidates for the *hsh* mutation at that time, it was necessary to set up a new mapping cross in which DNA markers from across the genome could be tested for linkage. This was initially carried out at Harwell using classical linkage analysis with visible markers to establish a chromosomal location. Within the first year of the study, linkage was found between *hsh* and two markers, brachury (T) and tufted (*tf*), on chromosome 17 (Beechey and Cattanach, 1996), the results of which indicated that the *hsh* locus lay distal to quaking, also on chromosome 17. Final results suggested that *hsh* was positioned about 29cM distal to *tf,* which is located at 12.5cM from the centromere. Incomplete penetrance of the *hsh* phenotype was identified on these backgrounds (Beechey and Cattanach, 1996). The *Mog* locus lies distal to quaking on chromosome 17 (Pham-Dinh *et al.*, 1993) and, being a CNS myelin-specfic gene, it was a strong candidate gene. The investigations of *Mog* gene expression using immunostaining and *in situ* hybridisation have been discussed previously in Analysis of candidate genes, page 146. Since there was no evidence for this as the altered gene, with positive immunostaining and strong hybridisation signal, and no other candidate genes were obvious, fine mapping of the chromosome 17 locus using molecular techniques and an intersubspecific backcross was initiated as part of the *hsh* study.

5.2 Breeding of mouse mapping panels

5.2.1 Introduction and aims

For fine mapping of the putative *hsh* locus on chromosome 17, it was necessary to establish a recombinational backcross to follow the inheritance of polymorphic microsatellite markers in the F2 offspring. The aim was to collect 500-1000 F2 mice from an appropriate backcross to map to a sufficiently small interval for the next stage of positional cloning.

5.2.2 Materials and Methods

5.2.2.1 Mouse breeding

Outcrosses to generate F1 mice were set up with *Mus spretus* (*spretus*), CAST/Ei (CAST), C57BL/6J (C57) and BALB/cJ (BALB) mice and where successful, F1 mice were backcrossed to *hsh* to produce F2 offspring as described in Breeding, page 68. Only *hsh* mice that had a marked tremor as young animals were used for breeding. The offspring from the backcross matings were graded on the basis of a shaky phenotype at 20 days of age and tissues retained after euthanasia as necessary.

5.2.2.2 Principles of phenotypic analysis

The principles underlying the expected distributions of F2 *hsh* versus wild type phenotypes are described in General principles of linkage analysis, page 71. In summary, since *hsh* is an autosomal recessive condition, two mutant alleles are required to express a shaky phenotype. Half of F2 mice inherit two *hsh* alleles and should therefore exhibit a shake. The other half are heterozygous at the *hsh* locus and should be phenotypically wild type.

5.2.2.3 Histopathology

The first 50 mice (*hsh* and wild type phenotypes) from the CAST backcross were phenotypically scored and their cervical cords processed for resin embedding (see Resin processing and sectioning, page 46). Thick sections were cut and stained with methlyene blue/azur II (see Methylene blue/azur II for resin sections, page 47) for light microscopic examination of white matter.

5.2.3 Results

5.2.3.1 Intersubspecific backcross

Two *spretus* males were obtained but failed to breed with *hsh* females and this attempt was abandoned. From the CAST backcross, 1122 F2 mice were weaned over a period of 20 months; litter sizes were subjectively comparable to wild type and *hsh* stock maintained under similar conditions and there was no apparent abnormal neonatal death. Only 93 (8.2%) phenotypically *hsh* animals were identified. The sex of the F1 *hsh*/CAST parent did not influence the production of *hsh* mice, with F1 males responsible for 42 of the 93 animals (45%). The sexes of the F2 mice were equally distributed with 46 females and 47 males. There was some variation in the intensity of the tremor and subjectively, mice did not appear as shaky as the outcross and backcross *hsh* parents had been at the equivalent age.

Examination of cervical cord sections obtained from the first 50 CAST backcross mice confirmed the accuracy of phenotypic identification. No mice had been misidentified phenotypically and only the cords from the phenotypic *hsh* mice (4/50) exhibited hypomyelination histologically.

5.2.3.2 Interstrain backcrosses

Over a ten month period, 176 F2 mice were weaned from an interstrain backcross using C57 mice. Of these, 68 mice (38%) of both sexes were scored as phenotypically *hsh*. The tremor was subjectively comparable in intensity to the *hsh* outcross and backcross parents and showed little variation between mice of the same age.

During the same time, 139 F2 mice were born from an interstrain backcross employing BALB as the second parental strain. Only 27 (19.4%) of these had a definitive shake. There was some variation in expressivity and the impression was that mice did not tremor with as much intensity as those on the C57 background.

Litter sizes in both crosses appeared normal and there was no apparent increased incidence of neonatal death.

5.2.4 Discussion

One of the first decisions to be made in the establishment of the backcross was the choice of the second parental species or strain. A balance had to be struck between the considerations of genetic distance and the ability to generate offspring in which segregation of the mutant allele could be observed. Initially an interspecific backcross using *Mus spretus* was considered as this is the most distant species from

M. musculus that still allows the production of fertile F1 hybrids (Avner *et al.*, 1988). DNA polymorphisms are therefore more numerous than between more closely related mice. However, the F1 males are infertile so that only female meiosis can be examined and there is an inversion on chromosome 17 that may suppress recombination (Hammer *et al.*, 1989). This strategy was therefore quickly abandoned when the mice failed to breed.

Intersubspecific crosses using *Mus musculus castaneus* (CAST) for mapping purposes have largely supplanted *spretus* for mapping. Although more closely related to laboratory strains, the degree of polymorphism is still high, mice breed readily and are easy to handle, and both F1 sexes are fertile.

A surprising finding was the small proportion of shaking F2 mice identified on the CAST backcross. Half of all animals were predicted to be homozygous at the *hsh* locus and should therefore have demonstrated a tremor. Instead, only 8.6% were classified as *hsh*. A number of possible reasons were mooted for this finding, namely embryonic or early neonatal death of homozygous *hsh* on the CAST background, misclassification of mice or incomplete penetrance of the phenotype on this cross. Litter sizes were subjectively comparable to wild type and *hsh* stock which would tend to rule against embryonic death as the explanation. Neonatal death was not a feature. Misclassification of the phenotype was eliminated by histological examination of a large number of previously scored mice. The only remaining explanation was the incomplete penetrance of *hsh* on the CAST background. Presumably only about 17% of homozygous animals carried a complement of enhancing/suppressing alleles from the C3H/101 and CAST backgrounds that was permissive for the shaky phenotype. Support for this came from similar findings on the backgrounds used for classical linkage analysis (Beechey and Cattanach, 1996) and the fact that *hsh* was only 90% penetrant on the C3H/101 background at the onset of the study (see General phenotypic description, page 83). It has long been recognised that mouse mutants can show considerable variation in the penetrance and expressivity of a phenotype despite a common genotype, due to the presence of genes at other non-disease loci (Erickson, 1996). The mechanism(s) by which modifiers achieve their effects are still unclear in many cases but several pathways have been suggested. Suppression or enhancement of other involved genes is likely, perhaps by altering transcription rates, mRNA stability or modifying the degree of DNA methylation (Wilkins, 1990). Alternatively, a redundant gene may come into play to compensate for the mutated locus (Rozmahel, 1996).

The penetrance/expressivity of a particular mutation may vary between several different backgrounds, as in curly tail (Neumann *et al.*, 1994), presumably due to species/strain-specific modifying alleles that are not present in other strains. It was therefore decided to investigate the penetrance of *hsh* on a small number of inbred laboratory strains. Incomplete penetrance was apparent in both of the interstrain crosses although it was less profound than on the CAST backcross. On the C57 background, 76% of animals predicted to have a shaky phenotype were identified as *hsh.* About 40% of homozygous animals exhibited a phenotype on the BALB background. Presumably the number of loci at which the strain-specific allele suppressed the *hsh* phenotype was reduced in comparison to CAST as a result of the lack of genetic diversity that exists between inbred laboratory strains (Ferris *et al.*, 1982).

The incomplete penetrance of the *hsh* phenotype on the genetic backgrounds used in the mapping crosses had profound implications in terms of the numbers of mice that were to be bred. Usually in mapping studies, both the phenotypic wild type and the mutant animals are examined for recombination. In this project, only the shaky F2 mice could be used in linkage analysis; the genotype of the non-shaky mice could not be ascertained and it was therefore impossible to examine these mice for recombination between the *hsh* and marker loci. Since only about 1/12 mice from the CAST backcross exhibited a shake, a large number of F2 mice were required to generate 500-1000 useful samples, the minimum number considered necessary for mapping sufficiently close to a mutated gene for positional cloning. The higher penetrance on the interstrain backcrosses was open to exploitation to provide shaky F2 mice faster, but at the cost of genetic polymorphism and again, only the phenotypic *hsh* animals could be utilised.

5.3 Fine mapping of chromosome 17

5.3.1 Aim

The aim was to identify a set of markers flanking the disease locus as closely as possible. The first step in this process was the evaluation of a number of microsatellite primer pairs to select an appropriate set for use with the CAST backcross. The heterogeneous genetic background of *hsh*, which contained C3H, 101 and possibly other uncharacterised alleles from the original strains (see Background to the *hsh* mutation, page 80), had to be considered when testing individual primer pairs. The next step was the testing of the selected microsatellite markers with individual DNA samples from the backcross to establish the interval containing the *hsh* locus. Finally, samples from the C57 and BALB backcrosses were typed for a single marker for detection of linkage on these backgrounds.

5.3.2 Materials and Methods

5.3.2.1 gDNA preparation

gDNA was extracted from the tails of shaky mice from the F2 generations of the CAST, C57 and BALB backcrosses as described (see Preparation of genomic DNA, page 75). Fifty phenotypically unaffected mice from the CAST backcross were also subjected to the same treatment.

5.3.2.2 Selection of microsatellite primer pairs

Primer pairs were selected as described (Microsatellite primer pairs, page 76) to cover the proximal two thirds of the chromosome in order to span the region of interest.

5.3.2.3 PCR

Primer pairs were tested using the PCR protocol given in Polymerase chain reaction, page 77 and the products detected as described in Analysis of PCR products, page 78. If primers failed to produce clearly defined product, manipulation of PCR conditions was attempted; magnesium (Mg^{2+}) concentration, annealing temperature and cycle number were adjusted as considered appropriate. Formamide and Q-solution (Qiagen) were sometimes added to the PCR reaction to improve priming. If primers still failed to generate suitable PCR products after these simple measures, they were abandoned.

5.3.2.4 Mapping protocol and statistical analysis

The principle of linkage analysis is described fully in Genome-wide linkage analysis, page 72. For a description of statistical analyses, see Statistical analysis, page 73. Due to incomplete penetrance of the *hsh* phenotype, only the shaky F2 population could be utilised for mapping as the non-shaky mice were of unknown genotype; it was not possible to classify them as homozygous or heterozygous at the *hsh* locus and recombination events could therefore not be evaluated.

5.3.2.5 Illustration of linkage

For the sake of succinct illustration of the findings of linkage, PCRs were performed on pools of DNAs made up of equal amounts of DNA from each of the backcross mice (see Preparation of pooled DNA samples, page 76). Pools of CAST, C57 and BALB backcross DNA were made and run for D17Mit10 only. With an unlinked marker, a quarter of the alleles will be derived from CAST and the remainder will be C3H/101, giving 1:3 proportionate band intensities on a gel. If the marker is linked, more alleles are C3H/101 so this band increases in intensity whilst the CAST band becomes fainter. With very tight linkage, only a C3H/101 band is identified.

5.3.3 Results

5.3.3.1 Microsatellite primer pair selection

The primers shown inTable 5, page 170 were found to be suitable. Their positions on the chromosome gave good coverage for an initial scan to position the *hsh* locus more precisely prior to finer mapping (Figure 47, page 180). The product sizes for C3H and 101 differed from CAST and could be resolved on 3% Nusieve agarose gels. In an equal mix of C3H/CAST, both the C3H and the CAST bands were amplified with approximately equal intensity.

5.3.3.2 Intersubspecific backcross

In total, 78 F2 shaky mice from the CAST backcross were typed. The first 29 mice were typed for all 9 markers whereas the remaining 49 were only typed for D17Mit248, D17Mit10 and D17Mit6. The haplotypes derived from these animals are represented in Figure 48, page 181. Recombination rates were calculated using all mice typed for each marker whilst LOD scores were derived from only the 29 mice typed for all markers. Results are given in Table 6, page 171.

The lowest recombination rate detected was 20.7 ± 7.52 at D17Mit36 but only 29 mice were typed for this marker and this result was not statistically significant (χ^2 = 9.96, $p<0.005$). A recombination rate of 23 ± 4.77% was found for D17Mit10

MIT marker	C3H-derived allele (bp)	CAST-derived allele (bp)	Distance from centromere (cM)
D17Mit18	241	256	3
D17Mit248	104	134	5
D17mit44	154	128	15.5
D17Mit47	226	210	20
D17Mit36	114	146	22.5
D17Mit10	148	131	24
D17Mit9	115	132	30
D17Mit6	102	88	32
D17Mit2	230	250	46

Table 5: D17Mit marker panel used to type CAST backcross. Markers are ordered from centromere to telomere. Distances are based on the Whitehead/MIT map.

Mit Marker	Recombination rate	LOD score
D17Mit18	27.6 ± 8.27%	3.7
D17Mit248	26.4 ±4.96%	3.7
D17Mit44	20.7 ± 7.52%	4.5
D17Mit47	24 ± 7.9%	3.7
D17Mit36	20.7 ± 7.52%	4.5
D17Mit10	23 ± 4.77%	4.5
D17Mit9	27.6 ± 8.3%	3.7
D17Mit6	27 ±5%	3.7
D17Mit2	34.5 ± 8.87%	2.9

Table 6: Recombination rates and LOD scores for the D17Mit panel. Recombination rates were calculated for all mice typed for that individual marker whilst LOD scores have been calculated for only those 29 mice typed for all markers. Markers are ordered from centromere to telomere.

(18/78 animals are heterozygous) which was consistent with demonstration of linkage at $p<0.001$ ($\chi^2=22.61$). Recombination rates increased to 26 ± 4.96% at D17Mit248 proximally (20/78 mice) and 27 ± 5% at D17Mit6 distally (21/78 mice). No region of complete concordance i.e. homozygosity, was present and eleven mice were heterozygous across the entire region, specifically Maps 6, 42, 43, 77, 90, 96, 97, 98, 105, 108 and 124. LOD scores were significant for all markers except D17Mit2, with the highest score of 4.5 for D17Mit44, D17Mit36 and D17Mit10. Linkage is illustrated in Figure 49, page 185 where the pooled sample has been run against D17Mit10; the very weak CAST band and the strong C3H/101 band indicate the presence of little CAST DNA in the pool due to most mice carrying two C3H/101 alleles.

To rule against transmission distortion, that is, the non-random inheritance of a C3H/101 allele as opposed to a CAST allele, 50 of the phenotypically normal mice were tested for D17Mit248, D17Mit10 and D17Mit6. The recombination fractions were 53 ± 7%, 50 ± 7% and 48 ± 7% respectively, consistent with random recombination.

5.3.3.3 Interstrain backcrosses

Shaky mice derived from the C57 backcross were tested against D17Mit10. A recombination fraction of 38 ± 6.2% was calculated (23/61 recombinant mice) which was not indicative of statistically significant linkage ($\chi^2=3.69$, $p<0.05$). PCR of a pooled DNA sample containing contributions from all shaking mice on this background shows that compared to the 1:1 ratio in the control sample, there is no convincing evidence of a departure from the expected 3:1 ratio in the test pool (Figure 50, page 186). The same marker was used to test the small population of shaky mice from the BALB backcross and this time, a recombination rate of 22.5 ± 7.5% (7/31) was detected. Although this is not a statistically significant result ($\chi^2=9.22$, $p<0.005$), it is highly suggestive of linkage. A pooled sample demonstrates the linkage; the C3H/101 band is considerably stronger than the BALB and appears to exceed the expected 3:1 ratio (Figure 50, page 186).

5.3.4 Discussion

Before the typing of the backcross population could be performed, individual primer pairs had to be tested to ensure suitability for this study. The selection of appropriate microsatellite markers was complicated by the presence of the 101 background which has not been characterised for marker polymorphism. The significance of this lay in the fact that *hsh* mice could carry either a 101 or a C3H allele at any locus throughout the genome, so mapping required being able to define

polymorphism between 101 and CAST in addition to C3H and CAST. C3H and 101 alleles did not have to demonstrate polymorphism since they both originated from the same background. Primers were therefore ordered on the basis of marker polymorphism between C3H and CAST and then tested to ensure that the 101 and CAST bands were distinguishable. A useful guide was found to be the existence of very little polymorphism between the characterised laboratory strains for a marker but a large polymorphism between these and CAST; the 101 allele tended to be close to the size of the other laboratory strains rather than the CAST. Large polymorphisms between CAST and C3H also increased the chance of polymorphism between CAST and 101. In addition, it was important to establish that the primer pairs did not preferentially amplify one allele in the heterozygote animal. This probably occurs as a result of strain-specific sequence differences in the region of primer complementarity. It is usually, although not always, the laboratory strain that is amplified (Taylor *et al.*, 1994), which would lead to misclassification of heterozygotes as homozygotes with the false impression of linkage to that marker. An equal mixture of C3H/CAST DNA was used to test for this phenomenon and although it was not encountered with any of these markers, it did occur later in the mapping study and has been reported previously (Taylor *et al.*, 1994).

It was rather surprising when early in the study, it became apparent that a number of mice from the CAST backcross were heterozygous across the whole region, implying that they carried entire segments of CAST chromosome 17 where they should have harboured a mutant *hsh* allele. Several possible explanations for this were considered; misclassification of mice, contamination or confusion of samples, double crossover events, expression of a shaky phenotype in heterozygotes, a more distal location of the *hsh* locus and the erroneous mapping of a modifying locus were all debated. It also had to be considered that the putative linkage could in fact have been a genetic phenomenon associated with this particular genetic cross that led to preferential inheritance of two C3H/101 alleles rather than a CAST allele. In this scenario, apparent linkage would not be associated specifically with the *hsh* mutation but rather, with the strains of mice used in the backcross.

Misclassification of mice was felt to be most unlikely in view of the great care taken in retaining only those mice with a definitive shaky phenotype. In addition, Maps 6, 42 and 43 had been perfused and confirmed histologically as *hsh*. Confusion or contamination of samples also appeared an inadequate explanation since phenotypic *hsh* tissue constituted the only samples being collected and processed at that time; hence contamination/confusion could only occur between mice that were all homozygous at the *hsh* locus. However, in the unlikely event that contamination of

tail fur and skin with urine or faeces from other mice was influencing PCR results, DNA was also extracted from the spleens of these mice collected using aseptic techniques. Identical PCR results were obtained from the spleens for all markers.

Double crossover events do occur but their frequency depends on the genetic distance separating the two markers (Silver, 1995b) and the distances here are far too small for the numbers of crossover events that would be required to explain all heterozygous mice. Also, it would be expected that regions of homozygosity would be detected between flanking heterozygous regions, which was not the case.

Heterozygotes have been reported to exhibit a phenotype with a mutation that is recessive on other backgrounds, for example, the curly tail mouse mutant was long considered recessive until a small proportion of heterozygotes on different backgrounds expressed the phenotype (Neumann *et al.*, 1994). This suggested that *ct* may exhibit dominance in the presence of particular combinations of modifier alleles. In light of the much reduced penetrance of the *hsh* mutation on the CAST background, it seemed improbable that such a large proportion (14%, 11/78) of shaking mice would be heterozygous, but the possibility could not be excluded on the sole basis of these results.

A more distal location of the *hsh* locus on chromosome 17 was most unlikely in view of the location of D17Mit2, only 14cM from the telomere. Also, the recombination fraction for the whole group was increasing distally, indicating that linkage was reducing towards the telomere. For linkage to then increase again would require an unfeasible number of double crossover events.

It was possible that the tendency towards homozygosity was in fact not due to linkage with the *hsh* mutation but was due to transmission distortion. This occurs when two alleles are not equally inherited from the parent, perhaps because one combination is lethal in the embryo. Litter sizes were good, tending to rule against this, but confirmation was sought by testing 50 of the non-affected mice for 3 of the markers across the region. If transmission distortion was occurring due to the incompatible combination of CAST alleles with C3H/101 in this region, this would be seen for all mice, not just those expressing a phenotype. This was not observed and in fact, proportions were evenly distributed between heterozygotes and homozygotes. The removal of a small number of homozygotes (8%) did not significantly move the wild type population towards heterozygosity.

The remaining explanation was that classical linkage analysis had identified a region that was incompletely linked to the *hsh* phenotype, that is, a modifying locus. This would be consistent with a proportion of mice being heterozygous across the region

but a larger proportion showing linkage. Rather than the *hsh* locus lying 29cM distal to *tf,* as was indicated by linkage analysis (Beechey and Cattanach, 1996), this figure was likely to have been distorted by a proportion of heterozygous animals. The locus of interest would therefore lie substantially closer to *tf* than the recombination fraction indicated. However, it was surprising that a similar recombination rate was found for a number of markers spanning about 30cM of the chromosome; for a single modifying locus, it would be expected that markers located proximally and distally to the locus would exhibit higher recombination rates than was found here. The reason for the apparent extension of the region of linkage is not clear but it may be that more than one modifying locus was present on proximal chromosome 17. It is interesting that the same region was probably modifying penetrance on both the *tf* and CAST backgrounds, and the fact that linkage achieved statistical significance in both molecular and classical mapping experiments suggested that this was a major modifying locus. Whether or not it was the same gene within this region that was involved in both cases is not known but seems likely. Also intriguing is the finding that a curly tail modifier maps to the very same region, being roughly localised near D17Mit11 (Letts *et al.*, 1995). This marker lies between D17Mit44 and D17Mit10 and it is therefore appealing to conjecture that the same locus may be modifying the pentrance of both *ct* and *hsh* phenotypes. Curly tail embryos show a reduced rate of cell proliferation in the notochord and hindgut epithelium but not the neuroepithelium (Neumann *et al.*, 1994), causing ventral curvature and delayed closure of the neural tube. It has been hypothesised that *ct* may code for a protein associated with the cell cycle and that the modifier could be a transcriptional regulator, although no strong candidates were identified (Letts *et al.*, 1995). Since the notochord is involved in induction of oligodendrocyte precursors (Orentas and Miller, 1996; Pringle *et al.*, 1996), and *hsh* exhibits a lack of oligodendrocytes, it is imaginable, although rather tenuous, that the same modifier may be involved in the pathobiological pathways of both mutations. It must be borne in mind, however, that a region of this size contains many hundreds of genes and it may be no more than coincidence that two neurological mutants have a modifying locus within it.

Final confirmation that this was not the *hsh* locus came later in the study when mice from the C57 interstrain backcross were tested for D17Mit10. There was only very weak evidence of linkage, with 38% of mice inheriting a CAST allele from the F1 parent. The 80% penetrance on this background was much higher than the CAST; presumably modifying genes were less significant in this cross because of the lack of genetic diversity between the laboratory strains (Ferris *et al.*, 1982), which may account for the weaker linkage to the chromosome 17 locus. The stronger linkage to chromosome 17 found with the BALB backcross may at least partly explain the

lower penetrance on this background compared to the C57 backcross. In both cases, larger populations of mice may lead to statistical demonstration of linkage.

The aim of the project was the mapping of the *hsh* locus. Although linkage at a probability of 95% had been found to a region of chromosome 17 with a CAST backcross, it had been unequivocally shown that this did not contain the *hsh* locus. Undoubtedly it will prove interesting to examine this region in greater detail in the future, but it was necessary to pursue the elusive *hsh* gene for this study. Classical linkage analysis had not proceeded far prior to the discovery of linkage to chromosome 17, so no other chromosomal regions had been excluded. Consequently, the whole genome, except the X chromosome and chromosome 17, was available for analysis. Although a return to classical linkage analysis with phenotypic markers was contemplated, the decision to perform a genome scan using molecular techniques was made; now that the intersubspecific backcross was underway, albeit slowly with the low penetrance, and the PCR technique was established, it was likely to be a faster and more accurate process. However, as with all these things, an element of luck is indispensable.

5.4 Genome scan for chromosomal identification

5.4.1 Background and aims

Having excluded chromosome 17 as harbouring the *hsh* locus, it was necessary to initiate a genome scan for location of an alternative subchromosomal region showing linkage to one or more markers. A stratified protocol is the most efficient approach so that only a small number of samples are typed for initial linkage detection and when linkage is found, the remainder of the animals are typed for these markers. Once this first stage is completed, it is possible to concentrate on the construction of a high resolution map in the vicinity of the locus using a selected set of markers and a handful of recombinant animals.

5.4.2 Materials and Methods

5.4.2.1 Preparation of DNA

Samples were prepared previously as described in Preparation of genomic DNA, page 75. Only backcross mice with a shaky phenotype were typed.

5.4.2.2 Selection of microsatellite primer pairs

Primer pairs were selected as discussed (Microsatellite primer pairs, page 76). Since markers cover 15cM proximally and distally, they were chosen to be no more than 30cM apart, and proximal and distal markers were no greater than 15cM from the centromere and telomere respectively. Markers from chromosomes 8, 9, 10, 11, 1, 2 and 3 were tested and a number of these typed for the CAST backcross.

5.4.2.3 PCR

Primer pairs were first tested on C3H, 101, CAST and a C3H/CAST pool using the standard protocol given in Polymerase chain reaction, page 77 and the products detected as described (Analysis of PCR products, page 78). Those that did not yield easily interpreted results were abandoned to allow progress with primer pairs that did. Useful markers were subsequently tested with 52 shaky CAST backcross mice.

5.4.2.4 Principles of linkage analysis

This is discussed fully in General principles of linkage analysis, page 71. The aim was to cover as much of the genome as rapidly as possible with primer pairs that were straightforward to use. Genetic distances, where given, were obtained from

the Whitehead/MIT map (http://www-genome.wi.mit.edu) which is based on a C57BL/6J-ob and CAST/Ei intercross.

5.4.2.5 Statistics

The calculation of recombination rates, genetic distances and significance values is described in Statistical analysis, page 73.

5.4.3 Results

The recombination rates for those markers which were successful are summarised in Table 7 below.

Mit marker	C3H-derived allele (bp)	CAST-derived allele (bp)	Distance from centromere	Recombination rate (± SE)
D11Mit36	240	302	44cM	42 ± 7.3%
D11Mit180	147	167	70cM	42 ± 7.3%
D8Mit211	166	186	50cM	37.5 ± 6.7%
D8Mit13	91	114	70cM	50 ± 6.9%
D8Mit64	156	106	15cM	50 ± 6.9%
D1Mit33	94	114	82cM	46 ± 6.9%
D1Mit224	142	120	111cM	41 ± 6.8%
D2Mit1	120	140	2cM	39 ± 6.7%
D2Mit25	138	116	85cM	46 ± 6.9%
D3Mit203	138	158	10cM	25 ± 5.4%
D3Mit127	168	106	49cM	20 ± 4.6%

Table 7: Microsatellite marker panel tested in genome scan. Product sizes, distance from the centromere and recombination rates are given.

Significant results were obtained for D3Mit203, positioned 10cM from the top of chromosome 3, which was found to recombine with a frequency of 25 ± 5.4% (16/64 mice) (χ^2=16, p<0.001), and D3Mit127, 49cM from the centromere, which gave a recombination fraction of 20 ± 4.6% (15/73 mice) (χ^2=25, p<0.001). Two mice were heterozygous for both markers. At this point, the genome scan was halted while a detailed analysis of chromosome 3 was performed.

5.4.4 Discussion

To analyse as much of the genome as expediently as possible, unsuitable markers *i.e.* those that did not give good PCR results or yielded 101 bands similar to CAST, were left to allow testing of potentially more profitable primer pairs. The regions covered by these markers were to be returned to at a later date if linkage had not been detected elsewhere in the genome. Seven out of 20 markers tested here did not prove useful, which is similar to findings in other projects (Taylor *et al.*, 1994) (C. Rasberry, I. Jackson, personal communications).

No linkage was detected on the distal two thirds of chromosome 11, on chromosome 8, the distal half of chromosome 1 or proximal and distal chromosome 2. Significant linkage was evident for two markers on chromosome 3, one proximal marker, D3Mit203 and one about 40cM distal to this, D3Mit127. The finding of a recombination fraction of 25 ± 5.41% for a marker only 10cM from the centromere suggested that the locus lay distally, or that weak linkage was present, such as might occur for a modifying locus. However, the finding of a recombination rate of 20 ± 4.68% for a more distal marker tended to suggest the former and that the locus lay in the intervening region. The addition of the two recombination fractions should be about equal to the genetic distance separating the markers and although a different cross has been used by the Whitehead/MIT, their distance of about 39cM was very close to the value of 45cM obtained here.

Two mice were heterozygous for both markers and may therefore not have possessed a region of homozygosity in the interval of interest. However, it was possible that they were double recombinants. Suppression of recombination occurs within the chromosomal vicinity of an initial crossover event and is responsible for a severe reduction in the expected frequency of double crossover events in 10-20cM lengths of the genome. These two markers are separated by about 40cM so the effects of recombination suppression are not strong and in fact, the double recombinant rate can be evaluated from multiplying the two single recombinant fractions, *i.e.* treating the events independently. Thus a double recombinant rate of 5% (5/100) can be expected for these markers based on a probability of recombination of 0.2 for one marker and 0.25 for the other. Thus, 2/64 doubly recombinant mice would not be surprising. Further linkage testing in the region of interest was therefore initiated with a very strong suspicion that linkage had been found with the disease locus rather than another modifier.

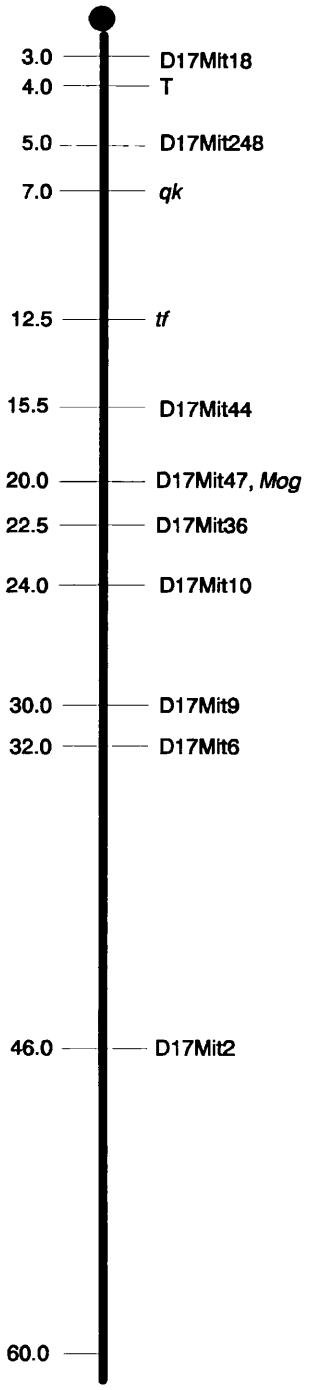

Figure 47: A genetic map of chromosome 17 showing the location of pertinent loci in terms of recombinational distance from the centromere. Microsatellite markers used in this study, brachyury (T), tufted (*tf*), quaking (*qk*) and myelin-oligodendrocyte glycoprotein (*Mog*) are shown. The putative *hsh* locus was mapped to about 29 cM distal to *tf*. Distances should be regarded as very approximate.

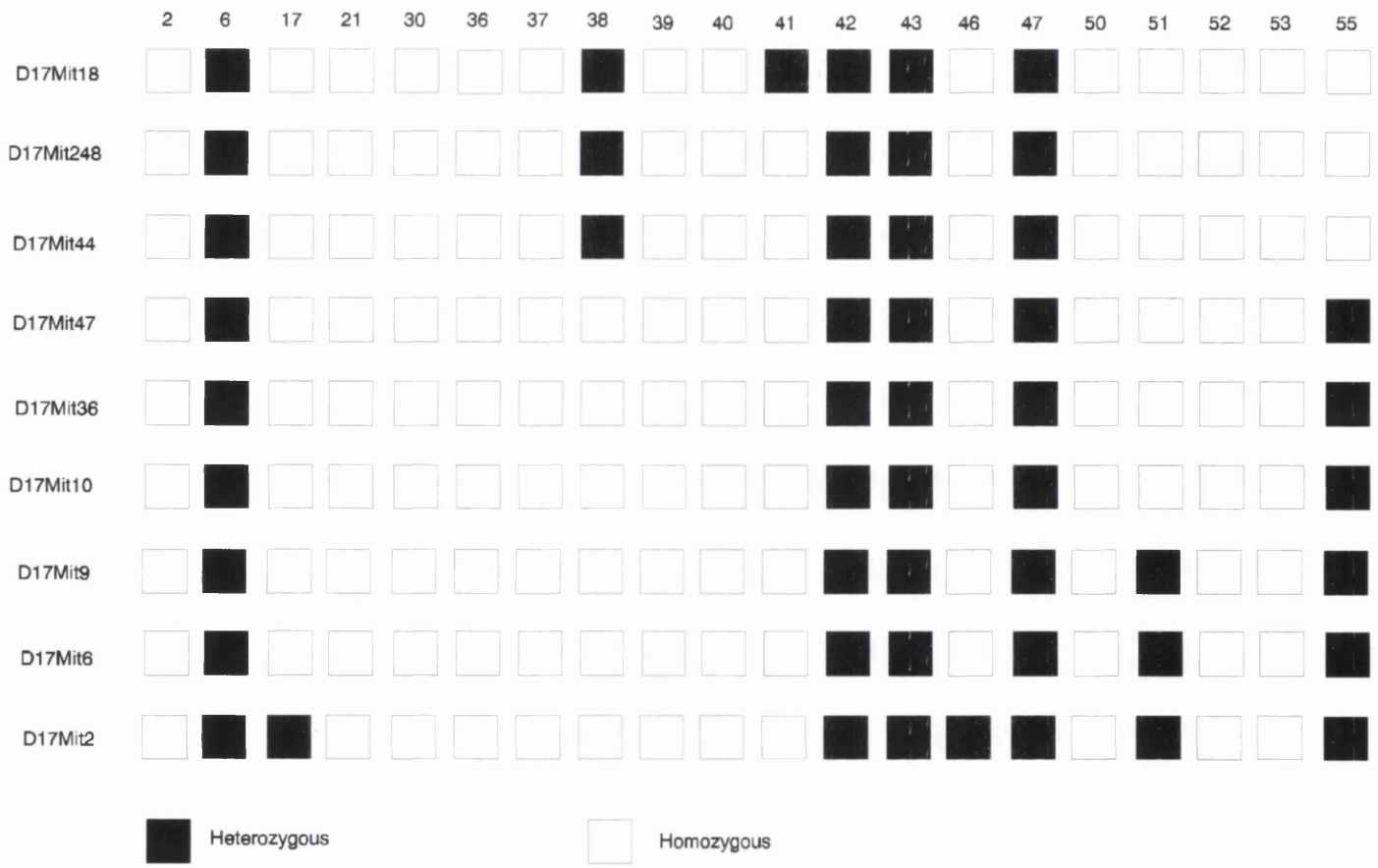

Figure 48: Haplotypes of F2 mice generated from the *hsh*/CAST backcross. All mice were homozygous at the *hsh* locus on the basis of a shaking phenotype and are identified numerically. Homozygosity for a marker is indicated by an open box whilst heterozygosity is shown as a filled box. Markers are ordered from centromere to telomere.

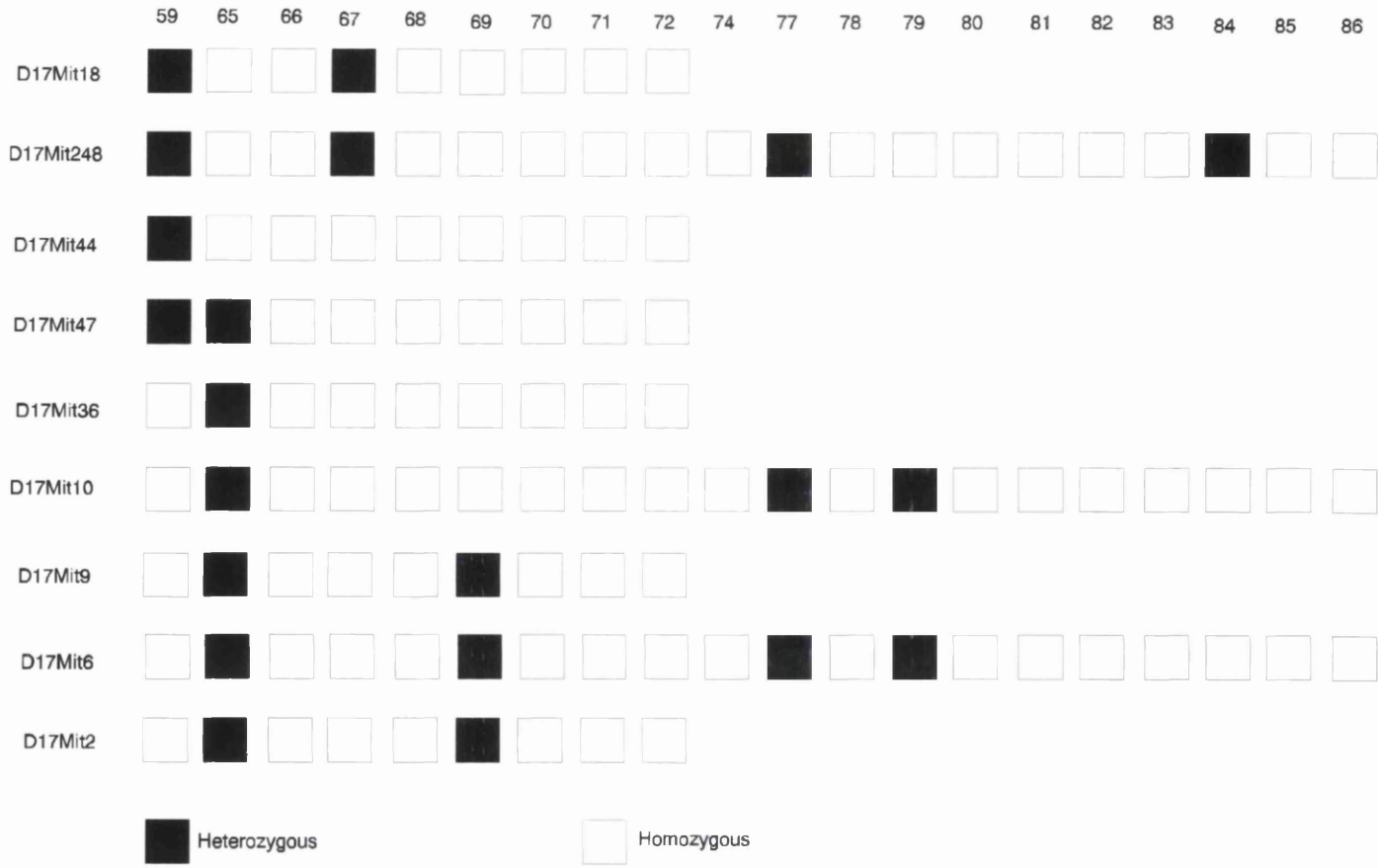

Figure 48 (cont): Tables showing the haplotypes of F2 mice generated from the *hsh*/CAST backcross. All mice were homozygous at the *hsh* locus on the basis of a shaking phenotype and are identified numerically. Homozygosity for a MIT marker is indicated by an open box whilst heterozygosity is shown as a black box. MIT markers are ordered from centromere to telomere.

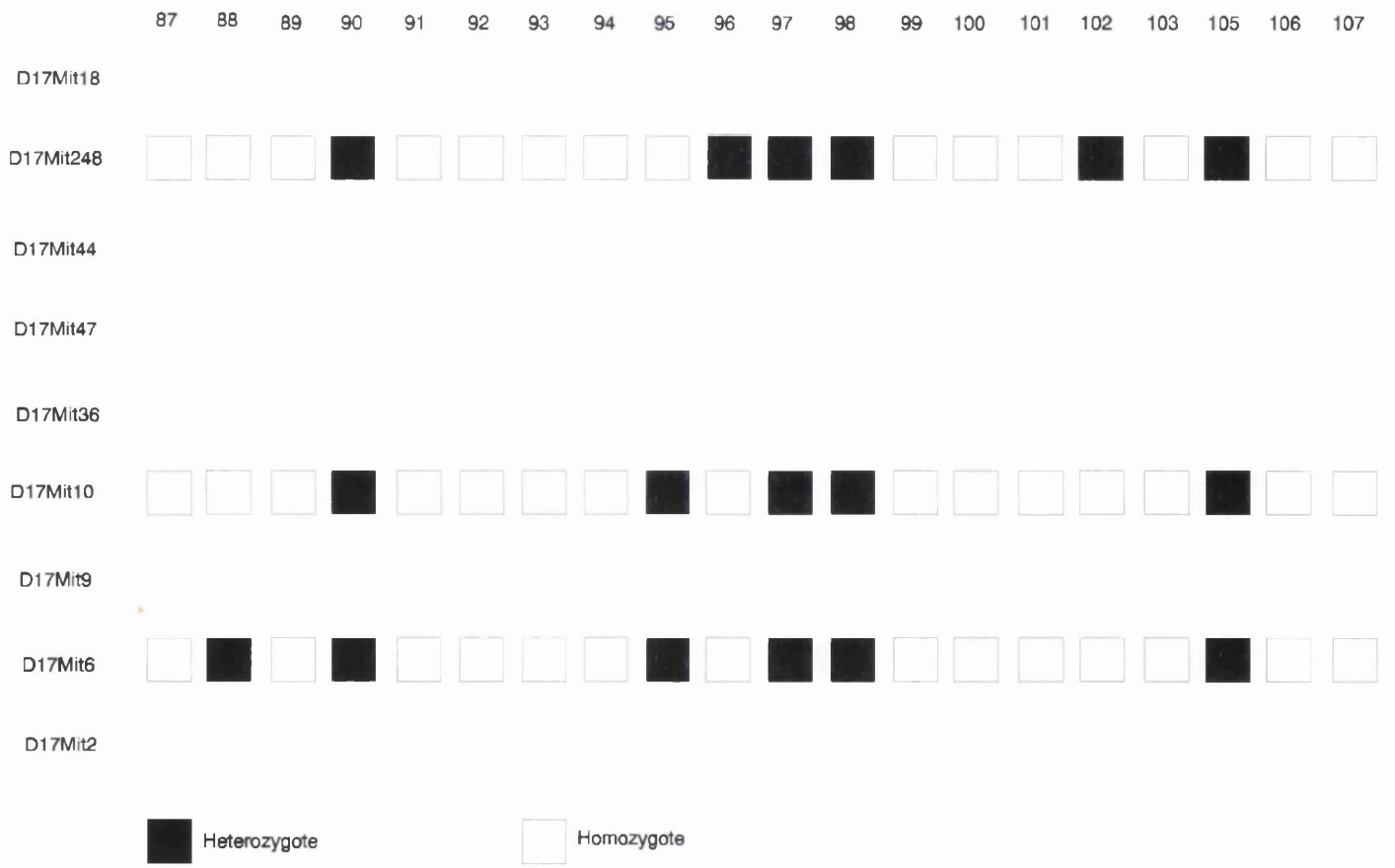

Figure 48 (cont): Tables showing the haplotypes of F2 mice generated from the *hsh*/CAST backcross. All mice were homozygous at the *hsh* locus on the basis of a shaking phenotype and are identified numerically. Homozygosity for a MIT marker is indicated by an open box whilst heterozygosity is shown as a black box. MIT markers are ordered from centromere to telomere.

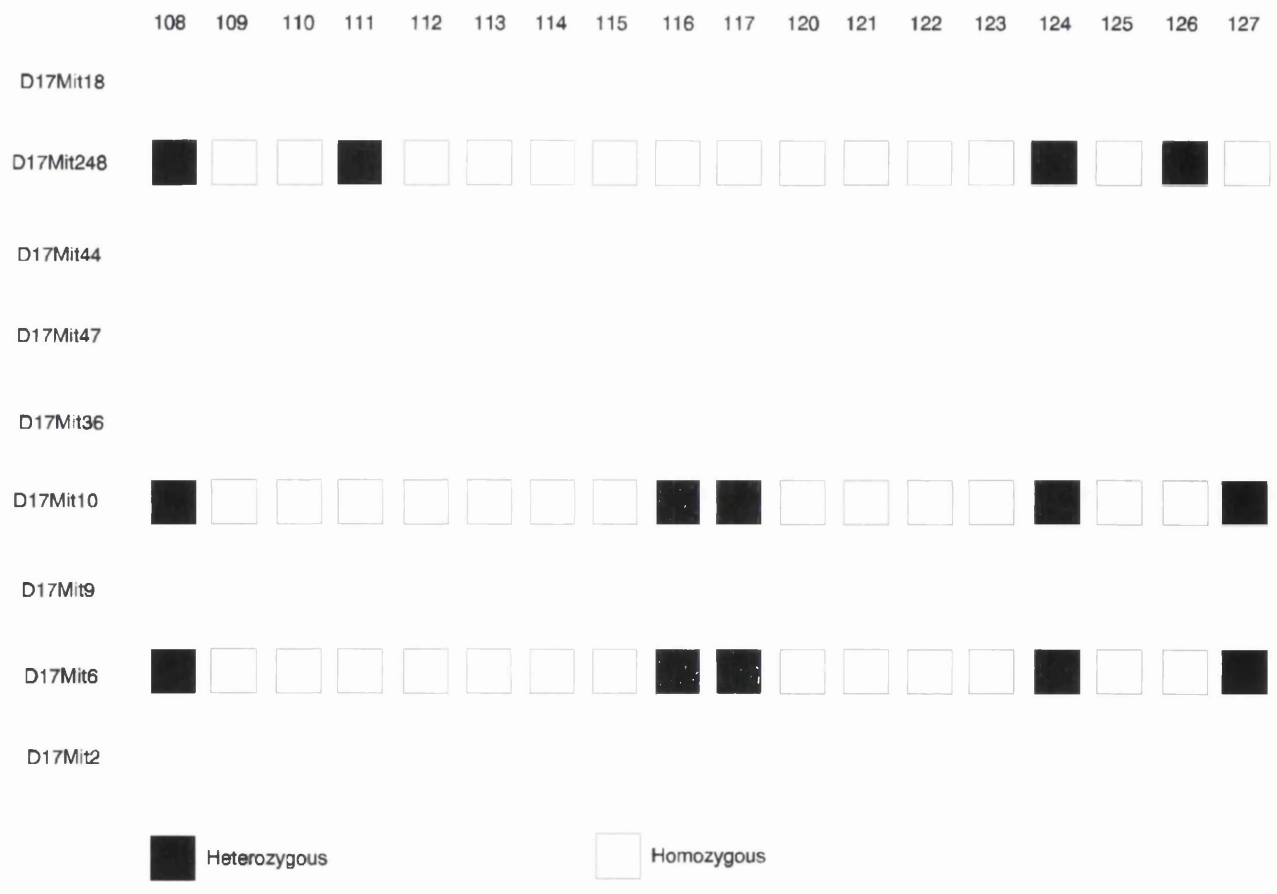

Figure 48 (cont): Tables showing the haplotypes of F2 mice generated from the *hsh*/CAST backcross. All mice were homozygous at the *hsh* locus on the basis of a shaking phenotype and are identified numerically. Homozygosity for a MIT marker is indicated by an open box whilst heterozygosity is shown as a black box. MIT markers are ordered from centromere to telomere.

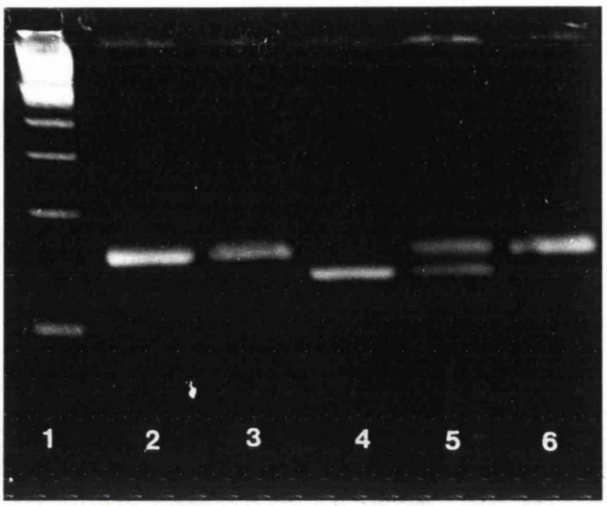

Figure 49: Gel showing a PCR with a CAST backcross pooled sample using D17Mit10. Lane 1 100 bp ladder, Lane 2 C3H, Lane 3 101, Lane 4, CAST, Lane 5, 50:50 ratio of C3H/CAST, Lane 6 CAST backcross pool. Equal band intensity is seen in the C3H/CAST pool whereas the test pool shows a very weak CAST band and a much stronger C3H/101 band, indicative of linkage to this marker. The 101 and C3H bands are very similar in size for this marker.

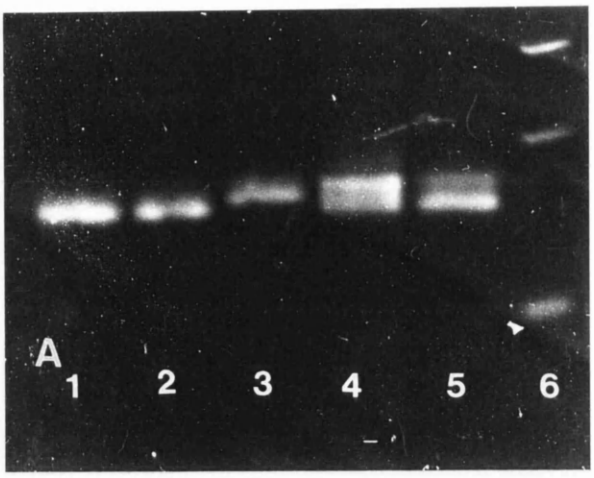

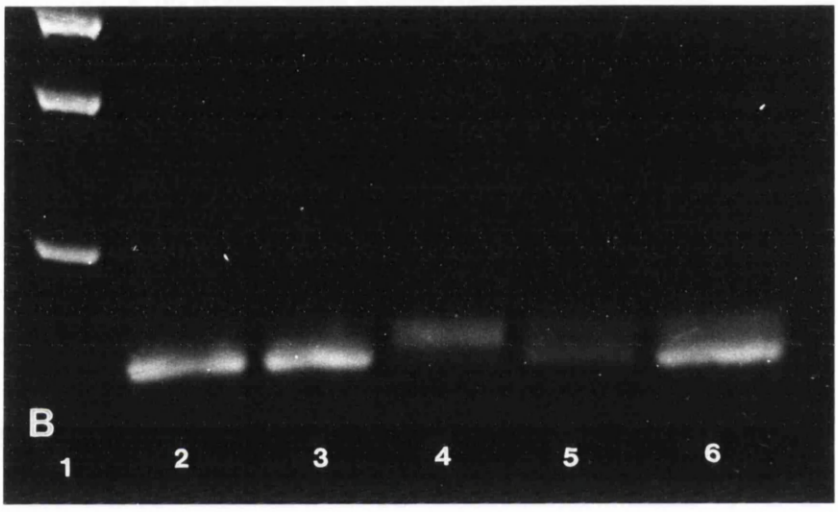

Figure 50: Gels showing the bands generated from PCRs using D17Mit10 and pooled DNA samples from the C57 and BALB backcrosses. (A) Lane 1 C3H, Lane 2 101, Lane 3 C57, Lane 4 50:50 ratio of C3H/C57, Lane 5 C57 backcross pool, Lane 6 100bp ladder. (B), Lane 1 100bp ladder, Lane 2 C3H, Lane 3 101, Lane 4 BALB, Lane 5 50:50 ratio of C3H/BALB, Lane 6 BALB backcross pool. The C57 pool appears to show about the expected band intensities for an unlinked marker (3:1 C3H/C57) although a recombination fraction of 38% had been found using individual samples. On the BALB pooled sample, there may be slight departure from these proportions, with a slightly stronger C3H/101 band and fainter BALB, which would be in accordance with the lower recombination rate of 22.5%.

5.5 Fine mapping of chromosome 3

5.5.1 Introduction

Now that linkage had been detected for two markers on chromosome 3, it was necessary to confirm that a region of homozygosity did exist and that no mice were heterozygous across the whole region. Heterozygosity might indicate the identification of a modifying locus or perhaps expression of a phenotype in heterozygotes. If it appeared that the disease locus had been flanked, the study was to be extended to encompass the C57 and BALB backcrosses. The ultimate goal was the identification of a handful of markers and recombinant mice that defined a very small interval containing the *hsh* gene so that this could be subjected to positional cloning.

5.5.2 Materials and Methods

5.5.2.1 Preparation of gDNA

New samples from shaky F2 mice were treated as described in Preparation of genomic DNA, page 75. Pools of DNA from CAST, C57 BALB backcrosses were utilised to illustrate linkage within the entire population. A ratio of 3:1 for C3H/101 and tester strain indicates no linkage; a stronger C3H/101 band suggests linkage.

5.5.2.2 PCR

The routine protocol is given in Polymerase chain reaction, page 77 and appropriate adjustments were made as necessary. Gel analysis is described in Analysis of PCR products, page 78.

5.5.2.3 Selection of microsatellite primer pairs

Primer pairs were selected initially from the region between D3Mit203 and D3Mit127 on the basis of the position of microsatellite markers on the Whitehead/MIT map and polymorphism between C3H and CAST. As the interval defined by flanking markers became smaller, the study was extended to include samples from the C57 and BALB backcrosses. At this point, data on the position of markers from the EUCIB and the MGD maps (see Genetic maps, page 74) were utilised to permit finer mapping. Genetic distances are different between the Whitehead/MIT map and the integrated maps so the derivation of map positions is given where necessary. Eventually all markers within the interval of interest that demonstrated polymorphism between C3H and any one of these strains were typed. A list of these markers can be seen in Figure 52, page 196.

5.5.2.4 Genetic maps

The genetic maps employed in this part of the study are discussed in Genetic maps, page 74.

5.5.2.5 Approach to mapping

All available CAST backcross samples were typed for a small number of markers. Mice that were homozygous for markers spanning the region of interest were abandoned and further markers typed against only recombinant animals. The aim was to identify proximal and distal markers as close as possible to the disease locus and to establish a region of complete concordance in the interval. Samples from the C57 and BALB crosses were also tested for linkage to this region. The integrated MGD and Chromosome Committee mouse genetic maps were examined for their gene content in the interval of interest and the syntenic human subchromosomal regions determined. The human genetic maps were also inspected for gene and disease loci in the syntenic regions.

5.5.3 Results

5.5.3.1 CAST backcross

5.5.3.1.1 *Mapping using the entire panel of mice*

D3Mit72 at 30cM, D3Mit11 at 37cM and D3Mit316 at 41cM on the Whitehead/MIT map were tested against all 97 CAST backcross samples available at that time. Details of these and the two previous markers on chromosome 3 are presented in Table 8 below.

Mit marker	C3H-derived allele (bp)	CAST-derived allele (bp)	Distance from centromere (cM)	Number of recombinants	Recombination rate (±SE)
D3Mit203	138	158	10cM	16/64	25 ± 5.4%
D3Mit72	142	120	30cM	3/97	3 ± 1.73%
D3Mit11	112	145	37cM	3/97	3 ± 1.73%
D3Mit316	114	146	41cM	7/97	7 ± 2.59%
D3Mit127	168	106	49cM	15/73	20 ± 4.6%

Table 8: D3Mit panel used for initial localisation of the interval containing the *hsh* locus. Distances are those given in the Whitehead/MIT map.

Haplotypes for the 64 backcross animals that were typed for all 5 markers are given in Figure 51, page 195. The two mice which were heterozygous for both of the original two markers, D3Mit203 and D3Mit127, were homozygous for all three intervening markers, indicating that they were double recombinants. A region of homozygosity containing the *hsh* locus lay between D3Mit72 and D3Mit11.

5.5.3.1.2 *Fine mapping using informative mice*

The 6 mice recombinant for D3Mit72 or D3Mit11 were typed for intervening polymorphic markers and haplotypes developed for them. Expected product sizes are given in Table 9, page 197 and the relative positions of the markers according to the EUCIB map are shown in Figure 52, page 196. The 3 markers that are not precisely ordered within their bin are indicated in red (D3Mit311, D3Mit141, D3Mit29) and the other markers from that bin that have been ordered are boxed in red (D3Mit156, D3Mit28, D3Mit232, D3Mit99, D3Mit76).

Additional mice born after identification of linkage on chromosome 3 were typed only for the flanking markers. After testing of all 120 CAST backcross samples that were collected during the study period, an interval was defined proximally by one recombination event for D3Mit74 at 39.16cM (0.83 ± 0.83cM proximal to *hsh*) and distally by three recombination events for D3Mit41 at 43.5cM (2.5 ± 1.42cM distal to *hsh*). The haplotypes of the 4 informative recombinant mice are shown in Figure 53, page 198. Those markers that have not been typed exhibited no detectable polymorphism between C3H/101 and CAST (D3Mit73, D3Mit139, D3Mit156, D3Mit99).

Examples of gels obtained for one proximal marker, D3Mit40 (Figure 54, page 199) and one distal primer pair, D3Mit102 (Figure 55, page 200), are given to illustrate the results. A pool of all 120 samples was also created to demonstrate linkage to the markers in the complete population, as is seen by the complete absence of a CAST band on the gel pictures. Homozygosity of all mice is shown for D3Mit232 (Figure 56, page 201) and D3Mit49 (Figure 57, page 202). This latter PCR is very interesting because the C3H and CAST bands are indistinguishable (this primer pair was originally selected for use on the C57 backcross) whilst the 101 allele is larger. All mice, including the pool of 120 samples, appear to carry the 101 allele.

5.5.3.2 C57 backcross

A set of 7 markers that showed polymorphism between C3H and C57 was tested against all 67 of these backcross mice and an identical region of complete concordance was identified. The use of the C57 backcross enabled the number of

markers tested to be extended (D3Mit73 was polymorphic for C57 but not CAST) and the interval containing the locus was further defined distally. The haplotypes of recombinant mice are shown with the CAST backcross haplotypes Figure 53, page 198. New distal flanking markers, D3Mit311 and D3Mit141 at about 42cM, were defined, for which 3 mice are heterozygous. This is equivalent to a genetic distance of 4.50 ± 2.53cM.

The following markers were not typed for the C57 backcross mice; D3Mit282, D3Mit139, D3Mit28, D3Mit232, D3Mit99, D3Mit41 (no polymorphism), D3Mit76 (4bp difference was not detected on polyacrylamide gel analysis) or because no further information was to be gained (D3Mit175, D3Mit74, D3Mit49). The region of homozygosity is illustrated by D3Mit73 (Figure 58, page 203). Again, a pooled sample containing DNA from all 67 mice is included for the purpose of illustrating linkage in the entire population. Only a single C3H/101 band can be seen in this pool, indicating a shortage of heterozygous mice.

5.5.3.3 BALB backcross

The 31 BALB backcross mice were all homozygous for D3Mit73, D3Mit49 and D3Mit156. Homozygosity in the entire population is illustrated with D3Mit73 in Figure 59, page 204.

5.5.4 Discussion

The region containing the *hsh* locus was localised to chromosome 3 between D3Mit74 proximally and D3Mit311/D3Mit141 distally. One intersubspecific and two interstrain backcrosses showed linkage to the same region, with all 215 mice being homozygous in this interval. Although penetrance is low on the CAST backcross and therefore identification of another major modifier with obligate homozygosity could not be completely excluded, the higher penetrance on the C57 background made this statistically impossible. With a penetrance of 76%, expression of the *hsh* phenotype on this backcross could not require homozygosity at two separate loci (penetrance would be reduced to 50% in that case, *i.e.* 25% of total mice born) and in fact, linkage to chromosome 17 had already been suggested, which would further reduce penetrance. In fact, it may be that chromosome 17 contains the sole modifying locus on the C57 background, although a much larger population will be required to confirm this hypothesis. It is interesting to note that results from one marker, D3Mit40, were consistent with the mutation arising on the 101 background rather than the C3H. However, there may still be some A/H or SN

strain specific microsatellite alleles present in the *hsh* genome and the possibility of these being the same size as the 101 alleles cannot be excluded.

Although markers have been placed in linkage groups known as "bins" by Whitehead/MIT, because only 98 meiotic events were used, resolution of greater than 1cM cannot be achieved. With over 6000 microsatellite markers across a genome of 1600cM, bins can obviously contain many markers. About 3200 of these markers have now been more finely positioned relative to one another on the much larger EUCIB backcross using 983 *Mus spretus* x C57BL/6 backcross mice, allowing mapping to a resolution of 0.1cM (European Backcross Collaborative Group, 1994). A proportion of the markers here in one bin, D3Mit311, D3Mit341 and D3Mit29, have not yet been positioned relative to other markers in that bin on either cross. This could be performed on the *hsh* backcrosses by assessing haplotypes if recombination events have occurred between these markers. Only one other marker in this bin with a known map position, D3Mit76, is polymorphic between C3H and C57 and this is only a 4bp difference (124bp versus 128bp). Polyacrylamide gel analysis has failed to separate the bands although PCR utilising radiolabelling techniques might be a successful approach. However, the 101 allele appeared to be the same size as the C57 on agarose gels, which may prevent typing. In addition, since distances between adjacent markers within a bin will be less than a centimorgan, fewer than 1/100 mice will demonstrate a recombination event between them and it may not yet be possible to place D3Mit311/D3Mit341 relative to other markers in the bin on this population of 67 mice.

Although there are no absolute cut-offs for determining what level of linkage is necessary before one can pursue a positional cloning exercise, it is generally accepted that 500-1000 backcross mice are required to map a locus to a sufficiently small interval (Silver, 1995a). Within the 2.17 ± 1.07cM interval that has been defined so far, there remain a number of potentially useful markers, and the rate-limiting step is now the generation of mice needed to define further recombination events. The very low penetrance on the CAST backcross resulted in only 120 mice over a period of over 2 years, and at this time, only 2/100 new mice is likely to demonstrate a recombination event in the defined interval. The C57 backcross in particular generates shaky mice considerably faster due to the higher penetrance. However, it may be worthwhile continuing with both backcrosses since they demonstrate polymorphisms with C3H for some different markers, increasing the number of useful markers. It is also possible that recombination differences between the two crosses will be helpful; certainly, more recombination events occurred distally on the C57 backcross compared to the CAST, whilst the reverse was true for the proximal region. Perhaps there are different "recombination

hotspots" in the crosses, *i.e.* areas where crossover events are more likely to occur. On the other hand, the BALB backcross exhibits lower penetrance and subjectively does not appear to be such a prolific cross. It is also polymorphic for only three of the markers currently mapped to the interval and not for the current flanking markers. As fine mapping progresses, it is possible that a vital recombination may occur for one of these markers, but the very small population size makes this unlikely, and it may not be worth continuing with this backcross.

Concomitant with continued breeding of backcross mice for fine mapping, other approaches to gene identification were attempted. High resolution mapping can greatly assist the candidate gene approach since genes that recombine outwith a defined interval can be excluded. This combination of positional cloning and candidate gene identification is increasingly successful as more genes are placed on the mouse genetic map, and will probably overtake positional cloning using contigs as the approach to identification of a novel mutant locus (Collins, 1995). However, with only about 5500 genes placed on the map out of an estimated 100,000, there is a very large probability that the guilty gene has not yet been mapped.

The integrated mouse genetic maps from the MGD and the Chromosome Committee were both examined for their gene content in the interval of interest. However, it must be borne in mind that often data have been mapped using different breeding strategies and species/strains or even different techniques, such as *in situ* hybridisation or somatic cell hybrids. Distances between loci may vary between studies and even the order of loci may be misrepresented on an integrated map. Therefore, the position of gene loci and the mapping of a gene to outwith the region of interest should be regarded with some caution.

Candidate genes would be those with a putative role in the CNS, especially with regard to oligodendrocytes and myelination. There were no obvious candidates from the 32 genes placed between D3Mit74 and the bin containing D3Mit311/341. A version of the map is shown in Figure 60, page 205 where genes are outlined in red, and the human homologues and their chromosomal loci are given where known. The full name for each locus is given in Table 10, page 223. Data for each gene was accessed through the MGD and examined for evidence of a putative role in the CNS but none appeared to have a specific CNS function. This failure to identify a candidate may be because the gene has not yet been identified or mapped, or that the culprit has a previously unrecognised role in the CNS.

Due to the inherent problems with allocating precise positions to loci, genes that were mapped close but outwith the region could not be definitively excluded. Other myelin-associated genes on chromosome 3 were therefore given consideration.

Cnp2 has been positioned at 38.4cM, 2.6cM proximal to D3Mit74 using analysis of recombinant inbred strains (Bernier *et al.*, 1988) and *Ugt8* has been cytogenetically mapped to bands E3-F1 in the middle of chromosome 3 using somatic cell hybrids and *in situ* hybridisation (Coetzee *et al.*, 1996). Neither has been mapped relative to microsatellite markers and their exact map positions must remain open to question. The role, if any, of the gene product from *Cnp2* in myelination is not known, while *Ugt8* has a key function in the biosynthesis of galactocerebroside, a frequently used marker for oligodendrocytes (Kagawa *et al.*, 1996). Both genes were subjected to further investigation but the phenotypic studies suggested that neither of these was a likely candidate. Western blotting for CNP levels indicated the presence of both CNP1 and CNP2 protein isoforms (see Western blotting for CNP, page 153), and *in situ* hybridisation using a *Ugt8* riboprobe demonstrated positive cells in the spinal cord white matter (see *In situ* hybridisation, page 120). However, mRNA and protein levels are not confirmation of a normal gene and to exclude them with certainty, the genes could be mapped on the recombinant mice using DNA polymorphisms such as intragenic polymorphic repeats or RFLPs to confirm their position outwith the interval of interest.

Since no further candidates were identified near to or within the defined interval, the human genetic map was examined for synteny. It is known that nearly all human genes have homologues in the mouse and *vice versa*, and that the order of genes is also conserved, to some extent, in segments up to 8cM in length along the chromosome (Nadeau, 1984). The practical implication of this is that the map position of a gene in one species may be applied to the other, although one should be cautious in overinterpreting synteny information; there are many examples of smaller genomic segments that have been inserted in or removed from larger syntenic regions. One gene in the interval of interest has its homologue on human chromosome 4 whilst the remaining 16 have homologues on with human chromosome 1 (Figure 60, page 205). Gene order does not appear to have been conserved, although it is possible that linkage mapping data are flawed in one of the species. Physical mapping advances may clarify the differences between man and mouse in this region in the future. No candidate genes or mutations associated with dysmyelinating disorders were gleaned from examination of the syntenic regions on the human map.

In order to progress further with the positional cloning of the *hsh* gene, it appears that the generation of more backcross mice is a priority. Once an interval of 0.1-0.5cM (200-1000kb) is achieved, the next stage of gene identification can be initiated. Although no likely candidates have been mapped to the region so far, the rate at which new loci are being placed on the mouse map is accelerating and it is

possible that, as fine mapping continues, a number of candidate genes may be discovered; this would potentially obviate the need for positional cloning using overlapping contigs and subsequent gene identification, which are labour intensive and slow processes.

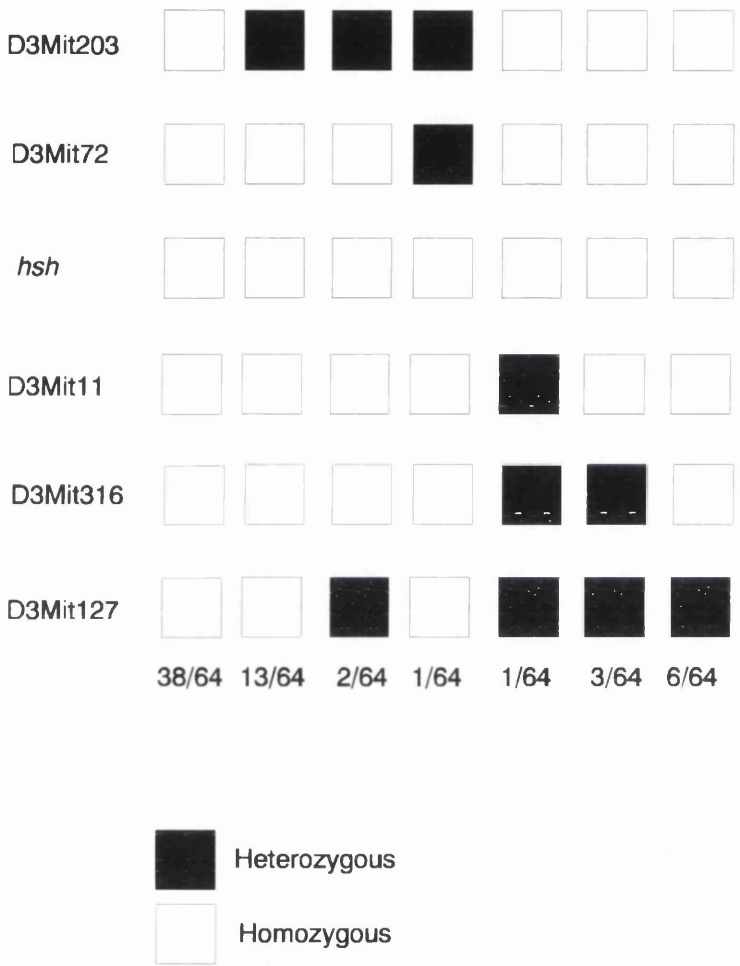

Figure 51: Haplotypes for the 64 CAST backcross animals typed for all 5 markers used in initial positioning of the *hsh* locus. Open boxes represent C3H/101 alleles, filled boxes CAST. The number of mice recombinant for each marker is given at the bottom of each column. The *hsh* locus has been positioned in a region of homozygosity between D3Mit72 and D3Mit11.

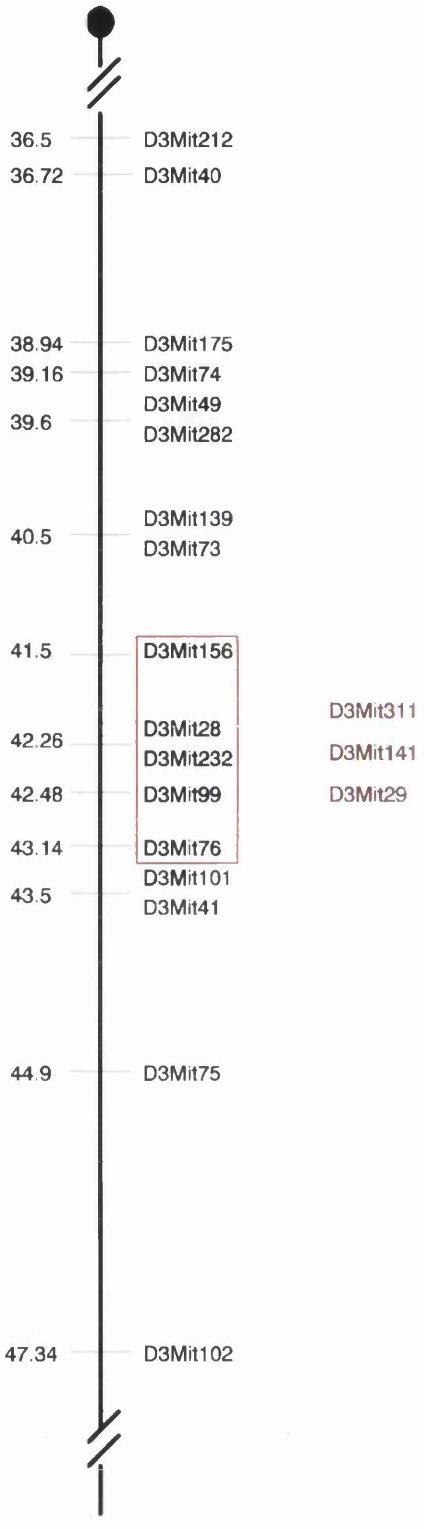

Figure 52: Location of markers mapped on the EUCIB backcross in the interval of interest. D3Mit311, D3Mit141 and D3Mit29 are in the same bin as the markers boxed in red on the Whitehead/MIT map but have not been positioned on the EUCIB map. D3Mit139 and D3Mit99 were not polymorphic for the crosses in this study and were therefore not used. Distances are those given on the EUCIB map.

Mit Marker	C3H-derived allele (bp)	CAST-derived allele (bp)	C57-derived allele (bp)	BALB-derived allele (bp)	Distance from centromere (cM)
D3Mit212	130	108	124	128	36.5
D3Mit40	110	120	140	110	36.72
D3Mit175	133	107	139	139	38.94
D3Mit74	148	170	152	148	39.16
D3Mit49	110	108	128	148	39.6
D3Mit282	123	109	123	119	39.6
D3Mit139	87	87	85	85	40.5
D3Mit73	106	106	148	144	40.5
D3Mit156	252	-1	252	260	41.5
D3Mit99	216	216	216	216	42.48
D3Mit232	154	170	154	152	42.26
D3mit76	124	112	128	124	43.14
D3Mit311	130	122	122	136	unknown
D3Mit141	159	147	149	157	unknown
D3Mit29	148	188	150	200	unknown
D3Mit101	126	118	108	-1	43.5
D3Mit41	210	236	210	210	43.5
D3Mit75	98	112	110	98	44.9
D3Mit102	142	162	152	142	47.34

Table 9: D3Mit panel available for fine mapping the *hsh* locus on the CAST, C57 and BALB backcrosses. D3Mit99 and D3Mit139 were not used due to insufficient polymorphism in all 3 backcrosses. All other markers were typed on informative mice from at least one backcross. The symbol -1 indicates that no product was generated for this strain.

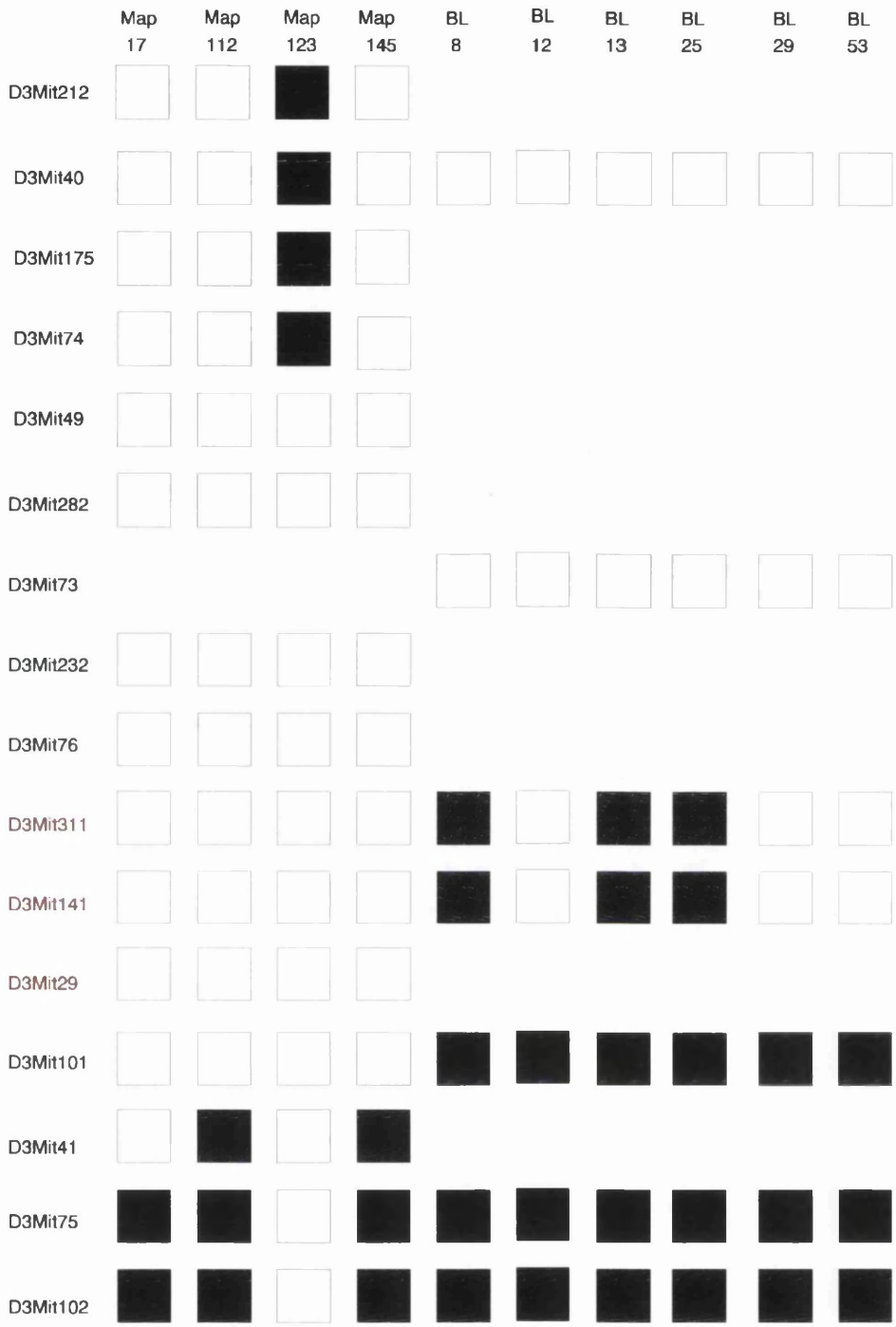

Figure 53: Haplotypes of recombinant F2 mice generated from the CAST and C57 backcrosses. CAST mice are indicated by the prefix MAP and C57 by BL. Homozygosity for a marker is indicated by an open box whilst heterozygosity is shown as a black box. Blank rows indicate there was no polymorphism for that marker or that testing was not be useful because mice were all homozygous for the preceding marker. Markers are ordered from centromere to telomere. The *hsh* locus is seen to lie between the proximal marker D3Mit74 and the distal markers D3Mit311 and D3Mit141.

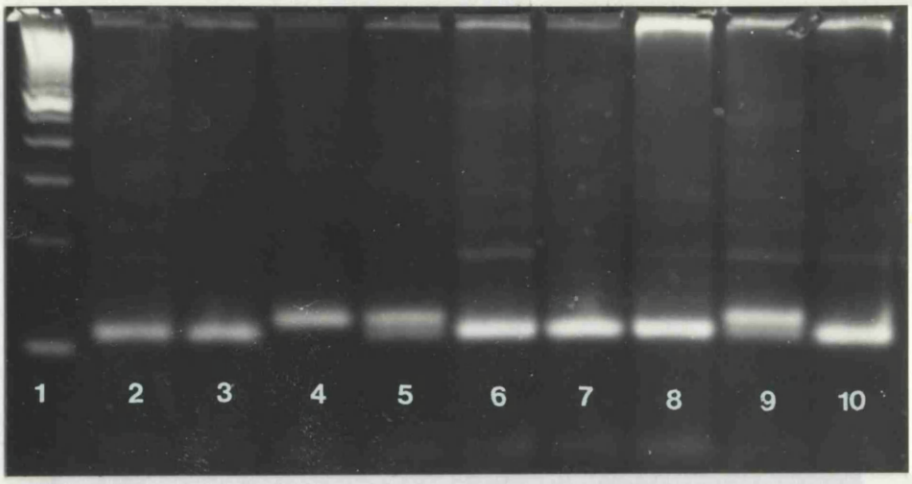

Figure 54: A gel showing PCR products for CAST mice and D3Mit40. Lane 1 100bp ladder, Lane 2 C3H, Lane 3 101, Lane 4 CAST, Lane 5 F1 *hsh*/CAST, Lane 6 pooled sample of 120 CAST backcross DNAs, Lane 7 Map17, Lane 8 Map112, Lane 9 Map123 and Lane 10 Map145. The C3H and 101 alleles are very similar in size and the CAST allele is amplified in the presence of a *musculus* allele. The pooled sample has been included to demonstrate the strong linkage to this marker in the whole population; no CAST band is visible at all. One mouse, Map123, is recombinant.

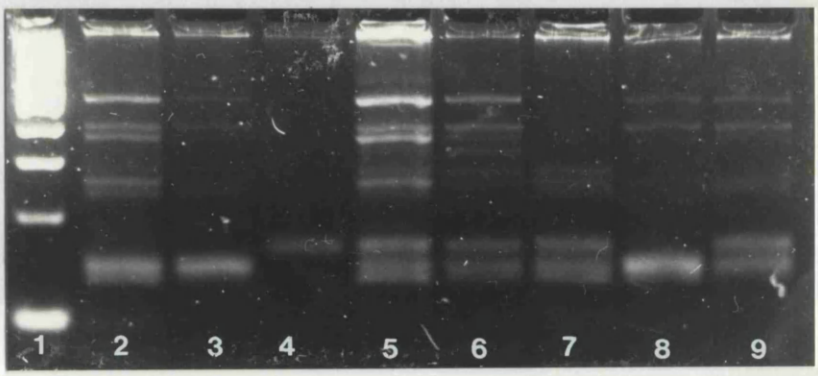

Figure 55: A gel showing PCR products for CAST mice and D3Mit102. Lane 1 100bp ladder, Lane 2 C3H, Lane 3 101, Lane 4 CAST, Lane 5 F1 *hsh*/CAST, Lane 6 Map17, Lane 7 Map112, Lane 8 Map123 and Lane 9 Map145. The C3H allele produces two bands but they are not similar to CAST. Maps 17, 112 and 145 are heterozygous while Map 123 is now homozygous.

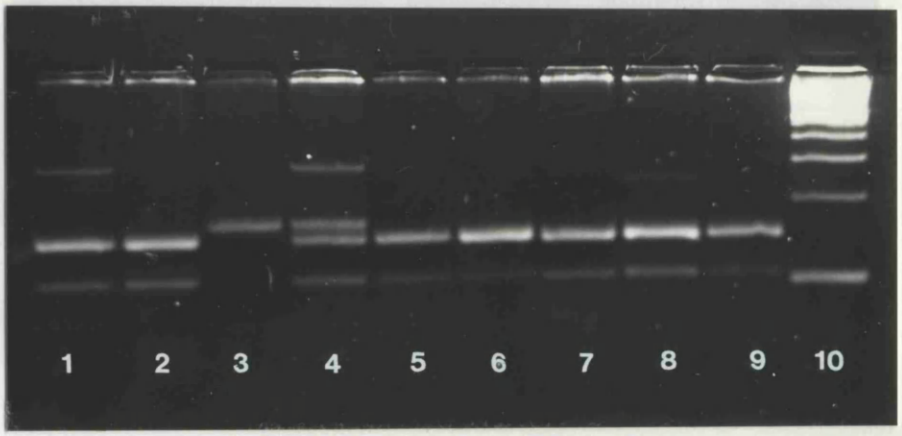

Figure 56: A gel showing PCR products for CAST mice and D3Mit232. Lane 1 C3H, Lane 2 101, Lane 3 CAST, Lane 4 F1 *hsh*/CAST, Lane 5 pooled sample of 120 CAST backcross mice, Lane 6 Map 17, Lane 7 Map 112, Lane 8 123, Lane 9 Map 145, Lane 10 100bp ladder. All four Map mice are now homozygous. No CAST band is seen in the pool, suggestive of a largely homozygous population.

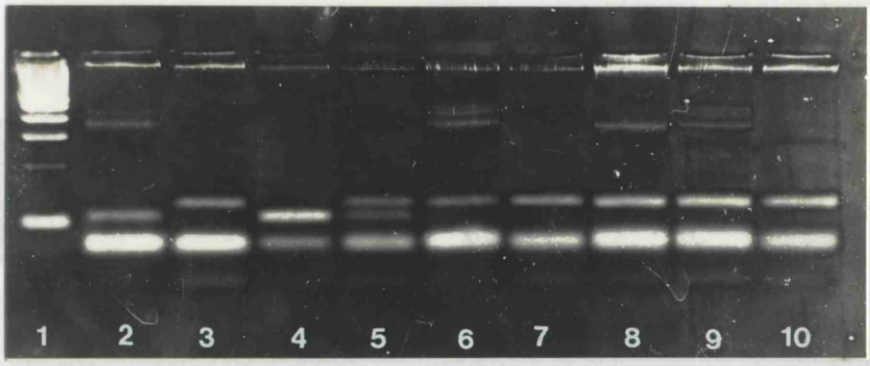

Figure 57: A gel showing PCR products for CAST mice and D3Mit49. Lane 1 100bp ladder, Lane 2 C3H, Lane 3 101, Lane 4 CAST, Lane 5 F1 *hsh*/CAST, Lane 6, pooled sample of 120 CAST backcross mice, Lane 7 Map17, Lane 8 Map 112, Lane 9 Map 123, Lane 10 145. The CAST and C3H alleles are very similar in size while the 101 is a heavier fragment. Only a 101 allele is identified in the pooled or 4 individual samples. Since this marker lies in the region of concordance where all mice are homozygous, it suggests the mutation may have arisen on the 101 background. The intense lower band is excess primer.

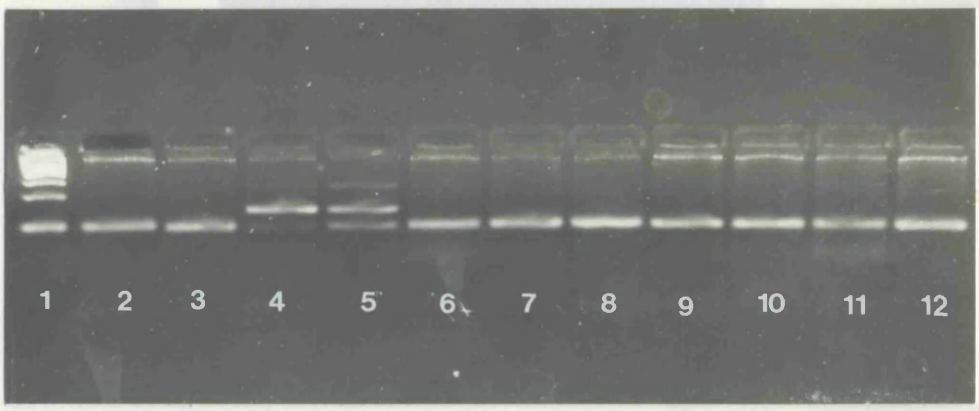

Figure 58: A gel showing PCR products for the C57 backcross and D3Mit73. Lane 1 100bp ladder, Lane 2 C3H, Lane 3 101, Lane 4 C57, Lane 5 F1 *hsh*/C57, Lane 6 BL8, Lane7 BL12, Lane 8 BL13, Lane 9 BL25, Lane 10 BL29, Lane 11 BL53, Lane 12 pooled sample of 67 C57 backcross mice. Only a C3H/101 allele is seen in the pool and the BL mice heterozygous for the next distal marker. An extra faint band is seen in the C57 sample but does not affect interpretation.

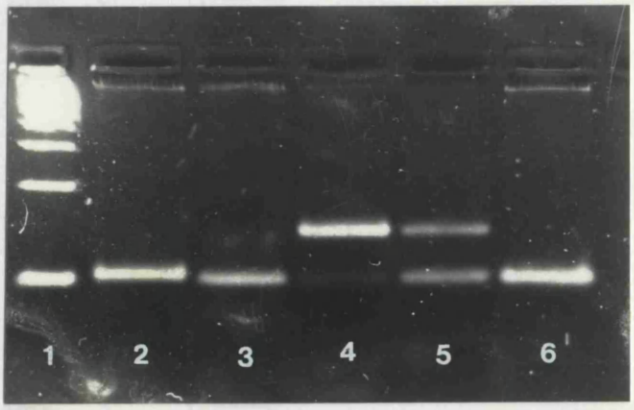

Figure 59: A gel showing PCR products for the BALB backcross and D3Mit73. Lane 1 100bp ladder, Lane 2 C3H, Lane 3 101, Lane 4 BALB, Lane 5 F1 *hsh*/BALB, Lane 6 pooled sample of 31 BALB backcross mice. A slight difference can be seen between the sizes of the C3H and 101 alleles. The pooled BALB sample has only a single band, at the level of the 101 allele. No BALB band can be seen at all in this sample.

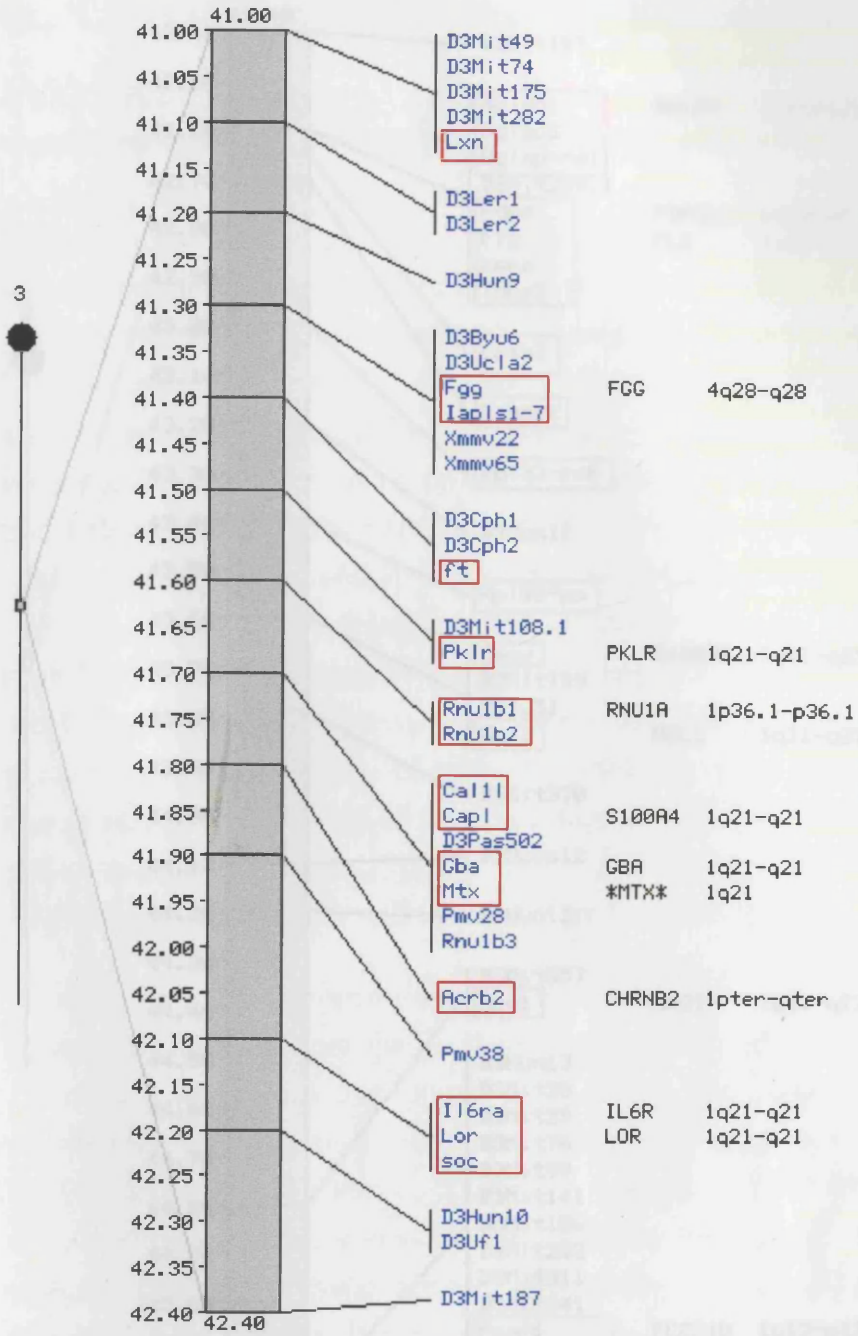

Figure 60: A composite genetic map of chromosome 3 between the two flanking markers D3Mit74 and D3Mit311/D3Mit141. Genes are boxed in red whilst other symbols represent microsatellite and other DNA segments or viral sequences. The known human homologues and their chromosomal loci are given in black type adjacent to the appropriate mouse gene. The centromere is towards the top of the page and genetic distances are those given on the MGD map. The full names of all loci are provided in Table 10, page 238.

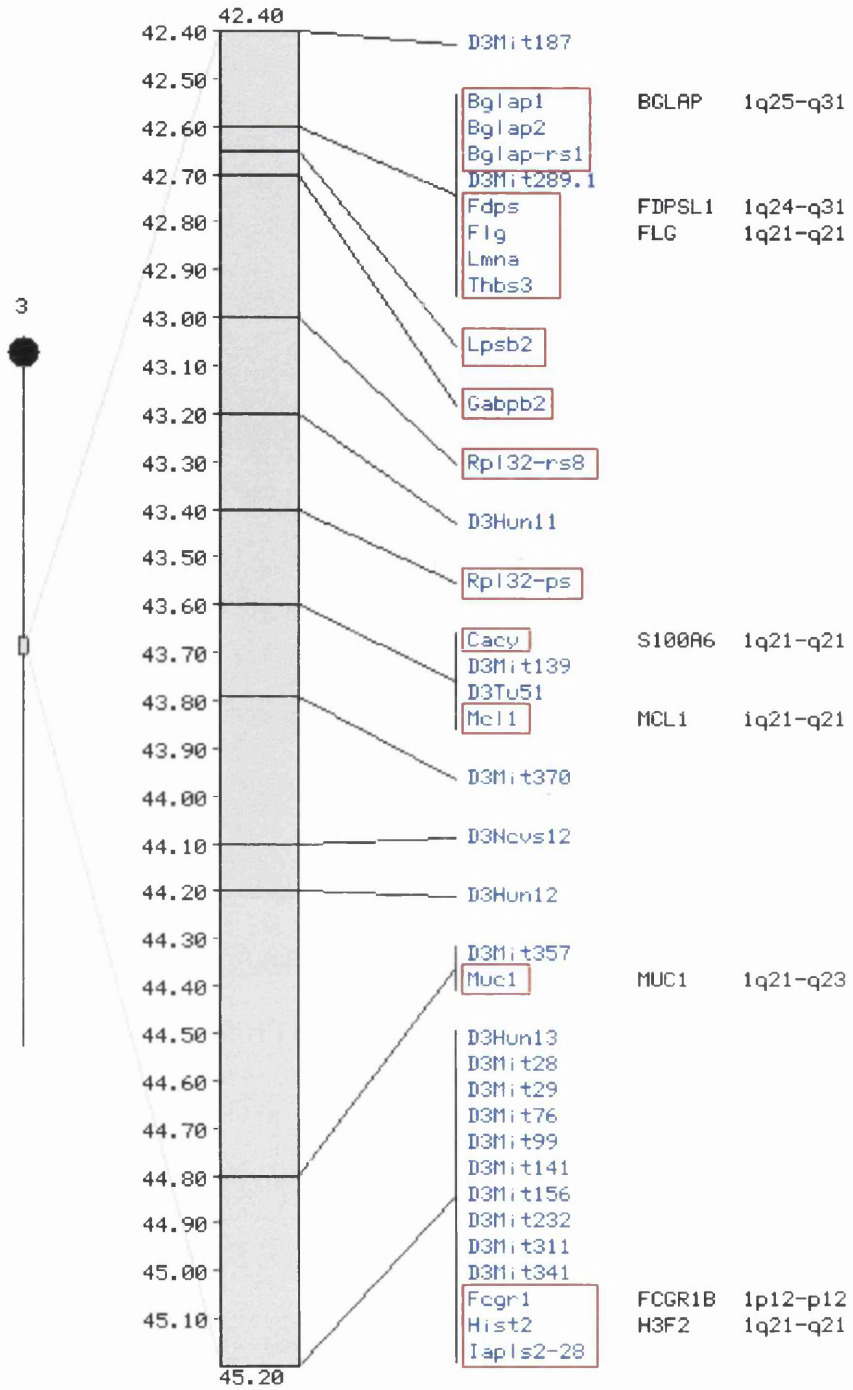

Figure 60 (cont.) A composite genetic map of chromosome 3 between the two flanking markers D3Mit74 and D3Mit311/D3Mit141.

6. Concluding remarks and future work

Historically, myelin mutants have added greatly to the wealth of knowledge concerning the complex processes of myelination in the CNS and PNS. The greatest benefits have come from those mutants in which a phenotypic abnormality has been related to a precise alteration in a gene product, for example, shiverer and the *Plp* mutants in the CNS and trembler in the PNS (see (Griffiths, 1996) for review). Thus, the ultimate goal of the *hsh* project must be both the definition of the phenotypic effects of the mutation and the identification and characterisation of the gene product. To that end, a multidisciplinary approach was employed in this study, with the dual aims of describing the effects of the novel hindshaker mutation on myelination, and mapping of the culprit gene to a sub-chromosomal locus. As the work presented here shows, both aims have been achieved; knowledge of the phenotype has been extended and a surprisingly complex genetic picture has been illuminated. The purpose of this final discussion is to bring together the genotypic and phenotypic studies, place them in context with current genetic and neurobiological research and to suggest future work for gene isolation.

In summary, the hypomyelinating phenotype appears to be due to a paucity of mature oligodendrocytes that is more profound in specific regions of the CNS (see Discussion of the *hsh* phenotype, page 157). This culminates in a retardation of myelination that is most severe in the spinal cord and cerebellum and less obvious in the forebrain and optic nerve. There is a subsequent partial resolution of the myelin deficit with age that is concomitant with an increase in the number of mature oligodendrocytes. Myelin appears structurally normal and it seems likely that the mutation does not involve a gene encoding for a major structural component of myelin, but more probably affects the biology of the oligodendrocytes. Autosomal recessive inheritance had already been shown although it is now known that there is variation in expressivity and penetrance of the mutation on different backgrounds. The *hsh* gene has been mapped to a 2cM interval in the middle of chromosome 3 and three flanking markers and five markers showing complete concordance have been identified using backcrosses with CAST/Ei or C57BL/6J as the second parental strains. A suppressor modifying locus has also been found on chromosome 17.

Inspection of the interval of interest on chromosome 3 for candidate genes has failed to yield any contenders to date. The *Cnp2* gene, mapped to 2cM proximal to the region of interest, was considered but no strong evidence for its involvement was

forthcoming (see Western blotting for CNP, page 153 for discussion). It is not yet clear whether the *Cnp2* gene generates any of the observed *Cnp* mRNA transcripts (Bernier *et al.*, 1988), or whether it encodes for a CNP-related polypeptide or is in fact a pseudogene. However, since the possibility of it generating a CNP protein isoform has not been completely excluded, further investigation would be warranted; certainly the putative functions of CNP protein could be consistent with a possible aetiology in the *hsh* phenotype. Although its precise function remains unknown, it is expressed early in myelination (Trapp, 1990), may have a role in signal transduction (Thompson, 1992) and appears to influence the development of filopodia in cultured cells (De Angelis and Braun, 1994). Thus, the suggestion has been made for a role in early development and differentiation of oligodendrocytes. In addition, extra copies of *Cnp* result in premature peak expression of myelin proteins (Gravel *et al.*, 1996). Thus, it appears that perturbation of these putative functions could correlate with the phenotypic abnormalities identified in *hsh*. The mapping data are not strong enough to exclude conclusively the gene from the interval and the identification of both protein isoforms in *hsh* does not necessarily indicate normal gene function. Mapping of the *Cnp2* gene on the CAST/Ei and/or C57BL/6 backcrosses should indicate whether the gene lies within the interval or is in fact, accurately mapped to a proximal locus. The difficulty comes in differentiating between the *Cnp* and *Cnp2* genes. A *Cnp2* specific restriction fragment length polymorphism has been identified using *Taq*1 digestion (Bernier *et al.*, 1988) but C57BL/6 and C3H/HEH yield fragments of the same size and CAST and 101 have not been tested. The next stage in elimination of *Cnp2* as a candidate could be investigation of possible *Taq*1 RFLPs between CAST, 101 and C3H to allow mapping of the gene on this backcross. Until it has been mapped outwith the interval, it must remain a potential candidate.

If the "positional candidate" approach, based on correlation of gene function with the *hsh* phenotype, fails to identify the affected gene, other strategies for gene cloning will be required. Positional cloning, where the gene is isolated purely on the basis of its position in the genome (Collins, 1992; Ballabio, 1993), is certainly one option. Currently, although only 2cM is contained within the region, this is a huge distance in terms of the number of genes that it may contain. Estimates place gene frequency at about 1 gene every 30kB (Silver, 1995c), although this can vary tremendously depending on gene density and size. Since 2cM is equivalent to about 4Mb in the mouse, over 130 genes may lie in this interval, of which about 30 have been mapped to date. A distance of this size far exceeds that amenable to positional cloning, but the bottleneck in further high resolution mapping is not the lack of markers but the ability to obtain further mice with recombination breakpoints close to the *hsh* gene. Ideally this should be well under 0.5cM, requiring a total of at least

500 backcross mice. At that stage, it should be possible to move to "chromosome walking" by developing large insert contigs, using either yeast or bacterial artificial chromosomes or bacteriophage P1 as cloning vectors. At the present rate of breeding, about 300 useful mice will be bred over the coming year, taking the total to more than 500. Approximately 6 (2/100) of these are likely to be recombinant in the interval of interest and may have breakpoints sufficiently close to the gene to permit higher resolution mapping. Obviously the larger the number of meiotic events being examined, the smaller the interval for contig construction. Also, markers later generated from overlapping YACs can be typed to define the interval even more tightly to reduce the number of genes that have to be examined.

The strategy outlined above does not require a large labour commitment and merely necessitates the breeding of sufficient mice and typing for flanking markers using PCR until chromosome walking can be attempted. It is, however, time consuming with the breeding of large numbers of mice now the rate limiting step. Therefore, consideration could be given to alternatives to increasing the cross size, for example, boosting of recombination frequency in gametes using cisplatin (see below) or gene identification based on non-breeding mapping strategies. The choice will partly depend on the profile of the study in the future; a higher financial and labour input would be necessary for either of these alternatives but may yield results sooner.

It has been shown that the anticancer drug cisplatin, which causes DNA strand breakage and is highly recombinogenic in some model organisms, has the ability to increase recombination in the offspring of treated male mice (Hanneman *et al.*, 1997). This was at a level of up to twice that of controls and could therefore reduce the number of meioses that must be screened to localise a gene by half. The protocol is simple and could markedly decrease the time, cost and effort that will still be required to map *hsh* to a suitably small interval. What is not clear, however, is the effect of cisplatin on females or different strains of mice. Also, only a small number of chromosomal regions were tested for recombination and it may be that the interval on chromosome 3 will be affected differently by cisplatin treatment.

The *hsh* locus maps to a region of mouse chromomsome 3 that exhibits synteny with regions of human chromosomes 1 and 4. It has not been possible to assign *hsh* to either of these homologous groups, and it was also difficult to define precisely the limits of the homologous regions on the respective human chromosomes; gene order does not appear to be completely conserved and some homologous genes have only been mapped to cytogenetic bands in man. However, the existence of homology could theoretically be exploited as a non-breeding mapping strategy for gene

identification. The emphasis on the human genome project in recent years has led to the development and mapping of a large number of partial cDNAs termed expressed sequence tags (ESTs). These are short incomplete sequences of cDNAs, usually derived from RNA prepared from tissues that are restricted temporally and spatially. ESTs therefore correspond to the genes that are being expressed in specific tissues at certain stages of development and provide a handle to many, as yet, uncharacterised genes. It is conceivable that the analysis of ESTs mapped to the homologous chromosomal regions on chromosomes 1 and 4 could eventually lead to identification of the mutated gene. Data on the expression of ESTs are accessible through the WWW (http://www.ncbi.nlm.nih.gov/dbEST/index.html) and could be used to select those ESTs that are CNS or glial cell specific. Assuming homology between human and mouse ESTs, the expression of appropriate ESTs could then be studied in normal and *hsh* CNS tissue from suitable ages. Differences in expression between these may suggest the involvement of that particular gene in the phenotype. The obstacles to such a strategy cannot be underestimated, however. The homologous regions are still enormous and cover large expanses of two chromosomes. The number of ESTs mapped to these regions runs into hundreds, and at the moment, many ESTs from the same gene may be mapped separately with no indication of their shared origin. The same gene may therefore be tested several times. Additionally, there is no reason *a priori* to suggest that expression will be altered either at RNA or protein level or that the gene will not be expressed in tissues other than the CNS. With these considerations, further fine mapping in an attempt to exclude one of the homologous human chromosomes and refine the interval would be expedient before sweeping analysis of human ESTs.

One unexpected discovery made during the study was the revelation of a rather more complex pattern of inheritance than had been anticipated. First it appeared that modifying genes were responsible for incomplete penetrance and variable expressivity on the C3H/101 background. Subsequently, incomplete penetrance was identified on the CAST/Ei, C57BL/6J and BALB/cJ backgrounds, again due to the presence of specific alleles at non-disease loci. This was a major setback for the mapping study because the rate of generation of mice for linkage analysis was severely curtailed. Since only those mice with a definitive shake could be classified genotypically, non-shaky mice could not be utilised and the number of useful samples was only a fraction of the total born. The positive aspect of the low penetrance was the opportunity to identify additional loci involved in the pathophysiological pathway that would have otherwise remained obscure.

A prediction of the number of modifying loci influencing penetrance on a particular genetic background cannot be made with precision; genes may be enhancers or

suppressors of a phenotype, and some may act in a recessive manner, some dominantly and many may be influenced by interaction with proteins encoded by other genes. However, with a penetrance of 16% on the CAST background, several loci are likely to be involved, of which one, on chromosome 17, has been identified. Since the CAST alleles are under-represented in this region in the phenotypic *hsh* population, this is a suppressor locus. The same locus also appears likely to influence penetrance of the *hsh* phenotype on several other backgrounds, including C57BL/6J and BALB/cJ. As discussed (Fine mapping of chromosome 17, page 168), curly tail, a murine model for neural tube defects, also has a modifying locus within the region identified on chromosome 17. It would be interesting to know whether the same gene is involved, but no obvious candidates have been found to date. Positional cloning of modifiers is extremely difficult due to the unknown genetic status of mice; it cannot be determined which are homozygous or heterozygous at the locus on the basis of the phenotype, and therefore the classification of recombinant animals cannot be authenticated. Thus, the identification of modifying genes is currently dependent on typing a large population of segregating mice to define a set of markers with the lowest recombination rate and then assessing candidate genes already mapped to that region. Definitive identification then requires careful characterisation of sequence and expression variation and, eventually, transgenesis experiments where the mutant genotype receives the non-permissive modifying allele and is then studied for a phenotype. The interval is still poorly defined in *hsh*, partly because of small population size but also because not all available markers in that region have been typed. A greater number of samples must be tested for a battery of markers on proximal chromosome 17 to define the region more precisely. This will allow a more directed search for candidate genes. Such procedures are being attempted for other murine mutants, for example, the mouse model for cystic fibrosis which has a modifier on chromosome 7 for which there are several contending genes (Rozmahel, 1996) and multiple intestinal neoplasia (*Min*) mice with a candidate modifying gene (the secretory phospholipase A2 gene) on chromosome 4 (MacPhee *et al.*, 1995). Interestingly, the $Plp^{jp\text{-}rsh}$ mutation, maintained at Glasgow on the C3H/101 background, has been shown to exhibit a far more severe phenotype on the C57BL/6 background with death of hemizygous males (I.R. Griffiths, personal communication). It might be fruitful to examine proximal chromosome 17 for evidence of linkage to the same region. A predominance of C3H/101 alleles in this region might suggest the presence of a modifying locus on chromosome 17 with a ubiquitous function in CNS development.

The identification of further modifying loci could be achieved by completing the genome scan using the statistical criteria employed in this study. Using $p<0.001$,

only 1 in 20 findings of positive linkage is likely to have occurred by chance. However, one must remember that regions that fall short of statistical significance may nonetheless be correct. Unfortunately there is no way of distinguishing between small peaks that represent weak true positives and peaks of the same height arising from random fluctuation. Thus, it is entirely possible that regions that exhibit only weak linkage to the *hsh* phenotype may be overlooked.

Although cloning of modifiers is still a major hurdle, it is now possible to clone virtually any mouse gene for which the genetic status of contributing animals is known, purely on the basis of its position in the genome. Consequently, it is likely to be merely a matter of time until the *hsh* gene is identified. The protein product may then be deduced and its expression in normal animals compared to that in *hsh* mutants. By correlating the precise genetic alteration in *hsh* with the phenotype, it may be possible to further clarify the role of the protein in normal myelination. In addition, transgenic/knock-out mice may be created to study myelination in the complete absence or in the presence of extra copies of the gene. Based on the data from the phenotypic studies to date, the premise is that characterisation of the *hsh* gene product will shed light on the development of oligodendrocytes and regulation of their heterogeneity in different regions of the CNS. However, the pleiotropic effects of many mutations obfuscate the correlation of protein function with phenotype and only a minority of currently defined mutations have an apparently simple pathogenesis due to lack of a functional protein. On the other hand, it has tended to be autosomal recessive mutations that have been more likely to yield clear indications of the role of the gene rather than X-linked or dominant mutations (Griffiths, 1996). Thus it is hoped that the hindshaker mouse may provide elucidation of at least one link, if not more, in the complex network of events called myelination. Through the addition of such small components, a thorough understanding of the interactive processes involved in normal myelination can be developed, allowing a rational approach to be extended to investigation and treatment of disease states affecting myelin.

7. Appendix

7.1 Fixatives

7.1.1 Buffered neutral formaldehyde, 4% (BNF)

For 1L of fixative:

40% formaldehyde	100ml
Tap water	900ml
sodium dihydrogen phosphate	4g
di-potassium hydrogen phosphate	8g

7.1.2 "Strong fix" (paraformaldehyde/glutaraldehyde 4%/5%)

For 500ml "strong fix":

8% formaldehyde[1]	250ml
25% glutaraldehyde	100ml
0.08M cacodylate buffer[2]	mix formaldehyde and glutaraldehyde and make up to 500ml
calcium chloride	250mg

Filter and store at 4°C for up to 2 weeks.

1 8% formaldehyde - 20g paraformaldehyde in 250ml distilled water; heat to 65°C and add 1M NaOH until the solution clears. Cool to 4°C.

2 0.08M sodium cacodylate buffer - 17.1224g sodium cacodylate made up to 1L with distilled water and pH adjusted to 7.2.

7.1.3 Periodate-lysine-paraformaldehyde

For 1L of fixative:

lysine monohydrochloride	13.7g in 375ml distilled water
sodium hydrogen phosphate	1.8g in 100ml distilled water
	mix to give 475ml at pH7.4

paraformaldehyde	20g in 200ml distilled water

The two components can be stored separately at 4°C until required, overnight if necessary.

Mix buffered lysine and parafomaldehyde and make up volume to 1L with 0.1M phosphate buffer. Add 2.14g sodium periodate and allow to dissolve. Use immediately as does not keep.

7.2 Tissue processing protocols

7.2.1 Paraffin wax processing

Tissues to be prepared for paraffin blocks were passed through the following solutions:

1)	70% methylated spirit/5% phenol	2 hr
2)	90% methylated spirit/5% phenol	2 hr
3)	methylated spirit	2 hr
4)	ethanol/5% phenol x3	2 hr, 1hr x2
5)	1% celloidin in methyl benzoate*	4 hr
6)	xylene x3	1 hr (x3)
7)	paraffin wax x2	6 hr, 7 hr

*Necoloidine (Merck) solution for microscopy was considered as 100%. Add 1ml/100ml methyl benzoate.

7.2.2 Resin processing

Processing of tissues for resin blocks involved the following solutions:

1)	isotonic cacodylate buffer	4°C	50 min
2)	1% osmium tetroxide in cacodylate buffer	room temperature	2 hr
3)	isotonic cacodylate buffer[1]	room temperature	30 min
4)	50% ethanol	4°C	5 min
5)	50% ethanol	4°C	10 min
6)	70% ethanol	4°C	5 min
7)	70% ethanol	4°C	10 min
8)	80% ethanol	4°C	5 min

9)	80% ethanol	4°C	10 min
10)	90% ethanol	4°C	5 min
11)	90% ethanol	4°C	10 min
12)	ethanol	4°C	20 min
13)	ethanol	4°C	20 min
14)	propylene oxide	room temperature	15 min
15)	propylene oxide	room temperature	15 min
16)	1:3 resin[2]:propylene oxide	room temperature	13 hr
17)	1:2 resin:propylene oxide	room temperature	6 hr
18)	1:2 resin:propylene oxide	room temperature	18 hr
19)	resin	30°C	4 hr

Processed samples were positioned in resin filled silicon moulds and left to polymerise overnight at 60°C.

7.2.2.1 [1]Isotonic sodium cacodylate buffer

sodium cacodylate	16.05g
sodium chloride	3.8g
calcium chloride	0.055g
magnesium chloride	0.102g

Make up to 1L with distilled water and adjust to pH7.2.

7.2.2.2 [2]Araldite resin

araldite CY212	30g	resin
dodecanyl succinic anhydride (DDSA)	25.2g	hardener
2,4,6-tri-dimethylaminomethyl -phenol (DMP 30)	1.2ml	accelerator
di-butyl phthalate	1.0ml	plasticiser

7.3 Staining protocols and stains

7.3.1 Haematoxylin and eosin

Paraffin sections were passed through the following solutions:

1)	xylene	2 min
2)	absolute alcohol	2 min
3)	methylated spirit	2 min
4)	water	2 min
5)	Lugol's iodine	1 min
6)	water	1 min
7)	5% sodium thiosulphate	1 min
8)	water	1 min
9)	Mayer's haematoxylin[1]	10 min
10)	1% acid alcohol	3 dips
11)	water	2 min
12)	Scot's tap water substitute[2]	1 min
13)	water	2 min
14)	methylated spirit	10 sec
15	saturated alcoholic eosin	2 min
16)	methylated spirit	2 min
17)	absolute alcohol	2 min
18)	histoclear	2 min
19)	xylene	5 min

[1] and [2] - see below

7.3.2 Haematoxylin

Sections for nuclear counterstaining were passed through:

1)	water	2 min
2)	Mayer's haematoxylin	50 sec
3)	water	wash off excess
4)	Scot's tap water substitute	30 sec

Dehydrate sections routinely before mounting in DPX.

7.3.2.1 [1]Mayer's haematoxylin

haematoxylin 1.0g

potassium alum 10.0g

sodium iodate 0.2g

made up in 1L distilled water. Bring to boiling point and allow to cool overnight. Then add 1g citric acid and 50g chloral hydrate.

7.3.2.2 [2]Scot's tap water

sodium bicarbonate 3.5g

magnesium sulphate 20.0g

in 1L distilled water.

7.3.3 Staining of tissues for electron microscopy

Thin resin sections for electronmicroscopy were stained as follows:

1)	saturated uranyl acetate in 50% ethanol	5-15 min
2)	50% ethanol	rinse
3)	50% ethanol	rinse
4)	distilled water	rinse x 2
5)	air dry	
6)	Reynold's lead citrate* (Sodium	5-10 min
7)	1M sodium hydroxide	rinse x 3
8)	distilled water	rinse x 5

7.3.3.1 *Reynold's lead citrate

lead nitrate 1.33g

sodium citrate 1.76g

Dissolve each in 15 ml water, mix together and shake vigorously for 1 min, then intermittently over the next 30 min. Add 8 ml 1M NaOH until the solution clears and make up the volume to 50 ml with water.

7.3.3.2 Methylene blue/azur II

This was used for staining thick resin sections used for light microscopy.

Methylene blue	1%
azur II	1%
borax	1%

Each of the above is made up with distilled water. Equal volumes of each are mixed to give final staining solution.

7.4 Buffers

7.4.1 Tris buffered saline (TBS)

Tris pH7.5	3g
sodium chloride	8g
potassium chloride	0.2g

Dissolve in 800ml distilled water, adjust pH to 7.4 with HCl and make up to 1L with further distilled water.

7.4.2 Phosphate buffered saline (PBS)

sodium chloride	8g
disodium hydrogen phosphate	1.44g
potassium dihydrogen phosphate	0.24g
potassium chloride	0.2g

Dissolve in 800ml distilled water, adjust pH to 7.4 with HCl and make up to 1L with further distilled water.

7.4.3 Tris-EDTA buffer (TE)

To make 10mM Tris.Cl (pH8.0), 1mM EDTA (pH8)

1M Tris pH8.0	500µl
0.5M EDTA	100µl

Add to 50ml distilled water.

7.4.4 Gel running buffers

7.4.4.1 Tris acetate EDTA buffer x10

0.04M Tris acetate, 0.001M EDTA.

tris base	48.4g
glacial acetic acid	11.4ml
0.5 M EDTA	20ml

made up to 1L in distilled water.

7.4.4.2 Tris borate EDTA buffer x5

tris base	54g
boric acid	27.5
0.5 M EDTA	20ml

made up to 1L in distilled water.

7.5 Loading dye

6x buffer for TAE/TBE conditions

30% glycerol (Sigma)

0.25% bromophenol blue

0.25% xylene cyanol FF (Sigma)

7.6 SSC (Sodium chloride/sodium citrate) X20

3M sodium chloride/0.3M sodium citrate

sodium chloride	1753g
sodium citrate	882g

made up to 10L with distilled water.

7.7 Bacteriological media

7.7.1 Luria-Bertani medium

tryptone (Oxoid) 10g

yeast extract (Oxoid) 5g

sodium chloride 10g

Add to 950ml distilled water, adjust to pH7.0 using about 0.2ml 5N sodium hydroxide. Make up to 1L with distilled water and sterilise by autoclaving for 20 min at 15lb/in^2. Store at 4°C.

7.7.2 SOC medium

tryptone (Oxoid) 20g

yeast extract (Oxoid) 5g

sodium chloride 0.5g

Make up to 970ml in DW, add 10ml 250mM potassium chloride and adjust to pH7.0 using about 0.2ml 5N sodium hydroxide. Autoclave for 20 min at 15lb/in^2. Cool to <60°C and add 20ml filter sterilised 1M glucose solution. Store at 4°C.

7.8 Tissue culture solutions

7.8.1 SD solution

soybean trypsin inhibitor (SD) (SIGMA)	0.52mg/ml
bovine pancreas DNAse (SIGMA)	0.04mg/ml
factor V bovine serum albumin (SIGMA).	3 mg/ml

Made up in L15/HBSS 1ml aliquots stored at -20°C.

7.8.2 SATO medium

Glucose	1g/l
Glutamine (SIGMA)	2mM
Insulin (bovine) (SIGMA)	10μg/ml
Transferrin (human) (SIGMA)	100μg/ml
BSA-pathocyte (ICN)	0.0286%
Progesterone (SIGMA)	0.2μM
Putrescine (SIGMA)	0.1mM
Thyroxine (SIGMA)	0.45μM
Selenite (SIGMA)	0.224μM
Tri-iodo-thyronine (SIGMA)	0.5μM

Made up in DMEM, 30ml aliquots stored at -20°C.

7.8.3 Blocking buffer

2% bovine serum albumin (BSA/Fraction V) (BDH)

0.1% porcine skin gelatin/type A (Sigma)

2% normal goat serum (Scottish antibody production unit)

0.02% biotin (Sigma)

0.1% saponin (Sigma)

Blocking buffer 2, used for dilution of antibodies, is identical to above except only contains 0.02% saponin.

7.8.4 Poly-L lysine coverslips

Coverslips were coated with poly-L lysine to encourage cell adhesion and were prepared as follows:

1. Wash in 70% ethanol
2. Rinse in distilled water
3. Soak in 1M nitric acid overnight
4. Rinse in distilled water
5. Rinse in absolute alcohol
6. Air dry on filter paper
7. Autoclave for 20 min and 15lb/in2
8. Immerse in poly-L lysine (100µg/ml in SDW) (Sigma) for at least 30 min
9. Rinse in SDW x2
10. Air dry

Post-autoclaving, all procedures were carried out in a tissue culture hood. Coverslips were stored at -20°C after coating.

7.9 Protein analysis

7.9.1 Polyacrylamide gel composition

7.9.1.1 Acrylamide/bisacrylamide solution

acrylamide-bisacrylamide (30:0.8)	5 ml
Tris-Hcl 3M (pH 8.8)	3.75 ml
10% SDS	0.3 ml
1.5% ammonium persulphate	0.7 ml
water	20.25 ml

7.9.1.2 Acrylamide/bisacrylamide solution

acrylamide-bisacrylamide (30:0.8)	20 ml
Tris-Hcl 3M (pH 8.8)	3.75 ml
10% SDS	0.3 ml
1.5% ammonium persulphate	0.7 ml
water	2.75 ml

7.9.1.3 Stacking gel

acrylamide-bisacrylamide (30:0.8)	2.5 ml
Tris-Hcl 0.125 M (pH 6.8)	5 ml
10% SDS	2 ml
1.5% ammonium persulphate	1 ml
water	11.3 ml
TEMED	0.015 ml

7.9.2 SDS-PAGE buffers

7.9.2.1 Discontinuous buffers

Resolving gel buffer: 0.375M Tris-HCl

Stacking gel buffer: 0.125M Tris-HCl

Reservoir buffer: 0.025M Tris-HCl, 0.192M glycine, 0.1% SDS

7.9.2.2 Sample buffer

0.0625M Tris-HCl (pH 6.8)

2% SDS

5% 2-mercaptoethanol

10% glycerol

0.002% bromophenol blue

Table 10: A list of the full names of all loci in the interval of interest on chromosome 3. No gene appeared to have a specific role in the CNS based on data available through the MGD.

cM	Symbol, Name
	D3Mit175, DNA segment, Massachusetts, Institute of Technology 175
41.0	***D3Mit282***, DNA segment, Massachusetts, Institute of Technology 282
41.0	***D3Mit49***, DNA segment, Massachusetts, Institute of Technology 49
41.0	***D3Mit74***, DNA segment, Massachusetts, Institute of Technology 74
41.0	***Lxn***, latexin
41.1	***D3Ler1***, DNA segment, Chr 3, Le Roy 1
41.1	***D3Ler2***, DNA segment, Chr 3, Le Roy 2
41.2	***D3Hun9***, DNA segment, Chr 3, Hunter 9
41.3	***D3Byu6***, DNA segment, Chr 3, Brigham Young, University 6
41.3	***D3Ucla2***, DNA segment, University of California at Los Angeles 2
41.3	***Fgg***, gamma-fibrinogen
41.3	***Iapls1-7***, intracisternal A particle, lymphocyte specific 1-7
41.3	***Xmmv22***, xenotropic-MCF leukemia virus 22
41.3	***Xmmv65***, xenotropic-MCF leukemia virus 65
41.4	***D3Cph1***, DNA segment, Chr 3, CEPH 1
41.4	***D3Cph2***, DNA segment, Chr 3, CEPH 2
41.4	***ft***, flaky tail
41.5	***D3Mit108.1***, DNA Segment, Massachusetts Institute of Technology-
41.5	***Pklr***, pyruvate kinase liver and red blood cell
41.6	***Rnu1b1***, U1b1 small nuclear RNA
41.6	***Rnu1b2***, U1b2 small nuclear RNA
41.7	***Cal1l***, calpactin I light chain
41.7	***Capl***, calcium binding protein, placental
41.7	***D3Pas502***, DNA segment, Chr 3, Pasteur Institute 502
41.7	***Gba***, acid beta glucosidase
41.7	***Mtx***, metaxin
41.7	***Pmv28***, polytropic murine leukemia virus 28
41.7	***Rnu1b3***, U1b3 small nuclear RNA
41.8	***Acrb***2, acetylcholine receptor beta 2 neural
41.9	***Pmv38***, polytropic murine leukemia virus 38
42.1	***Il6ra***, interleukin 6 receptor, alpha

42.1 ***Lor***, loricrin

42.1 ***soc***, soft coat

42.2 ***D3Hun10***, DNA segment, Chr 3, Hunter 10

42.2 ***D3Ufl***, DNA segment, Chr 3, University of Florida 1

42.4 ***D3Mit187***, DNA segment, Massachusetts Institute of Technology 187

42.6 ***Bglap-rs1***, bone gamma-carboxyglutamate protein, related sequence 1

42.6 ***Bglap1***, bone gamma carboxyglutamate protein 1

42.6 ***Bglap2***, bone gamma-carboxyglutamate protein 2

42.6 ***D3Mit289.1***, DNA Segment, Massachusetts Institute of Technology-

42.6 ***Fdps***, farnesyl diphosphate synthetase

42.6 ***Flg***, filaggrin

42.6 ***Lmna***, lamin A

42.6 ***Thbs3***, thrombospondin 3

42.65 ***Lpsb2***, liver protein, selenium binding, 56 kDa

42.7 ***Gabpb2***, GA repeat binding protein, beta 2

43.0 ***Rpl32-rs8***, ribosomal protein L32 related sequence 8

43.2 ***D3Hun11***, DNA segment, Chr 3, Hunter 11

43.4 ***Rpl32-ps***, ribosomal protein L32 pseudogene

43.6 ***Cacy***, calcyclin

43.6 ***D3Mit139***, DNA segment, Massachusetts Institute of Technology 139

43.6 ***D3Tu51***, DNA segment, Chr 3, Tubingen 51

43.6 ***Mcl1***, myeloid cell leukemia sequence 1

43.78 ***D3Mit370***, DNA segment, Massachusetts Institute of Technology 370

44.1 ***D3Ncvs12***, DNA segment, National Cardiovascular Center, Shionogi 12

44.2 ***D3Hun12***, DNA segment, Chr 3, Hunter 12

44.8 ***D3Mit357***, DNA Segment, Massachusetts Institute of Technology 357

44.8 ***Muc1***, tumor-associated mucin 1

45.2 ***D3Hun13***, DNA segment, Chr 3, Hunter 13

45.2 ***D3Mit141***, DNA segment, Massachusetts Institute of Technology 141

45.2 ***D3Mit156***, DNA segment, Massachusetts Institute of Technology 156

45.2 ***D3Mit232***, DNA segment, Massachusetts Institute of Technology 232

45.2 ***D3Mit28***, DNA segment, Massachusetts Institute of Technology 28

45.2 ***D3Mit29***, DNA segment, Massachusetts Institute of Technology 29

45.2 ***D3Mit311***, DNA Segment, Massachusetts Institute of Technology 311

45.2 ***D3Mit341***, DNA Segment, Massachusetts Institute of Technology 341

45.2 ***D3Mit76***, DNA segment, Massachusetts Institute of Technology 76

45.2 ***D3Mit99***, DNA segment, Massachusetts Institute of Technology 99

45.2 ***Fcgr1***, Fc receptor, IgG, high affinity I

45.2 ***Hist2***, histone gene complex 2

45.2 ***Iapls2-28***, intracisternal A particle, lymphocyte specific 2-28

8. Abbreviations

µl	microlitre
µm	micrometer
APES	3-aminopropyltriethoxy-silane
BAC	bacterial artificial chromosome
BALB	BALB/cJ
bFGF	basic fibroblast growth factor
BNF	buffered neutral paraformaldehyde
C57	C57BL/6J
cAMP	3',5'-cyclic AMP
CAST	*Mus musculus castaneus*
CIAP	calf intestinal alkaline phosphatase
cM	centimorgan
CNP	2',3',cyclic nucleotide 3'-phosphodiesterase
CNS	central nervous system
CNTF	ciliary neurotrophic factor
ct	curly tail
DAB	3,4,4',4',-tetraminobiphenyl hydrochloride
DAPI	4',6-diamidino-2-phenylindole
DEPC	diethyl pyrocarbonate
dl	downless
DM20	the small isoform of from the *Plp* gene
DNA	deoxyribonucleic acid
EGF	epidermal growth factor
EM	electron microscopy
EST	expressed sequence tag
EUCIB	European Collaborative Interspecific Backcross
FCS	foetal calf serum
FITC	fluorescein isothiocyanate
g	grams
GalC	galactocerebroside
GFAP	glial fibrillary acidic protein
golli-mbp	gene of oligodnedrocyte lineage
H&E	haematoxylin and eosin
HBSS	Hanks buffered salt solution
hh	*hedgehog*
hr	hour

hsh	hindshaker
IGF	insulin-like growth factor
IL6	interleukin 6
IPL	intraperiod line
ISH	*in situ* hybridisation
K+	potassium
kDa	kiloDalton
L-MAG	large isoform of the myelin associated glycoprotein
LIF	leukaemia inhibitory facotr
LM	light microscopy
LOD	logarithm of odds
M	molar
MAG	myelin-associated glycoprotein
MAL	myelin and lymphocyte protein
MBP	myelin basic protein
Mbp^{shi}	shiverer
Mbp$^{shi\text{-}mld}$	myelin deficient
md-rat	myelin deficient rat
MDL	major dense line
Mg^{2+}	magnesium
MGD	Mouse Genome Database
Mgf$^{sl\text{-}con}$	Steel contrasted
min	minute
Min	multiple intestinal neoplasia mutation
MOBP	myelin-associated oligodendrocytic basic protein
MOG	myelin/oligodendrocyte glycoprotein
MOSP	myelin oligodendrocyte specific protein
mRNA	messenger ribonucleic acid
NaCl	sodium chloride
NaOH	sodium hydroxide
NH_4^+	ammonia
O-2A	oligodendrocyte type-2 astrocyte
°C	degrees centigrade
Omgp	oligodendrocyte-myelin glycoprotein
OSP	oligodendrocyte specific protein
P	postnatal age (days)
P1	phage 1
PAP	peroxidase-anti-peroxidase
PBS	phosphate buffered saline

PCR	polymerase chain reaction
PDGF	platelet derived growth factor
PDGFRα	platelet derived growth factor α receptor
PLP	proteolipid protein
PLPjp	jimpy
PLPjp-rsh	rumpshaker
Plp^{msd}	myelin synthesis deficient
PMD	Pelizaeus Merzbacher disease
PNS	peripheral nervous system
POA	pre-oligodendrocyte antigen
pt	paralytic tremor rabbit
qk	quaking
R-mAb	Ranscht monoclonal antibody
RFLP	restriction fragment length polymorphism
RNA	ribonucleic acid
RNAseA	ribonuclease A
rpm	revolutions per minute
S-MAG	small isoform of the myelin associated glycoprotein
SDS	sodium dodecyl sulphate
SDS-PAGE	sodium dodecyl suplphate polyacrylamide gel electrophoresis
SDW	sterile distilled water
sec	second
sh-pup	shaking pup
Shh	sonic hedgehog
SSC	sodium chloride/sodium citrate
SSLP	simple sequence length polymorphism
T	Brachury
TAE	tris acetate EDTA
TBE	tris borate EDTA
TBS	tris buffered saline
TEMED	N,N,N,N',tetramethylethylenediamine
tf	tufted
TXR	Texas red
Ugt8	UDP-glucuronosyltransferase 8
UV	ultraviolet
WT	wild type
YAC	yeast artificial chromosome

9. Reference List

Afar, D.E.H., Salzer, J.L., Roder, J., Braun, P.E. and Bell, J.C. (1990) Differential phosphorylation of myelin-associated glycoprotein isoforms in cell culture. *Journal of Neurochemistry.* **55,** 1418-1426.

Agresti, C., Aloisi, F. and Levi, G. (1991) Heterotypic and homotypic cellular interactions influencing the growth and differentiation of bipotential oligodendrocyte-type-2 astrocyte progenitors in culture. *Developmental Biology.* **144,** 16-29.

Ainger, K., Avossa, D., Morgan, F., Hill, S.J., Barry, C., Barbarese, E. and Carson, J.H. (1993) Transport and localization of exogenous myelin basic protein mRNA microinjected into oligodendrocytes. *Journal of Cell Biology.* **123,** 431-441.

Armstrong, R.C., Harvath, L. and Dubois-Dalcq, M. (1990) Type 1 astrocytes and oligodendrocyte-type 2 astrocyte glial progenitors migrate toward distinct molecules. *Journal of Neuroscience Research.* **27,** 400-407.

Avner, P., Amar, L., Dandalo, I. and Guenet, J.-L. (1988) Genetic analysis of the mouse using interspecific crosses. *Trends in Genetics.* **4,** 18-23.

Ballabio, A. (1993) The rise and fall of positional cloning? *Nature Genetics.* **3,** 277-279.

Bambrick, L.L. and Braun, P.E. (1991) Phosphorylation of myelin-associated glycoprotein in cultured oligodendrocytes. *Developmental Neuroscience.* **13,** 412-416.

Bansal, R. and Pfeiffer, S.E. (1992a) Novel stage in the oligodendrocyte lineage defined by reactivity of progenitors with R-mAb prior to O1 anti-galactocerebroside. *Journal of Neuroscience Research.* **32,** 309-316.

Bansal, R., Stefansson, K. and Pfeiffer, S.E. (1992b) Proligodendroblast antigen (POA), a developmental antigen expressed by A007/O4-positive oligodendrocyte progenitors prior to the appearance of sulfatide and galactocerebroside. *Journal of Neurochemistry.* **58,** 2221-2229.

Bansal, R., Warrington, A.E., Gard, A.L., Ranscht, B. and Pfeiffer, S.E. (1989) Multiple and novel specificities of monoclonal antibodies O1, O4 and R-mAb used in the analysis of oligodendrocyte development. *Journal of Neuroscience Research.* **24,** 548-557.

Baron, P., Kamholz, J., Scherer, S., Honda, H., Shy, M., Scarpini, E., Scarlato, G. and Pleasure, D. (1993) Appearance of PLP mRNA in specific regions of the developing rat lumbosacral spinal cord as revealed by *in situ* hybridization. *Exp Neurol.* **121,** 139-147.

Barres, B.A., Hart, I.K., Coles, H.S.R., Burne, J.F., Voyvodic, J.T., Richardson, W.D. and Raff, M.C. (1992a) Cell death and control of cell survival in the oligodendrocyte lineage. *Cell.* **70,** 31-46.

Barres, B.A., Hart, I.K., Coles, H.S.R., Burne, J.F., Voyvodic, J.T., Richardson, W.D. and Raff, M.C. (1992b) Cell death in the oligodendrocyte lineage. *Journal of Neurobiology.* **23,** 1221-1230.

Barres, B.A., Jacobson, M.D., Schmid, R., Sendtner, M. and Raff, M.C. (1993) Does oligodendrocyte survival depend on axons? *Current Biology.* **3,** 489-497.

Barres, B.A., Lazar, M.A. and Raff, M.C. (1994) A novel role for thyroid hormone, glucocorticoids and retinoic acid in timing oligodendrocyte development. *Development.* **120,** 1097-1108.

Barres, B.A. and Raff, M.C. (1993) Proliferation of oligodendrocyte precursor cells depends on electrical activity in axons. *Nature.* **361,** 258-260.

Barres, B.A. and Raff, M.C. (1994a) Control of oligodendrocyte number in the developing rat optic nerve. *Neuron.* **12,** 935-942.

Barres, B.A., Raff, M.C., Gaese, F., Bartke, I., Dechant, G. and Barde, Y.-A. (1994b) A crucial role for neurotrophin-3 in oligodendrocyte development. *Nature.* **367,** 371-375.

Barres, B.A., Schmid, R., Raff, M.C. and Sendtner, M. (1993) Multiple extracellular signals are required for long-term oligodendrocyte survival. *Development.* **118,** 283-295.

Bartlett, W.P., Knapp, P.E. and Skoff, R.P. (1988) Glial conditioned medium enables jimpy oligodendrocytes to express properties of normal oligodendrocytes: production of myelin antigens and membranes. *Glia.* **1,** 253-259.

Bassell, G. and Singer, R.H. (1997) MRNA and cytoskeletal filaments. *Current Opinion in Cell Biology.* **9,** (1)109-115.

Baumann, N., Jacque, C. and Dupouey, P. (1986) Astrocyte modifications in neurological mutations of the mouse. *Astrocytes: Cell biology and pathology of astrocytes.* Fedoroff, S. and Vernadakis, A., editors: Academic Press, Orlando, pp. 325-335.

Beechey, C.V. (1993) A new spontaneous neurological mutant. *Mouse Genome.* **91,** 114-115.

Beechey, C.V. and Cattanach, B.M. (1996) Linkage of hindshaker, *hsh* . *Mouse Genome.* **94,** (2)486-486.

Bernier, L., Alvarez, F., Norgard, E.M., Raible, D.W., Mentaberry, A., Schembri, J.G., Sabatini, D.D. and Colman, D.R. (1987) Molecular cloning of a 2',3'-cyclic nucleotide 3'-phosphodiesterase: mRNAs with different 5' ends encode the same set of proteins in nervous and lymphoid tissues. *Journal of Neuroscience.* **7,** 2703-2710.

Bernier, L., Colman, D.R. and D'Eustachio, P. (1988) Chromosomal locations of genes encoding 2',3' cyclic nucleotide 3'-phosphodiesterase and glial fibrillary acidic protein in the mouse. *Journal of Neuroscience Research.* **20,** 497-504.

Bignami, A., Eng, L.F. and Uyeda, C.T. (1972) Localization of the glial fibrillary acidic protein in astrocytes by immunofluorescence. *Brain Research.* **43,** 429-435.

Billings-Gagliardi, S., Kirschner, D.A., Nadon, N.L., DiBenedetto, L.M., Karthigasan, J., Lane, P., Pearsall, G.B. and Wolf, M.K. (1995) Jimpy 4J: A new X-linked mouse mutation producing severe CNS hypomyelination. *Developmental Neuroscience.* **17,** 300-310.

Bjartmar, C., Hildebrand, C. and Loinder, K. (1994) Morphological heterogeneity of rat oligodendrocytes: Electron microscopic studies on serial sections. *Glia.* **11,** 235-244.

Black, J.A., Foster, R.E. and Waxman, S.G. (1982) Rat optic nerve: freeze-fracture studies during development of myelinated axons. *Brain Research.* **250,** 1-20.

Blakemore, W.F., Harding, J.D.J. and Done, J.T. (1974a) Ultrastructural observations on the spinal cord of a Landrace pig with congenital tremor type AIII. *Research in Veterinary Science.* **17,** 174-178.

Blakemore, W.F., Palmer, A.C. and Barlow, R.M. (1974b) Progressive ataxia of Charolais cattle associated with disordered myelin. *Acta Neuropathologica (Berlin).* **29,** 127-139.

Boison, D., Büssow, H., D'Urso, D., Müller, H.-W. and Stoffel, W. (1995) Adhesive properties of proteolipid protein are responsible for the compaction of CNS myelin sheaths. *Journal of Neuroscience.* **15,** 5502-5513.

Boison, D. and Stoffel, W. (1989) Myelin-deficient rat: a point mutation in exon III (A->C, Thr75->Pro) of the myelin proteolipid protein causes dysmyelination and oligodendrocyte death. *EMBO J.* **8,** 3295-3302.

Boison, D. and Stoffel, W. (1994) Disruption of the compacted myelin sheath of axons of the central nervous system in proteolipid protein-deficient mice. *Proceedings of the National Academy of Sciences USA.* **91,** 11709-11713.

Bonhomme, F., Catalan, J., Britton-Davidian, J., Moriwaki, K., Nevo, E. and Thaler, L. (1984) Biochemical diversity and evolution in the genus Mus. *Biochem Genet.* **22,** 275-303.

Bonhomme, F., Guenet, J.-L., Dod, B., Moriwaki, K. and Bullfield, G. (1987) The polyphyletic origin of laboratory inbred mice and their rate of evolution. *J Linnean Soc.* **30,** 51-58.

Bonhomme, F., Guenet, J.-L. (1989) The wild house mouse and its relatives. *Genetic variants and strains of the laboratory mouse.* Lyon, M. and Searle, A.G., editors: Oxford University Press, pp. 649-662.

Botstein, D., White, R., skolnick, m. and davis, r. (1980) Contruction of a genetic linkage map in man using restriction fragment length polymorphisms. *Am J Hum Genet.* **32,** 314-331.

Bögler, O., Wren, D., Barnett, S.C., Land, H. and Noble, M. (1990) Cooperation between two growth factors promotes extended self-renewal and inhibits differentiation of O-2A progenitor cells. *Proceedings of the National Academy of Sciences USA.* **87,** 6368-6372.

Bronstein, J.M., Kozak, C.A., Chen, X.N., Wu, S., Danciger, M., Korenberg, J.R. and Farber, D.B. (1996) Chromosomal localization of murine and human oligodendrocyte-specific protein genes. *Genomics.* **34,** 255-257.

Brown, S.D. (1992) The mouse genome project and human genetics. A report from the 5th international mouse genome mapping workshop, Lunteren, Holland. *Genomics.* **13,** 490-492.

Butt, A.M., Ibrahim, M. and Berry, M. (1997) The relationship between developing oligodendrocyte units and maturing axons during myelinogenesis in the anterior medullary velum of neonatal rats. *Journal of Neurocytology.* **26,** (5)327-338.

Butt, A.M. and Ransom, B.R. (1989) Visualization of oligodendrocytes and astrocytes in the intact rat optic nerve by intracellular injection of lucifer yellow and horseradish peroxidase. *Glia.* **2,** 470-475.

Cameron-Curry, P. and Le Douarin, N.M. (1995) Oligodendrocyte precursors originate from both the dorsal and the ventral parts of the spinal cord. *Neuron.* **15,** 1299-1310.

Campagnoni, C.W., Garbay, B., Micevych, P., Pribyl, T., Kampf, K., Handley, V.W. and Campagnoni, A.T. (1992) DM20 mRNA splice product of the myelin proteolipid protein gene is expressed in the murine heart. *Journal of Neuroscience Research.* **33,** 148-155.

Carson, J.H., Nielson, M.L. and Barbarese, E. (1983) Developmental regulation of myelin basic protein expression in mouse brain. *Developmental Biology.* **96,** 485-492.

Cattanach, B.M. and Beechey, C.V. (1991) Evidence of allelism between rumpshaker and jimpy. *Mouse Genome.* **89,** 271.

Chernoff, G.F. (1981) Shiverer: an autosomal recessive mutant mouse with myelin deficiency. *The Journal of Heredity.* **72,** 128.

Choi, B.H., Kim, R.C. and Lapham, L.W. (1983) Do radial glia give rise to both astroglial and oligodendroglial cells. *Developmental Brain Research.* **8,** 119-130.

Coetzee, G.A., Li, X., Fujita, N., Marcus, J., Suzuki, K., Francke, U. and Popko, B. (1996) Molecular cloning, chromosomal mapping and characterization of the mouse UDP-galactose:ceramide galactosyltransferase gene. *Genomics.* **35,** 215-222.

Coffey, J.C. and McDermott, K.W. (1997) The regional distribution of myelin oligodendrocyte glycoprotein (MOG) in the developing rat CNS: An *in vivo* immunohistochemical study. *Journal of Neurocytology.* **26,** (3)149-161.

Colello, R.J., Devey, L.R., Imperato, E. and Pott, U. (1995) The chronology of oligodendrocyte differentiation in the rat optic nerve: Evidence for a signaling step initiating myelination in the CNS. *Journal of Neuroscience.* **15,** 7665-7672.

Colello, R.J., Pott, U. and Schwab, M.E. (1994) The role of oligodendrocytes and myelin on axon maturation in the developing rat retinofugal pathway. *Journal of Neuroscience.* **14,** 2594-2605.

Collins, F.S. (1992) Positional cloning: Let's not call it reverse anymore. *Nature Genetics.* **1,** 3-6.

Collins, F.S. (1995) Positional cloning moves from perditional to traditional. *Nature.* **9,** 347-350.

Copeland, N.G., Jenkins, N.A., Gilbert, D.J., Eppig, J.T., Maltais, L.J., Miller, J.C., Dietrich, W.F., Weaver, A., Lincoln, S.E., Steen, R.G., *et al.* (1993) A genetic linkage map of the mouse: Current applications and future prospects. *Science.* **262,** 57-66.

Cornall, R.J., Aitman, T.J., Hearne, C.M. and Todd, J.A. (1991) The generation of a library of PCR-analysed microsatellite variants for genetic mapping of the mouse genome. *Genomics.* **10,** 874-881.

Cox, K.H., DeLeon, D.V., Angerer, L.M. and Angerer, R.C. (1984) Detection of mRNAs in sea urchin embryos by in situ hybridization using asymmetric RNA probes. *Developmental Biology.* **101,** 485-502.

Côté, F., Collard, J.-F., Houle, D. and Julien, J.-P. (1994) Copy-dependent and correct developmental expression of the human neurofilament heavy gene in transgenic mice. *Molecular Brain Research.* **26,** 99-105.

Cummings, J.F., Summers, B.A., de Lahunta, A. and Lawson, C. (1986) Tremors in samoyed pups with oligodendrocyte deficiencies and hypomyelination. *Acta Neuropathologica (Berlin).* **71,** 267-277.

Daubas, P., Pham-Dinh, D. and Dautigny, A. (1994) Structure and polymorphism of the mouse myelin/oligodendrocyte glycoprotein gene. *Genomics.* **23,** 36-41.

De Angelis, D.A. and Braun, P.E. (1994) Isoprenylation of brain 2',3'-cyclic nucleotide 3'-phosphodiesterase modulates cell morphology. *Journal of Neuroscience Research.* **39,** 386-397.

De Angelis, D.A. and Braun, P.E. (1996) 2',3'-cyclic nucleotide 3'-phosphodiesterase binds to actin- based cytoskeletal elements in an isoprenylation-independent manner. *Journal of Neurochemistry.* **67,** 943-951.

de Ferra, F., Engh, H., Hudson, L., Kamholz, J., Puckett, C., Molineaux, S. and Lazzarini, R.A. (1985) Alternative splicing accounts for the four forms of myelin basic protein. *Cell.* **43,** 721-727.

De Waegh, S.M., Lee, V.M.Y. and Brady, S.T. (1992) Local modulation of neurofilament phosphorylation, axonal caliber, and slow axonal transport by myelinating Schwann cells. *Cell.* **68,** 451-463.

Del Rio Hortega, P. (1921) Estudios sobre la neuroglia: La glia de escasas radiaciones (oligodendroglia). *Boletin Ral Sociedad Espanola de Histologia Natural.* **21,** 63-92.

Del Rio Hortega, P. (1922) Son homologables la glia de escasas radiaciones y la celula de Schwann? *Boletin Ral Sociedad Espanola de Histologia Natural.* **10,** 25-29.

Del Rio Hortega, P. (1924) La glie a radiations peu nombreuses et la cellule de Schwann sont elles homologables. *Compte Rendu Seances Societe Biologie.* **91,** 818-820.

Dentinger, M.P., Barron, K.D. and Csiza, C.K. (1982) Ultrastructure of the central nervous system in a myelin deficient rat. *Journal of Neurocytology.* **11,** 671-691.

Dickinson, P.J., Fanarraga, M.L., Griffiths, I.R., Barrie, J.A., Kyriakides, E. and Montague, P. (1996) Oligodendrocyte progenitors in the embryonic spinal cord express DM-20. *Neuropathology and Applied Neurobiology.* **22,** 188-198.

Dietrich, W., Katz, H., Lincoln, S.E., Shin, H.-S., Friedman, J., Dracopoli, N.C. and Lander, E.S. (1992) A genetic map of the mouse suitable for typing intraspecific crosses. *Genetics.* **131,** 423-447.

Douglas, A.J. and Thompson, R.J. (1993) Structure of the myelin membrane enzyme 2',3'-cyclic nucleotide 3'-phosphodiesterase: Evidence for two human mRNAs. *Biochem Soc Trans.* **21,** 295-297.

Dubois-Dalcq, M., Behar, T., Hudson, L.D. and Lazzarini, R.A. (1986) Emergence of three myelin proteins in oligodendrocytes cultured without neurons. *Journal of Cell Biology.* **102,** 384-392.

Duncan, I.D. (1987) Abnormalities of myelination of the central nervous system associated with congenital tremor. *Journal of Veterinary Internal Medicine.* **1,** 10-23.

Duncan, I.D. (1990) Dissection of the phenotype and genotype of the X-linked myelin mutants. *Annals of the New York Academy of Sciences.* **605,** 110-121.

Duncan, I.D. (1995) Inherited disorders of myelination of the central nervous system. *Neuroglia.* Kettenmann, H. and Ransom, B.R., editors: Oxford University Press, Oxford, pp. 843-858.

Duncan, I.D., Griffiths, I.R. and Munz, M. (1983) "Shaking pup": a disorder of central myelination in the spaniel dog. III. Quantitative aspects of the glia and myelin in the spinal cord and optic nerve. *Neuropathology and Applied Neurobiology.* **9,** 355-368.

Duncan, I.D., Hammang, J.P., Goda, S. and Quarles, R.H. (1989) Myelination in the jimpy mouse in the absence of proteolipid protein. *Glia.* **2,** 148-154.

Duncan, I.D., Hammang, J.P. and Jackson, K.F. (1986) Mosaicism in the CNS of two myelin mutants, the shaking pup and the myelin deficient (md) rat. *Journal of Neuropathology and Experimental Neurology.* **45,** 373.

Duncan, I.D., Hammang, J.P. and Trapp, B.D. (1987) Abnormal compact myelin in the myelin-deficient rat: absence of proteolipid protein correlates with a defect in the intraperiod line. *Proceedings of the National Academy of Sciences USA.* **84,** 6287-6291.

Duncan, I.D., Jackson, K.F., Hammang, J.P., Marren, D. and Hoffman, R. (1993) Development of myelin mosaicism in the optic nerve of heterozygotes of the X-linked myelin-deficient (*md*) rat mutant. *Developmental Biology.* **157,** 334-347.

Duncan, I.D., Lunn, K.F., Holmgren, B., Urba-Holmgren, R. and Brignolo-Holmes, L. (1992) The taiep rat: A myelin mutant with an associated oligodendrocyte microtubular defect. *Journal of Neurocytology.* **21,** 870-884.

Dyer, C.A., Hickey, W.F. and Geisert, E.E., Jr. (1991) Myelin/oligodendrocyte-specific protein: A novel surface membrane protein that associates with microtubules. *Journal of Neuroscience Research.* **28,** 607-613.

Ebersole, T., Rho, O. and Artzt, K. (1992) The proximal end of mouse chromosome 17: new molecular markers identify a deletion associated with *quaking*^{viable}. *Genetics.* **131,** 183-190.

Ebersole, T.A., Chen, Q., Justice, M.J. and Artzt, K. (1996) The *quaking* gene product necessary in embryogenesis and myelination combines features of RNA binding and signal transduction proteins. *Nature Genetics.* **12,** 260-265.

Edwards, A.M., Braun, P.E. and Bell, J.C. (1989) Phosphorylation of myelin-associated glycoprotein in vivo and in vitro occurs only in the cytoplasmic domain of the large isoform. *Journal of Neurochemistry.* **52,** 317-320.

Einsenbarth, G.S., Walsh, F.S. and Nirenberg, M. (1979) Monoclonal antibody to a plasma membrane antigen of neurons. *Proceedings of the National Academy of Sciences USA.* **76,** 4913-4917.

Ellison, J.A., Scully, S.A. and de Vellis, J. (1996) Evidence for neuronal regulation of oligodendrocyte development: Cellular localization of platelet-derived growth factor α

receptor and A-chain mRNA during cerebral cortex development in the rat. *Journal of Neuroscience Research.* **45,** 28-39.

Erickson, R.P. (1996) Mouse models of human genetic disease: Which mouse is more like a man? *BioEssays.* **18,** (12)993-998.

European Backcross Collaborative Group (1994) Towards high resolution maps of the mouse and human genomes - a facility for ordering markers to 0.1cM resolution. *Human Molecular Genetics.* **3,** 621-627.

Fanarraga, M.L., Griffiths, I.R., McCulloch, M.C., Barrie, J.A., Cattanach, B.M., Brophy, P.J. and Kennedy, P.G.E. (1991) Rumpshaker: an X-linked mutation affecting CNS myelination. A study of the female heterozygote. *Neuropathology and Applied Neurobiology.* **17,** 289-297.

Fanarraga, M.L., Griffiths, I.R., McCulloch, M.C., Barrie, J.A., Kennedy, P.G.E. and Brophy, P.J. (1992) Rumpshaker: an X-linked mutation causing hypomyelination. Developmental differences in myelination and glial cells between the optic nerve and spinal cord. *Glia.* **5,** 161-170.

Fanarraga ML, Griffiths IR, Zhao M, Duncan ID. Oligodendrocytes are not inherently programmed to myelinate a specific size of axon. [In Press] J Neurosci 1997;

Ferris, S.D., Sage, R.D., Prager, E.M., Titte, U. and Wilson, A.C. (1983) Mitochondrial DNA evolution in mice. *Genetics.* **105,** 681-721.

Ferris, S.D., Sage, R.D. and Wilson, A.C. (1982) Evidence from mtDNA sequences that common laboratory strains are descended from a single female. *Nature.* **295,** 163-165.

ffrench-Constant, C. and Raff, M.C. (1986) Proliferating bipotential glial progenitor cells in adult rat optic nerve. *Nature.* **319,** 499-502.

Fox, M.W., Inman, O.R. and Himwich, W.A. (1967) The postnatal development of the spinal cord of the dog. *Journal of Comparative Neurology.* **130,** 233-240.

Fremeau, R.T., Jr. and Popko, B. (1990) *In situ* analysis of myelin basic protein gene expression in myelin-deficient oligodendrocytes: antisense hnRNA and readthrough transcription. *EMBO J.* **9,** 3533-3538.

Friede, R.L. and Bischhausen, R. (1982) How are sheath dimensions affected by axon caliber and internode length. *Brain Research.* **235,** 335-350.

Friedman, B., Hockfield, S., Black, J.A., Woodruff, K.A. and Waxman, S.G. (1989) In situ demonstration of mature oligodendrocytes and their processes: an immunocytochemical study with a new monoclonal antibody, Rip. *Glia.* **2,** 380-390.

Friedrich, V.L., Jr. (1974) The myelin deficit in quaking mice. *Brain Research.* **82,** 168-172.

Friedrich, V.L., Jr. (1975) Hyperplasia of oligodendrocytes in quaking mice. *Anatomy and Embryology.* **147,** 259-271.

Fulton, B.P., Burne, J.F. and Raff, M.C. (1992) Visualization of O-2A progenitor cells in developing and adult rat optic nerve by quisqualate-stimulated cobalt uptake. *Journal of Neuroscience.* **12,** 4816-4833.

Gard, A.L. and Pfeiffer, S.E. (1990) Two proliferative stages of the oligodendrocyte lineage (A2B5+O4- and GalC-) under different mitogenic control. *Neuron.* **5,** 615-625.

Gardinier, M.V. and Macklin, W. (1988) Myelin proteolipid protein gene expression in jimpy and jimpy^{msd} mice. *Journal of Neurochemistry.* **51,** 360-369.

Gencic, S. and Hudson, L.D. (1990) Conservative amino acid substitution in the myelin proteolipid protein of jimpy^{msd} mice. *Journal of Neuroscience.* **10,** 117-124.

Gillespie, C.S., Wilson, R., Davidson, A. and Brophy, P.J. (1989) Characterization of a cytoskeletal matrix associated with myelin from rat brain. *Biochem J.* **260,** 689-696.

Gilmore, S.A. (1971) Neuroglial population in the spinal white matter of neonatal and early post-natal rats: an autoradiographic study of numbers of neuroglial and changes in their proliferative activity. *The Anatomical Record.* **171,** 283-292.

Gonye, G.E., Warrington, A.E., DeVito, J.A. and Pfeiffer, S.E. (1994) Oligodendrocyte precursor quantitation and localization in perinatal brain using a retrospective bioassay. *Journal of Neuroscience.* **14,** 5365-5372.

Gould, R.M., Byrd, A.L. and Barbarese, E. (1995) The number of Schmidt-Lanterman incisures is more than doubled in *shiverer* PNS myelin sheaths. *Journal of Neurocytology.* **24,** 85-98.

Gow, A., Friedrich, V.L., Jr. and Lazzarini, R.A. (1994) Many naturally occurring mutations of myelin proteolipid protein impair its intracellular transport. *Journal of Neuroscience Research.* **37,** 574-583.

Gow, A., Gragerov, A., Gard, A.L., Colman, D.R., Lazzarini, R.A. and Gard, A. (1997) Conservation of topology, but not conformation, of the proteolipid proteins of the myelin sheath Conservation of topology, but not conformation, of the proteolipid proteins of the myelin sheath. *Journal of Neuroscience.* **17,** (1)181-189.

Gravel, M., Peterson, J., Yong, V.W., Kottis, V., Trapp, B. and Braun, P.E. (1996) Overexpression of 2',3'-cyclic nucleotide 3'-phosphodiesterase in transgenic mice alters oligodendrocyte development and produces aberrant myelination. *Molecular and Cellular Neuroscience.* **7,** 453-466.

Greenfield, S., Brostoff, S.W. and Hogan, E.L. (1977) Evidence for defective incorporation of proteins in myelin of the quaking mutant mouse. *Brain Res.* **120,** 507-515.

Griffiths, I.R. (1996) Myelin mutants: model systems to study normal and abnormal myelination. *BioEssays.* **18,** 789-797.

Griffiths, I.R., Dickinson, P. and Montague, P. (1995) Expression of the proteolipid protein gene in glial cells of the post-natal peripheral nervous system of rodents. *Neuropathology and Applied Neurobiology.* **21,** 97-110.

Griffiths, I.R., Duncan, I.D., McCulloch, M. and Harvey, M.J.A. (1981) Shaking pups: a disorder of central myelination in the spaniel dog. *Journal of the Neurological Sciences.* **50,** 423-433.

Griffiths, I.R., Schneider, A., Anderson, J. and Nave, K.-A. (1995) Transgenic and natural mouse models of proteolipid protein (PLP) related dysmyelination and demyelination. *Brain Pathology.* **5,** 275-281.

Griffiths, I.R., Scott, I., McCulloch, M.C., Barrie, J.A., McPhilemy, K. and Cattanach, B.M. (1990) Rumpshaker mouse: a new X-linked mutation affecting myelination: evidence for a defect in PLP expression. *Journal of Neurocytology.* **19,** 273-283.

Haldane, J.B.S., Sprunt, A.D. and Haldane, N.M. (1915) Reduplication in mice. *J Genet.* **5,** 133-135.

Hall, A., Giese, N.A. and Richardson, W.D. (1996) Spinal cord oligodendrocytes develop from ventrally derived progenitor cells that express PDGF alpha-receptors. *Development.* **122,** (12)4085-4094.

Hamada, H., Petrino, M.G. and Kakunaga, T. (1982) A novel repeated element with Z-DNA-forming potential is widely found in evolutionarily diverse eukaryotic genomes. *Proceedings of the National Academy of Sciences USA.* **79,** 6465-6469.

Hammer, M.F., Schimenti, J. and Silver, L.M. (1989) Evolution of mouse chromosome 17 and the origin of inversions associated with *t* haplotypes. *Proceedings of the National Academy of Sciences USA.* **86,** 3261-3265.

Hanneman, W.H., Legare, M.E., Sweeney, S. and Schimenti, J.C. (1997) Cisplatin increases meiotic crossing-over in mice. *Proceedings of the National Academy of Sciences of the United States of America.* **94,** (16)8681-8685.

Hardy, R. and Reynolds, R. (1991) Proliferation and differentiation potential of rat forebrain oligodendroglial progenitors both *in vitro* and *in vivo*. *Development.* **111,** 1061-1080.

Hardy, R.J. and Friedrich, V.L., Jr. (1996) Oligodendrocyte progenitors are generated throughout the embryonic mouse brain, but differentiate in restricted foci. *Development.* **122,** 2059-2069.

Hartman, B.K., Agrawal, H.C., Agrawal, D. and Kalmbach, S. (1982) Development and maturation of central nervous system myelin: comparison of immunohistochemical localization of proteolipid protein and basic protein in myelin and oligodendrocytes. *Proceedings of the National Academy of Sciences USA.* **79,** 4217-4220.

Helynck, G., Luu, B., Nussbaum, J.L., Picken, D., Skalidis, G., Trifilieff, E., Van Dorsselaer, A., Seta, P., Sandeaux, R., Gavach, D., *et al.* (1983) Brain proteolipids, isolation, purification and effects on ionic permeability of membranes. *European Journal of Biochemistry.* **133,** 689-695.

Hildebrand, C. and Waxman, S.G. (1984) Postnatal differentiation of rat optic nerve fibers:electron microscopic observations on the development of nodes of Ranvier and axoglial relations. *Journal of Comparative Neurology.* **224,** 25-37.

Hirano, M. and Goldman, J.E. (1988) Gliogenesis in rat spinal cord: evidence for origin of astrocytes and oligodendrocytes from radial precursors. *Journal of Neuroscience Research.* **21,** 155-167.

Holz, A., Schaeren-Wiemers, N., Schaefer, C., Pott, U., Colello, R.J. and Schwab, M.E. (1996) Molecular and developmental characterization of novel cDNAs of the myelin-associated oligodendrocytic basic protein. *Journal of Neuroscience.* **16,** 467-477.

Hsieh, S.-T., Kidd, G.J., Crawford, T.O., Xu, Z., Lin, W.-M., Trapp, B.D., Cleveland, D.W. and Griffin, J.W. (1994) Regional modulation of neurofilament organization by myelination in normal axons. *Journal of Neuroscience.* **14,** 6392-6401.

Jackson, K.F. and Duncan, I.D. (1988) Cell kinetics and cell death in the optic nerve of the myelin deficient rat. *Journal of Neurocytology.* **17,** 657-670.

Kagawa, T., Ikenaka, K., Inoue, Y., Kuriyama, S., Tsujii, T., Nakao, J., Nakajima, K., Aruga, J., Okano, H. and Mikoshiba, K. (1994) Glial cell degeneration and hypomyelination caused by overexpression of myelin proteolipid protein gene. *Neuron.* **13,** 427-442.

Kagawa, T., Oba, A., Okumura, S. and Ikenaka, K. (1996) Localization of mRNA for UDP-galactose: Ceramide galactosyltransferase in the brain during mouse development. *Developmental Neuroscience.* **18,** 309-318.

Klugmann, M., Schwab, M.H., Pühlhofer, A., Schneider, A., Zimmermann, F., Griffiths, I.R. and Nave, K.-A. (1997) Assembly of CNS myelin in the absence of proteolipid protein. *Neuron.* **18,** 59-70.

Knapp, P.E., Benjamins, J.A. and Skoff, R.P. (1996) Epigenetic factors up-regulate expression of myelin proteins in the dysmyelinating jimpy mutant mouse. *Journal of Neurobiology.* **29,** 138-150.

Knapp, P.E., Booth, C.S. and Skoff, R.P. (1993) The pH of jimpy glia is increased: Intracellular measurements using fluorescent laser cytometry. *Int J Dev Neurosci.* **11,** 215-226.

Knapp, P.E. and Skoff, R.P. (1987) A defect in the cell cycle of neuroglia in the myelin deficient jimpy mouse. *Developmental Brain Research.* **35,** 301-306.

Knapp, P.E. and Skoff, R.P. (1993) Jimpy mutation affects astrocytes: Lengthening of the cell cycle in vitro. *Developmental Neuroscience.* **15,** 31-36.

Knapp, P.E., Skoff, R.P. and Redstone, D.W. (1986) Oligodendroglial cell death in jimpy mice: an explanation for the myelin deficit. *Journal of Neuroscience.* **6,** 2813-2822.

Knight, A.M. and Dyson, P.J. (1990) Detection of DNA polymorphisms between two inbred mouse strains - limitations of restriction fragment length polymorphisms (RFLPs). *Mol Cell Probes.* **4,** 497-504.

Kondo, A., Sato, Y. and Nagara, H. (1991) An ultrastructural study of oligodendrocytes in zitter rat: A new animal model for hypomyelination in the CNS . *Journal of Neurocytology.* **20,** 929-939.

Kondo, A., Sendoh, S., Akazawa, K., Sato, Y. and Nagara, H. (1992) Early myelination in zitter rat: Morphological, immunocytochemical and morphometric studies. *Developmental Brain Research.* **67,** 217-228.

Kornegay, J.N., Goodwin, M.A. and Spyridakis, L.K. (1987) Hypomyelination in a Weimaraner dog. *Acta Neuropathologica (Berlin).* **72,** 394-401.

Kuhlmann-Krieg, S., Sommer, I. and Schachner, M. (1988) Ultrastructural features of cultured oligodendrocytes expressing stage-specific cell-surface antigens. *Developmental Brain Research.* **39,** 269-280.

Kunishita, T., Tabira, T., Umezawa, H., Mizutani, M. and Katsuie, Y. (1986) A new myelin-deficient hamster: biochemical and morphological studies. *Journal of Neurochemistry.* **46,** 105-111.

Kurihara, T., Monoh, K., Sakimura, K. and Takahashi, Y. (1990) Alternative splicing of mouse brain 2',3'-cyclic-nucleotide 3'-phosphodiesterase mRNA. *Biochemical and Biophysical Research Communications.* **170,** 1074-1081.

Kurihara, T., Takahashi, Y., Fujita, N., Sato, S. and Miyatake, T. (1989) Developmental expression of 2',3'-cyclic nucleotide 3'-phosphodiesterase mRNA in brains of normal and quaking mice. *Molecular Brain Research.* **5,** 247-250.

Kusumi, K., Smith, J.S., Segre, J.A., Koos, D.S. and Lander, E.S. (1993) Construction of a large-insert yeast artifical chromosome library of the mouse genome. *Mammalian Genome.* **4,** 391-392.

Lachapelle, F. (1995) Glial transplants: An *in vivo* analysis of extrinsic and intrinsic determinants of dysmyelination in genetic variants. *Brain Pathology.* **5,** 289-299.

Lander, E. and Kruglyak, L. (1995) Genetic dissection of complex traits: guidelines for interpreting and reporting linkage results. *Nature Genetics.* **11,** 241-247.

Langworthy, O.R. (1928) The behavior of pouch young opossums correlated with the myelinization of tracts in the nervous system. *Journal of Comparative Neurology.* **46,** 201-248.

Langworthy, O.R. (1933) Development of behavior patterns and myelinization of the nervous system in the human fetus and infant. *Contributions to Embryology, Carnegie Institute of Washington.* **443,** No139 1-57.

LeRoy, H., Simon-Chazottes, D., Montagutelli, X. and Guenet, J.-L. (1992) A set of anonymous DNA clones as markers for mouse gene mapping. *Mammalian Genome.* **3,** 244-246.

Letts, V.A., Schork, N.J., Copp, A.J., Bernfield, M. and Frankel, W.N. (1995) A curly-tail modifier locus, *mct1*, on mouse chromosome 17. *Genomics.* **29,** 719-724.

Levi, G., Agresti, C., D'Urso, D. and Aloisi, F. (1991) Is the oligodendroglial differentiation of bipotential oligodendrocyte- type 2 astrocyte progenitors promoted by autocrine factors. *Neuroscience Letters.* **128,** 37-41.

Levi, G., Aloisi, F. and Wilkin, G.P. (1987) Differentiation of cerebellar bipotential glial precursors into oligodendrocytes in primary culture: developmental profile of surface antigens and mitotic activity. *Journal of Neuroscience Research.* **18,** 407-417.

Levine, J.M., Stincone, F. and Lee, Y.-S. (1993) Development and differentiation of glial precursor cells in the rat cerebellum. *Glia.* **7,** 307-321.

Levison, S.W., Chuang, C., Abramson, B.J. and Goldman, J.E. (1993a) The migrational patterns and developmental fates of glial precursors in the rat subventricular zone are temporally regulated. *Development.* **119,** 611-622.

Levison, S.W. and Goldman, J.E. (1993b) Both oligodendrocytes and astrocytes develop from progenitors in the subventricular zone of postnatal rat forebrain. *Neuron.* **10,** 201-212.

Li, C., Tropak, M.B., Gerlai, R., Clapoff, S., Abramow-Newerly, W., Trapp, B., Peterson, A. and Roder, J. (1994) Myelination in the absence of myelin-associated glycoprotein. *Nature.* **369,** 747-750.

Ling, E.-A. and Leblond, C.P. (1973) Investigation of glial cells in semithin sections. II. Variation with age in the numbers of the various glial cell types in rat cortex and corpus callosum. *Journal of Comparative Neurology.* **149,** 73-82.

Ling, E.-A. and Wong, W.-C. (1993) The origin and nature of ramified and amoeboid microglia: A historical review and current concepts. *Glia.* **7,** 9-18.

Linington, C., Webb, M. and Woodhams, P.L. (1984) A novel myelin-associated glycoprotein defined by a mouse monoclonal antibody. *Journal of Neuroimmunology.* **6,** 387-396.

Lord, K.E. and Duncan, I.D. (1987) Early postnatal development of glial cells in the canine cervical spinal cord. *Journal of Comparative Neurology.* **265,** 34-46.

Love, J.M., Knight, A.M., Mcaleer, M.A. and Todd, J.A. (1990) Towards construction of a high resolution map of the mouse genome using PCR-analysed microsatellites. *nucleic acid research* . **18,** 4123-4130.

Lunn, K.F., Fanarraga, M.L. and Duncan, I.D. (1995) Myelin mutants: New models and new observations. *Microsc Res Tech.* **32,** 183-203.

Luskin, M.B. and McDermott, K. (1994) Divergent lineages for oligodendrocytes and astrocytes originating in the neonatal forebrain subventricular zone. *Glia.* **11,** 211-226.

Luskin, M.B., Parnavelas, J.G. and Barfield, J.A. (1993) Neurons, astrocytes, and oligodendrocytes of the rat cerebral cortex originate from separate progenitor cells: An ultrastructural analysis of clonally related cells. *Journal of Neuroscience.* **13,** 1730-1750.

Macklin, W.B., Gardinier, M.V., King, K.D. and Kampf, K. (1987) An AG-GG transition at a splice site in the myelin proteolipid protein gene in jimpy mice results in the removal of an exon. *FEBS Letters.* **223,** 417-421.

Macklin, W.B., Gardinier, M.V., Obeso, Z.O., King, K.D. and Wight, P.A. (1991) Mutations in the myelin proteolipid protein gene alter oligodendrocyte gene expression in jimpy and jimpy^{msd} mice. *Journal of Neurochemistry.* **56,** 163-171.

MacPhee, M., Chepenik, K.P., Liddell, R.A., Nelson, K.K., Siracusa, L.D. and Buchberg, A.M. (1995) The secretory phospholipase A2 gene is a candidate for the *Mom1* locus, a major modifier of *Apc^{min}*-induced intestinal neoplasia. *Cell.* **81,** 957-966.

Magyar, J.P., Ebensperger, C., Schaeren-Wiemers, N. and Suter, U. (1997) Myelin and lymphocyte protein (MAL/MVP17/VIP17) and plasmolipin are members of an extended gene family. *Gene.* **189,** (2)269-275.

Martini, R., Mohajeri, M.H., Kasper, S., Giese, K.P. and Schachner, M. (1995) Mice doubly deficient in the genes for P0 and myelin basic protein show that both proteins contribute to the formation of the major dense line in peripheral nerve myelin. *Journal of Neuroscience.* **15,** 4488-4495.

Matthews, M.A. and Duncan, D. (1971) A quantitative study of morphological changes accompanying the initiation and progress of myelin production in the dorsal funiculus of the rat spinal cord. *Journal of Comparative Neurology.* **142,** 1-22.

McCallion, A.S., Guenet, J.-L., Montague, P., Griffiths, I.R., Savioz, A. and Davies, R.W. (1996) The mouse gene (*Mobp*) encoding myelin-associated oligodendrocytic basic protein maps to distal chromosome 9. *Mammalian Genome.* **7,** 847-849.

McKinnon, R.D., Matsui, T., Dubois-Dalcq, M. and Aaronson, S.A. (1990) FGF modulates the PDGF-driven pathway of oligodendrocyte development. *Neuron.* **5,** 603-614.

McKinnon, R.D., Piras, G., Ida, J.A., Jr. and Dubois-Dalcq, M. (1993) A role for TGF-β in oligodendrocyte differentiation. *Journal of Cell Biology.* **121,** 1397-1407.

McMorris, F.A. and Dubois-Dalcq, M. (1988) Insulin-like growth factor I promotes cell proliferation and oligodendroglial commitment in rat glial progenitor cells developing in vitro. *Journal of Neuroscience Research.* **21,** 199-209.

Mikol, D.D., Rongnoparut, P., Allwardt, B.A., Marton, L.S. and Stefansson, K. (1993) The oligodendrocyte-myelin glycoprotein of mouse: Primary structure and gene structure. *Genomics.* **17,** 604-610.

Mikoshiba, K., Aoki, E. and Tsukada, Y. (1980) 2'-3'cyclic nucleotide 3'-phosphohydrolase activity in the central nervous system of a myelin deficient mutant (shiverer). *Brain Research.* **192,** 195-204.

Miller, R.H., David, S., Patel, R., Abney, E.R. and Raff, M.C. (1985) A quantitative immunohistochemical study of macroglial cell development in the rat optic nerve: *in vivo* evidence for two distinct astrocyte lineages. *Developmental Biology.* **111,** 35-41.

Miller, R.H. and Raff, M.C. (1984) Fibrous and protoplasmic astrocytes are biochemically and developmentally distinct. *Journal of Neuroscience.* **4,** 585-592.

Milner, R., Anderson, H.J., Rippon, R.F., McKay, J.S., Franklin, R.J.M., Marchionni, M.A., Reynolds, R. and ffrench-Constant, C. (1997) Contrasting effects of mitogenic growth factors on oligodendrocyte precursor cell migration. *Glia.* **19,** (1)85-90.

Milner, R., Edwards, G., Streuli, C. and ffrench-Constant, C. (1996) A role in migration for the αvβ1 integrin expressed on oligodendrocyte precursors. *Journal of Neuroscience.* **16,** (22)7240-7252.

Mitchell, L.S., Gillespie, C.S., McAllister, F., Fanarraga, M.L., Kirkham, D., Kelly, B., Brophy, P.J., Griffiths, I.R., Montague, P. and Kennedy, P.G.E. (1992) Developmental expression of the major myelin protein genes in the CNS of the X-linked hypomyelinating mutant rumpshaker. *Journal of Neuroscience Research.* **33,** 205-217.

Monoh, K., Kurihara, T., Sakimura, K. and Takahashi, Y. (1989) Structure of mouse 2',3'-cyclic nucleotide 3'-phosphodiesterase gene. *Biochemical and Biophysical Research Communications.* **165,** 1213-1220.

Montag, D., Giese, K.P., Bartsch, U., Martini, R., Lang, Y., Blüthmann, H., Karthigasan, J., Kirschner, D.A., Wintergerst, E.S., Nave, K.-A., *et al.* (1994) Mice deficient for the myelin-associated glycoprotein show subtle abnormalities in myelin. *Neuron.* **13,** 229-246.

Montague, P., Dickinson, P.J., McCallion, A.S., Stewart, G.J., Savioz, A., Davies, R.W., Kennedy, P.G.E. and Griffiths, I.R. (1997) Developmental expression of the murine *Mobp* gene. *Journal of Neuroscience Research.* **49,** (2)133-143.

Mori, S. and Leblond, C.P. (1970) Electron microscopic identification of three classes of oligodendrocytes and a preliminary study of their proliferative activity in the corpus callosum of young rats. *Journal of Comparative Neurology.* **139,** 1-30.

Morse, H.C. (1978) Introduction. *Origins of inbred mice.* Morse, H.C. , editor: Academic Press, New York, pp. 1-31.

Morse, H.C. (1981) The Laboratory Mouse - a historical perspective. *The mouse in biomedical research.* Foster, H., Small, J.D. and Fox, J.G., editors: Academic Press, pp. 1-16.

Murray, J.A. and Blakemore, W.F. (1980) The relationship between internodal length and fibre diameter in the spinal cord of the cat. *Journal of the Neurological Sciences.* **45,** 29-41.

Nadeau, J.H. (1984) Lengths of chromosomal segments conserved since divergence of man and mouse. *Proceedings of the National Academy of Sciences USA.* **81,** 814-818.

Nadon, N.L., Arnheiter, H. and Hudson, L.D. (1994) A combination of PLP and DM20 transgenes promotes partial myelination in the jimpy mouse. *Journal of Neurochemistry.* **63,** 822-833.

Nadon, N.L. and Duncan, I.D. (1996) Molecular analysis of glial cell development in the canine 'shaking pup' mutant. *Developmental Neuroscience.* **18,** 174-184.

Nadon, N.L., Duncan, I.D. and Hudson, L.D. (1990) A point mutation in the proteolipid protein gene of the "shaking pup" interupts oligodendrocyte development. *Development.* **110,** 529-537.

Nagara, H. and Suzuki, K. (1981) Chronological study of oligodendroglial alterations and myelination in quaking mice. *Neuropathology and Applied Neurobiology.* **7,** 135-150.

Nave, K.-A. (1994) Neurological mouse mutants and the genes of myelin. *Journal of Neuroscience Research.* **38,** 607-612.

Nave, K.-A. (1995) Neurological mouse mutants: a molecular-genetic analysis of myelin proteins. *Neuroglia.* Kettenmann, H. and Ransom, B.R., editors: Oxford University Press, Oxford, pp. 843-858.

Nave, K.-A. and Milner, R.J. (1989) Proteolipid proteins: structure and genetic expression in normal and myelin-deficient mutant mice. *Critical Reviews in Neurobiology.* **5,** 65-91.

Neumann, P.E., Frankel, W.N., Letts, V.A., Coffin, J.M., Copp, A.J. and Bernfield, M. (1994) Multifactorial inheritance of neural tube defects: localization of the major gene and recognition of modifiers in *ct* mutant mice . *Nature Genetics.* **6,** 357-362.

Noble, M. and Murray, K. (1984) Purified astrocytes promote the division of a bipotential glial progenitor cell. *EMBO J.* **3,** 2243-2247.

Noble, M., Murray, K., Stroobant, P., Waterfield, M.D. and Riddle, P. (1988) Platelet-derived growth factor promotes division and motility and inhibits premature differentiation of the oligodendrocyte/type-2 astrocyte progenitor cell. *Nature.* **333,** 560-562.

Noll, E. and Miller, R.H. (1993) Oligodendrocyte precursors originate at the ventral ventricular zone dorsal to the ventral midline region in the embryonic rat spinal cord. *Development.* **118,** 563-573.

Nornes, H.O. and Das, G.D. (1974) Temporal pattern of neurogenesis in spinal cord of rat. I. An autoradiographic study-time and sites of origin and migration and settling patterns of neuroblasts. *Brain Research.* **73,** 121-138.

Norton, W.T., Cammer, W. (1984) Isolation and characterization of myelin. *Myelin.* Morell, P., editor: Plenum Press, New York and London, pp. 147-196.

Nunoya, T., Tajima, M., Mizutani, M. and Umezawa, H. (1985) A new mutant strain of Syrian hamster with myelin deficiency. *Acta Neuropathologica (Berlin).* **65,** 305-312.

Okano, H., Tamura, T., Miura, M., Aoyama, A., Ikenaka, K., Oshimura, M. and Mikoshiba, K. (1988) Gene organization and transcription of duplicated MBP genes of *myelin deficient (shi^{mld})* mutant mouse. *EMBO J.* **7,** 77-83.

Ono, K., Bansal, R., Payne, J., Rutishauser, U. and Miller, R.H. (1995) Early development and dispersal of oligodendrocyte precursors in the embryonic chick spinal cord. *Development.* **121,** 1743-1754.

Orentas, D.M. and Miller, R.H. (1996) The origin of spinal cord oligodendrocytes is dependent on local influences from the notochord. *Developmental Biology.* **177,** 43-53.

Owens, G.C., Boyd, C.J., Bunge, R.P. and Salzer, J.L. (1990) Expression of recombinant myelin-associated glycoprotein in primary Schwann cells promotes the initial investment of axons by myelinating Schwann cells. *Journal of Cell Biology.* **111,** 1171-1182.

Palmer, A.C., Blakemore, W.F., Barlow, R.M., Fraser, J.A. and Ogden, A.L. (1972) Progressive ataxia of Charolais cattle associated with a myelin disorder. *Veterinary Record.* **91,** 592-594.

Panagopoulos, G., King, R.H.M., Gabriel, G., Stolinski, C., Soffer, D., Lachapelle, F. and Thomas, P.K. (1989) Morphometric and freeze-fracture studies on peripheral nerve in shiverer mice. *Journal of Comparative Neurology.* **286,** 337-344.

Pasquini, J.M., Guarna, M.M., Besio-Moreno, M.A., Iturregui, M.T., Oteiza, P.I. and Soto, E.F. (1989) Inhibition of the synthesis of glycosphingolipids affect the translocation of proteolipid protein to the myelin membrane. *Journal of Neuroscience Research.* **22,** 289-296.

Pedraza, L., Fidler, L., Staugaitis, S.M. and Colman, D.R. (1997) The active transport of myelin basic protein into the nucleus suggests a regulatory role in myelination. *Neuron.* **18,** (4)579-589.

Perry, V.H. and Gordon, S. (1988) Macrophages and microglia in the nervous system. *Trends in Neurosciences.* **11,** 273-277.

Peters A, Palay SL, Webster Hd. Saunders WB, editor.The fine structure of the nervous system. Philadelphia: W.B.Saunders; 1976;

Pfeiffer, S.E., Warrington, A.E. and Bansal, R. (1993) The oligodendrocyte and its many cellular processes. *Trends in Cell Biology.* **3,** 191-197.

Pham-Dinh, D., Mattei, M.-G., Nussbaum, J.-L., Roussel, G., Pontarotti, P., Roeckel, N., Mather, I.H., Artzt, K., Lindahl, K.F. and Dautigny, A. (1993) Myelin/oligodendrocyte

glycoprotein is a member of a subset of the immunoglobulin superfamily encoded within the major histocompatibility complex. *Proceedings of the National Academy of Sciences USA.* **90,** 7990-7994.

Pierce, J.C. and Sternberg, N. (1992a) Using bacteriophage P1 system to clone high molecular weight genomic DNA. *Methods in Enzymology.* **216,** 549-574.

Pierce, J.C., Sternberg, N. and Sauer, B. (1992b) A mouse genomic library in the bacteriophage P1 cloning system: Organisation and characterisation. *Mammalian Genome.* **3,** 550-558.

Placzek, M. (1995) The role of the notochord and floor plate in inductive interactions. *Curr Opin Genet Dev.* **5,** 499-506.

Placzek, M., Tessier-Lavigne, M., Yamada, T., Jessell, T. and Dodd, J. (1990) Mesodermal control of neural cell identity: Floor plate induction by the notochord. *Science.* **250,** 985-988.

Popko, B., Puckett, C. and Hood, L. (1988) A novel mutation in myelin-deficient mice results in unstable myelin basic protein gene transcripts. *Neuron.* **1,** 221-225.

Popko, B., Puckett, C., Lai, E., Shine, H.D., Readhead, C., Hunt, S.W.1., Sidman, R.L. and Hood, L. (1987) Myelin deficient mice: expression of myelin basic protein and generation of mice with varying levels of myelin. *Cell.* **48,** 713-721.

Popot, J.-L., Dinh, D.P. and Dautigny, A. (1991) Major myelin proteolipid: The 4-α-helix topology. *Journal of Membrane Biology.* **120,** 233-246.

Pribyl, T.M., Campagnoni, C.W., Kampf, K., Kashima, T., Handley, V.W., McMahon, J. and Campagnoni, A.T. (1993) The human myelin basic protein gene is included within a 179-kilobase transcription unit: Expression in the immune and central nervous systems. *Proceedings of the National Academy of Sciences USA.* **90,** 10695-10699.

Pringle, N., Collarini, E.J., Mosley, M.J., Heldin, C.-H. and Richardson, W.D. (1989) PDGF A chain homodimers drive proliferation of bipotential (O2A) glial progenitor cells in the developing rat optic nerve. *EMBO J.* **8,** 1049-1056.

Pringle, N.P., Mudhar, H.S., Collarini, E.J. and Richardson, W.D. (1992) PDGF receptors in the rat CNS: During late neurogenesis, PDGF alpha-receptor expression appears to be restricted to glial cells of the oligodendrocyte lineage. *Development.* **115,** 535-551.

Pringle, N.P. and Richardson, W.D. (1993) A singularity of PDGF alpha-receptor expression in the dorsoventral axis of the neural tube may define the origin of the oligodendrocyte lineage. *Development.* **117,** 525-533.

Pringle, N.P., Yu, W.-P., Guthrie, S., Roelink, H., Lumsden, A., Peterson, A.C. and Richardson, W.D. (1996) Determination of neuroepithelial cell fate: induction of the oligodendrocyte lineage by ventral midline cells and sonic hedgehog. *Developmental Biology.* **177,** 30-42.

Privat, A., Jacque, C., Bourre, J.M., Dupouey, P. and Baumann, N. (1979) Absence of the major dense line in myelin of the mutant mouse shiverer. *Neuroscience Letters.* **12,** 107-112.

Puckett, C., Hudson, L.D., Ono, K., Benecke, J., Dubois-Dalcq, M. and Lazzarini, R.A. (1987) Myelin-specific proteolipid protein is expressed in myelinating Schwann cells but is not incorporated into myelin sheaths. *Journal of Neuroscience Research.* **18,** 511-518.

Quarles, R.H., Colman, D.R., Salzer, J.L. and Trapp, B.D. (1992) Myelin-associated glycoprotein:structure-function relationships and involvement in neurological diesases. *Myelin: biology and chemistry.* Martenson, R.E., editor: CRC Press Inc., Boca Ranton, pp. 413-448.

Raff, M.C. (1989) Glial cell diversification in the rat optic nerve. *Science.* **243,** 1450-1455.

Raff, M.C. (1992) Social controls on cell survival and cell death. *Nature.* **356,** 397-400.

Raff, M.C., Abney, E.R. and Fok-Seang, J. (1985) Reconstitution of a developmental clock in vitro: a critical role for astrocytes in the timing of oligodendrocyte differentiation. *Cell.* **42,** 61-69.

Raff, M.C., Lillien, L.E., Richardson, W.D., Burne, J.F. and Noble, M. (1988) Platelet-derived growth factor from astrocytes drives the clock that times oligodendrocyte development in culture. *Nature.* **333,** 562-565.

Raff, M.C., Miller, R.H. and Noble, M. (1983) A glial progenitor that develops *in vitro* into an astrocyte or an oligodendrocyte depending on culture medium. *Nature.* **303,** 390-396.

Raff, M.C., Mirsky, R., Fields, K.L., Lisak, R.P., Dorfman, S.H., Silberberg, D.H., Gregson, N.A., Liebowitz, S. and Kennedy, M.C. (1978) Galactocerebroside is a specific marker for oligodendrocytes in culture. *Nature.* **274,** 813-816.

Raible, D.W. and McMorris, F.A. (1993) Oligodendrocyte differentiation and progenitor cell proliferation are independently regulated by cyclic AMP. *Journal of Neuroscience Research.* **34,** 287-294.

Readhead, C., Popko, B., Takahashi, N., Shine, H.D., Saavedra, R.A., Sidman, R.L. and Hood, L. (1987) Expression of a myelin basic protein gene in transgenic shiverer mice: correction of the dysmyelinating phenotype. *Cell.* **48,** 703-712.

Readhead, C., Schneider, A., Griffiths, I.R. and Nave, K.-A. (1994) Premature arrest of myelin formation in transgenic mice with increased proteolipid protein gene dosage. *Neuron.* **12,** 583-595.

Remahl, S. and Hildebrand, C. (1982) Changing relation between onset of myelination and axon diameter range in developing feline white matter. *Journal of the Neurological Sciences.* **54,** 33-45.

Remahl, S. and Hildebrand, C. (1990) Relation between axons and oligodendroglial cells during initial myelination. I. The glial unit. *Journal of Neurocytology.* **19,** 313-328.

Roach, A., Boylan, K., Horvath, S., Prusiner, S.B. and Hood, L. (1983) Characterization of cloned cDNA representing rat myelin basic protein: absence of expression in brain of shiverer mutant mice. *Cell.* **34,** 799-806.

Roach, A., Takahashi, N., Pravtcheva, D., Ruddle, F. and Hood, L. (1985) Chromosomal mapping of mouse myelin basic protein gene and structure and transcription of the partially deleted gene in shiverer mutant mice. *Cell.* **42,** 149-155.

Rosenbluth, J. (1980) Central myelin in the mouse mutant shiverer. *Journal of Comparative Neurology.* **194,** 639-648.

Rosenbluth, J., Stoffel, W. and Schiff, R. (1996) Myelin structure in proteolipid protein (PLP)-null mouse spinal cord. *Journal of Comparative Neurology.* **371,** 336-344.

Rozmahel, R. (1996) Modulation of disease severity in cystic fibrosis transmembrane conductance regulator deficient mice by a secondary genetic factor. *Nature Genetics.* **12,** 280-287.

Rubin, B.P., Dusart, I. and Schwab, M.E. (1994) A monoclonal antibody (IN-1) which neutralises neurite growth inhibitory proteins in the rat CNS recognises antigens localized in CNS myelin. *Journal of Neurocytology.* **23,** 209-217.

Sadler, T.W. (1985) Central nervous system. *Langman's Medical Embryology.* Tracy, T., editor: pp. 334-371.

Salzer, J.L. and Colman, D.R. (1989) Mechanisms of cell adhesion in the nervous system: Role of the immunoglobulin gene superfamily. *Developmental Neuroscience.* **11,** 377-390.

Salzer, J.L., Holmes, W.P. and Colman, D.R. (1987) The amino acid sequence of the myelin-associated glycoproteins: homology to the immunoglobulin gene superfamily. *Journal of Cell Biology.* **104,** 957-965.

Sánchez, I., Hassinger, L., Paskevich, P.A., Shine, H.D. and Nixon, R.A. (1996) Oligodendroglia regulate the regional expansion of axon caliber and local accumulation of neurofilaments during development independently of myelin formation. *Journal of Neuroscience.* **16,** 5095-5105.

Scherer, S.S., Braun, P.E., Grinspan, J., Collarini, E., Wang, D. and Kamholz, J. (1994) Differential regulation of the 2',3'-cyclic nucleotide 3'- phosphodiesterase gene during oligodendrocyte development. *Neuron.* **12,** 1363-1375.

Schneider, A., Griffiths, I.R., Readhead, C. and Nave, K.-A. (1995) Dominant-negative action of the *jimpy* mutation in mice complemented with an autosomal transgene for myelin proteolipid protein. *Proceedings of the National Academy of Sciences USA.* **92,** 4447-4451.

Schneider, A., Montague, P., Griffiths, I.R., Fanarraga, M.L., Kennedy, P.G.E., Brophy, P.J. and Nave, K.-A. (1992) Uncoupling of hypomyelination and glial cell death by a mutation in the proteolipid protein gene. *Nature.* **358,** 758-761.

Schwab, M.E. and Schnell, L. (1989) Region-specific appearance of myelin constituents in the developing rat spinal cord. *Journal of Neurocytology.* **18,** 161-169.

Seitelberger, F. (1995) Neuropathology and genetics of Pelizaeus-Merzbacher disease. *Brain pathol.* **5,** 267-273.

Silver, L.M. (1995a) Classical linkage analysis and mapping panels. *Mouse genetics.* Silver, L.M., editor: Oxford university press, pp. 195-263.

Silver, L.M. (1995b) Mapping in the mouse: an overview. *Mouse genetics.* Silver, L.M., editor: Oxford University Press, pp. 133-155.

Silver, L.M. (1995c) The mouse genome . *Mouse genetics.* Silver, L.M., editor: Oxford University Press, New York, pp. 76-113.

Sinoway, M.P., Kitagawa, K., Timsit, S., Hashim, G.A. and Colman, D.R. (1994) Proteolipid protein interactions in transfectants: Implications for myelin assembly. *Journal of Neuroscience Research.* **37,** 551-562.

Skoff, R.P. (1976) Myelin deficit in the jimpy mouse may be due to cellular abnormalities in astroglia. *Nature.* **264,** 560-562.

Skoff, R.P. (1982) Increased proliferation of oligodendrocytes in the hypomyelinated mouse mutant-jimpy. *Brain Research.* **248,** 19-31.

Skoff, R.P. (1990) Gliogenesis in rat optic nerve: astrocytes are generated in a single wave before oligodendrocytes. *Developmental Biology.* **139,** 149-168.

Skoff, R.P. and Ghandour, M.S. (1995) Oligodendrocytes in female carriers of the jimpy gene make more myelin than normal oligodendrocytes. *Journal of Comparative Neurology.* **355,** 124-133.

Skoff, R.P., Price, D.L. and Stocks, A. (1976a) Electron microscopic autoradiographic studies of gliogenesis in rat optic nerve. *Journal of Comparative Neurology.* **169,** 291-312.

Skoff, R.P., Price, D.L. and Stocks, A. (1976b) Electron microscopic autoradiographic studies of gliogenesis in rat optic nerve. II. Time of origin. *Journal of Comparative Neurology.* **169,** 313-334.

Skoff, R.P., Toland, D. and Nast, E. (1980) Pattern of myelination and distribution of neuroglial cells along the developing optic system of the rat and rabbit. *Journal of Comparative Neurology.* **191,** 237-253.

Small, R.K., Riddle, P. and Noble, M. (1987) Evidence for migration of oligodendrocyte-type-2 astrocyte progenitor cells into the developing rat optic nerve. *Nature.* **328,** 155-157.

Smith, K.J., Blakemore, W.F., Murray, J.A. and Patterson, R.C. (1982) Internodal myelin volume and axon surface area. A relationship determining myelin thickness? *Journal of the Neurological Sciences.* **55,** 231-246.

Sorg, B.A., Smith, M.M. and Campagnoni, A.T. (1987) Developmental expression of the myelin proteolipid protein and basic protein mRNA in normal and dysmyelinating mutant mice. *Journal of Neurochemistry.* **49,** 1146-1154.

Sprinkle, T.J., Lanclos, K.D. and Lapp, D.F. (1992) Assignment of the human 2',3'-cyclic nucleotide 3'-phosphohydrolase gene to chromosome 17. *Genomics.* **13,** 877-880.

Sprinkle, T.J., Zarube, M.E. and McKhann, G.M. (1978) Activity of 2'3'-cyclic nucleotide 3'-phosphodiesterase in regions of rat brain during development: quantitative relationship to myelin basic protein. *Journal of Neurochemistry.* **30,** 309-314.

Stensaas, L.J. and Stensaas, S.S. (1968) Astrocytic neuroglial cells, oligodendrocytes and microgliacytes in the spinal cord of the toad. II. Electron microscopy. *Zeitschrift Zellforschung Microskopische Anatomie.* **86,** 184-213.

Stoffel, W., Boison, D. and Bussow, H. (1997) Functional analysis in vivo of the double mutant mouse deficient in both proteolipid protein (PLP) and myelin basic protein (MBP) in the central nervous system. *Cell and Tissue Research.* **289,** (2)195-206.

Sturrock RR. Crevos-Navarr J and Sarkander IH, editors.Problems of glial identification and quantification in the ageing central nervous system. New York: Raven press; 1983; 179p.

Suzuki, K. and Nagara, H. (1982) Quaking mouse: vacuolar degeneration of spinal roots. *Acta Neuropathologica (Berlin).* **58,** 269-274.

Suzuki, K. and Zagoren, J.C. (1977) Quaking mouse: an ultrastructural study of the peripheral nerves. *Journal of Neurocytology.* **6,** 71-84.

Takahashi, N., Roach, A., Teplow, D.B., Prusiner, S.B. and Hood, L. (1985) Cloning and characterization of the myelin basic protein gene from mouse: one gene can encode both 14kd and 18.5kd MBPs by alternate use of exons. *Cell.* **42,** 139-148.

Taylor, B.A., Navin, A. and Phillips, S.J. (1994) PCR-amplification of simple sequence repeat variants from pooled DNA samples for rapidly mapping new mutations of the mouse. *Genomics.* **21,** 626-632.

Temple, S. and Raff, M.C. (1985) Differentiation of a bipotential glial progenitor cell in single cell microculture. *Nature.* **313,** 223-225.

Temple, S. and Raff, M.C. (1986) Clonal analysis of oligodendrocyte development in culture: evidence for a developmental clock that counts cell divisions. *Cell.* **44,** 773-779.

Thompson, R.J. (1992) 2',3'-Cyclic nucleotide-3'-phosphohydrolase and signal transduction in central nervous system myelin. *Biochem Soc Trans.* **20,** 621-626.

Timsit, S., Martinez, S., Allinquant, B., Peyron, F., Puelles, L. and Zalc, B. (1995) Oligodendrocytes originate in a restricted zone of the embryonic ventral neural tube defined by DM-20 mRNA expression. *Journal of Neuroscience.* **15,** 1012-1024.

Timsit, S.G., Bally-Cuif, L., Colman, D.R. and Zalc, B. (1992) DM-20 mRNA is expressed during the embryonic development of the nervous system of the mouse. *Journal of Neurochemistry* . **58,** 1172-1175.

Tokuda, M. (1935) An eighteenth century Japanese guide book on mouse-breeding. *Journal of Heredity.* **26,** 481-484.

Tosic, M., Roach, A., de Rivaz, J.-C., Dolivo, M. and Matthieu, J.-M. (1990) Post-transcriptional events are responsible for low expression of myelin basic protein in myelin deficient mice: role of antisense RNA. *EMBO J.* **9,** 401-406.

Trapp, B.D. (1990) Myelin-associated glycoprotein: location and potential functions. *Annals of the New York Academy of Sciences.* **605,** 29-43.

Trapp, B.D., Andrews, S.B., Wong, A., O'Connell, M. and Griffin, J.W. (1989) Co-localization of the myelin-associated glycoprotein and the microfilament components F-actin and spectrin in Schwann cells of myelinated nerve fibres. *Journal of Neurocytology.* **18,** 47-60.

Trapp, B.D., Bernier, L., Andrews, B. and Colman, D.R. (1988) Cellular and subcellular distribution of 2',3'-cyclic nucleotide 3'-phosphodiesterase and its mRNA in the rat central nervous system. *Journal of Neurochemistry.* **51,** 859-868.

Trapp, B.D., Moench, T., Pulley, M., Barbosa, E., Tennekoon, G.I. and Griffin, J.W. (1987) Spatial segregation of mRNA encoding myelin-specific proteins. *Proceedings of the National Academy of Sciences USA.* **84,** 7773-7777.

Trapp, B.D., Nishiyama, A., Cheng, D. and Macklin, E. (1997) Differentiation and death of premyelinating oligodendrocytes in developing rodent brain. *Journal of Cell Biology.* **137,** (2)459-468.

Trotter, J. and Schachner, M. (1989) Cells positive for the O4 surface antigen isolated by cell sorting are able to differentiate into astrocytes or oligodendrocytes. *Developmental Brain Research.* **46,** 115-122.

Tucker, P.K., Lee, B.K., Lundrigan, B.L. and Eicher, E.M. (1992) Geographic origin of the Y chromosome in "old" inbred strains of mice. *Mammalian Genome.* **3,** 254-261.

Umemori, H., Sato, S., Yagi, T., Aizawa, S. and Yamamoto, T. (1994) Initial events of myelination involve Fyn tyrosine kinase signalling. *Nature.* **367,** 572-576.

Van Dorsselaer, A., Nebhl, R., Sorokine, O., Schindler, P. and Luu, B. (1987) The DM-20 proteolipid is a major brain protein. It is synthesised earlier in foetal life than the major myelin proteolipid (PLP). *Compte Rendu Academy Science Paris.* **305,** 555-560.

Vela, J.M., Dalmau, I., González, B. and Castellano, B. (1996) The microglial reaction in spinal cords of jimpy mice is related to apoptotic oligodendrocytes. *Brain Res.* **712,** 134-142.

Verity, A.N. and Campagnoni, A.T. (1988) Regional expression of myelin protein genes in the developing mouse brain: in situ hybridization studies. *Journal of Neuroscience Research.* **21,** 238-248.

Warf, B.C., Fok-Seang, J. and Miller, R.H. (1991) Evidence for the ventral origin of oligodendrocyte precursors in the rat spinal cord. *Journal of Neuroscience.* **11,** 2477-2488.

Warrington, A.E., Barbarese, E. and Pfeiffer, S.E. (1993) Differential myelinogenic capacity of specific developmental stages of the oligodendrocyte lineage upon transplantation into hypomyelinating hosts. *Journal of Neuroscience Research.* **34,** 1-13.

Watanabe, I. and Bingle, G.J. (1972) Dysmyelination in "quaking" mouse. Electron microscopic study. *Journal of Neuropathology and Experimental Neurology.* **31,** 352-369.

Weber, J.L. and May, P.E. (1989) Abundant class of human DNA polymorphisms which can be typed using the polymerase chain reaction. *American Journal of Human Genetics.* **44,** 388-396.

Weimbs, T. and Stoffel, W. (1992) Proteolipid protein (PLP) of CNS myelin: Positions of free, disulfide-bonded, and fatty acid thioester-linked cysteine residues and implications for the membrane topology of PLP. *Biochemistry.* **31,** 12289-12296.

Wilkins, A.S. (1990) Position effects, methylation and inherited epigenetic states. *BioEssays.* **12,** 385-386.

Wilkinson, H.J., Bailes, J.A. and McMahon, A.P. (1987) Expression of the proto-oncogene interleukin-1 is restricted to specific neural cells in the developing mouse embryo. *Cell.* **50,** 79-88.

Willard, H.F. and Riordan, J.R. (1985) Assignment of the gene for myelin proteolipid protein to the X chromosome: implications for X-linked myelin disorders. *Science.* **230,** 940-942.

Williams, B.P. and Price, J. (1995) Evidence for multiple precursor cell types in the embryonic rat cerebral cortex. *Neuron.* **14,** 1181-1188.

Williams, M.A. (1977) Stereological techniques. *Practical Methods in Electron Microscopy. Vol. 6. Quantitative Methods in Biology.* Glauert, A.M., editor: North Holland, Amsterdam, pp. 5-84.

Wolswijk, G. (1995) Strongly G_{D3}^{+} cells in the developing and adult rat cerebellum belong to the microglial lineage rather than to the oligodendrocyte lineage. *Glia.* **13,** 13-26.

Wolswijk, G. and Noble, M. (1989) Identification of an adult-specific glial progenitor cell. *Development.* **105,** 387-400.

Wren, D., Wolswijk, G. and Noble, M. (1992) In vitro analysis of the origin and maintenance of O-2A^{adult} progenitor cells. *Journal of Cell Biology.* **116,** 167-176.

Yamada, T., Placzek, M., Tanaka, H., Dodd, J. and Jessell, T.M. (1991) Control of cell pattern in the developing nervous system: polarizing activity of the floor plate and notochord. *Cell.* **64,** 635-647.

Yamamoto, Y., Mizuno, R., Nishimura, T., Ogawa, Y., Yoshikawa, H., Fujimura, H., Adachi, E., Kishimoto, T., Yanagihara, T. and Sakoda, S. (1994) Cloning and expression of myelin-associated oligodendrocytic basic protein. A novel basic protein constituting the central nervous system myelin. *Journal of Biological Chemistry.* **269,** 31725-31730.

Yan, Y., Lagenaur, C. and Narayanan, V. (1993) Molecular cloning of M6: Identification of a PLP/DM20 gene family. *Neuron.* **11,** 423-431.

Yanagisawa, K., Duncan, I.D., Hammang, J.P. and Quarles, R.H. (1986) Myelin-deficient rat: analysis of myelin proteins. *Journal of Neurochemistry.* **47,** 1901-1907.

Yeh, H.-J., Ruit, K.G., Wang, Y.-X., Parks, W.C., Snider, W.D. and Deuel, T.F. (1991) PDGF A-chain gene is expressed by mammalian neurons during development and in maturity. *Cell.* **64,** 209-216.

Young, G.M. and Levison, S.W. (1996) Persistence of multipotential progenitors in the juvenile rat subventricular zone. *Developmental Neuroscience.* **18,** 255-265.

Yu, W.-P., Collarini, E.J., Pringle, N.P. and Richardson, W.D. (1994) Embryonic expression of myelin genes: Evidence for a focal source of oligodendrocyte precursors in the ventricular zone of the neural tube. *Neuron.* **12,** 1353-1362.

Zhang, H. and Miller, R.H. (1996) Density-dependent feedback inhibition of oligodendrocyte precursor expansion. *Journal of Neuroscience.* **16,** 6886-6895.